

EPA/600/2-88/022
March 1988

AERATION EQUIPMENT EVALUATION:
PHASE I - CLEAN WATER TEST RESULTS

by

Fred W. Yunt
Tim O. Hancuff
County Sanitation Districts of Los Angeles County
Los Angeles, California 90607

Contract No. 14-12-150

Project Officer

Richard C. Brenner
Wastewater Research Division
Water Engineering Research Laboratory
Cincinnati, Ohio 45268

WATER ENGINEERING RESEARCH LABORATORY
OFFICE OF RESEARCH AND DEVELOPMENT
U.S. ENVIRONMENTAL PROTECTION AGENCY
CINCINNATI, OHIO 45268

DISCLAIMER

Development of the information in this report has been funded in part by the U.S. Environmental Protection Agency under Contract No. 14-12-150 to the County Sanitation Districts of Los Angeles County. The report has been subjected to Agency peer and administrative review and approved for publication as an EPA document. Mention of trade names or commercial products does not constitute endorsement or recommendation for use.

FOREWORD

The U.S. Environmental Protection Agency (EPA) is charged by Congress with protecting the Nation's land, air, and water systems. Under a mandate of national environmental laws, the agency strives to formulate and implement actions leading to a compatible balance between human activities and the ability of natural systems to support and nurture life. The Clean Water Act, the Safe Drinking Water Act, and the Toxics Substances Control Act are three of the major congressional laws that provide the framework for restoring and maintaining the integrity of our Nation's water, for preserving and enhancing the water we drink, and for protecting the environment from toxic substances. These laws direct EPA to perform research to define our environmental problems, measure the impacts, and search for solutions.

The Water Engineering Research Laboratory is that component of EPA's Research and Development program concerned with preventing, treating, and managing municipal and industrial wastewater discharges; establishing practices to control and remove contaminants from drinking water and to prevent its deterioration during storage and distribution; and assessing the nature and controllability of releases of toxic substances to the air, water, and land from manufacturing processes and subsequent product uses. This publication is one of the products of that research and provides a vital communication link between the researcher and the user community.

As part of these activities, an aeration equipment evaluation was undertaken at the Joint Water Pollution Control Plant of Los Angeles County Sanitation Districts using the non-steady state clean water test procedure. Systems chosen for evaluation represented various submerged generic aeration devices. Seven manufacturers participated in the study. Information documented herein should be of particular interest to design engineers and municipal officials charged with selecting aeration equipment for new activated sludge treatment plants and/or considering a retrofit to new equipment in existing plants.

Francis T. Mayo, Director
Water Engineering Research Laboratory

ABSTRACT

This research project was initiated with the principle objective of evaluating the oxygen transfer performance of various generic aeration systems used in activated sludge wastewater treatment. A secondary objective of the project was to evaluate various oxygen transfer data analysis methods in current use.

Working in conjunction with an EPA-retained consultant and the equipment manufacturers, clean water tests were conducted on eight types of submerged aerators. All aerator testing was conducted in the same tank and used the same procedures in order to provide standard test conditions.

Results of this work indicated that, of the systems tested, fine bubble diffusion equipment transferred oxygen most efficiently in clean water. Results also indicated that, in clean water, jet aeration equipment transfers oxygen more efficiently than do coarse bubble aeration systems. However, because the value of wastewater correction factors (α and β) are dependent on the type of aerator tested, the relative performance of the aerators to one another in wastewater may be different.

This report was submitted in fulfillment of Contract No. 14-12-150 by the County Sanitation Districts of Los Angeles County under partial sponsorship of the U.S. Environmental Protection Agency. This report covers the test period February 15, 1978, through March 16, 1979.

CONTENTS

Foreword	iii
Abstract	iv
Figures	viii
Tables	xi
Nomenclature	xiii
Conversion Factors	xxi
Acknowledgements	xxii
1. Introduction	1
Background and Overview.....	1
Project Outline.....	2
2. Conclusions and Recommendations.....	4
3. Equipment and Testing Procedures.....	6
Test Facility.....	6
Test Procedures.....	6
Airflow measurements.....	6
Dissolved oxygen sample collection.....	11
Dissolved oxygen measurements.....	16
Aerator power determinations.....	16
Power density calculations.....	23
Headloss measurements.....	24
Deoxygenation procedure.....	25
Field Experiment Procedure.....	25

CONTENTS (continued)

4. Oxygen Transfer Data Analysis.....	29
Field Measurements.....	29
Basic Theory.....	29
Determination of $K_L a_t$ and C^*	35
Least Squares Regression Methods.....	37
Need for Data Truncation.....	38
Parameters at Standard Conditions.....	39
K_{La20} determination.....	39
C^*_0 determination.....	40
Evaluation of Data Acceptability.....	42
Primary Data Analysis Method.....	42
Standard Oxygen Transfer Calculations.....	43
Determination of Standard Aeration Efficiency.....	44
5. Aeration System Descriptions.....	45
Overview.....	45
Fine Bubble Dome Diffusers.....	45
Fine Bubble Tube Diffusers.....	48
Jet Aerators.....	48
Static Tube Aerators.....	53
Variable Orifice Coarse Bubble Diffusers.....	53
Fixed Orifice Coarse Bubble Diffusers - D-24.....	60
Fixed Orifice Coarse Bubble Diffusers - Superfuser.....	65
Fixed Orifice Coarse bubble Diffusers - Deflectofuser.....	70
6. Test Results.....	73
Overview.....	73
Tabular Presentations.....	74
Presentation of analysis results for the Exponential and Equilibrium Methods.....	74
Comparison of analysis results for the Exponential and Equilibrium Methods.....	74
Graphical Presentations.....	91
Water depth relationships.....	92
Delivered power density relationships.....	95
7. Problems Associated with Clean Water Testing.....	112
Overview.....	112
Degassing of High Level Dissolved Oxygen Samples.....	112
Blower Pulsation.....	113
Excessive $K_L a$ Variation.....	115
Jet Aerator Pump Power Measurement.....	116
Tap Water Foaming.....	117

CONTENTS (continued)

8. Follow-On Research Activities.....	123
References.....	124
Appendices	
A. Airflow Meter Equations.....	125
B. Preamble to Appendices C through J.....	128
C. Individual Performance Results for Norton Fine Bubble Dome Diffusers.....	129
D. Individual Performance Results for FMC Fine Bubble Tube Diffusers.....	136
E. Individual Performance Results for Pentech Jet Aerators.....	143
F. Individual Performance Results for Kenics Static Tube Aerators.....	150
G. Individual Performance Results for Bauer Variable Orifice Diffusers.....	157
H. Individual Performance Results for Sanitaire Coarse Bubble Diffusers.....	164
I. Individual Performance Results for Envirex Coarse Bubble Diffusers.....	171
J. Individual Performance Results for FMC Coarse Bubble Diffusers.....	178

FIGURES

<u>Number</u>		<u>Page</u>
1	Clean Water Testing Facility	7
2	Orifice Plate for 3-in. Air Line	12
3	Orifice plate for 4-in. Air Line	13
4	Annubar Flow Measurement Device	14
5	Horsepower Schematics	21
6	Primary Curve Plots for Equilibrium and Exponential Data Analysis Methods.....	36
7	Test Tank Configuration for the Norton Dome Diffuser Aeration System.....	46
8	Norton Dome Diffuser.....	47
9	Test Tank Configuration for the FMC Pearlcomb Tube Diffuser Aeration System.....	49
10	FMC Pearlcomb Diffuser.....	50
11	Test Tank Configuration for the Pentech EMJA Unit at the 10-ft Water Depth.....	51
12	Pentech Directional Mix Jet Aerator (DMJA).....	52
13	Test Tank Configuration for the Pentech DMJA Unit at the 15-ft Water Depth.....	54
14	Pentech Eddy Mix Jet Aerator (EMJA).....	55
15	Test Tank Configuration for the Pentech EMJA Unit at the 20- and 25-ft Water Depths.....	56

FIGURES (continued)

16	Test Tank Configuration for the Kenics Static Tube Aeration System at the 10- and 15-ft Water Depths.....	57
17	Kenics Static Tube Aerator.....	58
18	Test Tank Configuration for the Kenics Static Tube Aeration System at the 20- and 25-ft Water Depths....	59
19	Bauer Airpac Diffuser.....	61
20	Test Tank Configuration for the Bauer Model II Airpac Aeration System at the 10- and 20-ft Water Depths.....	62
21	Test Tank Configuration for the Bauer Model III Airpac Aeration System at the 15- and 25-ft Water Depths.....	63
22	Sanitaire D-24 Diffuser.....	64
23	Test Tank Configuration for the Sanitaire D-24 Aeration System at the 10- and 20-ft Water Depths.....	66
24	Test Tank Configuration for the Sanitaire D-24 Aeration System at the 15- and 25-ft Water Depths.....	67
25	Envirex Superfuser Diffuser.....	68
26	Test Tank Configuration for the Envirex Superfuser Aeration System.....	69
27	FMC Deflectofuser Diffuser.....	71
28	Test Tank Configuration for the FMC Deflectofuser (Sparger) Aeration System at the 15-ft Water Depth.....	72
29	Comparative Plot of SOTR vs. Water Depth at Middle Power Density Tested.....	93
30	Comparative Plot of SOTE vs. Water Depth at Middle Power Density Tested.....	94
31	Comparative Plot of SWAE vs. Water Depth at Middle Power Density Tested.....	96
32	Comparative Plot of SOTR vs. Delivered Power Density at 10-ft Water Depth.....	97

FIGURES (continued)

33	Comparative Plot of SOTE vs. Delivered Power Density at 10-ft Water Depth.....	98
34	Comparative Plot of SWAE vs. Delivered Power Density at 10-ft Water Depth.....	100
35	Comparative Plot of SOTR vs. Delivered Power Density at 15-ft Water Depth.....	101
36	Comparative Plot of SOTE vs. Delivered Power Density at 15-ft Water Depth.....	102
37	Comparative Plot of SWAE vs. Delivered Power Density at 15-ft Water Depth.....	103
38	Comparative Plot of SOTR vs. Delivered Power Density at 20-ft Water Depth.....	105
39	Comparative Plot of SOTE vs. Delivered Power Density at 20-ft Water Depth.....	106
40	Comparative Plot of SWAE vs. Delivered Power Density at 20-ft Water Depth.....	107
41	Comparative Plot of SOTR vs. Delivered Power Density at 25-ft Water Depth.....	108
42	Comparative Plot of SOTE vs. Delivered Power Density at 25-ft Water Depth.....	109
43	Comparative Plot of SWAE vs. Delivered Power Density at 25-ft Water Depth.....	111

TABLES

<u>Number</u>		<u>Page</u>
1	Summary of Water Quality Characteristics.....	8
2	Field Measurements.....	30
3	Summary of Exponential Method Results: Norton Fine Bubble Dome Diffusers.....	75
4	Summary of Equilibrium Method Results: Norton Fine Bubble Dome Diffusers.....	76
5	Summary of Exponential Method Results: FMC Fine Bubble Dome Diffusers.....	77
6	Summary of Equilibrium Method Results: FMC Fine Bubble Dome Diffusers.....	78
7	Summary of Exponential Method Result: Pentech Jet Aerators.....	79
8	Summary of Equilibrium Method Results: Pentech Jet Aerators.....	80
9	Summary of Exponential Method Results: Kenics Static Tube Aerators.....	81
10	Summary of Equilibrium Method Results: Kenics Static Tube Aerators.....	82
11	Summary of Exponential Method Results: Bauer Course Bubble Diffusers.....	83
12	Summary of Equilibrium Method Results: Bauer Variable Orifice Diffusers.....	84
13	Summary of Exponential Method Results: Sanitaire Course Bubble Diffusers.....	85

TABLES (continued)

14	Summary of Equilibrium Method Results: Sanitaire Course Bubble Diffusers.....	86
15	Summary of Exponential Method Results: Envirex Course Bubble Diffusers.....	87
16	Summary of Equilibrium Method Results: Envirex Course Bubble Diffusers.....	88
17	Summary of Exponential Method Results: FMC Course Bubble Diffusers.....	89
18	Summary of Equilibrium Method Results: FMC Course Bubble Diffusers.....	90
19	Comparison of Analysis Methods.....	91
20	Foaming Problem Comparison Tests.....	121

NOMENCLATURE

List of Basic Symbols

<u>Symbol</u>	<u>Description</u>	<u>Symbol</u>	<u>Description</u>
C	dissolved oxygen (D.O.) concentration	P	aerator power
C*	D.O. saturation value	PD	power density
D	D.O. deficit (driving force)	p	pressure
e	efficiency	Q	measured airflow at standard conditions
F	airflow correction factor	T	temperature
h	differential pressure	t	time
$K_L a$	overall volumetric mass transfer coefficient	V	volume of liquid in aeration tank
N	aeration efficiency	z	water depth

List of Specific Symbols

<u>Symbol</u>	<u>Description</u>	<u>Units</u>
C_c	calculated D.O. concentration at time t	mg/L

NOMENCLATURE (continued)

List of Specific Symbols (continued)

<u>Symbol</u>	<u>Description</u>	<u>Units</u>
C_f	final D.O. concentration corresponding to time t_f	mg/L
C_i	initial D.O. concentration corresponding to time t_i	mg/L
C_m	measured D.O. concentration at time t	mg/L
C_t	D.O. concentration at time t	mg/L
C^*	D.O. saturation value	mg/L
C^*_{hT}	handbook D.O. saturation value at temperature T , 14.70 psia, dry air, and 20.9% O_2 by volume	mg/L
C^*_{h20}	handbook D.O. saturation value at 20°C, 14.70 psia, dry air and 20.9% O_2 by volume (9.17 mg/L)	mg/L
C^*_{md}	measured or derived D.O. saturation value at temperature T and barometric pressure p_a	mg/L
C^*_o	projected field D.O. saturation value at standard conditions of 20°C, 14.70 psia, and 0 mg/L D.O.	mg/L
C^*_{∞} (T_o, p_{ao})	projected field D.O. saturation value at time $t = \infty$, 20°C, and 14.70 psia, based on the concept of equivalent depth	mg/L
D_f	final D.O. deficit corresponding to time t_f	mg/L
D_i	initial D.O. deficit corresponding to time t_i	mg/L
D_o	D.O. deficit at standard conditions of 20°C, 14.70 psia, and 0 mg/L D.O.	mg/L
d	actual internal pipe diameter	in.
dC/dt	oxygen transfer rate per unit volume	mg/L
dC/dt_o	oxygen transfer rate per unit volume at standard conditions of 20°C, 14.70 psia, and 0 mg/L D.O.	mg/L
e_b	blower efficiency	decimal %

NOMENCLATURE (continued)

List of Specific Symbols (continued)

<u>Symbol</u>	<u>Description</u>	<u>Units</u>
e_d	drive or coupling efficiency	decimal %
e_m	motor efficiency	decimal %
e_p	pump efficiency	decimal %
F_a	orifice area correction factor	--
F_m	manometer fluid temperature correction factor	--
F_{pe}	pipe expansion correction factor	--
F_{wv}	relative humidity correction factor	--
h_a	Annubar differential pressure	in. H ₂ O
h_L	measured diffuser headloss	in. H ₂ O
h_{Ld}	estimated aeration system piping headloss	psig
h_{Ls}	estimated suction piping headloss	psig
h_o	orifice plate differential pressure	in. H ₂ O
K	flow meter constant	--
K_{La}	overall volumetric mass transfer coefficient	1/hr
K_{Lat}	overall volumetric mass transfer coefficient at temperature T	1/hr
K_{La20}	overall volumetric mass transfer coefficient at 20°C	1/hr
N_{bo}	brake aeration efficiency in clean water at standard conditions of 20°C, 14.70 psia, and 0 mg/L D.O.	lb of oxygen per hp-hr
N_{do}	delivered aeration efficiency in clean water at standard conditions of 20°C, 14.70 psia, and 0 mg/L D.O.	lb of oxygen per hp-hr
N_{wo}	wire aeration efficiency in clean water at standard conditions of 20°C, 14.70 psia, and 0 mg/L D.O.	lb of oxygen per hp-hr

NOMENCLATURE (continued)

List of Specific Symbols (continued)

<u>Symbol</u>	<u>Description</u>	<u>Units</u>
N_o	aeration efficiency in clean water at standard conditions of 20°C, 14.70 psia, and 0 mg/L D.O.	lb of oxygen per hp-hr
OSR	oxygen supply rate	lb of oxygen per hr
OTE	oxygen transfer efficiency at 0 mg/L D.O. (maximum deficit)	%
OTR	oxygen transfer rate at 0 mg/L D.O. (maximum deficit)	lb of oxygen per hr
P_a	air power	hp
P_{ab}	air brake power	hp
P_{abs}	air brake power at standard conditions of 20°C, 14.70 psia, and 36% relative humidity	hp
P_{ad}	air delivered power	hp
P_{ads}	air delivered power at standard conditions of 20°C, 14.70 psia, and 36% relative humidity	hp
P_{ans}	air nominal power at standard conditions of 20°C, 14.70 psia, 36% relative humidity, and a blower inlet pressure of 14.60 psia	hp
P_{aw}	air wire power	hp
P_{aws}	air wire power at standard conditions of 20°C, 14.70 psia, and 36% relative humidity	hp
P_b	total brake power	hp
P_{bs}	total brake power at standard conditions of 20°C, 14.70 psia, and 36% relative humidity	hp
P_d	total delivered power	hp

NOMENCLATURE (continued)

List of Specific Symbols (continued)

<u>Symbol</u>	<u>Description</u>	<u>Units</u>
P_{ds}	total delivered power at standard conditions of 20°C, 14.70 psia, and 36% relative humidity	hp
P_{ns}	total nominal power at standard conditions of 20°C, 14.70 psia, 36% relative humidity, and a blower inlet pressure of 14.60 psia	hp
P_{pb}	pump brake power	hp
P_{pd}	pump delivered power	hp
P_{pw}	pump wire power	hp
P_w	total wire power	hp
PD_{ds}	delivered power density at standard conditions	hp per 1000 ft ³
PD_{ns}	nominal power density at standard conditions	hp per 1000 ft ³
p_a	barometric pressure	mm of mercury
p_{ao}	barometric pressure at standard conditions (14.70 psia)	in. of mercury
p_c	aerator air pressure	in. of mercury
p_f	flow meter flowing gas pressure	in. of mercury
p_{fa}	Annubar flowing gas pressure	in. of mercury
p_{fo}	orifice plate flowing gas pressure	in. of mercury
p_i	assumed blower inlet pressure (14.6 psia)	psia
P_{sh}	aerator static head	in. of mercury

NOMENCLATURE (continued)

List of Specific Symbols (continued)

<u>Symbol</u>	<u>Description</u>	<u>Units</u>
p_t	Annubar stagnation pressure	in. of mercury
p_{vpT}	vapor pressure of water at temperature T	psig
p_{vp20}	vapor pressure of water at 20°C (0.34 psig)	psig
p_{wa}	partial pressure of water vapor in ambient air	psig
p_{wl}	partial pressure of water vapor in the air line	psig
p_1	calculated blower inlet pressure	psia
p_2	calculated blower discharge pressure	psia
Q_a	measured airflow at standard conditions using Annubar	scfm
Q_{max}	maximum test airflow for a system at each water depth	scfm
Q_o	measured airflow at standard conditions using orifice plate	scfm
Q_p	liquid flow rate produced by jet aerator pump	cfs
Q_{test}	averaged airflow value associated with a test	scfm
Re	Reynolds number of airflow in pipe	--
RH	relative humidity	%
S_o	orifice factor	--
SOTE	oxygen transfer efficiency in clean water at standard conditions of 20°C, 14.70 psia, and 0 mg/L D.O.	%
SOTR	oxygen transfer rate in clean water at standard conditions of 20°C, 14.70 psia, and 0 mg/L D.O.	lb of oxygen per hr
SWD	side water depth	ft
T_a	ambient air temperature	°F

NOMENCLATURE (continued)

List of Specific Symbols (continued)

<u>Symbol</u>	<u>Description</u>	<u>Units</u>
T_{am}	manometer board air temperature	°F
T_d	diffuser air temperature	°F
T_f	flow meter air temperature	°F
T_i	temperature at blower inlet	°F
T_o	water temperature at standard conditions (20°C)	°C
T_w	water temperature	°C
TDH	total dynamic head of jet aerator pump	ft of H ₂ O
t_j	time, corresponding to D.O. measurement C_j	sec
t_f	time corresponding to D.O. measurement C_f	sec
V_j	inflated water volume (aerated)	ft ³
V_w	deflated water volume (not aerated)	ft ³
Y_e	orifice plate gas expansion factor	--
z_d	diffuser submergence	ft
z_{emd}	equivalent depth corresponding to the measured or derived D.O. saturation value	ft
z_j	inflated water depth (same as side water depth)	ft
z_w	deflated water depth	ft
α	(alpha) ratio of $K_L a$ in wastewater to $K_L a$ in clean water under identical conditions	--
β	(beta) ratio of the oxygen saturation in wastewater to oxygen saturation in clean water under identical conditions	--
γ_{air}	(gamma) specific weight of air at the temperature, pressure, and relative humidity for which Q is reported	lb per ft ³

NOMENCLATURE (continued)

List of Specific Symbols (continued)

<u>Symbol</u>	<u>Description</u>	<u>Units</u>
γ_{water}	(gamma) specific weight of water at 20°C (62.4 lb/ft ³)	lb per ft ³
θ	(theta) $K_L a$ temperature adjustment factor	--
μ	(mu) gas absolute viscosity	cps

CONVERSION FACTORS

<u>Measurement</u>	<u>To Convert From U.S. Customary Unit</u>	<u>To SI Unit</u>	<u>Divide By</u>
Aeration Efficiency	lb O ₂ /hp-hr	kg O ₂ /kWh	1.644
Airflow	cfm	L/sec	2.119
Barometric Pressure	psia	kPa	0.1451
Density	lb/ft ³	kg/m ³	0.06243
Depth	ft	m	3.281
Headloss	in. of H ₂ O	mm H ₂ O	0.03937
Headloss	psi	kPa	0.1451
Oxygen Supply Rate	lb O ₂ /hr	kg O ₂ /hr	2.205
Oxygen Transfer Rate	lb O ₂ /hr	kg O ₂ /hr	2.205
Power	hp	kW	1.341
Power Density	hp/1000 ft ³	W/m ³	0.03797
Temperature	°F	°C	*
Water Volume	ft ³	m ³	35.31

* °C = 5 (°F-32)/9

ACKNOWLEDGEMENTS

The untiring effort, cooperation, and numerous contributions of Gerry Shell of Gerry Shell Environmental Engineers, LaVergne, Tennessee, are gratefully acknowledged. The generous assistance rendered by all equipment manufacturers participating in the aeration equipment evaluation is greatly appreciated. The contributions of the consultants working for the equipment manufacturers and Michael K. Stenstrom of the University of California, Los Angeles, are also gratefully acknowledged.

SECTION 1

INTRODUCTION

BACKGROUND AND OVERVIEW

This project was originally conceived by the U.S. Environmental Protection Agency (EPA) and County Sanitation Districts of Los Angeles County (LACSD) in the spring of 1977. An arrangement was made to have the Districts conduct clean oxygen transfer tests on seven different types of submerged aeration devices; the deflectofuser (sparger) was later added because it was widely used both nationwide and in the Districts' treatment plants. EPA partially funded the project and retained Gerry Shell of Gerry Shell Environmental Engineers as a consulting engineer. The project was referred to as the "Aeration Equipment Evaluation - Phase I". A second phase of the project was considered essential at a later date to compare oxygen transfer performance in clean water to that in mixed liquor.

The "Aeration Equipment Evaluation - Phase I" project was conducted in order to accomplish three major objectives. The main purpose was to evaluate the clean water oxygen transfer performance of various generic types of aeration equipment under identical testing conditions and using identical testing methods. A second purpose of the study was to demonstrate the effects of changing depths and operating power levels on various types of aeration equipment. Finally, a subobjective of the project was to evaluate various oxygen transfer data analysis methods in current use.

Analysis of clean water test results for various generic aeration devices is the first step toward defining the performance expected from such equipment. Clean water tests indicate general trends in an aerator's performance, but they do not necessarily reflect an aerator's performance under actual conditions. The logical second step, therefore, was the evaluation of selected submerged aeration equipment under mixed liquor conditions. Subsequent to the clean water testing studies, LACSD evaluated three generic types of aeration equipment under mixed liquor conditions at their Whittier Narrows Water Reclamation Plant in El Monte, California. This phase of the project is referred to as the "Aeration Equipment Evaluation - Phase II". The three systems tested were selected on the basis of their performance during the clean water project. It is hoped that information obtained from both phases of the "Aeration Equipment Evaluation" can be used to determine wastewater correction factors (alpha and beta) that may have applicability to other aeration system designs. Field test work for the mixed liquor phase of the project was completed in 1982, and a report of these activities is in preparation.

PROJECT OUTLINE

This study was to be an evaluation of distinct generic types of equipment; it was not intended to be an evaluation of various manufacturers' equipment of the same generic type. Due to the large variety of fixed orifice coarse bubble diffusers on the market, more than one of this generic type was tested. The following is a complete list of the equipment tested:

<u>System</u>	<u>Description</u>	<u>Manufacturer</u>
A	Fine bubble ceramic dome diffusers applied in a total floor coverage configuration	Norton Company
B	Fine bubble plastic tube diffusers applied in a dual aeration configuration	FMC Corporation
C	Jet aerators	Pentech-Houdaille Industries, Inc.
D	Static tube aerators	Kenics Corporation
E	Variable orifice coarse bubble diffusers	C-E Bauer of Combustion Engineering, Inc.
F	Fixed orifice coarse bubble diffusers	Sanitaire - Water Pollution Control Corporation
G	Fixed orifice coarse bubble diffusers	Envirex, Inc.
H	Fixed orifice coarse bubble diffusers [sparger tests conducted at a 4.6-m (15-ft) depth only]	FMC Corporation

The tests were conducted at the Districts' Joint Water Pollution Control Plant in Carson, California. The study was structured to provide clean water test information at water depths of 3.0 m (10 ft), 4.6 m (15 ft), 6.1 m (20 ft), and 7.6 m (25 ft). A range of nominal power densities was evaluated at each depth. The manufacturers were given the choice to test at one of two power options, as follows:

Option 1: 13.2, 26.3, and 39.5 nominal W/m^3
(0.5, 1.0, and 1.5 nominal hp/1000 ft³)

Option 2: 7.9, 13.2, and 26.3 nominal W/m^3
(0.3, 0.5, and 1.0 nominal hp/1000 ft³)

It was hoped that each manufacturer would select the range that was most typical of the equipment's application in mixed liquor. All

manufacturers tested chose Option 1, with the exception of the Norton Company, which selected Option 2. The 3 to 1 range in power for both options was intended to demonstrate the aeration equipment's ability to handle diurnal variations in process loading.

The manufacturers were responsible for designing the layout of their equipment subject to the constraints of this study. Each manufacturer was allowed, if desired, to change its equipment configuration at each depth tested. It was required, however, that the same configuration be used for all tests at a given depth.

Testing procedures and testing equipment were decided on by the LACSD Project Engineers and approved by the EPA consultant. Manufacturers and other experts in the field reviewed and commented on the test procedures. All tests were conducted by the LACSD Project Engineers, with each system's initial tests being witnessed by both the EPA consultant and a representative of the equipment manufacturer.

Actual testing on the first aeration system (fine bubble dome diffusers) began in November 1977. Due to technical problems related to airflow and dissolved oxygen (D.O.) measurements, the official tests of this system were not completed until May, 1978. The tests on the last aeration system (coarse bubble sparger) were completed in March, 1979.

SECTION 2

CONCLUSIONS AND RECOMMENDATIONS

The clean water study provided considerable insight into the performance characteristics of various submerged aeration devices. The following conclusions were reached:

- (1) For a given water depth and delivered power density, the Standard Wire Aeration Efficiency (SWAE) of the fine bubble dome diffusers in a total floor coverage mode was substantially better than that of any other system tested.
- (2) For a given water depth and delivered power density, the SWAE of the fine bubble tube diffusers in a dual aeration mode was substantially better than that of either the jet aerators or the various coarse bubble diffusers.
- (3) For a given water depth and delivered power density, the SWAE of the jet aerators was usually better than that of the various coarse bubble diffusers (with the exception of the Sanitaire fixed orifice coarse bubble diffusers in a total floor coverage mode).
- (4) For a given water depth, delivered power density, and with similar configurations, the SWAE's of the various coarse bubble diffusers were similar.
- (5) For a given configuration and water depth, and for an increase in delivered power density, the SWAE decreased significantly for the fine bubble tube diffusers, showed a local maximum for the jet aerators, and showed very little change for the coarse bubble diffusers.
- (6) For a given configuration and delivered power density, and for an increase in water depth, the SWAE was relatively unaffected for the fine bubble diffusers and usually increased significantly for the other types with the exception of the static tube aerators at the upper water depths.
- (7) For a given water depth and delivered power density, the Standard Oxygen Transfer Efficiency (SOTE) of the fine bubble dome diffusers in a total floor coverage mode was substantially better than that of any other system tested.

- (8) For a given water depth and delivered power density, the SOTE's of the fine bubble tube diffusers in a dual aeration mode and the jet aerators were similar and significantly better than that of the various coarse bubble diffusers.
- (9) For a given water depth and delivered power density, the SOTE's of the various coarse bubble diffusers were very similar when installed in similar configurations.
- (10) For a given configuration and water depth, and for an increase in delivered power density, the SOTE decreased significantly for the fine bubble diffusers and jet aerators, and usually increased slightly for the various coarse bubble diffusers (with the exception of the static tube aerators, where the SOTE was not significantly affected by changes in delivered power density).
- (11) For a given configuration and delivered power density, the SOTE increased substantially with an increase in water depth for all systems tested.
- (12) The use of a total floor coverage configuration with the Sanitaire fixed orifice coarse bubble diffusers appeared to improve the performance of this system significantly.
- (13) With the exception of the Sanitaire system, the changes in configuration experienced during this study did not appear to result in significant changes in performance.
- (14) The exponential and equilibrium methods of clean water data analysis provided nearly identical results under the conditions of this study. Based on 100 test analyses, the average ratio of the SWAE obtained by the exponential method to the SWAE obtained by the equilibrium method was 0.995, with a standard deviation in the ratio of 0.0169.

Clean water testing can only show the performance trends of an aeration device and cannot be used alone to determine performance under process water conditions. For this reason, it is recommended that further testing be conducted in process water to establish characteristic alpha factors for the devices evaluated during this study.

SECTION 3

EQUIPMENT AND TESTING PROCEDURES

TEST FACILITY

The test facility used for all tests was an all steel rectangular aeration tank (Figure 1) located at the LACSD Joint Water Pollution Control Plant. The dimensions of this tank are 6.1 m X 6.1 m X 7.6 m (20 ft X 20 ft X 25 ft) side water depth (SWD). Prior to the start of this project, the tank was steam cleaned and all exposed metal surfaces were coated with coal tar epoxy. Potable water was used in all clean water tests conducted in this study. The majority of this water was supplied by the Los Angeles Metropolitan Water District and was a blend of roughly 45% northern California water and 55% Colorado River water. Additional amounts of local well water also contributed to the delivered water supply. Average characteristics of the supplied water were: total dissolved solids (TDS) level of 500 mg/L, pH of 8.25, hardness of 225 mg/L as CaCO₃, and turbidity of less than 0.1 turbidity units.^{1/} Additional laboratory measurements (those made during the testing) are presented in Table 1. The temperature range of water used in the study was 16.2 to 25.2°C (61.2 to 77.4°F).

The air delivery system used for this project consisted of a Roots Model RAS-60 rotary positive blower driven by a 56-kW (75-hp) electric motor. System air was filtered by an Air Maze DA dry type filter. A 1-m³ (35-ft³) pulsation dampening tank was also included in the system between the blower and the airflow measurement elements. System air rate was adjusted by bleeding off excess air at the blower.

TEST PROCEDURES

The tests were of the non-steady state nature using sodium sulfite to deoxygenate the clean water and cobalt chloride as a catalyst. Samples were withdrawn from the tank and collected in BOD bottles and chemically fixed for later D.O. measurement by the Iodometric (Winkler) method. In addition, a sample stream was pumped from the tank for continuous D.O. monitoring with an in-line probe. The official results of this study, however, were based solely on D.O. measurements using the Winkler technique.^{2/} Details of each aspect of the test procedure follow.

Airflow Measurements

Airflow measurements were made with two different primary flow elements: an orifice plate and an Annubar (a velocity head measuring device

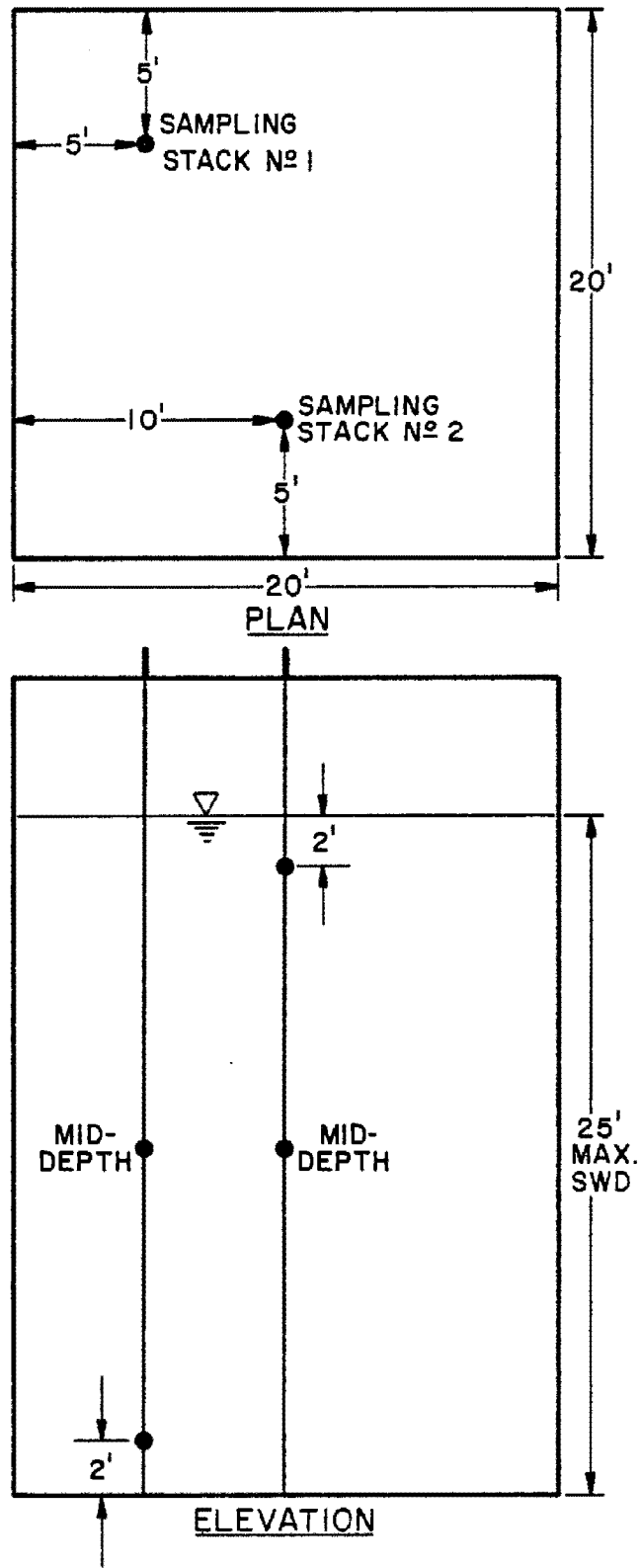


Figure 1. Clean water testing facility.

TABLE 1. SUMMARY OF WATER QUALITY CHARACTERISTICS

Sample Date	Manufacturer	Water Batch Number	Pre-test Sample	Post-test Sample	Assumed # Na ₂ SO ₃ Conc. (mg/L)	Laboratory Results							
						Alkalinity (mg/L CaCO ₃)	pH	Total Hardness (mg/L CaCO ₃)	Total SO ₄ (mg/L SO ₄)	T.D.S. (mg/L)	Co (mg/L)	Fe (mg/L)	Mn (mg/L)
02/15/78	Norton	1	✓		0								
03/23/78	Norton	1		✓	142								
03/24/78	Norton	2	✓		0	124	8.00	252		624	0.01		
04/11/78	Norton	2		✓	162	149	8.10	255	---	778	0.10	---	---
04/12/78	Norton	3	✓		0	248	8.05	226	---	620	0.05	---	---
05/06/78	Norton	3		✓	944	132	8.35	219	810	1536	0.10	0.05	0.01
05/08/78	Norton	4	✓		0	139	7.98	181	69	414	<0.01	0.05	0.01
05/18/78	Norton	4		✓	565	111	8.31	179	557	1025	0.11	0.09	0.01
05/25/78	Kenics	1	✓		0	87	7.11	164	109	303	0.11	0.07	0.01
06/02/78	Kenics	1		✓	956	98	8.19	161	778	1417	0.10	0.08	0.02
06/08/78	Kenics	2	✓		0	132	8.10	189	109	428	<0.01	0.02	0.01
06/14/78	Kenics	2		✓	1127	137	8.50	182	1090	1872	0.12	0.14	0.02
06/15/78	Kenics	3	✓		0	95	7.50	181	141	446	0.01	0.07	0.01
06/26/78	Kenics	3		✓	749	115	8.38	187	683	1317	0.10	0.15	0.03
06/28/78	Kenics	4	✓		0								
06/29/78	Kenics	4		✓	302	91	6.10	208	620	1173	0.10	0.09	<0.01
07/01/78	Pentech	1	✓		0	94	8.31	214	182	528	0.03	0.16	<0.01
07/08/78	Pentech	1		✓	1031	96	8.39	214	967	1692	0.09	0.21	0.01
07/10/78	Pentech	2	✓		0	92	6.20	210	172	498	<0.01	0.09	<0.01
07/17/78	Pentech	2		✓	441								
07/17/78	Pentech	3	✓		0								
07/29/78	Pentech	3		✓	734	86	7.90	216	746	1372	0.09	0.14	0.01
07/31/78	Pentech	4	✓		0	81	8.03	193	305	831	0.10	0.14	0.01
08/02/78	Pentech	4		✓	299								
08/03/78	Pentech	5	✓		0	125	7.87	198	176	592	0.11	0.08	<0.01
08/16/78	Pentech	5		✓	517								
08/21/78	FMC	1	✓		0	93	8.02	211	152	476	0.02	0.08	<0.01
08/23/78	FMC	1		✓	1132	91	7.91	218	965	1721	0.11	0.08	<0.01

* Calculated values based on actual sodium sulfite additions.

(continued)

TABLE 1. SUMMARY OF WATER QUALITY CHARACTERISTICS (continued)

Sample Date	Manufacturer	Water Batch Number	Pre-test Sample	Post-test Sample	Assumed Na ₂ SO ₃ * Conc. (mg/L)	Laboratory Results							
						Alkalinity (mg/L CaCO ₃)	pH	Total Hardness (mg/L CaCO ₃)	Total SO ₄ (mg/L SO ₄)	T.D.S. (mg/L)	Co (mg/L)	Fe (mg/L)	Mn (mg/L)
08/29/78	FMC	2	✓		0								
08/31/78	FMC	2		✓	752	93	8.21	216	681	1280	0.11	0.08	<0.01
09/02/78	FMC	3	✓		0	92	7.98	213	149	490	0.03	0.18	0.01
09/29/78	FMC	3		✓	321								
10/13/78	FMC	4	✓		0	166	7.15	116	2.3	384	0.02	0.03	0.01
10/14/78	FMC	4		✓	323								
10/19/78	FMC	5	✓		0	190	8.55	127	4	290	0.01	0.02	0.02
10/20/78	FMC	5		✓	319								
10/23/78	FMC	6	✓		0	141	8.45	190	105	508	0.02	0.01	0.02
10/26/78	FMC	6		✓	944	144	8.70	186	719	1327	0.07	0.06	0.02
10/30/78	FMC	7	✓		0	192	8.29	118	132	468	0.07	0.06	0.02
10/31/78	FMC	7		✓	612	193	8.60	112	487	926	0.08	0.04	0.02
02/08/79	FMC	8	✓		0	181	8.07	104	1	332	<0.01	0.02	<0.01
02/10/79	FMC	8		✓	970								
11/06/78	Sanitaire	1	✓		0	192	8.50	117	2	286	0.01	0.06	0.01
11/07/78	Sanitaire	1		✓	926	195	8.70	107	721	1268	0.12	0.08	0.02
11/08/78	Sanitaire	2	✓		0	192	8.22	107	4	225	0.01	0.04	0.02
11/15/78	Sanitaire	2		✓	664	193	8.48	119	612	1120	0.12	0.10	0.02
12/05/78	Bauer	1	✓		0	191	8.18	106	107	480	0.02	0.08	0.02
12/06/78	Bauer	1		✓	1017	195	8.60	109	846	1506	0.14	0.24	0.02
12/07/78	Bauer	2	✓		0	192	8.21	104	3	318	0.02	0.04	0.02
12/09/78	Bauer	2		✓	805								
12/15/78	Bauer	3	✓		0								
12/16/78	Bauer	3		✓	292								
01/08/79	Envirex	1	✓		0	148	7.71	137	66	376	0.02	0.10	0.02
01/09/79	Envirex	1		✓	931	197	8.43	113	847	1492	0.14	0.06	0.02
01/10/79	Envirex	2	✓		0	191	8.18	112	70	405	0.02	0.08	0.02
01/20/79	Envirex	2		✓	886	164	8.50	106	613	1149	0.06	0.02	<0.01

* Calculated values based on actual sodium sulfite additions.

(continued)

made by Ellison Instrument Company). Dual flow measurements were taken to insure greater accuracy. Furthermore, to provide accuracy over the wide range of flow rates encountered, two different sized air lines were used, both with appropriately sized orifice plates and Annubar equipment. A third and smaller air line was used for two tests on the jet aeration system; this line was equipped with an Annubar.

The airflow measurement system was designed by staff of the Sanitation Districts according to References 3/, 4/, and 5/. Drawings of the orifice plate and Annubar equipment used are given in Figures 2, 3, and 4. The pertinent flow equations are shown in Appendix A. It is beyond the scope of this report to explain the equations in any detail. It is sufficient to say that the equations contain somewhat complicated terms, many of which are correction factors and refinements and are often of only minor significance. These factors were accounted for in the analysis primarily because the flow calculations were performed using a hand-held programmable calculator.

The differential pressure from the primary elements was measured with manometers. Air line temperature and pressure, ambient temperature and pressure, and relative humidity were recorded. The airflow readings were converted to standard conditions of 20°C (68°F), 101.325 kPa (14.70 psia), and 36% relative humidity.

Dissoved Oxygen Sample Collection

Sample Locations--

Water samples to be analyzed by the Winkler method^{2/} were collected from four locations in the aeration tank (Figure 1). There were two vertical sampling "stacks", each with two sampling locations. Schematically, the 6.1-m X 6.1-m (20-ft X 20-ft) tank surface was divided into four quadrants, labeled 1 to 4 in a clockwise direction. The first stack was located in the middle of quadrant 1; the second stack was located between quadrants 3 and 4, halfway between the center of the tank and the aeration tank wall. Submersible sample pumps were installed in the first stack at mid-depth and at 0.6 m (2.0 ft) off the bottom of the tank; the second stack had submersible pumps installed at mid-depth and 0.6 m (2.0 ft) below the surface of the tank. The heights of the pumps were adjustable for proper placement at the various water depths. The sample pump for the in-line probe was installed near mid-depth on the first sampling stack.

Anti-Air Entrainment Device--

An anti-air entrainment device was installed on each pump to avoid the collection of air bubbles in the samples. These devices consisted of a 152-mm (6.0-in.) length of 38-mm (1.5-in.) diameter pipe mounted pointing vertically upward on the suction side of the pump. Theoretically, the velocity in the suction line was less than the rise velocity of the air bubbles in the tank to help avoid the collection of bubbles in the water samples.

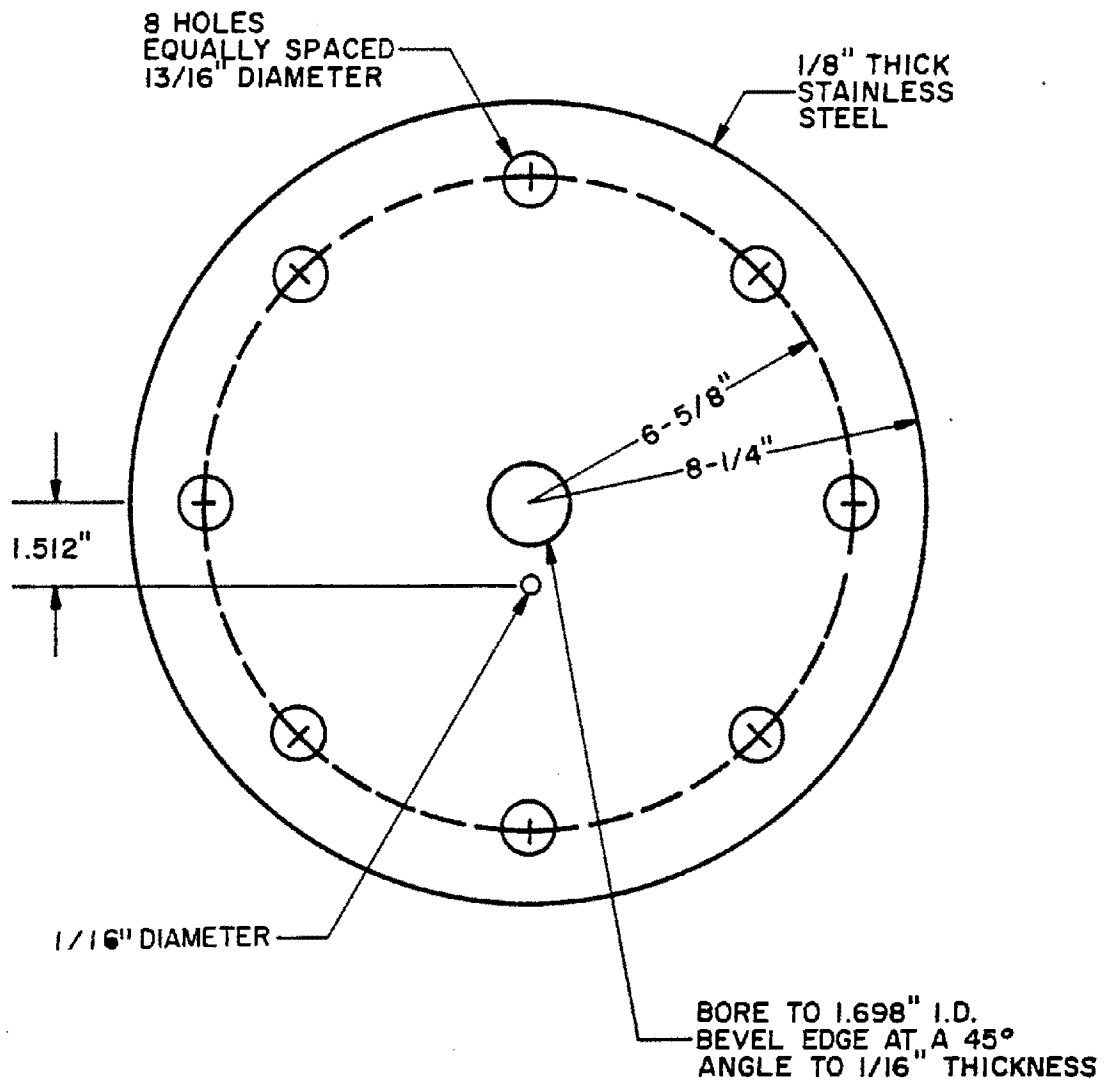


Figure 2. Orifice plate for 3-in. air line.

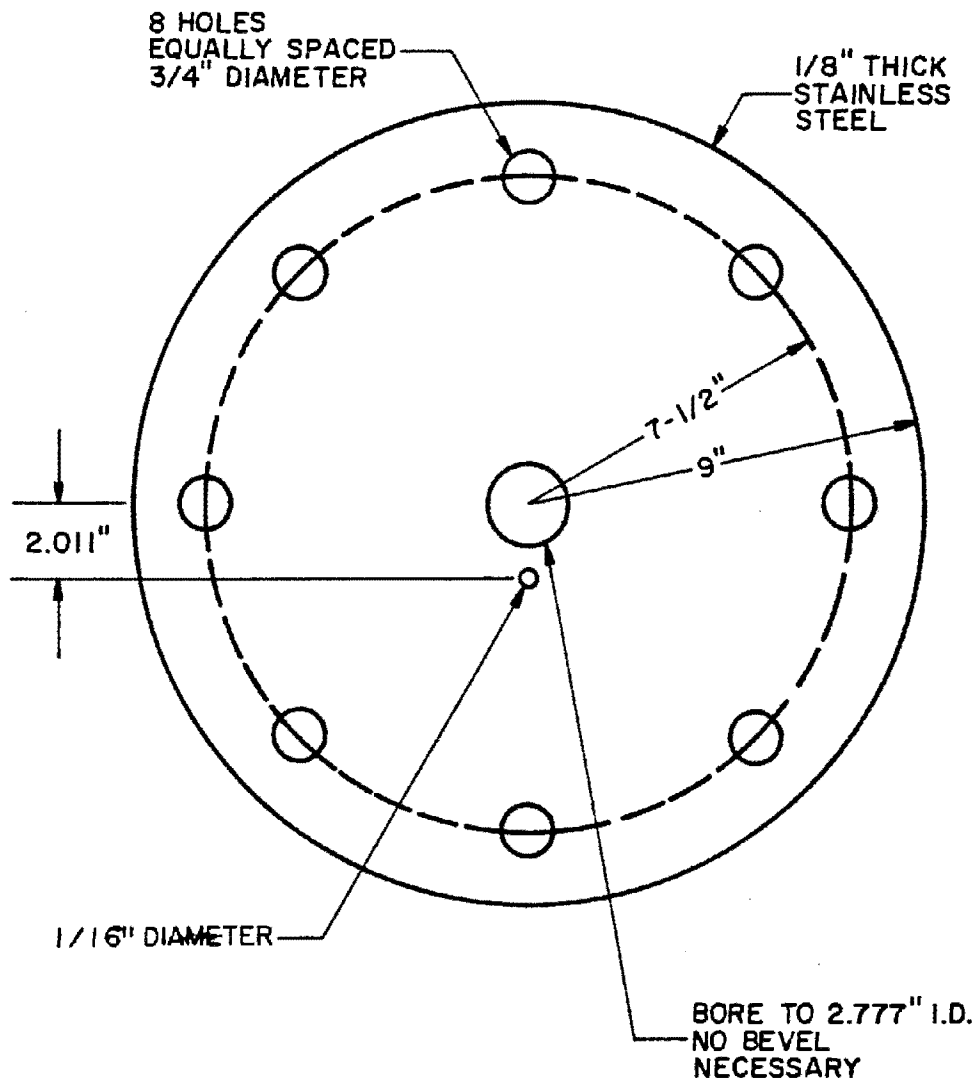
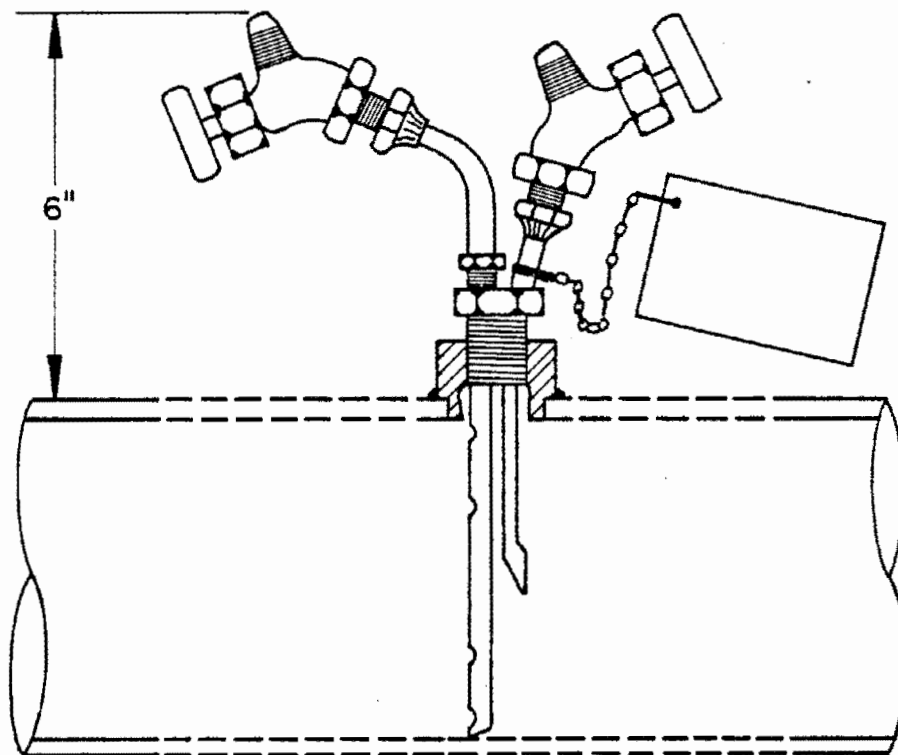


Figure 3. Orifice plate for 4-in. air line.



3 Different Annubars were used for the Aeration Equipment Evaluation (3/4", 2", and 3" pipe sizes)

(Courtesy of Ellison Instrument Co.)

Figure 4. Annubar flow measurement device.

Sampling Devices--

D.O. was measured by two methods. These two methods consisted of 1) an in-line mounted D.O. probe/analyzer and 2) sample collection and analysis. In both cases, samples were pumped through plastic tubing by submersible pumps from the aeration tank to the sampling station. At the sampling station, the water was discharged through sampling devices into a steel drum and pumped back into the aeration tank. The D.O. probe/analyzer was mounted in the line just upstream of the discharge nozzle. This apparatus allowed instantaneous measurement of aeration tank D.O. concentrations. The other four pumped samples were used for sample collection in "BOD"-type bottles. Copper discharge nozzles for the four pumped samples were mounted on a plywood board to enable one operator to control the four samples simultaneously. Each nozzle consisted of a 9.5-mm (3/8-in.) I.D. copper tube and a valve for flow regulation. These nozzles were mounted so they fitted easily into four BOD bottles when fully inserted, and there was room at the neck of the BOD bottles for the displaced air to escape during filling.

Sample Collection Procedure--

An attempt was made to collect approximately eight samples for the Winkler analysis between 20% and 80% saturation, although additional samples were taken below 20% and above 80% saturation. Time was monitored with a stopwatch. Sample water was pumped continuously to purge the BOD bottles until the desired time "t", after which the sampling device was withdrawn and the BOD bottles stoppered. If necessary, 1 or 2 sec were allowed before stoppering the BOD bottles to allow any small air bubbles to rise to the surface and escape. The overflow water from the BOD bottles was caught in a 208-L (55-gal) tank and was continuously pumped back to the aeration tank.

Sampling Rates--

The submersible pumps for the Winkler samples were sized so a BOD bottle could be filled three to five times in 15 sec (0.06 to 0.10 L/sec = 1.0 to 1.6 gpm). This was done to insure adequate displacement of the water in the BOD bottle and to minimize the detention time in the sample lines (approximately 10 sec). All pump rates and sample line lengths were equal so that the samples from the various locations would represent the same time "t". Furthermore, the velocity of the water into the BOD bottles was kept below 1.5 m/sec (5.0 ft/sec) to avoid air entrainment upon insertion or withdrawal of the copper nozzles in the bottles.

The sampling rate for the in-line probe was approximately 0.28 L/sec (4.5 gpm). This rate was chosen to minimize fluid pressure on the probe while maintaining an adequate velocity of water past the probe tip.

Dissolved Oxygen Measurements

The official D.O. measurements were made by the Winkler method on captured samples. The azide modification of the Winkler titration method was used with alkali-iodide-azide reagent #2 as stated in Standard Methods.^{2/} This reagent was selected because it reportedly reduced the volatility of iodine and thus provided a more accurate D.O. measurement. Samples were set up immediately after capture and titrated within 1.5 hr. The thiosulfate used for the titrations was standardized once each day. Two burets were available to titrate the Winkler samples in an effort to expedite the procedure.

In the study, it was recognized that Winkler titrations may be affected by agents that either oxidize iodide to iodine or reduce iodine to iodide. Two steps were taken to insure that the occurrence of such interferences would not take place unknowingly. The first was to measure the D.O. saturation level before and after each test by both the Winkler (iodometric) method and the electrometric method (using a D.O. probe/analyzer). The second step was the daily evaluation of interferences using a blank. In this method, the iodine present in a sample of tank water (with iodide salt added) was measured to detect any positive interference (oxidation of iodide to iodine). No interferences were detected during the study.

The in-line D.O. probe was calibrated by the air calibration method. A BOD bottle was filled approximately 1/4 to 1/3 full with tap water. Time was allowed for the contents of the bottle to equilibrate with the ambient temperature. The bottle was stoppered and shaken vigorously to saturate the water with oxygen. The stopper was then removed, allowing fresh air to enter the bottle. The bottle was restoppered and shaken vigorously again, this time to saturate air with water vapor. The probe was then inserted into the bottle. Time was allowed for the probe thermistor to equilibrate with the air temperature in the bottle before measuring the temperature and setting the corresponding D.O. saturation.^{6/} Finally, the probe was adjusted for the salinity correction of the tank water. Salinity was assumed to be the initial water batch TDS plus TDS addition as sulfate. This adjustment was a minor correction.

The D.O. measurements from the D.O. probe were recorded with a strip chart recorder. Care was taken to check the recorder's calibration and zero indication.

Aerator Power Determinations

In addition to power for an air supply, aeration equipment may also require power for a mixer or a pump. Of the eight systems evaluated in this study, only the jet aeration system required pump power in addition to the power for the air supply. The following power determination discussion is divided into two subsections, Air Power and Pump Power.

Air Power--

Due to the fact that the test facility blowers operate at a fixed speed, it was necessary to "waste" air to obtain the desired airflow rates. This means that no direct measurement of air horsepower was possible. Air power was calculated by the adiabatic compression equation using measured airflow, measured diffuser static head, and assumed suction and pressure losses.

The following relationship was used to determine air power. Pressure losses on the suction side of the blower were estimated by the relationship:

$$P_a = 0.005729 (\gamma_{\text{air}}) (Q) (T_i + 460) \left[\left(\frac{p_2}{p_1} \right)^{0.283} - 1 \right] \quad (1)$$

in which:

P_a = air power, hp

γ_{air} = specific weight of air at the temperature, pressure, and relative humidity for which Q is reported, lb/ft³

Q = airflow rate, cfm

T_i = blower inlet temperature, °F

p_1 = blower inlet pressure, psia

p_2 = discharge pressure, psia

Air power is that power associated with the blower portion of the aeration system. Reference can be made to nominal, delivered, brake, or wire power for the air blower. These various powers are described in the following paragraphs.

Air nominal power--The aeration equipment evaluation was based on testing at one of two power density ranges, either 13.2, 26.3, and 39.5 W/m³ (0.5, 1.0, and 1.5 hp/1000 ft³) or 7.9, 13.2, and 26.3 W/m³ (0.3, 0.5, and 1.0 hp/1000 ft³). These power density ranges were based on nominal and not delivered, brake, or wire power. Nominal power, which does not account for certain system-specific headlosses, was the most appropriate parameter on which to control power in the study because it more closely approximated the power delivered to the basin. Air nominal power is calculated using the adiabatic compression equation. In the nominal power determination, blower inlet pressure is assumed to be 100.6 kPa (14.60 psia). Also assumed in the calculations is that the discharge pressure is the diffuser submergence. The following relationship is used to determine air nominal power:

$$P_{\text{ans}} = 0.227 Q \left[\left(\frac{p_{\text{ao}} + p_{\text{sh}} (.491)}{p_i} \right)^{0.283} - 1 \right] \quad (2)$$

in which:

P_{ans} = air nominal power at standard conditions of 20°C (68°F), 101.3 kPa (14.70 psia), 36% relative humidity, and a blower inlet pressure of 100.6 kPa (14.60 psia), hp

P_{ao} = barometric pressure at standard conditions, 101.3 kPa (14.70 psia), psia

P_{sh} = aerator static head, in. of mercury

P_i = assumed blower inlet pressure, 100.6 kPa (14.60 psia), psia

Air delivered power--Air delivered power is considered to be the theoretical adiabatic power required at the blower to supply air through a diffuser system operating under a given static head. In determining the air delivered power, various headlosses are taken into account that were previously ignored in the evaluation of air nominal power. These headlosses include estimated aerator headloss, estimated system piping headloss, and estimated blower suction headloss. Aeration headloss values included here are those values that were actually measured in the study. Aeration system piping headloss and the blower suction headloss were both estimated using relationships presented below.

In this study, air delivered power is reported in terms of standard conditions of 20°C (68°F), 101.3 kPa (14.70 psia), and 36% relative humidity. The following equation is used for determining the air delivered power values:

$$P_{ads} = 0.227 Q_{test} \left[\left(\frac{P_2}{P_1} \right)^{0.283} - 1 \right] \quad (3)$$

in which:

Q_{test} = average airflow rate associated with a test, scfm

P_{ads} = air delivered power at standard conditions of 20°C (68°F), 101.3 kPa (14.70 psia), and 36% relative humidity, hp

The only question remaining in this equation is the values to use for p_1 and p_2 . The blower inlet pressure, p_1 , is determined according to the following equation:

$$P_1 = P_{ao} - h_{Ls} \quad (4)$$

in which:

h_{Ls} = estimated suction piping headloss, psi.

This estimated headloss value is determined using the following relationship:

$$h_{Ls} = 0.1 \left(\frac{Q_{test}}{Q_{max}} \right)^2 \quad (5)$$

in which:

Q_{max} = maximum test airflow rate for a system at each water depth, scfm

The parameter h_{Ls} was determined for each test. At each depth, a manufacturer was assigned a 0.7-kPa (0.1-psig) suction headloss at the maximum airflow rate. The values of the suction headlosses at the lower power levels were obtained according to a square root relationship with airflow rate. This was done to simulate losses that resulted from a diurnal variation in airflow.

The blower discharge pressure, p_2 , is determined according to the following equation:

$$p_2 = p_{a0} + 0.491 p_{sh} + 0.0361 h_L + h_{Ld} \quad (6)$$

in which:

p_{sh} = aerator static head, in. of mercury

h_L = measured diffuser headloss, in. of water

h_{Ld} = estimated aeration system piping headloss, psig

The estimated headloss value is determined using the following relationship:

$$h_{Ld} = 1.0 \left(\frac{Q_{test}}{Q_{max}} \right)^2 \quad (7)$$

Actual field measurements of static head and diffuser headloss are used in Equation 6 above.

The discharge piping headloss, h_{Ld} , is determined in a manner similar to the suction piping headloss. Each aeration system is assigned a 6.9-kPa (1.0-psig) line loss corresponding to the maximum airflow at each depth.

The values of the discharge piping headloss at the lower power levels are obtained according to a square root relationship with airflow rate. As with the suction piping headloss, this is done to simulate losses that result from a diurnal variation in airflow.

Air brake power--Air brake power is usually considered to be the power required at the output shaft of the blower motor (Figure 5). Standard air brake power is determined from standard air delivered power by the following expression:

$$P_{abs} = \frac{P_{ads}}{e_b \cdot e_d} \quad (8)$$

in which:

P_{abs} = air brake power at standard conditions of 20°C (68°F)
101.3 kPa (14.70 psia), and 36% relative humidity, hp

e_b = blower efficiency, decimal %

e_d = drive or coupling efficiency, decimal %

For the purposes of this study, the blower efficiency assumed is 0.70 and the drive efficiency assumed is 0.95. Therefore:

$$P_{abs} = P_{ads} / [(0.70)(0.95)] = P_{ads} / 0.665$$

Air wire power--Air wire power is the electrical power required to run the blower motor (Figure 5). Standard air wire power is determined from standard air brake power using the following equation:

$$P_{aws} = P_{abs} / e_m \quad (9)$$

in which:

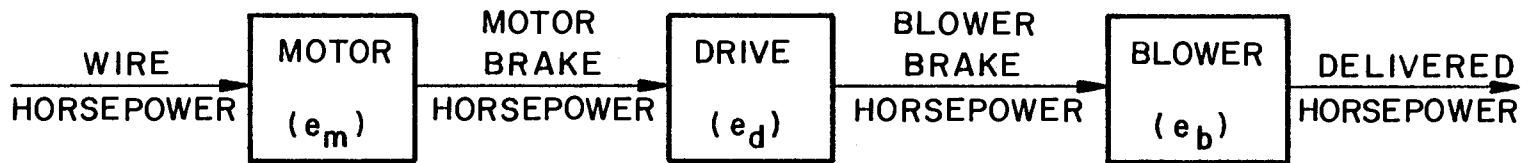
P_{aws} = air wire power at standard conditions of 20°C (68°F),
101.3 kPa (14.70 psia), and 36% relative humidity, hp

e_m = motor efficiency, decimal %

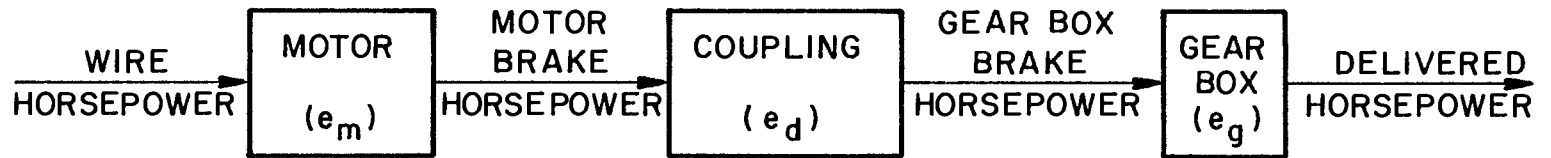
For the purposes of this study, the motor efficiency assumed is 0.92. Therefore:

$$P_{aws} = P_{abs} / 0.92 = P_{ads} / [(0.665)(0.92)] = P_{ads} / 0.612$$

GAS HORSEPOWER



TURBINE HORSEPOWER



NOTE: EFFICIENCIES ARE IN PARENTHESES

Figure 5. Horsepower schematics.

Pump Power--

Pump power is the power associated with the pump portion of an aeration system. In this study, only one system, the jet aeration system, used a pump. Because the jet aeration system employed a pump in addition to a blower, a suitable method for determining pump horsepower had to be developed.

Pump delivered power--To determine pump delivered power, the following procedure was used. During each test, determinations were made of the pump total dynamic head. This information was then used with the manufacturer's pump performance curves to determine pump flow rate. Using this flow rate, the following equation was used to determine pump power:

$$P_{pd} = \frac{Q_p (\gamma_{\text{water}}) (\text{TDH})}{550} \quad (10)$$

in which:

P_{pd} = pump delivered power, hp

γ_{water} = specific weight of water, 62.4 lb/ft³

TDH = total dynamic head, ft of water

Q_p = pump discharge, cfs

Pump brake power--The pump brake power is considered to be the power required at the output shaft of the pump motor (Figure 5). The standard pump brake power is determined from the standard pump delivered power by the following expression:

$$P_{pb} = P_{pd} / (e_p)(e_d) \quad (11)$$

in which:

P_{pb} = pump brake power, hp

e_p = pump efficiency, decimal %

e_d = drive or coupling efficiency, decimal %

For the purposes of this study, the pump efficiency assumed is 0.805. This is an average of typical efficiencies for full-scale submersible and dry pit pumps. The drive efficiency assumed is 0.95. Thus:

$$P_{pb} = P_{pd}/[(0.805)(0.95)] = P_{pd}/0.765$$

Pump wire power--The pump wire power is considered to be the electrical power required to run the pump motor (Figure 5). The standard pump wire power is determined from the standard pump brake power by the following relationship:

$$P_{pw} = P_{pb}/e_m \quad (12)$$

in which:

P_{pw} = pump wire power, hp

e_m = motor efficiency, decimal %

For the purposes of this study, the motor efficiency assumed is 0.92. Therefore:

$$P_{pw} = P_{pb}/0.92 = P_{pd}/[(0.92)(0.765)] = P_{pd}/0.704$$

Direct watt meter readings were also recorded during the jet aerator testing. They were not used in determining the results presented in this report because of problems associated with readability and assumed pump efficiencies. Additional information on the estimation of pump power can be found in Section 7.

For the jet aeration system, the total power requirements are the sum of the air and pump horsepowers.

Power Density Calculations

Power density is the power input per unit volume of aeration tank liquid. Power density is a term that makes the comparison of test results at different volumes possible. It was used in this study for both test control and comparison of results for the tests conducted at various aeration tank water depths. In general, power density is calculated according to the following equation:

$$PD = P(1000)/V_i \quad (13)$$

in which:

PD = power density, hp/1000 ft³

P = power, hp

V_i = inflated water volume, ft³

In addition to SWD, nominal power density (from Equation 13 on a nominal power basis) was chosen as a control parameter. In this study, the aeration equipment manufacturers were given a choice of two nominal power

density ranges: 7.9, 13.2, and 26.3 W/m³ (0.3, 0.5, and 1.0 hp/1000 ft³) and 13.2, 26.3, and 39.5 W/m³ (0.5, 1.0, and 1.5 hp/1000 ft³). Adjustment of the power density was accomplished by increasing or decreasing airflow to the aeration tank. When the specified nominal power density was set, the test was run. As in the equation above, standard nominal power density is calculated as follows:

$$PD_{ns} = P_{ns}(1000)/V_i \quad (14)$$

in which:

PD_{ns} = nominal power density at standard conditions, hp/1000 ft³

P_{ns} = total nominal power at standard conditions of 20°C (68°F), 101.3 kPa (14.70 psia), 36% relative humidity, and a blower inlet pressure of 100.6 kPa (14.60 psia), hp

Nominal power density is a term well suited as a controlling parameter in the study. However, for purposes of taking into account additional effects representative of actual system operation, the term "delivered power density" was developed. This value takes into consideration additional power loss factors due to blower suction loss, air piping headloss, and aeration device headloss. While headlosses for the aeration devices are actual measurements, the piping headloss and blower suction loss are estimated values (Equations 5 and 7). The effects of diurnal variation are, therefore, more accurately reflected in the delivered power density expression. Delivered power density is defined to be the delivered power divided by the inflated liquid volume in the aeration basin. Determination of delivered power density is made using the following equation:

$$PD_{ds} = P_{ds}(1000)/V_i \quad (15)$$

in which:

PD_{ds} = delivered power density at standard conditions, hp/1000 ft³

P_{ds} = total delivered power at standard conditions of 20°C (68°F), 101.3 kPa (14.70 psia), 36% relative humidity, and a blower inlet pressure of 100.6 kPa (14.60 psia), hp

Headloss Measurements

Aerator headloss was determined by subtracting aerator pressure from the static head using a differential water-filled manometer. The static head was determined with a bubbler system. The bubbler system consisted of a small air pump and a discharge pipe. The air pump provided a constant supply of air to the pipe that discharged at the aerator air release point. The pipe was large in diameter and the airflow rate low so that there were no pressure losses in the piping. A pressure tap was made in the pipe so

that this "bubbler pressure" could be measured. The pressure measured with the bubbler device is also referred to as the static head. A second pressure tap was installed in the center of the air distribution piping for the measurement of aerator pressure. A manometer was used to measure the headloss (the difference between the diffuser pressure and the static head). Additional measurements included aerator pressure, aerator air temperature, and water temperature.

If the air supply had been shut off, when air was resupplied to the aeration system, the aeration system was first blown out at a high air rate for at least 15 min. After that, a minimum of 30 min at the proper air rate was maintained before the headloss readings were taken.

Deoxygenation Procedure

Cobalt chloride was used as a catalyst in the deoxygenation reactions. It was added once at a dosage of 0.1 mg/L as cobalt ion to each batch of test water. The chemical crystals were added to the mix tank and allowed to dissolve for at least 30 min prior to discharging the solution into the aeration tank. After cobalt addition to the aeration tank, at least another 30 min was allowed prior to the start of the first test.

Anhydrous sodium sulfite was used to deoxygenate the water prior to the start of each test. The amount of sodium sulfite added was approximately 1.5 times the stoichiometric requirement for oxygen removal. The salt was dissolved in approximately 379 L (100 gal) of water prior to the start of each run. The brine addition to the tank was accomplished within a 2 min period. The solution was pumped equally into the four tank quadrants through a 4-hose addition system. Distribution was, therefore, as even and rapid as possible. The chemical mix tank and delivery hoses were immediately flushed with tap water to wash all residual sodium sulfite into the aeration tank.

A decision was made to discard each water batch after the accumulated sodium sulfite concentration had reached 1000 mg/L. At that time, samples were taken for laboratory analyses to determine the chemical properties of the "post-test" water. Analyses were also conducted prior to using a water batch to determine the "pre-test" condition. These measurements included pH, alkalinity, hardness, sulfate, total dissolved solids, cobalt, iron, and manganese. A presentation of these results was given previously in Table 1.

FIELD EXPERIMENT PROCEDURE

Each field experiment was conducted according to the rigid step-by-step procedure itemized below.

1. Collect a water sample for laboratory analysis prior to the first test on a batch of water.
2. Prior to a given test, run a high airflow rate through the aeration system for approximately 15 min.

3. Set the aeration tank water level at the approximate depth desired.
4. Set the airflow rate to the approximate power level under investigation.
5. Adjust the water level to the desired depth.
6. Measure the aeration tank static head with a bubbler device.
7. Calculate the exact airflow rate required for the test.
8. Set the airflow rate to the desired value and maintain these conditions prior to the start of the test.
9. Add the cobalt chloride (if required) in solution form to the aeration tank water.
10. Mix the required amount of dry sodium sulfite with water in the mix tank.
11. Position the sampling pumps at the proper elevations.
12. Adjust the chemical distribution hoses so that they discharge just above the surface of the water.
13. Adjust the BOD bottle fill rates so the bottles are filled in 3 to 5 sec (0.06 to 0.10 L/sec = 1 to 1.6 gpm). Also adjust the in-line probe sampler flow rate so that it is approximately 0.28 L/sec (4.5 gpm).
14. Prior to the first official test on a new water batch, deoxygenate the water with the sodium sulfite solution and reaerate it back to saturation. Prepare another batch of sodium sulfite solution for the official test.
15. Determine the normality of the sodium thiosulfate for the (Winkler) D.O. measurements.
16. Check the condition of the in-line D.O. probe membrane. Calibrate the probe and record the pre-test D.O. reading.
17. Check the condition of the D.O. probe strip chart recorder.
18. Collect a pre-test equilibrium sample from each sample location.
19. Compare the pre-test equilibrium values from all sources.
20. After a minimum of 30 min and just prior to the start of the test, record

- a. ambient temperature, barometric pressure, and relative humidity,
 - b. flow meter differential pressure (both Annubar and orifice plate), line temperature, line pressure, Annubar stagnation pressure, and manometer board temperature,
 - c. blower differential and discharge pressure,
 - d. air temperature at the aerator,
 - e. aerator headloss,
 - f. aeration tank water temperature,
 - g. aeration tank water level,
 - h. aerator static head, and
 - i. pump power measurements (pump discharge pressure).
21. Turn on the D.O. strip chart recorder, and set the D.O. probe to the proper scale.
 22. Add the sodium sulfite solution, and flush the chemical lines with tap water.
 23. Monitor the D.O. level in the tank with the in-line probe. Make sure that the tank D.O. remains at zero for a minimum of 2 min (the estimated time required for complete mixing of sulfite to occur).
 24. Start the test when the D.O. level begins to rise (indicated by the in-line probe).
 25. Collect samples at the preselected time intervals.
 26. Add the first two Winkler reagents (manganese sulfate and alkali-iodide-azide) as soon as possible. Shake the samples, allow them to settle half-way down in the bottle, and then shake again.
 27. Take a second set of readings at the end of the run (the same readings as those shown in Step 20 above).
 28. Acidify, shake, and titrate all the Winkler samples. This step starts as soon as possible.
 29. Determine if there are chemical interferences in the Winkler method

30. After there has been no increase in the recorded D.O. for a period of at least 15 min, collect a set of equilibrium samples.
31. Perform a Winkler analysis on the final samples.
32. Read and record the D.O. probe reading on the aeration tank water. Compare this with the recorder reading. Check the recorder zero.
33. Compare the equilibrium results from all sources.
34. Photograph the aeration system in operation.
35. Shut off the blower and accessory aeration equipment (i.e., jet system pump).
36. Measure the non-aerated tank water level.
37. After the last test run for a given water batch, collect a water sample for laboratory analysis.

SECTION 4

OXYGEN TRANSFER DATA ANALYSIS

FIELD MEASUREMENTS

The majority of the field measurements were collected both before and after a test, primarily to insure that test conditions remained steady and sometimes to determine an average value of the parameter. An "arithmetic" average was used in this study for a particular variable if it was felt that the variation observed was random; a "time" or "weighted" average was used if it was felt that the variation observed was non-random. Water level measurement is an example of a parameter that was arithmetically averaged during a test. Airflow measurement is an example of a parameter that was time averaged during a test.

Time averages are calculated assuming that the measured parameter varies in a linear fashion from the start to the end of the run. The value of the variable at any time t is then calculated according to a linear interpolation. For the purposes of this study, t is taken to be the time midway between the start and finish of the water sample collection. The field measurements taken during each test along with other pertinent information associated with the measurements are summarized in Table 2.

Several measurements deserve special mention. Winkler D.O. measurements were obtained on samples from four locations. Each location was analyzed separately; no averaging of the four D.O. data values at a given time t was done. The data between 20 and 90% D.O. saturation were used in the final analysis with both analysis methods. Note that the data truncation used in the final analysis was different from that applied in the initial evaluation of test data (20 to 80% D.O. saturation). This change was made to accommodate the evaluation of data by an analysis method that requires D.O. data near saturation. Two different flow measurement elements were used to measure airflow rates. Airflow measurements were taken with these elements both before and after each run to insure accuracy. One of the devices was an orifice plate; the other was an averaging pitot tube called an Annubar. The time-average airflow rate was first determined for each flow meter. An arithmetic average of these two time-averaged airflow rates was then used in the oxygen transfer calculations.

BASIC THEORY

The transfer of a gas into a liquid can be described by the two-film

TABLE 2. FIELD MEASUREMENTS

Measurement	Symbol	Units	Frequency 1 of Measurement	Measurement Devices Used	Type 2 of Average
water depth (inflated)	z_i	ft	B/A	1	AR
water depth (deflated)	z_d	ft	A		none
air flow	Q	scfm	B/A	2	T (each meter) AR (overall)
BOD bottle fill rate	--	mL/sec	once/depth-day	1	none
in-line probe sample flow rate	--	gpm	once/depth-day	1	none
D.O. concentration	C	mg/L	continuous	2-3	none
time	t	sec	continuous	1	none
aeration tank water temperature	T_w	°C	B/A	2	T (each probe) AR (overall)
flow meter air temperature	T_f	°F	B/A	1	none
diffuser air temperature	T_d	°F	B/A	1	T
manometer board temperature	T_{am}	°F	B/A	1	none
ambient air temperature	T_a	°F	B/A	1	T
orifice plate flowing gas pressure	p_{f0}	in. Hg	B/A	1	none

TABLE 2. (continued)

Measurement	Symbol	Units	Frequency ¹ of Measurement	Measurement Devices Used	Type ² of Average
annubar flowing gas pressure	p_{fa}	in. Hg	B/A	1	none
annubar stagnation pressure	p_t	in. Hg	B/A	1	none
orifice plate differential pressure	h_o	in. H ₂ O	B/A	1	none
annubar differential pressure	h_a	in. H ₂ O	B/A	1	none
aerator static head	p_{sh}	in. Hg	B/A	1	AR
aerator headloss	h_L	in. H ₂ O	B/A	1	T
blower discharge pressure	p_d	in. Hg	B/A	1	none
blower differential pressure	p_{bd}	in. Hg	B/A	1	none
pump discharge pressure	TDH	in. H ₂ O	B/A (jet aerator only)	1	none
barometric pressure	p_a	mm Hg	B/A	1	T
relative humidity	R.H.	%	B/A	1	T
pump wire power	P_{pw}	kW	continuous	1	T

1. B = before test, A = after test, B/A = before and after test.
2. AR = arithmetic, T = time.

theory proposed by Lewis and Whitman.⁷ This theory is expressed by the following mathematical relationship:

$$dC/dt = K_L a_t (C^* - C) \quad (16)$$

in which:

dC/dt = oxygen transfer rate per unit volume, mg/L/hr

$K_L a_t$ = overall volumetric mass transfer coefficient for test conditions, 1/hr

C^* = D.O. saturation value, mg/L

C = D.O. concentration, mg/L

This is the differential form of the basic equation and states that the oxygen transfer rate per unit volume is directly proportional to the D.O. deficit ($C^* - C$). Note that dC/dt is greatest when C is assumed to be zero. The mass transfer coefficient, $K_L a_t$, is a function of many variables, including the type of aerator, the aeration tank geometry, the nature of the liquid, and the liquid temperature. Equation 16 was originally developed to describe the oxygen transfer in small, shallow containers. It has been generalized to the case of large, deep aeration basins that are completely mixed. If complete mixing is not achieved, the use of Equation 16 to define the oxygen capabilities of the aeration system may lead to significant errors. The relationship embodied in this equation, therefore, constitutes the basic mathematical model describing oxygen transfer, if the assumption of complete mixing is accurate.

All data analysis methods share one common trait; they define an analytical procedure to calculate oxygen transfer rate. This always includes the fundamental determination of both the volumetric mass transfer coefficient, $K_L a_t$, and the D.O. saturation value, C^* .

Eight data analysis methods were originally planned to be incorporated in this report. The methods included three that use the integrated or log-deficit form of the basic equation: the Mid-Depth, Surface, and Equilibrium Measured methods. Also planned was a single method that uses the transformed integrated form of the basic equation, the Exponential method. The final four methods use the differential form of the basic equation for parameter determination. These four are the Direct, Log Mean Driving Force, Log Mean Saturation, and Equilibrium Corrected methods of analysis. A computer program was developed to analyze data using all eight methods. It was, however, decided to include only the analysis results of the two most highly regarded methods. This decision was based on a review of the results of the various methods, the difficulties involved in presenting results from each method, and a wish to not confuse the reader regarding the primary purpose of this study - an evaluation of the oxygen transfer performance of various generic aeration systems. The two methods the Districts considered to be the most highly regarded were 1) the log-deficit model with a measured

equilibrium, hereinafter to be referred to as the Equilibrium method, and 2) the Exponential model.

The differences between primary data analysis methods include

1. the form of the basic mathematical relationship on which a regression analysis will be run,
2. the method for determining C^* ,
3. the use of a correction for gas-side oxygen depletion[†] (no correction is used in either the Exponential or Equilibrium methods), and
4. data truncation requirements.

At least three forms of the fundamental relationship expressed in Equation 16 are used for the analysis of clean water test data. These are the differential, integrated, and transformed integrated equation forms. It is in the differential form of the basic equation that Equation 16 is expressed. In the Equilibrium method analysis, the integrated equation form is used. The Exponential method analysis uses the transformed integrated equation form. Detailed information on the methods of analysis used in determining the study results follows.

The differential form of the basic equation can be rearranged and integrated to obtain the "integrated" or "log-deficit" form. In the past, this form of the equation has been the most commonly used. After rearrangement, Equation 16 becomes:

$$dC/(C^*-C) = K_L a_t (dt)$$

Letting $D = C^* - C$ and assuming C^* is constant:

$$-dD/D = K_L a_t (dt)$$

Upon integration between (t_i, D_i) and (t_f, D_f) , this becomes:

$$\ln D \Big|_{D_i}^{D_f} = -K_L a_t (t) \Big|_{t_i}^{t_f}$$

in which:

D_i = initial D.O. deficit, mg/L

D_f = final D.O. deficit, mg/L

[†] Gas-side oxygen depletion is defined as the decrease in a bubble's oxygen purity as it rises through the aeration tank.

Substituting for D:

$$\ln (C^*-C_f) - \ln (C^*-C_i) = - K_L a_t (t_f-t_i)$$

or:

$$\ln (C^*-C_f) = - K_L a_t (t_f-t_i) + \ln (C^*-C_i) \quad (17)$$

in which:

C_i = initial D.O. concentration, mg/L

C_f = final D.O. concentration, mg/L

This is the integrated form of the basic equation. It is this form that is used by the Equilibrium method. In the analysis of data, t_i is 0, t_f is total elapsed time t , and C_f represents the various C values corresponding to values of t . Making these assumptions, the relationship between C and t is as follows:

$$\ln (C^*-C) = - K_L a_t(t)/3600 + \ln (C^*-C_i) \quad (18)$$

This is the exact equation used in the Equilibrium method data analysis. A conversion factor of 3600 is used to make compatible the units of $K_L a$, 1/hr, and t , sec.

The second method used in this report is referred to as the Exponential method. An exponential form of the equation has been favored by the ASCE Subcommittee on Oxygen Transfer Standards.^{8/} Equation 17 can be transformed to obtain the exponential form of the basic oxygen transfer relationship. From Equation 17, it follows that:

$$e^{\ln (C^*-C_f)} = e^{[- K_L a_t (t_f-t_i) + \ln (C^*-C_i)]}$$

or:

$$C^*-C_f = [e^{-K_L a_t (t_f-t_i)}] [e^{\ln (C^*-C_i)}]$$

and finally:

$$C^*-C_f = (C^*-C_i) e^{-K_L a_t (t_f-t_i)} \quad (19)$$

In the analysis of data, t_i is 0, t_f is t , and C_f is C . This reduces Equation 19 to the relationship between C and t as follows:

$$C = C^* - (C^*-C_i) e^{-K_L a_t (t)/3600} \quad (20)$$

Again, a conversion factor of 3600 is used to make compatible the units of $K_L a$, 1/hr, and t , sec.

The fundamental curves associated with the above two forms of the basic oxygen transfer equation are shown in Figure 6. While the Equilibrium method employs a linear curve fitting technique, the Exponential method requires the use of a non-linear curve fitting technique.

The method of determining C^* is the major difference between various data analysis techniques. The specifics of the C^* determination used in this study are discussed in the next subsection. Suffice it to say at this time some models use a "measured" value while others use a "derived" value. "Measured" means the saturation value is experimentally measured in the field. "Derived" means the saturation value is derived from the data by a curve fitting technique. The Equilibrium method uses a measured saturation, while the Exponential method uses a derived saturation.

DETERMINATION OF $K_L a_t$ AND C^*

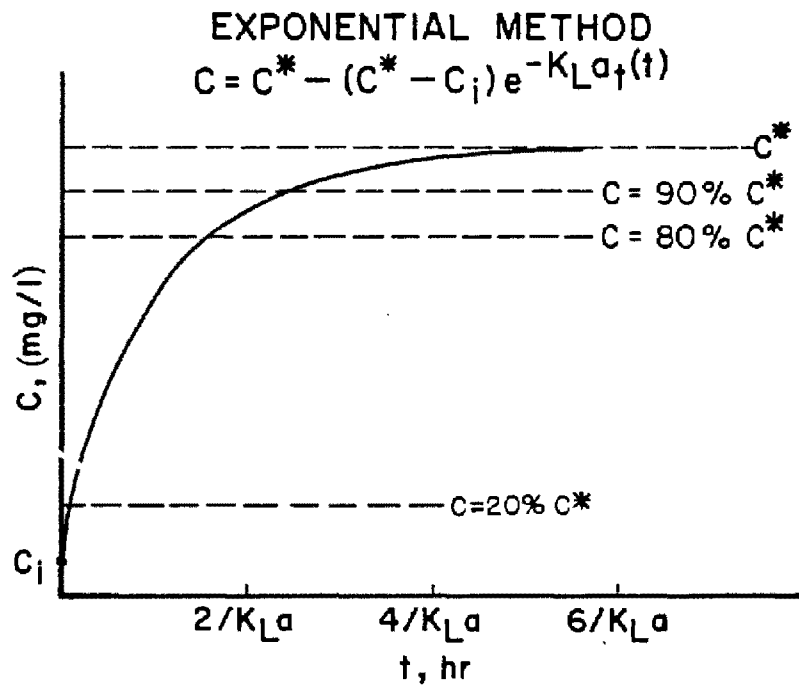
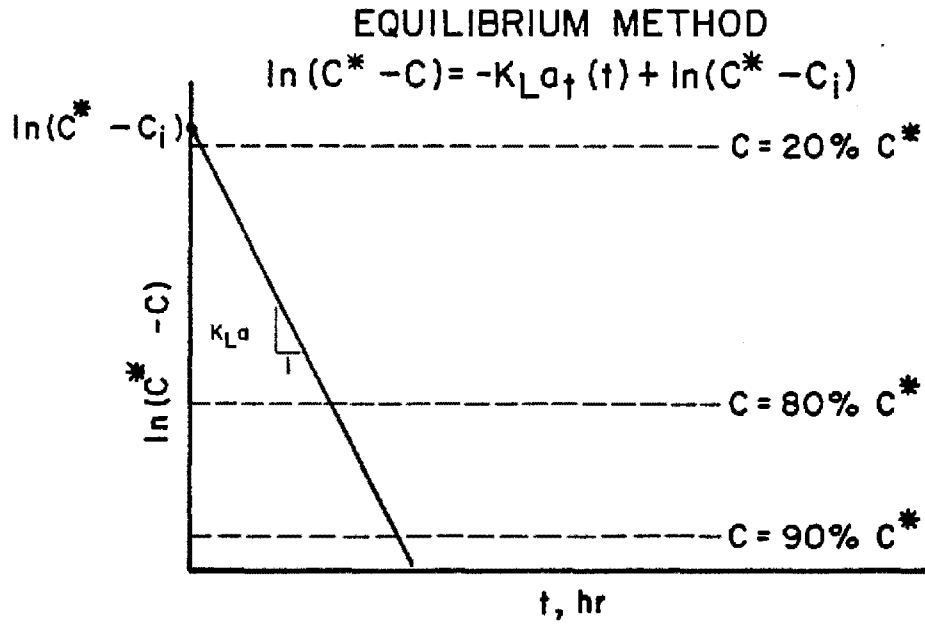
For both methods, the measured oxygen transfer data (C, t) for each of the four sample locations are analyzed separately. The resulting $K_L a_t$ and C^* values for the individual sample locations are then averaged to obtain the $K_L a_t$ and C^* results.

According to Equations 17 and 18, $K_L a_t$ is the negative slope of the straight line through a semi-logarithmic plot of the test data. Data plotted on the ordinate axis is the natural logarithm of the D.O. deficit, while time is plotted on the abscissa (Figure 6). A linear least squares regression analysis is used to determine the line of best fit.

The Equilibrium method assumes that the appropriate C^* in Equations 17 and 18 is the measured equilibrium D.O. concentration. In practice, the clean water test is conducted until D.O. saturation is observed (no further change in the D.O. concentration). A time equivalent to $6/K_L a_t$ is usually sufficient to achieve this condition.^{9/} Equilibrium samples are taken at each of the four sample locations in the tank.

With Equations 19 and 20, a non-linear least squares regression analysis is required to determine the best estimate of the parameters $K_L a_t$, C^* , and C_i (Figure 6). As opposed to the Equilibrium method, the Exponential method does not assume the C^* value; instead the value is derived from the data. This equation form, however, assumes that C^* is constant throughout the test (no correction for gas-side oxygen depletion).

Numerous non-linear optimization techniques could be used to determine the best estimates of the parameters C_i , C^* , and $K_L a_t$. All these techniques should yield approximately the same results. For purposes of this study, analysis was done using the Complex Method of Box technique.^{10/}



Note: The saturation values were directly measured for the Equilibrium method and analytically derived for the Exponential method.

Figure 6. Primary curve plots for Equilibrium and Exponential data analysis methods.

LEAST SQUARES REGRESSION METHODS

A regression analysis is normally of the linear least squares variety, but it may also be performed using non-linear techniques. A linear least squares regression of data defines one straight line. This straight line is specified by the constraints that the sum of the deviations (vertical distances between the data points and regression line) must equal zero and the sum of the deviations squared is the minimum value. In the log-deficit form of the gas transfer equation, a linear regression is employed (Equations 17 and 18). In this analysis, the ordinate axis is represented by the natural log of the oxygen deficit (difference between measured oxygen concentration and the saturation value). Time is plotted on the abscissa. The resulting slope of the "best fit" straight line is $-K_L a_t$. The Exponential method defines the non-linear relationship between C and t to be a function of three constants, C^* , C_j , and $K_L a_t$. Non-linear regression analysis is used to define these three values. In the case of the non-linear least squares analysis, a number of different optimization techniques may be applied. For the non-linear least squares analysis, the objective is that the sum of the initial deviations squared equal the minimum value. In the Exponential method of analysis, the ordinate axis represents the measured D.O. concentrations. The corresponding values of time are plotted on the abscissa. The determination of the best fit line is accomplished by an iterative searching technique referred to as the Complex Method of Box.^{10/}

The Complex Method of Box is used here to determine the values of C_j , C^* , and $K_L a_t$ that best describe the relationship (Equations 19 and 20) between time and D.O. As with a linear regression, the objective here is to minimize the sum of the squares of the deviations (SSD). (Deviations are the differences between calculated and measured values of D.O.) SSD is defined by the following expression:

$$SSD = \sum (C_c - C_m)^2 \quad (21)$$

in which:

$$C_c = C^* - (C^* - C_j) e^{-K_L a_t (t - t_j)}$$

and:

C_m = measured values of D.O. concentration, mg/L

Consider a point with coordinates $(C_j, C^*, K_L a_t)$. This point can be evaluated in terms of SSD to show how well the point describes the relationship between time and measured D.O. concentration: the lower the value of SSD, the better the relationship. Note that if all calculated D.O. values are exactly equal to the measured values of D.O., then $SSD = 0$.

The Complex Method of Box is a technique for selecting new points for SSD evaluation. To begin the process, six different arbitrary points are

chosen, each with coordinates (C_i , C^* , $K_L a_t$). The six points are then evaluated in terms of SSD. From this group of points, the worst point, P_W (largest SSD value), is then identified and set aside. Using the remaining five points, the centroid, P_C , is determined. The coordinates of the centroid are the mean values of C_i , C^* , and $K_L a_t$. For the five points in the next step, the program searches for a new sixth point, one with a SSD less than P_W . The new point is located on the line that runs through both P_W and P_C . The distance between P_C and the new point is 1.3 times the distance between P_W and P_C . This new point is located on the side of P_C opposite P_W . After determining the coordinates of this new point, it is evaluated in terms of SSD. If the SSD of the new point is not less than that of P_W , a second new point midway between the first new point and P_C is chosen and evaluated. This process continues until an improvement in SSD (better than SSD of P_W) is accomplished. When a better point is determined, it is placed in the group and the six points are reviewed to identify the new worst point and the search for a replacement point is again started.

To determine the final values of C_i , C^* , and $K_L a_t$, the process requires over 300 iterations (the determination of over 300 new points). In a few instances (less than 1% of the time), the method may produce erroneous values for the parameters. However, when an error does occur, it is substantial in magnitude; detection requires only a brief review of results. The correction of errors requires only changing the value of one of the six original starting points and reanalyzing the data.

NEED FOR DATA TRUNCATION

Most all data analysis methods require data truncation near the start of the test and then again at the end of the test, near equilibrium. The truncation near the start of the test (low D.O. values) is done primarily because of problems with sulfite distribution and because of the very high initial oxygen transfer rates. The truncation at the end of the test (high D.O. values) is done because near equilibrium, the D.O. may oscillate up and down very slightly with time. This can result in the calculation of negative driving forces and transfer rates, resulting in improper computational commands during electronic data processing.

One method is different from all others in this regard. The Exponential method not only does not require but should not have data truncation near equilibrium. These D.O. values are used in establishing the final equilibrium value. Furthermore, with the Exponential method, the data near the start of the test have significance in describing the adequacy of the method. The final oxygen transfer result for the Exponential method, however, should be reported identifying the data (if any) that have been truncated.

The low and high cut-off points for truncation are usually referred to in terms of percent of D.O. saturation. For this study, the low cut-off point was 20% and the high cut-off point was 90% of the measured saturation value. These truncation limits were chosen so that the results of analysis by both methods would be based on the same data, even though ideally no high cut-off point for the Exponential method analysis would have been preferred.

It is important to point out that while the determined values of $K_L a_t$ and C^* may be substantially different for some of the data analysis methods, it is possible that the product $(K_L a_t)(C^*)$ may be very similar for many of the methods. It is this product, the volumetric transfer rate, that is really the important result from the clean water test. It is hoped that this study will help to show how two methods can provide similar transfer rate results as well as similar $K_L a_t$ and C^* results.

PARAMETERS AT STANDARD CONDITIONS

Once $K_L a_t$ and C^* are determined for a test using a particular data analysis method, it is possible to make the oxygen transfer rate and efficiency calculations. Normally, test results are reported in terms of standard conditions of 20°C (68°F), 101.3 kPa (14.70 psia) and 0 mg/L D.O. (implies maximum driving force). To calculate oxygen transfer results in terms of standard conditions, it is necessary to determine each parameter at standard conditions ($K_L a_{20}$ and C^*_0).

$K_L a_{20}$ Determination

The basic oxygen transfer equation is used to make oxygen transfer rate determinations:

$$dC/dt = K_L a_t (C^* - C) \quad (16)$$

Normally, the values expressed in this equation are presented in forms of standard conditions and expressed as follows:

$$dC/dt = K_L a_{20} C^*_0 \quad (22)$$

One relationship between $K_L a_t$ and $K_L a_{20}$ that is commonly used 10/ is:

$$K_L a_t = K_L a_{20} (\theta)^{T_w - 20} \quad (23)$$

in which:

$K_L a_{20}$ = overall volumetric mass transfer coefficient at 20°C, 1/hr

θ = $K_L a$ temperature adjustment factor

T_w = water temperature, °C

The value of θ used for this study was 1.024. In reality, the temperature variation in $K_L a$ has been shown to be a function of the type of aerator, as well as other factors. Due to the lack of available information on this subject, however, a decision was made to use Equation 23 with $\theta = 1.024$ for all the aerators tested in this study.

When Equation 23 is substituted into Equation 16, the basic oxygen transfer relationship becomes:

$$dC/dt = K_L a_{20} (C^* - C) 1.024^{T_w - 20}$$

At standard conditions of 20°C (68°F), 101.3 kPa (14.70 psig), and 0 mg/L D.O. (maximum driving force), the equation reduces to:

$$(dC/dt)_0 = K_L a_{20} C^*_0$$

in which:

$(dC/dt)_0$ = standard oxygen transfer rate per unit volume at standard conditions, mg/L/hr

C^*_0 = projected field D.O. saturation value at standard conditions, mg/L

C*₀ Determination

The correction of C^* to standard conditions is somewhat more involved. The D.O. saturation value, C^* , for a given aeration system in a given tank under a given set of operating conditions is a complex function of temperature, pressure, and oxygen purity. However, assumptions can be made that make an estimation of C^*_0 possible. The actual procedure used is a function of the particular data analysis method employed; for the two methods used here, only one procedure is necessary.

The following procedure applies to data analysis methods that employ either a "measured" or "derived" D.O. saturation value. In this procedure, it is necessary to postulate a relationship between the measured or derived saturation value (at temperature T and pressure P_a) and the saturation value at standard conditions [20°C (68°F) and 101.3 kPa (14.70 psia)].

The relationship between oxygen solubility and temperature has been documented.^{6/} By attributing the difference between the measured or derived D.O. saturation value, C^*_{md} , and the textbook value of C^* (at the testing water temperature, T_w) to a pressure correction, the value of C^*_0 may be calculated. This procedure involves determining the absolute pressure (expressed in terms of "equivalent depth") that corresponds to the difference between C^*_{md} and textbook C^* at temperature T . This pressure correction is then applied to the textbook C^* value at 20°C (68°F) to determine C^*_0 .

The equivalent depth is that increase in pressure that explains the difference between the measured or derived D.O. saturation value and the textbook value of C^* at temperature T . The following equations show the relationship of equivalent depth to the other pertinent variables:

$$C^*_{md} = \left(\frac{0.01934p_a + 0.434z_{emd} - P_{vpT}}{14.70} \right) C^*_{hT} \quad (25)$$

and:

$$z_{emd} = 33.87 \left(\frac{C^*_{md}}{C^*_{hT}} \right) - 2.30(0.01934p_a - P_{vpT}) \quad (26)$$

in which:

C^*_{md} = measured or derived D.O. saturation value at temperature T and barometric pressure p_a , mg/L

C^*_{hT} = handbook D.O. saturation value at temperature T and pressure 101.3 kPa (14.70 psia) (dry air, 20.9% O_2 by volume), mg/L

p_a = barometric pressure, mm of mercury

z_{emd} = equivalent depth corresponding to the measured or derived D.O. saturation value, ft

P_{vpT} = vapor pressure of water at temperature T , psig

The factor preceding C^*_{hT} in Equation 25 is known as a pressure correction factor. The numerator of this factor represents the total pressure of dry air at the equivalent depth in the field. Dividing by 14.70 is necessary since C^*_{hT} is defined in terms of standard pressure conditions.

To calculate C^*_o , it is assumed that the equivalent depth calculated at temperature T and barometric pressure p_a is equal to the equivalent depth at 20°C (68°F) and 101.3 kPa (14.70 psia). Thus, at standard conditions:

$$C^*_o = \left(\frac{14.70 + 0.434 z_{emd} - P_{vp20}}{14.70} \right) C^*_{h20} \quad (27)$$

in which:

C^*_{h20} = handbook D.O. saturation value at 20°C (68°F) and 101.3 kPa (14.70 psia) (dry air, 20.9% O_2 by volume), mg/L

P_{vp20} = vapor pressure of water at 20°C (68°F), psig

Upon substitution of the handbook values:

$$C^*_o = \left(\frac{14.70 + 0.434 z_{emd} - 0.34}{14.70} \right) 9.17$$

which may be reduced to:

$$C^*_o = 8.96 + 0.271 z_{emd} \quad (28)$$

in which z_{emd} is calculated using Equation 26.

EVALUATION OF DATA ACCEPTABILITY

From the start of the testing, the need for a method of evaluating the validity of a test was recognized. At that time and throughout the testing, the following criterion was used as the basis for clean water test acceptability. A minimum of five D.O. concentration measurements was required from each sampling location between truncation limits of 20 and 80% of the D.O. saturation value. Each valid test was required to have all four sampling locations meet the five D.O. measurements criterion. Data between 20 and 80% of the saturation were then analyzed by the Equilibrium Measured technique for each location independently. The four resulting $K_L a$ values were then required to be within 6% of the average $K_L a$ value. Note that while the original truncation limits used were 20 to 80% of saturation for the evaluation of data acceptability, the final analysis presented in this report used limits of 20 to 90% of saturation.

Included in the analysis of data was the determination of the value of the correlation coefficient. While this factor did not influence the staff's judgement of the validity of the run directly, those analyses showing low correlations were more closely scrutinized. It should also be noted that it is impossible to determine a correlation coefficient for a non-linear regression analysis (as used in the Exponential method). A relative measurement of the goodness-of-fit of the data to the regression line, however, was determined for the non-linear regression. This number was determined by summing of the squares of the vertical deviations and subtracting the total from 1.

PRIMARY DATA ANALYSIS METHOD

The Exponential method was the primary data analysis method used in this study. Results from this analysis are presented in both tabular and graphical form; results from the Equilibrium method are presented in tabular form only. Due to recent work conducted by the ASCE Subcommittee on Oxygen Transfer Standards,^{8/} it is becoming increasingly clear that the

Exponential method embodies many desirable features. First, it determines the best estimates of the parameters C^* , $K_L a_t$, and C_i from an analysis of the data. Second, the form of the equation used allows for the determination of more precise estimates of the parameters C^* , $K_L a_t$, and C_i than are possible with other methods. This is because the curve fitting is done with the primary variables C and t , which are known more precisely than secondary variables such as C^*-C . Finally, upper end data truncation is not necessary near the end of the oxygen transfer test.

Disadvantages of the Exponential method are that 1) it requires a complex non-linear curve fitting procedure, 2) it may sometimes unfairly weight the data collected near the start of the test, and 3) it does not account for the effect of gas-side oxygen depletion. These shortcomings, however, are relatively minor and appear to be more than offset by the advantages of the method. The complex curve fitting technique is not a problem if access to computer facilities is available (modern hand-held programmable calculators are also being investigated for this purpose).^{10/} Because of items 2 and 3 above, use of the Exponential method leads to the calculation of an apparent (rather than true) $K_L a_t$. But as long as the apparent (rather than true) C^* is used to calculate the transfer rate, the results are nearly the same.

STANDARD OXYGEN TRANSFER CALCULATIONS

The basic oxygen transfer relationship is the product of the overall volumetric mass transfer coefficient at 20°C (68°F), $K_L a_{20}$, and the oxygen deficit, C^*-C . In a simplified form, assuming C is 0, this equation appears as:

$$(dC/dt)_0 = K_L a_{20} C^*_0 \quad (24)$$

The standard oxygen transfer rate, SOTR, can be determined by multiplying $(dC/dt)_0$, the oxygen transfer rate per unit volume at standard conditions, by the aeration tank volume and the appropriate conversion factor as shown below:

$$SOTR = 0.0000624 (dC/dt)_0 V_w \quad (29)$$

in which:

$$V_w = \text{deflated aeration tank water volume, ft}^3$$

To calculate the oxygen transfer efficiency, it is first necessary to know the oxygen supply rate, OSR. For the purposes of this study, the OSR is assumed to be constant during the entire test. It is calculated using the following expression:

$$OSR = Q \left[\frac{\text{ft}^3 \text{ dry air}}{\text{ft}^3 \text{ wet air}} \right] \left[\frac{\text{lb dry air}}{\text{ft}^3 \text{ dry air}} \right] \left[\frac{\text{lb oxygen}}{\text{lb dry air}} \right] \left[\frac{\text{min}}{\text{hr}} \right]$$

$$OSR = Q (0.9917) (0.0752) (0.231) (60) \quad (30)$$

$$OSR = 1.034 Q \quad (24)$$

in which:

OSR = oxygen supply rate, lb O₂/hr

Q = airflow at standard conditions of 20°C (68°F), 101.3 kPa (14.70 psia), and 36% relative humidity, scfm.

Knowing the SOTR and the OSR, the next step is to determine the standard oxygen transfer efficiency, SOTE. SOTE is the percentage of oxygen in air that is transferred into the water during aeration of water at a 0-mg/L D.O. concentration. SOTE is calculated according to the equation:

$$SOTE = \frac{SOTR}{OSR} \times 100\% \quad (31)$$

in which:

SOTE = standard oxygen transfer efficiency during aeration of water at 0-mg/L D.O., decimal %.

DETERMINATION OF STANDARD AERATION EFFICIENCY

The aeration efficiency is the pounds of oxygen per hour that are transferred into the water per unit of power used. The standard aeration efficiency, N₀, is the aeration efficiency at the standard conditions of 20°C (68°F), 101.3 kPa (14.70 psia), and 0-mg/L D.O.

Thus:

$$N_0 = \frac{\text{Standard Oxygen Transfer Rate}}{\text{Power Input}} = \frac{SOTR}{P} \quad (32)$$

Since power can be reported as either delivered, brake, or wire power, it follows that N₀ can be reported as either delivered, brake, or wire aeration efficiency (N_{d0}, N_{b0}, and N_{w0}, respectively). For a discussion of delivered, brake, and wire power and the equipment efficiencies used for the study, refer to the Aerator Power Determinations subsection of Section 3.

SECTION 5

AERATION SYSTEM DESCRIPTIONS

OVERVIEW

The different generic aeration systems tested included fine bubble dome diffusers, fine bubble tube diffusers, jet aerators, and various coarse bubble diffusers. Originally, seven manufacturers were contacted and asked to participate in this evaluation. Near the conclusion of the program, it was felt that the evaluation of a coarse bubble sparger system would be beneficial because it is widely used both nationwide and in LACSD treatment plants. Testing of the spargers was conducted at the 4.6-m (15-ft) water depth only.

For the original seven system installations, the manufacturer was responsible for designing the system layout to be tested, providing drawings for the installation, providing all required materials and equipment, and inspecting the completed installation.

Testing was conducted at three different nominal power densities for each of four SWDs. The manufacturers were allowed to change the configuration of their equipment for each depth, subject to the constraints of this study. It was required, however, that the manufacturer use the same configuration for all tests at a given depth.

FINE BUBBLE DOME DIFFUSERS

The manufacturer of the fine bubble dome diffusion equipment tested was the Norton Company. At all four depths tested, the manufacturer chose a single floor coverage system installation. This design consisted of 126 ceramic dome diffusers mounted on seven 10-cm (4-in.) diameter PVC headers (Figure 7). Each dome measured 17.8 cm (7 in.) in diameter and 3.8 cm (1.5 in.) in height (Figure 8). Dry dome permeability was 7.1 L/sec (15 scfm) at a headloss of 2.5 cm (1 in.) of water. Norton domes were mounted to the header plates with an orifice bolt. The size of the air control orifice in the bolt was 5.2 mm (13/64 in.). The diffused air release point was at an elevation of 28 cm (11 in.) above the tank floor. Support for this system was provided by pipe stands attached to the tank floor. All parts of this manufacturer's system were of non-corroding material.

This manufacturer chose to be tested at the lower power density range. The nominal power density levels selected were 7.9, 13.2, and

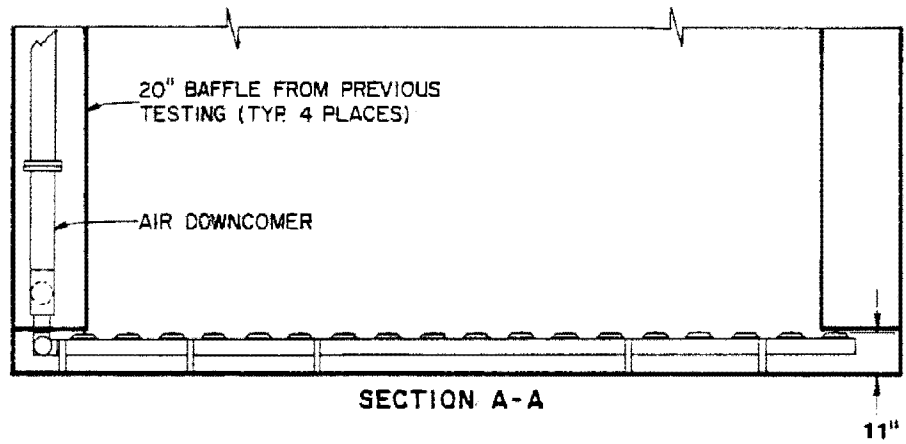
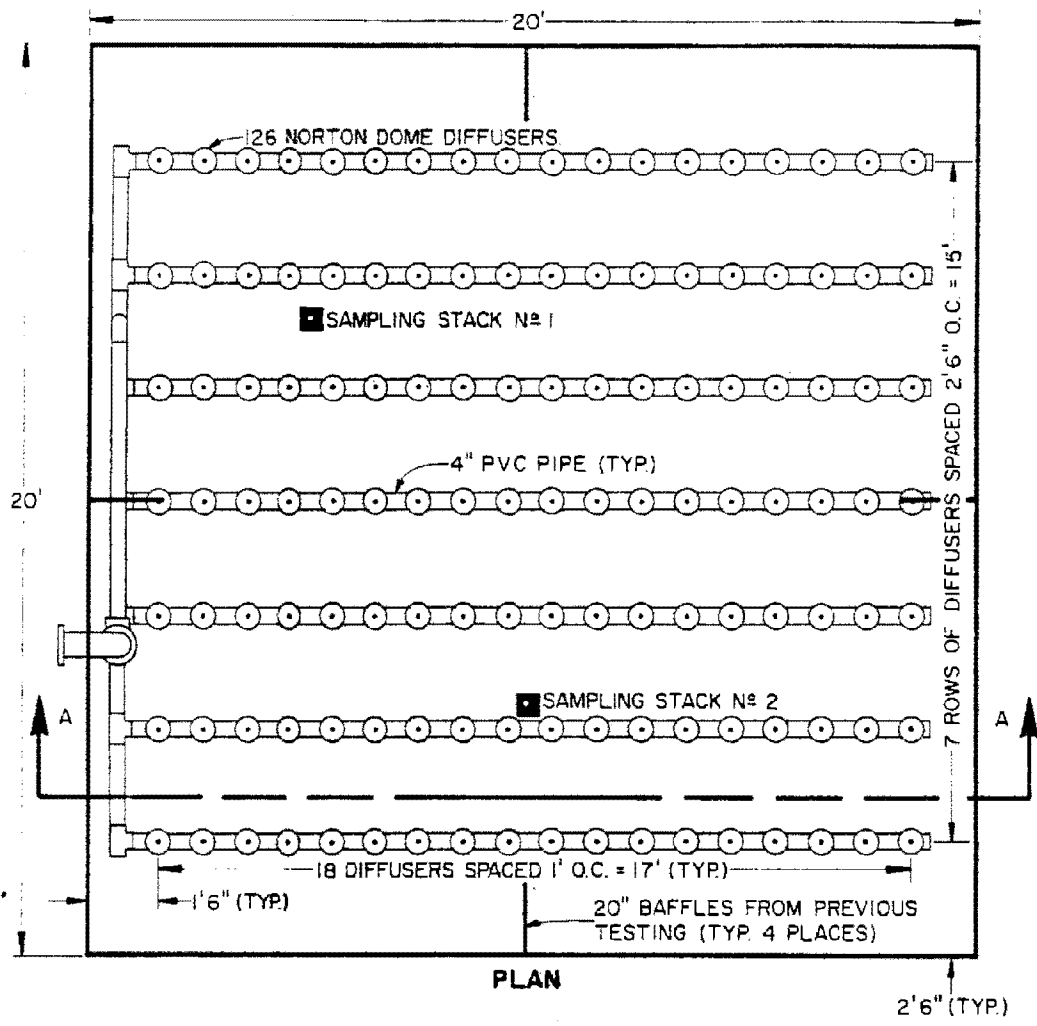
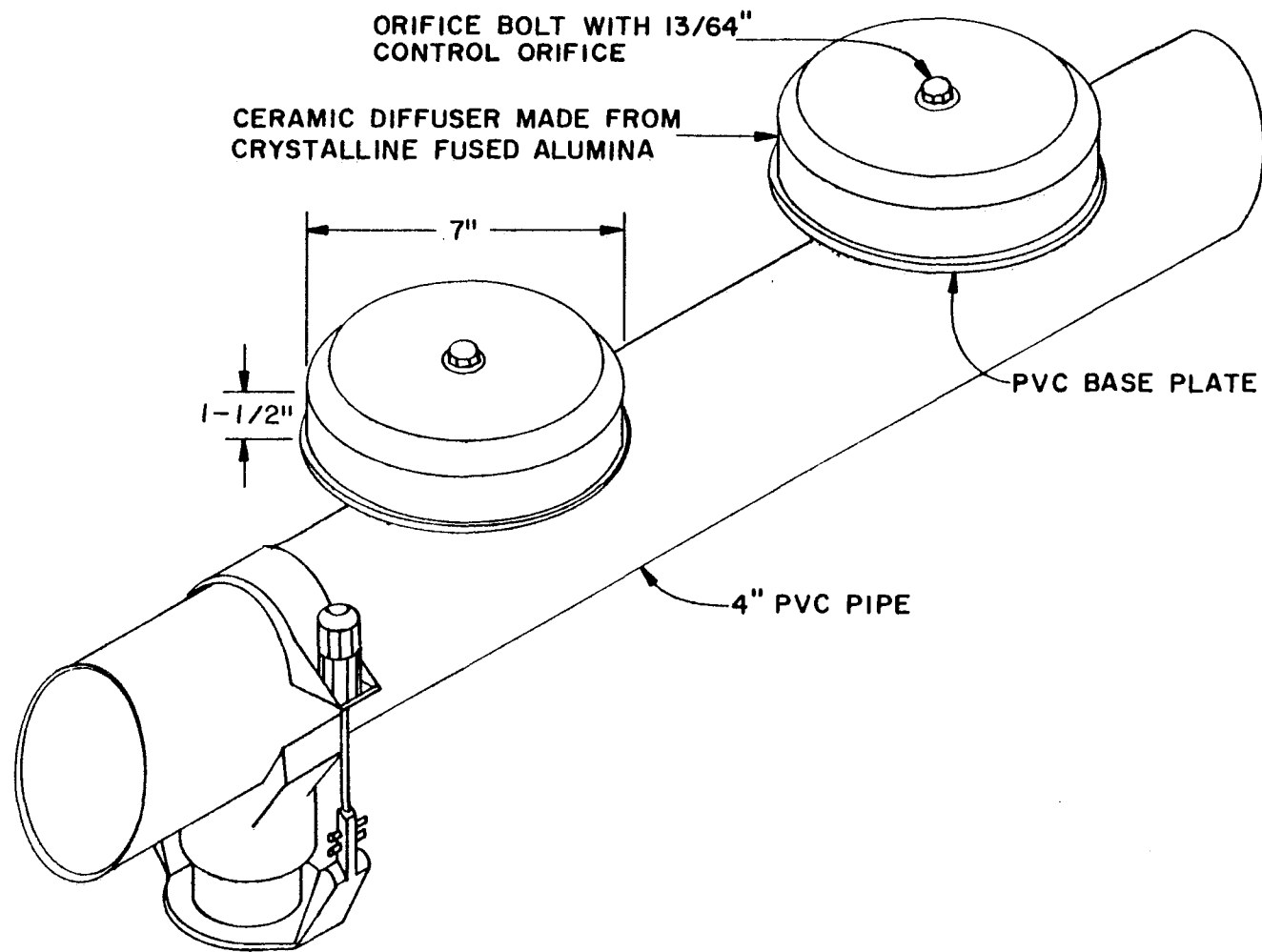


Figure 7. Test tank configuration for the Norton dome diffuser aeration system.



47

Figure 8. Norton dome diffuser.

26.3 W/m³ (0.3, 0.5, and 1.0 hp/1000 ft³). Testing air rates ranged from 35 to 128 L/sec (74 to 272 scfm). This corresponded to airflow rates per diffuser of 0.3 to 1.0 L/sec (0.6 to 2.2 scfm). Diffuser headlosses for the system ranged from 17 cm (6.7 in.) to 49 cm (19.4 in.) of water.

FINE BUBBLE TUBE DIFFUSERS

The fine bubble tube diffuser system tested was manufactured by the FMC Corporation. The manufacturer designed a single configuration for testing of this system at all four depths. A wide-band dual aeration installation consisting of two headers, each with 21 tube diffusers was mounted at opposite sides of the tank (Figure 9). The manufacturer referred to the diffuser tested as the Pearlcomb diffuser (Figure 10). The diffuser media was a white porous modified acrylonitrile-styrene copolymer material and was available in a number of porosities. The medium porosity grade, SP-35, was selected for this study and is the most widely used. These tube diffusers had a dry tube permeability of 23.7 L/sec (50.3 scfm) at a headloss of 2.54 cm (1 in.) of water. Control orifices for this diffuser were 11.91 mm (15/32 in.). This installation was supported off the floor with pipe stands. The diffused air release point was at an elevation of 65 cm (25 in.) above the tank floor.

The nominal power density levels selected by the manufacturer were 13.2, 26.3, and 39.5 W/m³ (0.5, 1.0, and 1.5 hp/100 ft³). Testing air rates ranged from 62 to 197 L/sec (132 to 417 scfm). This corresponds to airflow rates per diffuser of 1.5 to 4.7 L/sec (3.1 to 9.9 scfm). Diffuser headlosses for the system ranged from 6 cm (2.4 in.) to 31 cm (12.2 in.) of water.

JET AERATORS

The principle of jet aeration is that a primary or motive fluid (the tank liquid) is directed through a nozzle into a mixing chamber in the aerator. Air supplied by the blower enters the mixing chamber and is sheared into minute bubbles when entrained in the motive fluid. The combined gas-liquid mixture is then jetted into the aeration tank. This mixture forms a plume that travels horizontally while spreading through the tank before rising to the surface. It is significant to note that the air headloss through the jet aerator was usually very low or negative due to the ejecting action of the motive fluid.

The manufacturer of the jet aeration equipment tested was Pentech-Houdaille Industries, Inc. The manufacturer chose to test three different systems in the evaluation. At the 3.0-m (10-ft) SWD, the manufacturer used a six-nozzle eddy mix jet aeration (EMJA) cluster connected to a 3.7-kW (5-hp) recirculation pump (Figure 11). At the 4.6-m (15-ft) SWD, the manufacturer chose to test a 4.9-m (16-ft) directional mix jet aerator (DMJA) with four nozzles (Figure 12). Recirculation water was pumped to the DMJA unit by a

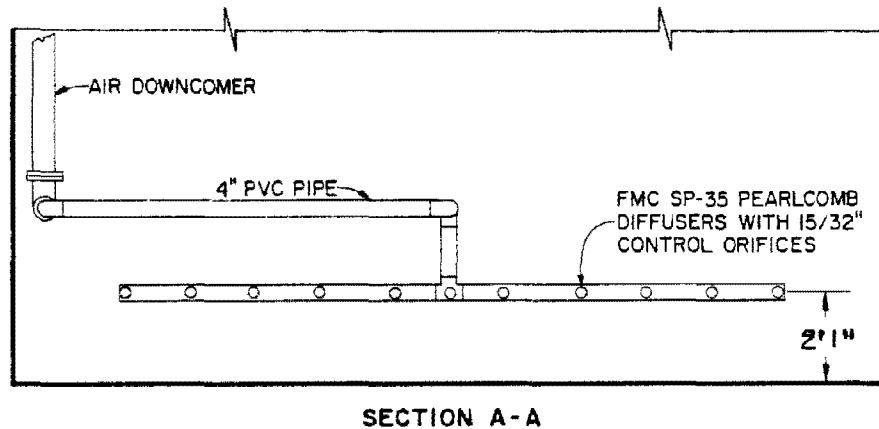
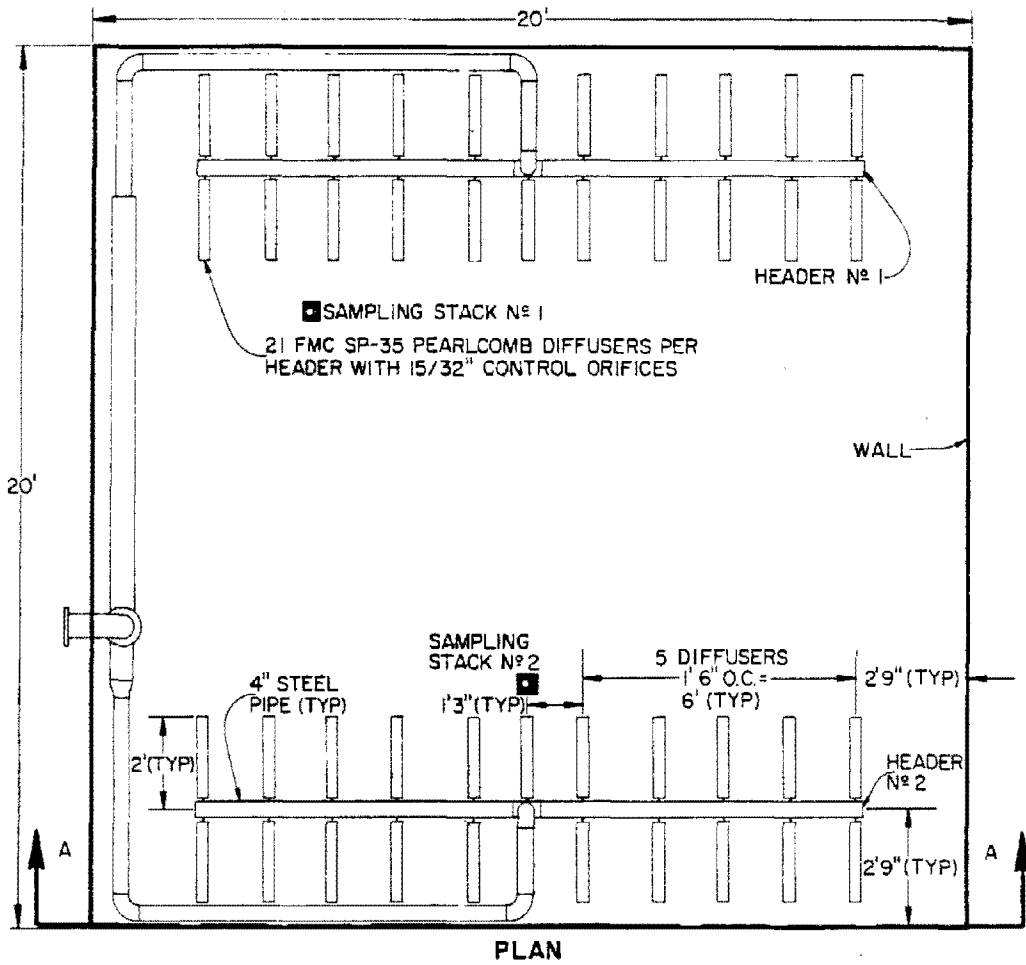


Figure 9. Test tank configuration for the FMC Pearlcomb tube diffuser aeration system.

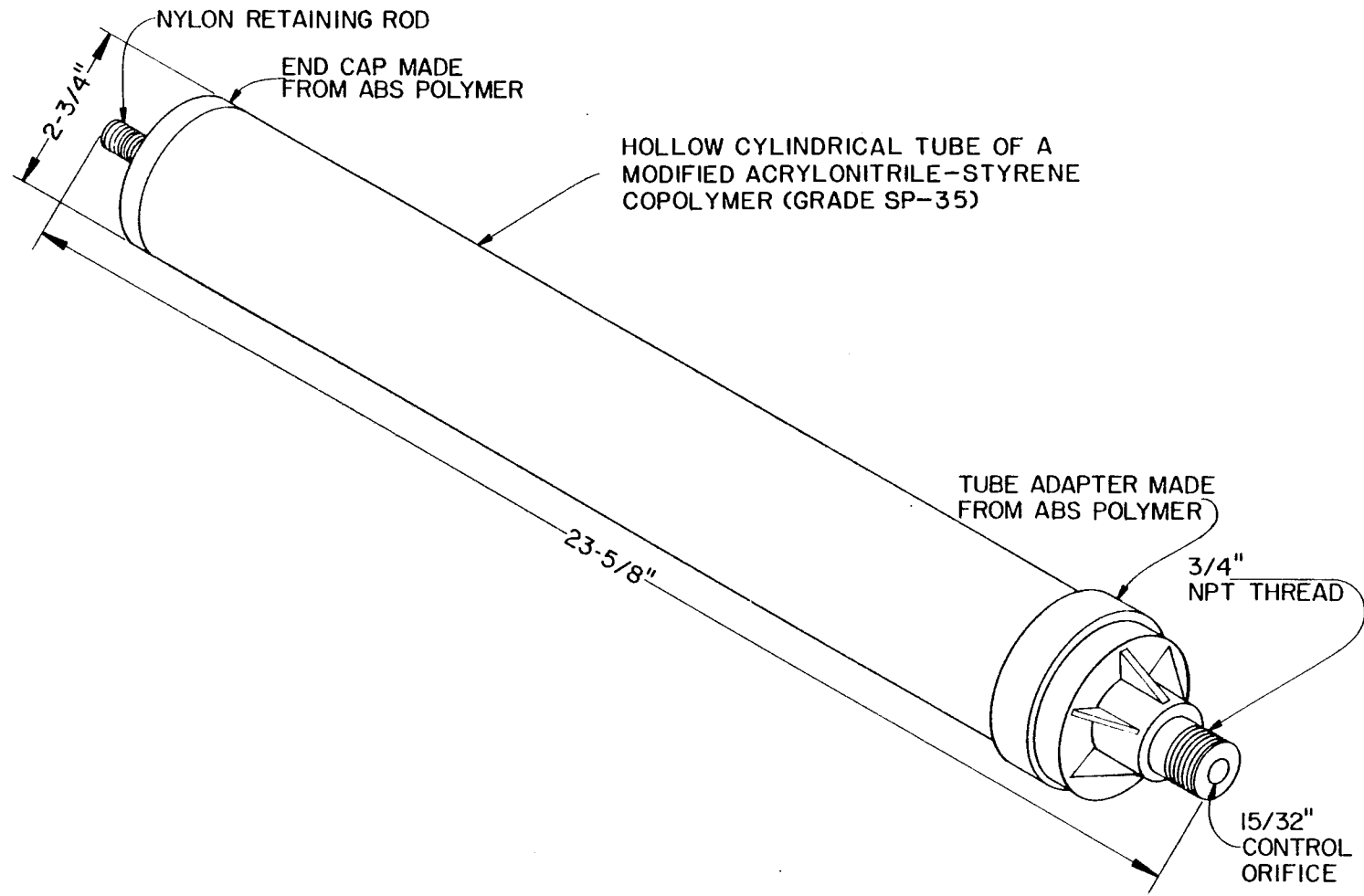
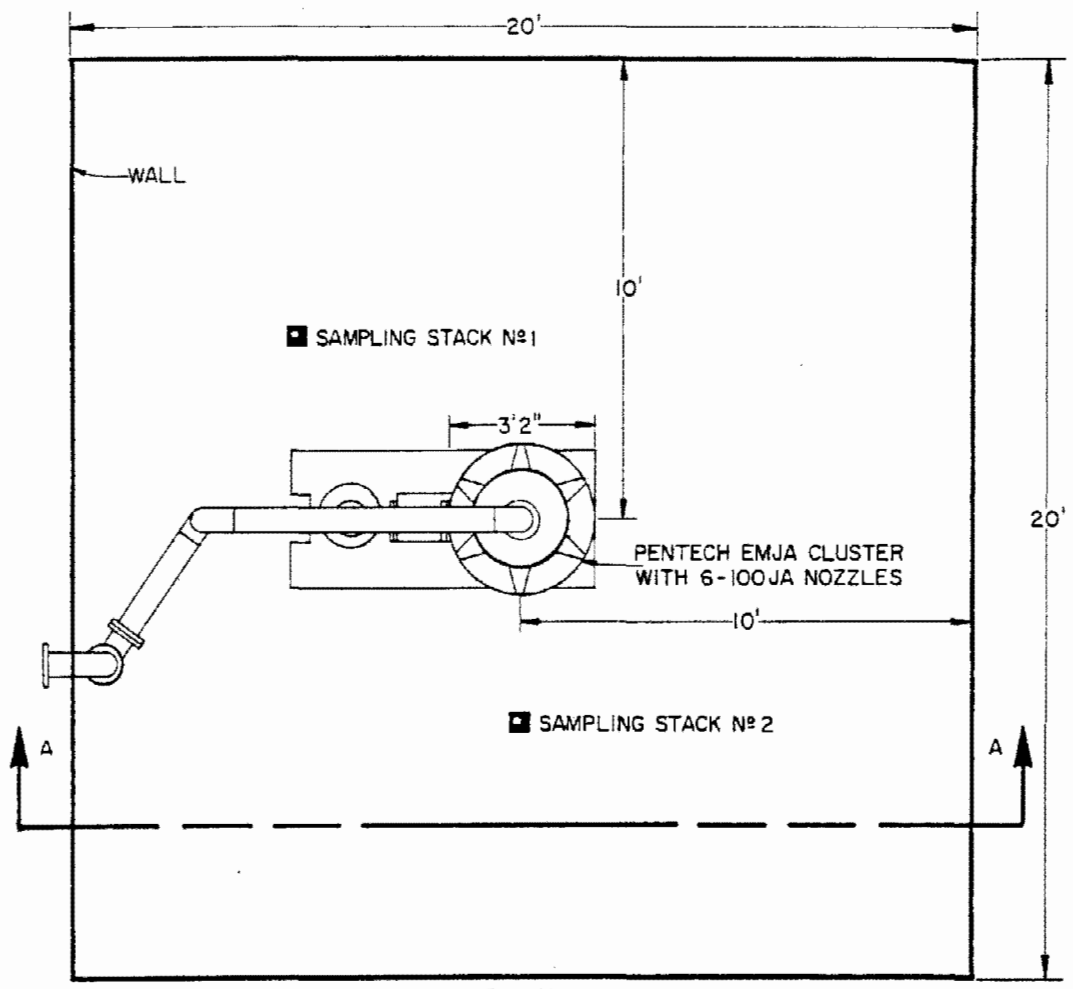
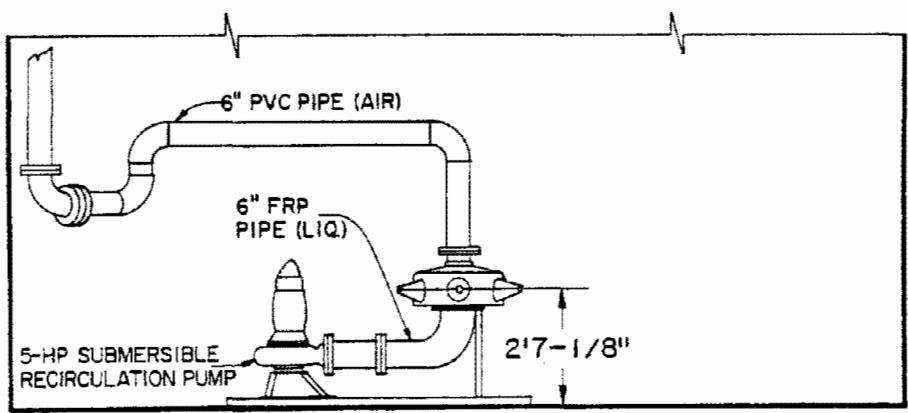


Figure 10. FMC Pearlcomb diffuser.



PLAN



SECTION A-A

Figure 11. Test tank configuration for the Pentech EMJA unit at the 10-ft water depth.

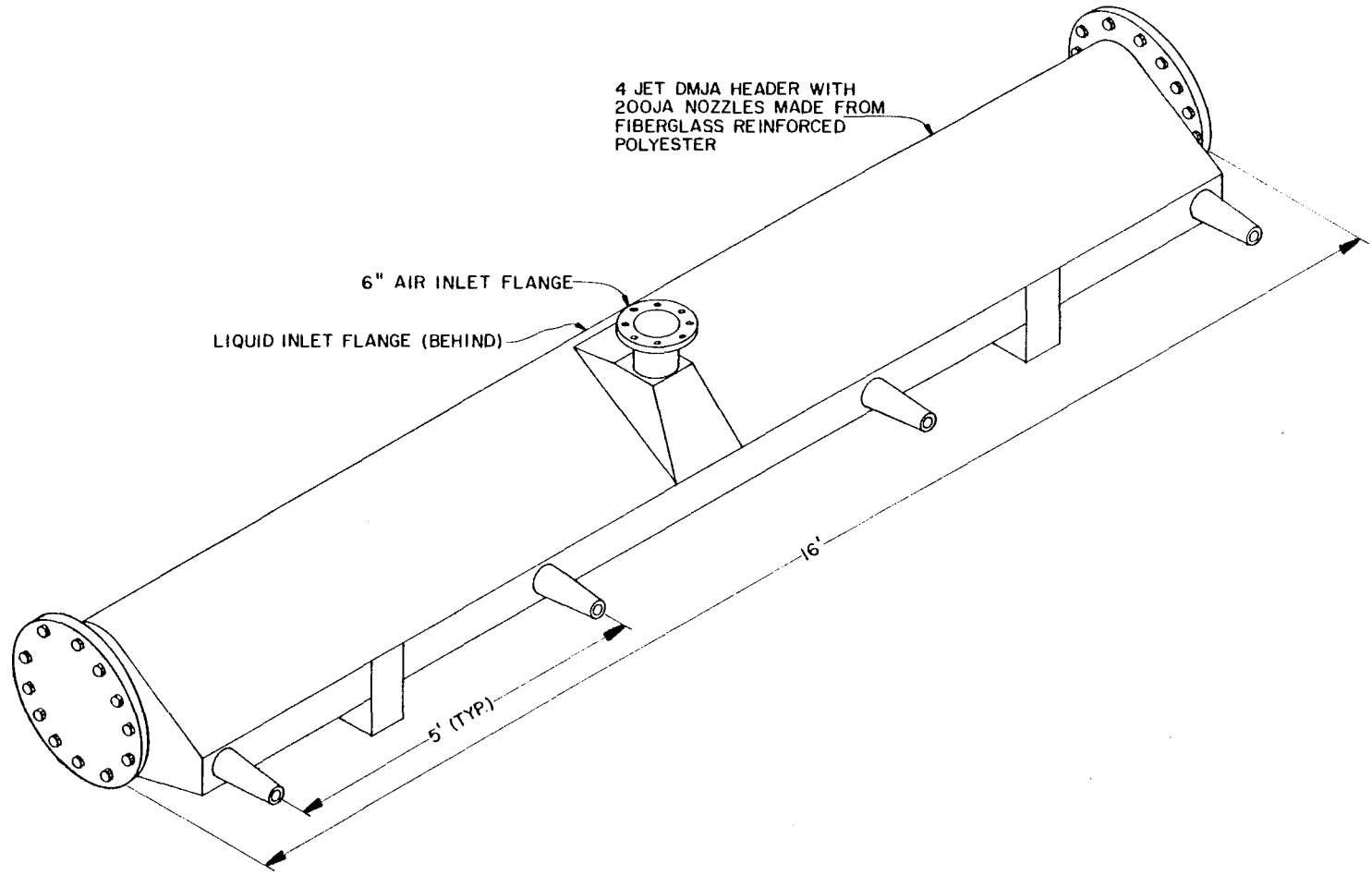


Figure 12. Pentech directional mix jet aerator (DMJA).

3.7-kW (5-hp) recirculation pump (Figure 13). At the 6.1-m (20-ft) and 7.6-m (25-ft) SWDs, the choice was a 10 nozzle EMJA cluster system (Figure 14). Recirculation water was again supplied to the jets by a 3.7-kW (5-hp) pump (Figure 15). For all depths, the EMJA cluster was mounted on a skid centered in the tank. Both the EMJA and DMJA units were fabricated of a fiberglass material. The DMJA unit was constructed so it could be bolted to the tank floor along one edge of the tank.

Nominal power testing densities chosen by the manufacturer were 13.2, 26.3, and 39.5 W/m³ (0.5, 1.0, and 1.5 hp/1000 ft³). This manufacturer's systems were the only ones tested that utilized power in addition to that required to supply air. Because the recirculation pump could only be operated at one speed, the power consumption by the pump was essentially constant. To vary the nominal power supplied, the air rates had to be adjusted greatly. Air rates supplied to the system ranged from 16 to 159 L/sec (33 to 336 scfm). Airflow rates per jet ranged from 2.3 to 36 L/sec (4.9 to 76 scfm). The DMJA jets discharged air/water at an elevation of 44 cm (17.4 in.) above the tank floor. The EMJA jets discharged air/water at an elevation of 79 cm (31.1 in.) above the tank floor.

STATIC TUBE AERATORS

The static tube aerators were supplied by Kenics Corporation. This manufacturer chose to use two different configurations. At the 3.0- and 4.6-m (10- and 15- ft) SWDs, the manufacturer chose to cover the floor evenly with nine 30-cm (1-ft) diameter static tube aerator units, each measuring 0.9-m (3-ft) high (Figure 16). At the 6.1- and 7.6-m (20- and 25-ft) SWDs, the nine-unit floor coverage was again chosen; however, this time the static aerators were 1.5 m (5 ft) high (Figures 17 and 18). Control orifices for this system consisted of two drilled holes 15.9 mm (5/8 in.) in diameter located on the bottom of the air header passing beneath each static tube aerator.

The nominal power density levels selected by the manufacturer were 13.2, 26.3, and 39.5 W/m³ (0.5, 1.0, and 1.5 hp/1000 ft³). System air rates ranged from 54 to 190 L/sec (115 to 402 scfm). This corresponded to airflow rates per aerator of 6 to 21 L/sec (13 to 45 scfm). Aerator headlosses for the system ranged from 4.3 cm (1.7 in.) to 28 cm (11.2 in.) of water. In this system, air was discharged 11.4 cm (4.5 in.) above the floor.

VARIABLE ORIFICE COARSE BUBBLE DIFFUSERS

The principle of operation of the variable orifice diffuser is that air passing through holes in the diffuser cause a high frequency oscillation of a spring that shears the passing air into small bubbles, thus promoting oxygen transfer. The spring also acts as a check valve to keep mixed liquor solids out of the air header when the air is shut off. The headloss of the device is due primarily to the

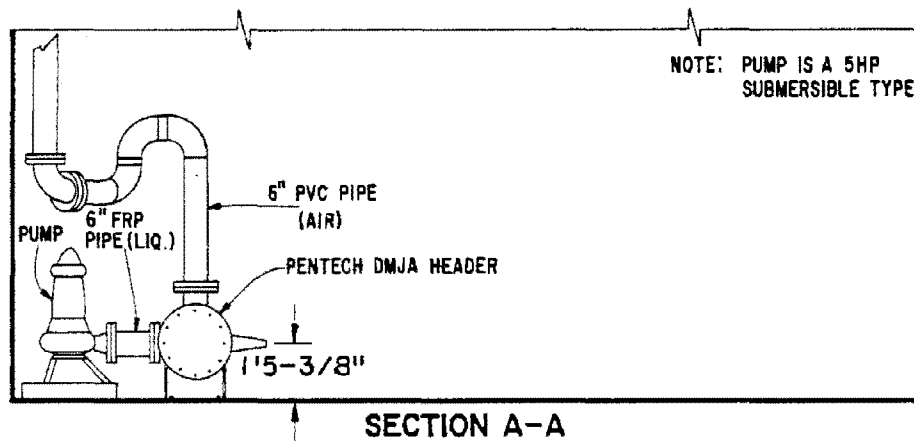
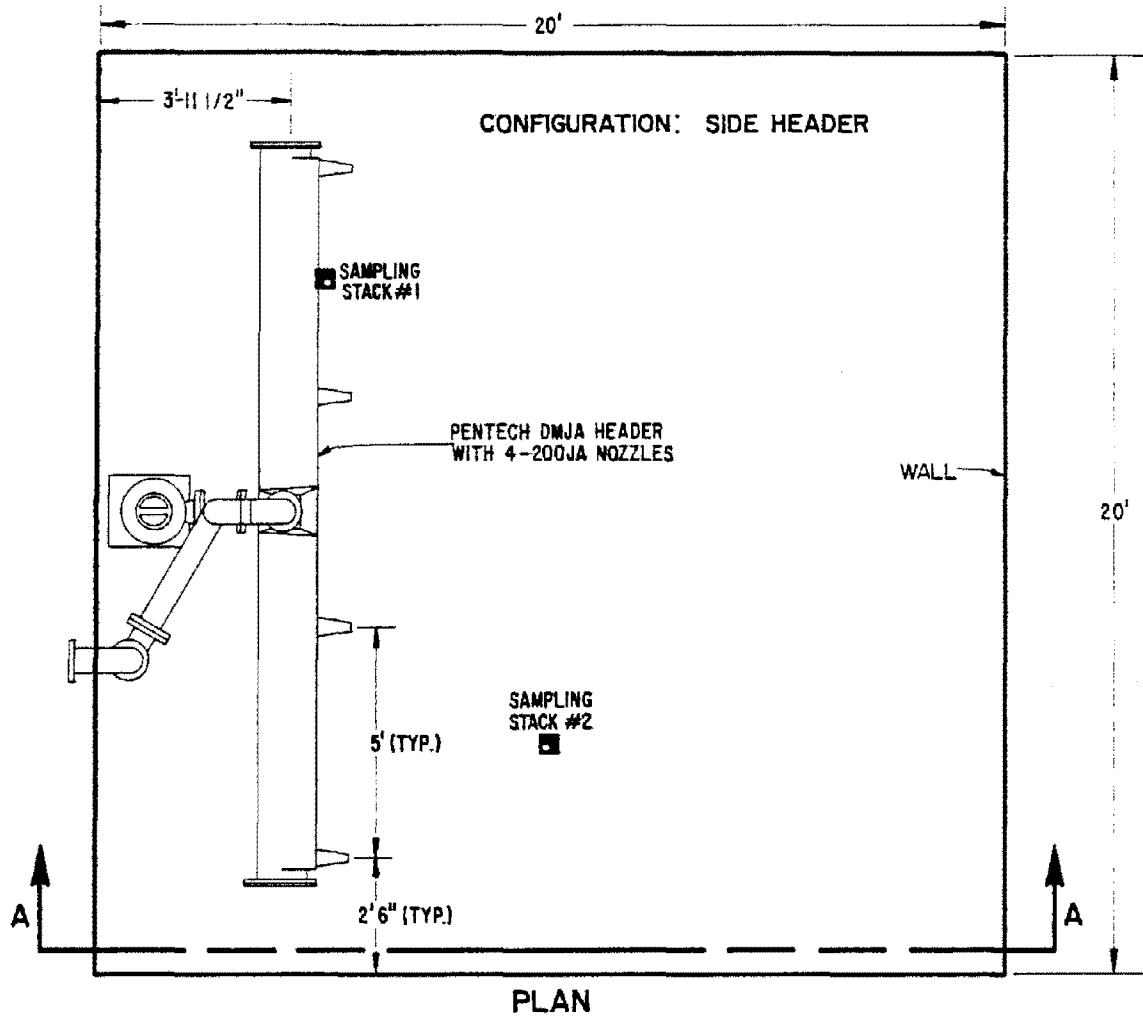
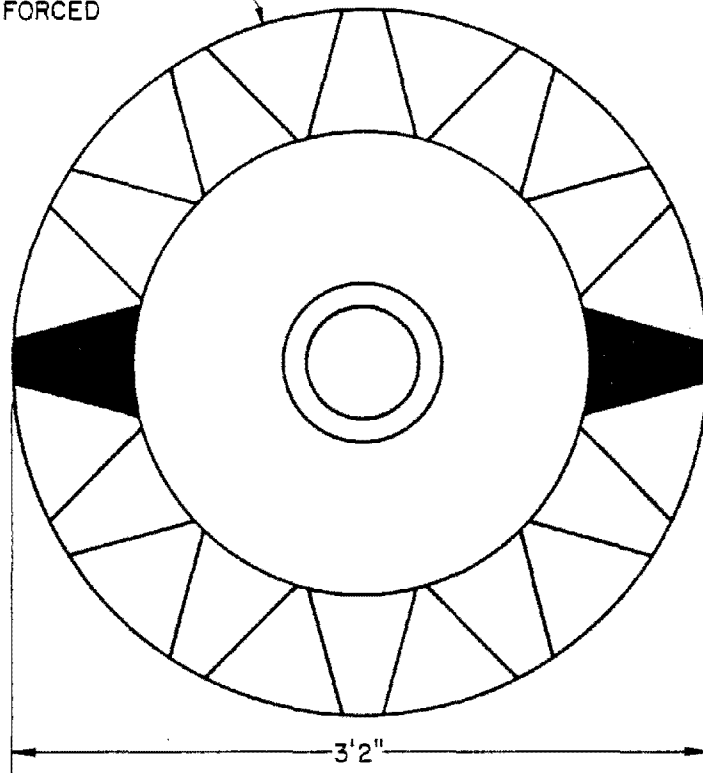
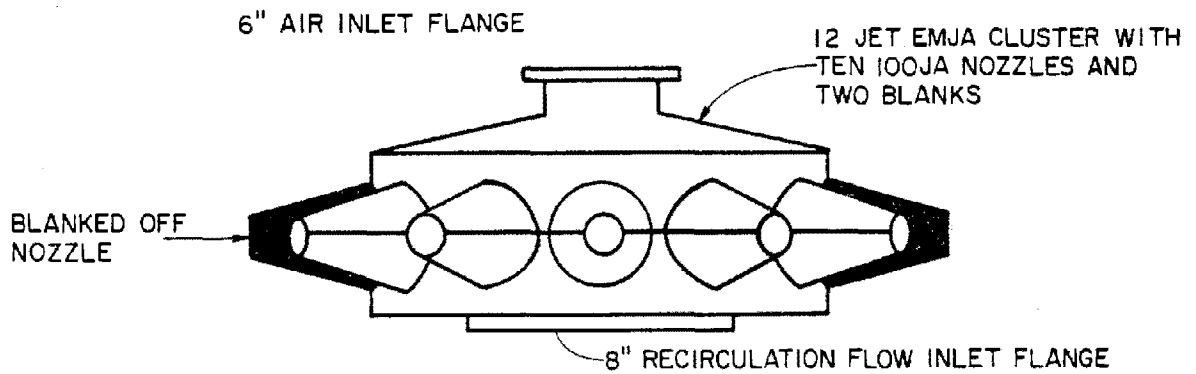


Figure 13. Test tank configuration for the Pentech DMJA unit at 15-ft water depth.

12 JET EMJA CLUSTER WITH
TEN 100JA NOZZLES AND
TWO BLANKS MADE FROM
FIBERGLASS REINFORCED
POLYESTER

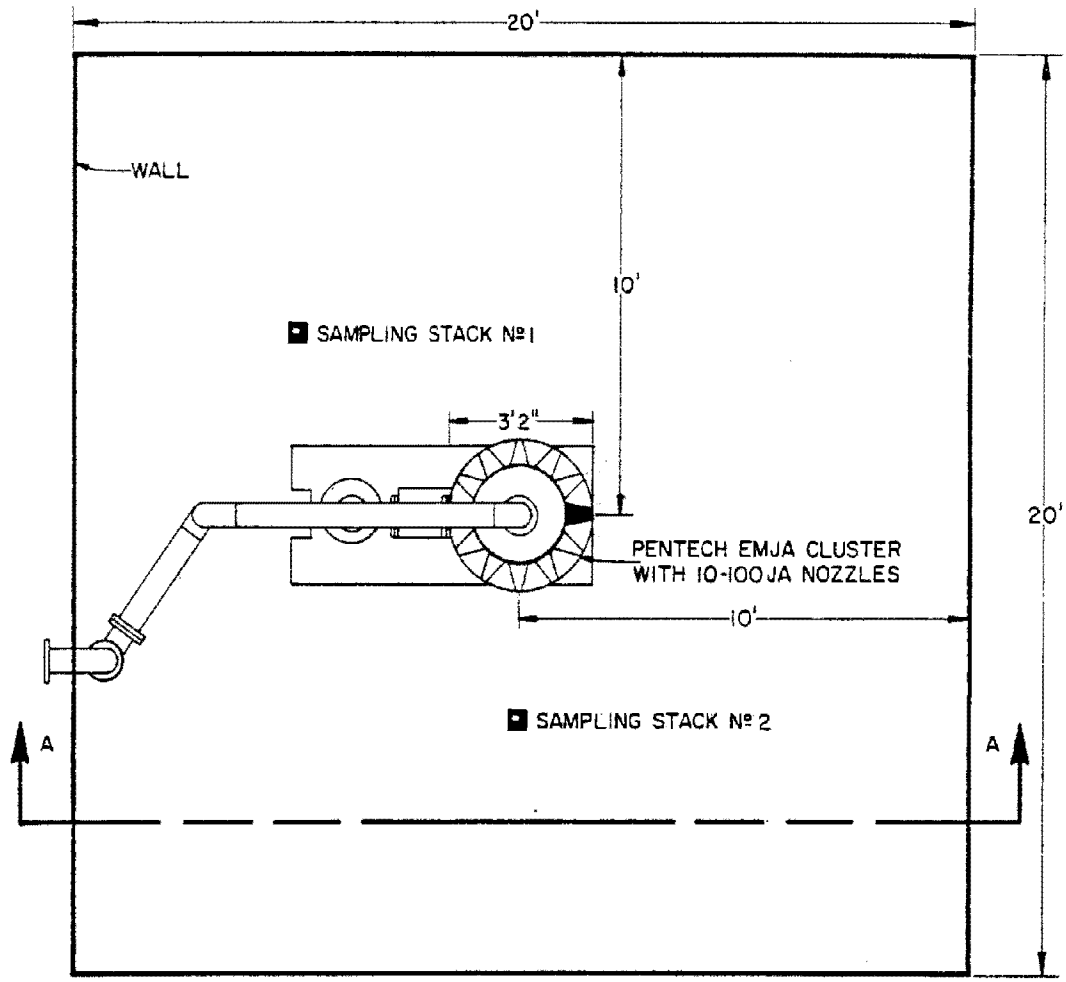


PLAN

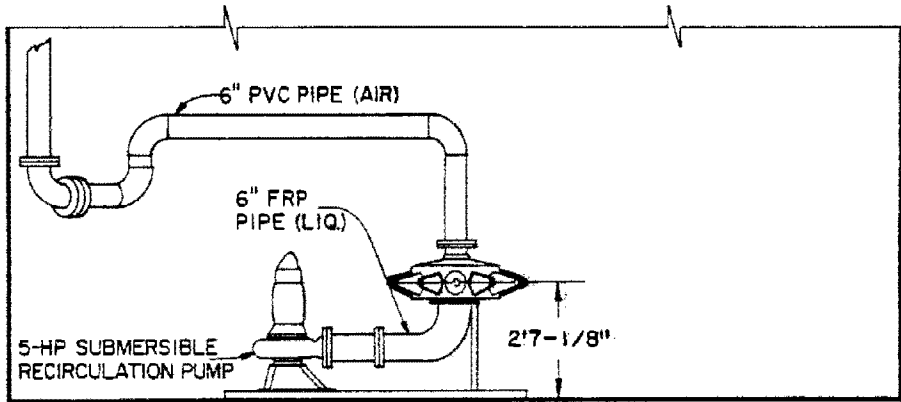


ELEVATION

Figure 14. Pentech eddy mix jet aerator (EMJA).



PLAN



SECTION A-A

Figure 15. Test tank configuration for the Pentech EMJA unit at the 20- and 25-ft water depths.

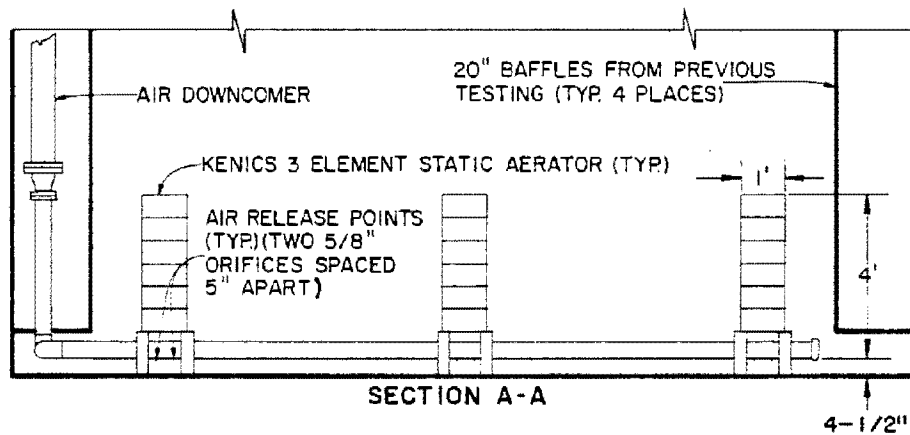
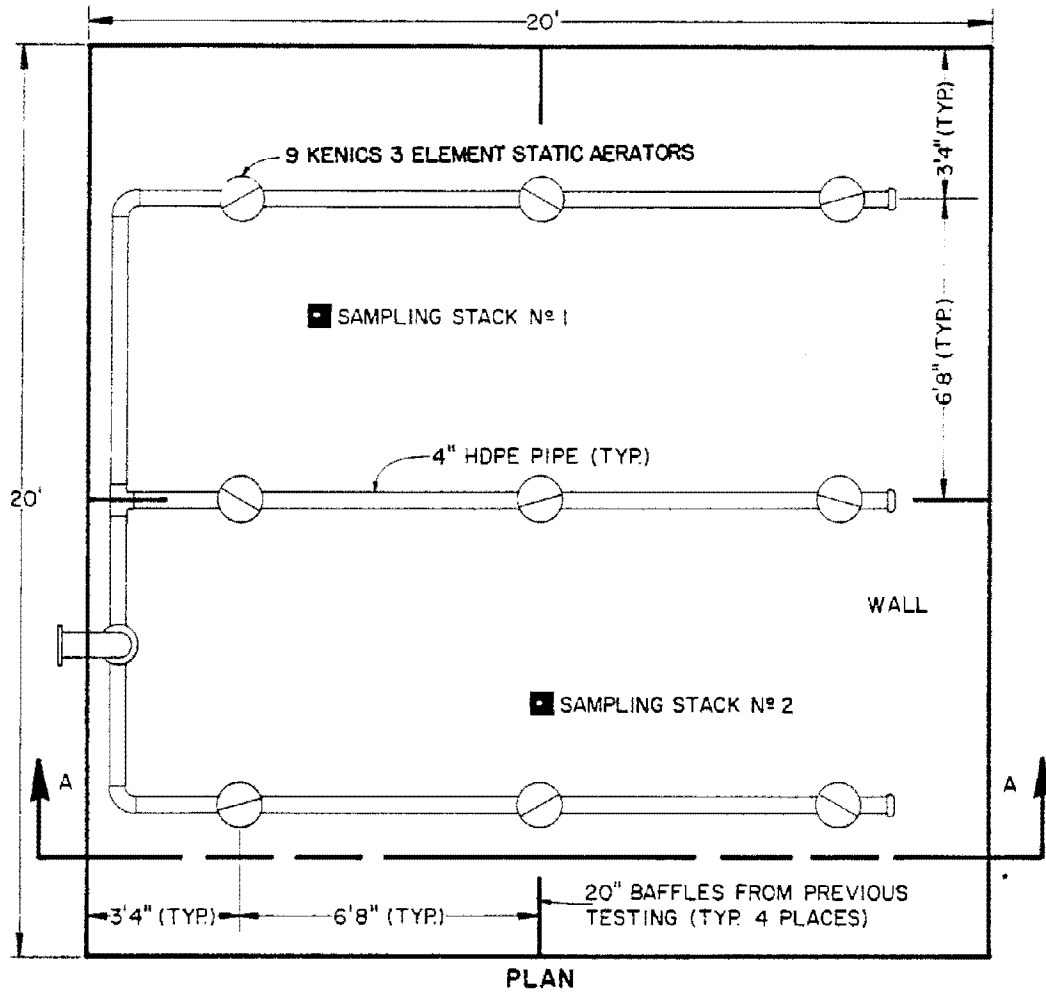


Figure 16. Test tank configuration for the Kenics static tube aeration system at the 10- and 15-ft water depths.

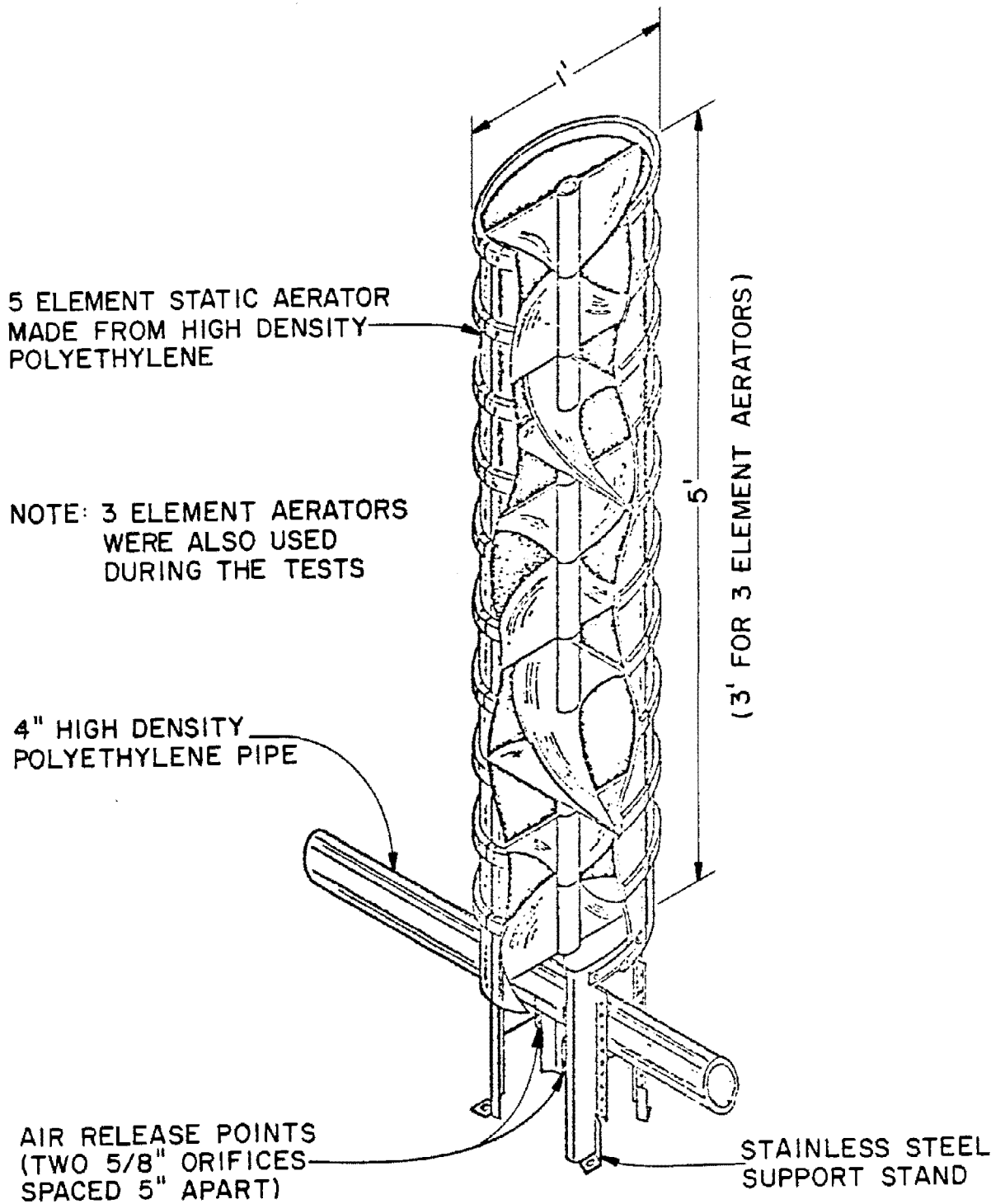
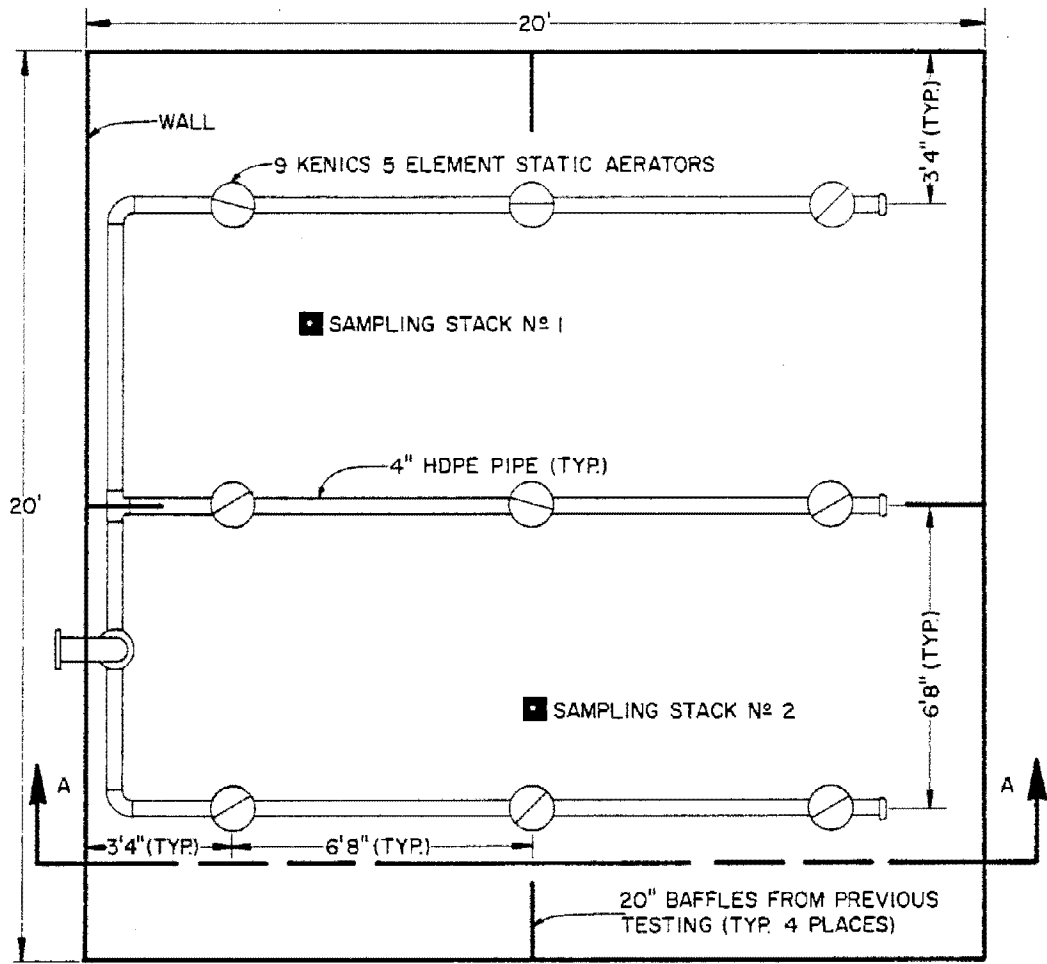
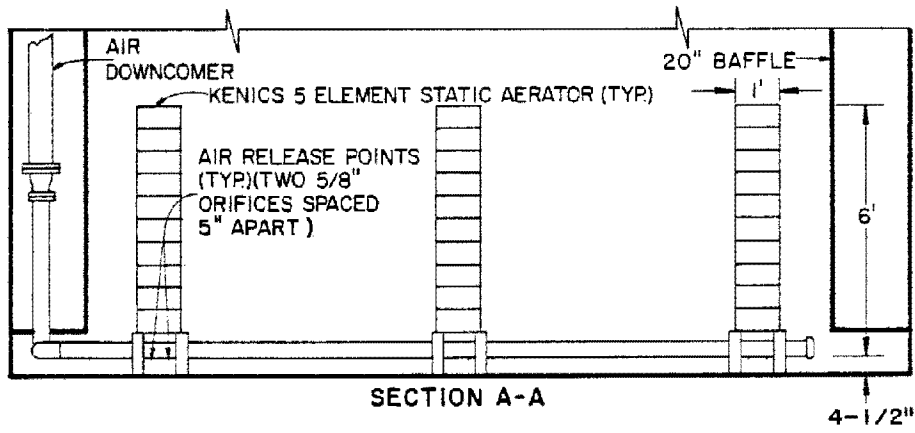


Figure 17. Kenics static tube aerator.



PLAN



SECTION A-A

Figure 18. Test tank configuration for the Kenics static tube aeration system at the 20- and 25-ft water depths.

action of the spring; the loss through the holes is almost insignificant by comparison. The spring opening is dependent on the magnitude of the airflow rate, thus the term "variable orifice." This also means that the diffuser has a somewhat flat headloss-airflow curve, which can be considered very desirable if a wide range of flow rates is to be encountered.

The variable orifice diffuser was manufactured by C-E Bauer of Combustion Engineering, Inc. The variable orifice diffuser was available in a number of different models. The diffuser was composed of a stainless steel channel approximately 38 mm (1.5 in.) square and had a number of thin, flat leaf springs mounted over holes in the channel. Different models had different numbers of springs per diffuser. Models with two and three springs per diffuser were tested in this study. A three-spring model is shown in Figure 19. Springs were 17 cm (6-3/4 in.) long by 3 cm (1-3/16 in.) wide and, for this testing, were 0.5 mm (0.02 in.) thick. Each spring was manufactured to maintain a 227-g (8-oz) spring tension. Each spring covered a total of four 2.2-cm (7/8-in.) diameter holes through which air passed. Springs were attached to the channel by means of rivets, which served as pivot points for the spring.

This manufacturer elected to use two configurations in the evaluation. At the 3.0- and 6.1-m (10- and 20-ft) SWDs, ten Model II Airpac diffusers were mounted on a central header (Figure 20). At the SWDs of 4.6 and 7.6 m (15 and 25 ft), eight Model III Airpac diffusers were mounted on a central header (Figure 21). This system was mounted across the tank center and supported by wall-mounted hangers.

The testing power densities selected by the manufacturer were 13.2, 26.3, and 39.5 W/m³ (0.5, 1.0, and 1.5 hp/1000 ft³). System aeration rates ranged from 55 to 190 L/sec (118 to 404 scfm). Corresponding airflow rates per diffuser ranged from 5.7 to 19 L/sec (12 to 40 scfm). Diffuser headlosses for the system ranged from 27 cm (10.7 in.) to 59 cm (23.2 in.) of water. The diffuser discharged air 23 cm (9.2 in.) above the tank floor for both configurations.

FIXED ORIFICE COARSE BUBBLE DIFFUSERS - D-24

This fixed orifice coarse bubble diffuser was manufactured by Sanitaire - Water Pollution Control Corporation. The company referred to this unit as the Model D-24 stainless steel non-clog diffuser. The unit was a fixed orifice coarse bubble diffuser and was fabricated of stainless steel sheet stock. It was somewhat tubular in appearance and was 61 cm (24 in.) in length (Figure 22). A total of 24 holes was cut along the length of the tube on the sides; 12 holes were 4.8 mm (3/16 in.) in diameter, and 12 holes were 9.5 mm (3/8 in.) in diameter. For the most part, the smaller holes were located on a horizontal line above that of the larger holes. In addition to the holes, an open slot 9.5 mm (3/8 in.) wide on both sides of the tube below the level of the holes was provided. Air was discharged through

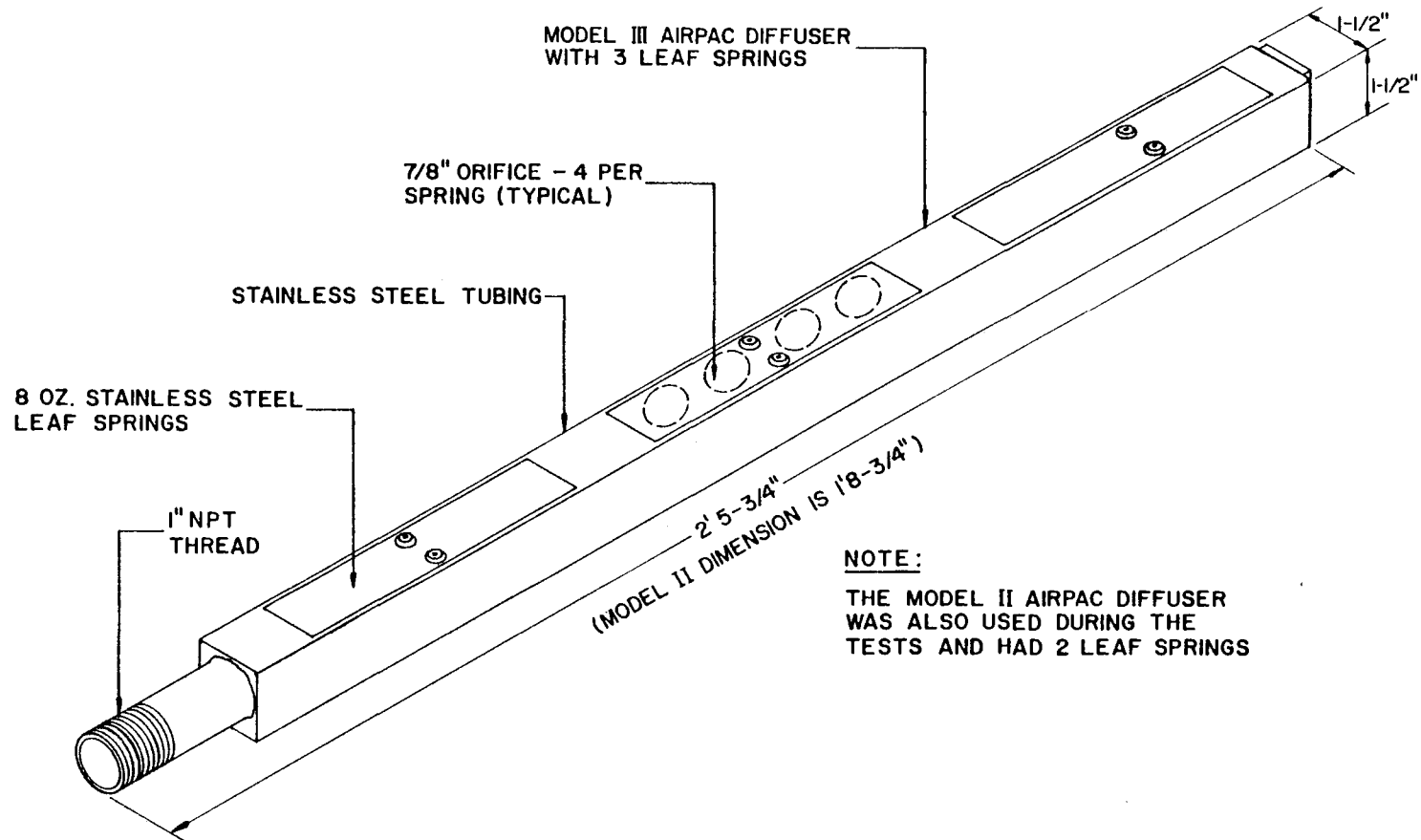


Figure 19. Bauer Airpac diffuser.

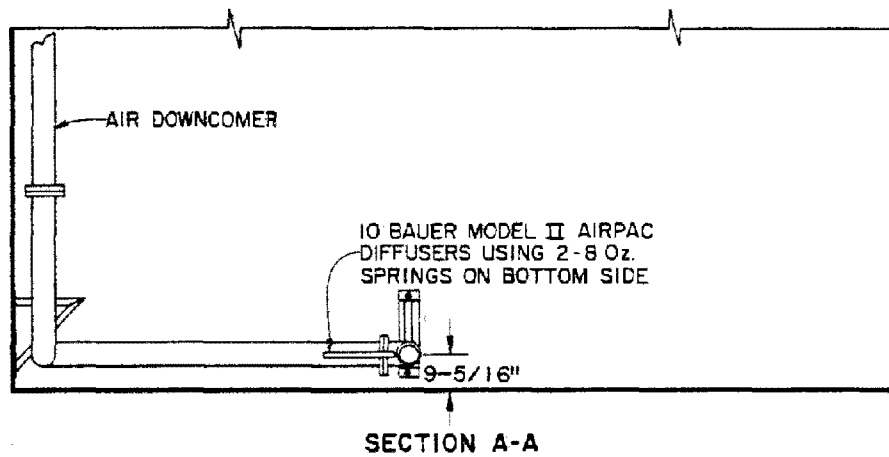
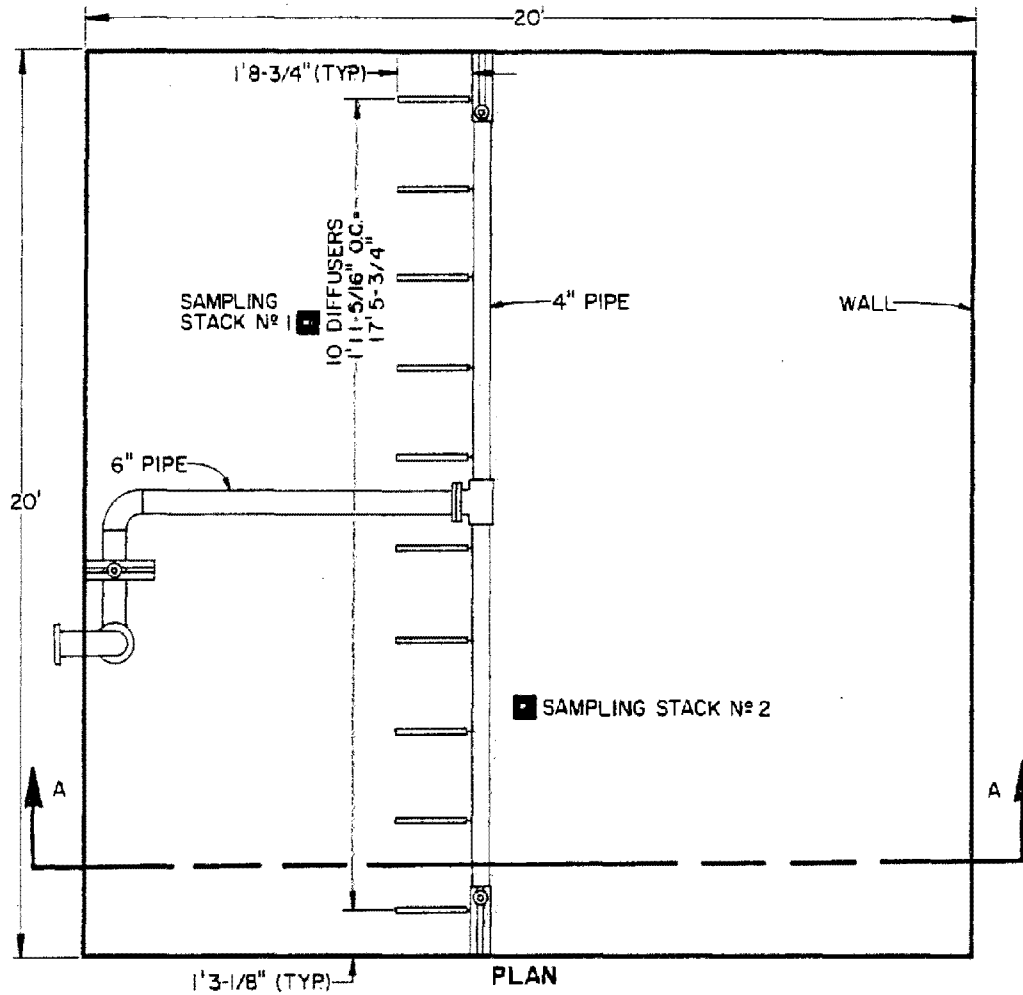


Figure 20. Test tank configuration for the Bauer Model II Airpac aeration system at the 10- and 20-ft water depths.

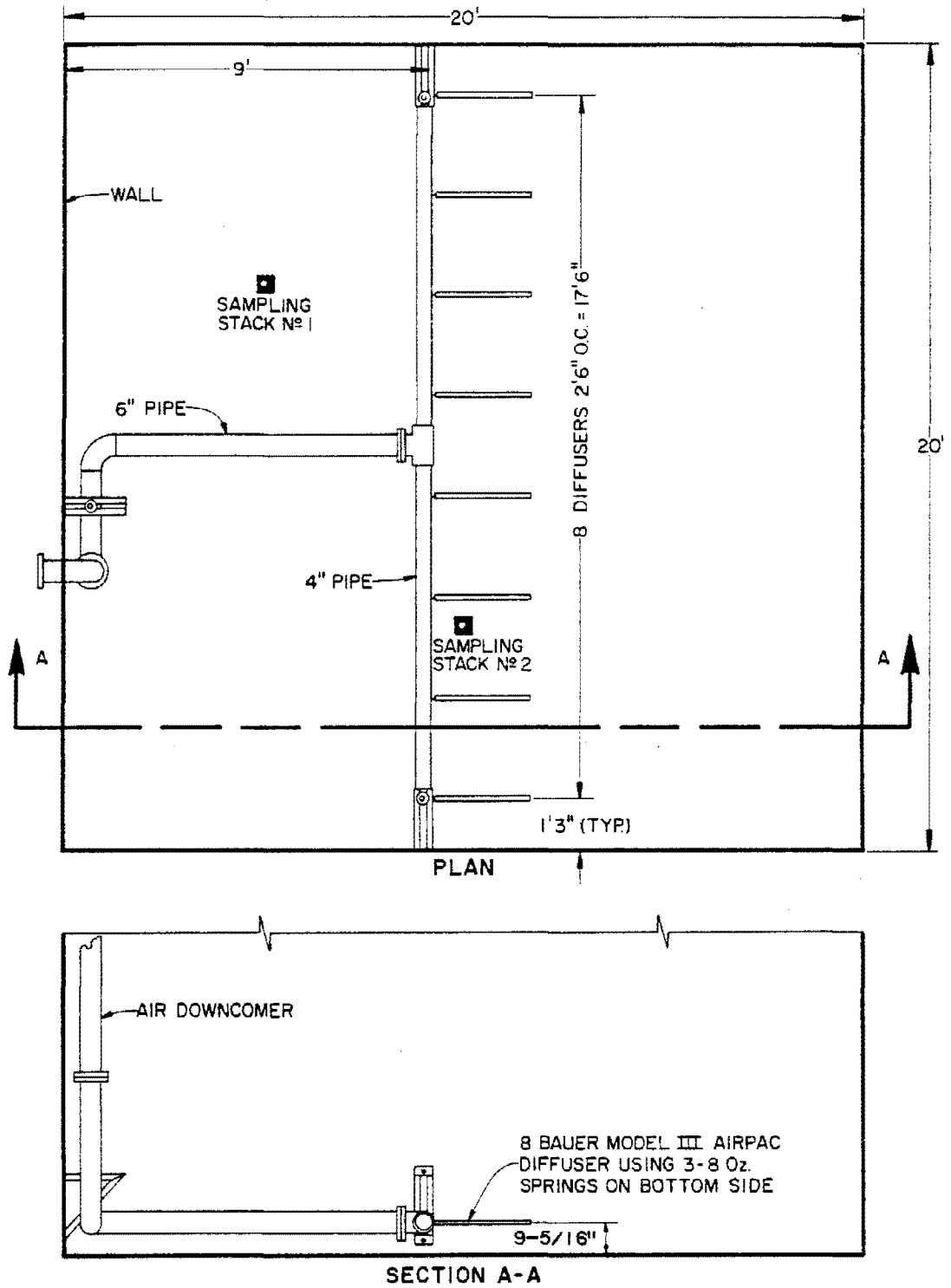
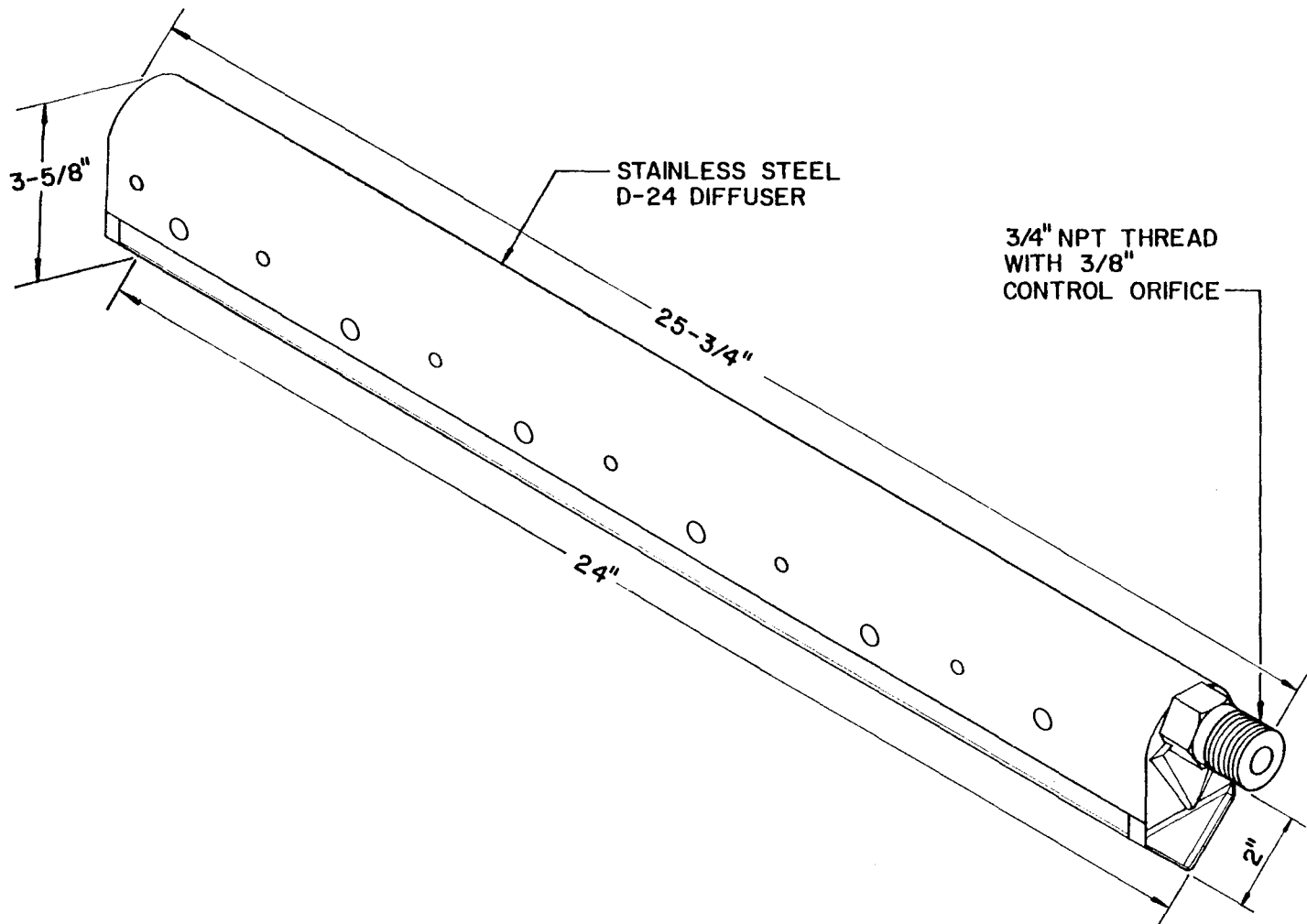


Figure 21. Test tank configuration for the Bauer Model III Airpac aeration system at the 15- and 25-ft water depths.



64

Figure 22. Sanitaire D-24 diffuser.

these openings. As low airflow rates increased, air began to discharge through the larger holes and slots. For the four testing depths, the manufacturer chose two configurations. At the 3.0- and 6.1-m (10- and 20-ft) SWDs, a 24 diffuser floor coverage layout was chosen (Figure 23). At the 4.6- and 7.6-m (15- and 25-ft) SWDs, the manufacturer chose to test a single, center-mounted, wide-band layout using 30 diffusers (Figure 24). The system was attached to the steel tank walls for support. The air discharge point was 16 cm (6.4 in.) above the floor.

The nominal power densities selected by the manufacturer were 13.2, 26.3, and 39.5 W/m³ (0.5, 1.0, and 1.5 hp/1000 ft³). Airflow rates ranged from 54 to 190 L/sec (115 to 402 scfm). Corresponding airflow rates per diffuser were 1.8 to 6.3 L/sec (3.8 to 13.4 scfm). Each diffuser used a 9.53-mm (3/8-in.) control orifice. Diffuser headlosses for the system ranged from 3.6 cm (1.4 in.) to 88 cm (34.6 in.) of water.

FIXED ORIFICE COARSE BUBBLE DIFFUSERS - SUPERFUSER

This system was a fixed orifice coarse bubble diffuser manufactured by Envirex, Inc. The company name for this diffuser was the Superfuser. A sketch of the diffuser is shown in Figure 25. Each diffuser consisted of a plenum chamber made out of molded resin material with 16 6.4-mm (1/4-in.) diameter holes drilled at two different elevations in the chamber wall. The bottom of each diffuser was completely open and was located 17.3 cm (6.8 in.) below the level of the lowest row of holes in the plenum chamber wall. The diffuser was open at the bottom to insure that air would always be supplied to the aeration tank, even in the remote case where the upper holes became plugged. During normal operation, all the air escaped through the drilled holes in the plenum chamber; none escaped out of the bottom of the diffuser. At all four testing depths, this company chose a single configuration. The installation consisted of a single-row, center-mounted diffuser configuration (Figure 26). Ten equally spaced superfusers were mounted on the center header. The header was supported by floor mounts so as to release air at an elevation of 32 cm (12.7 in.) above the tank floor. For the installation tested, no control orifices were used. With the exception of the floor stands, all parts of this system were non-metallic.

The nominal power density testing levels chosen by the manufacturer were 13.2, 26.3, and 39.5 W/m³ (0.5, 1.0, and 1.5 hp/1000 ft³). Air ranges ranged from 56 to 189 L/sec (119 to 400 scfm). Corresponding airflow rates per diffuser were from 5.7 to 19 L/sec (12 to 40 scfm). Diffuser headlosses for the system ranged from 4.1 cm (1.6 in.) to 29 cm (11.5 in.) of water.

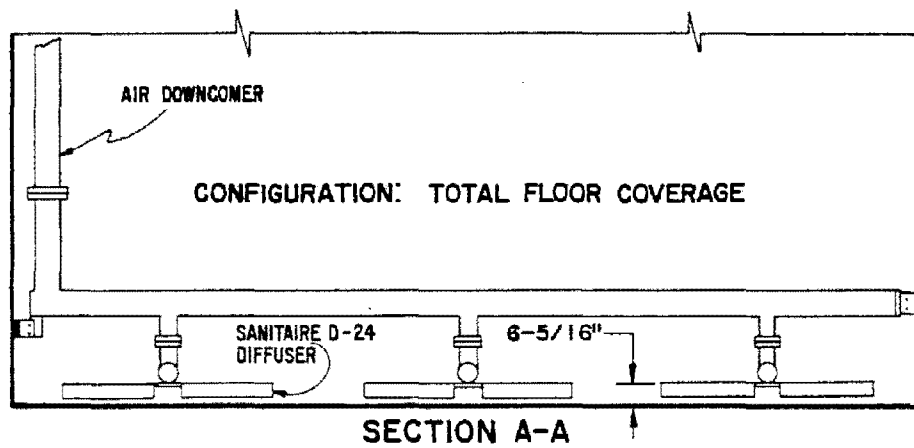
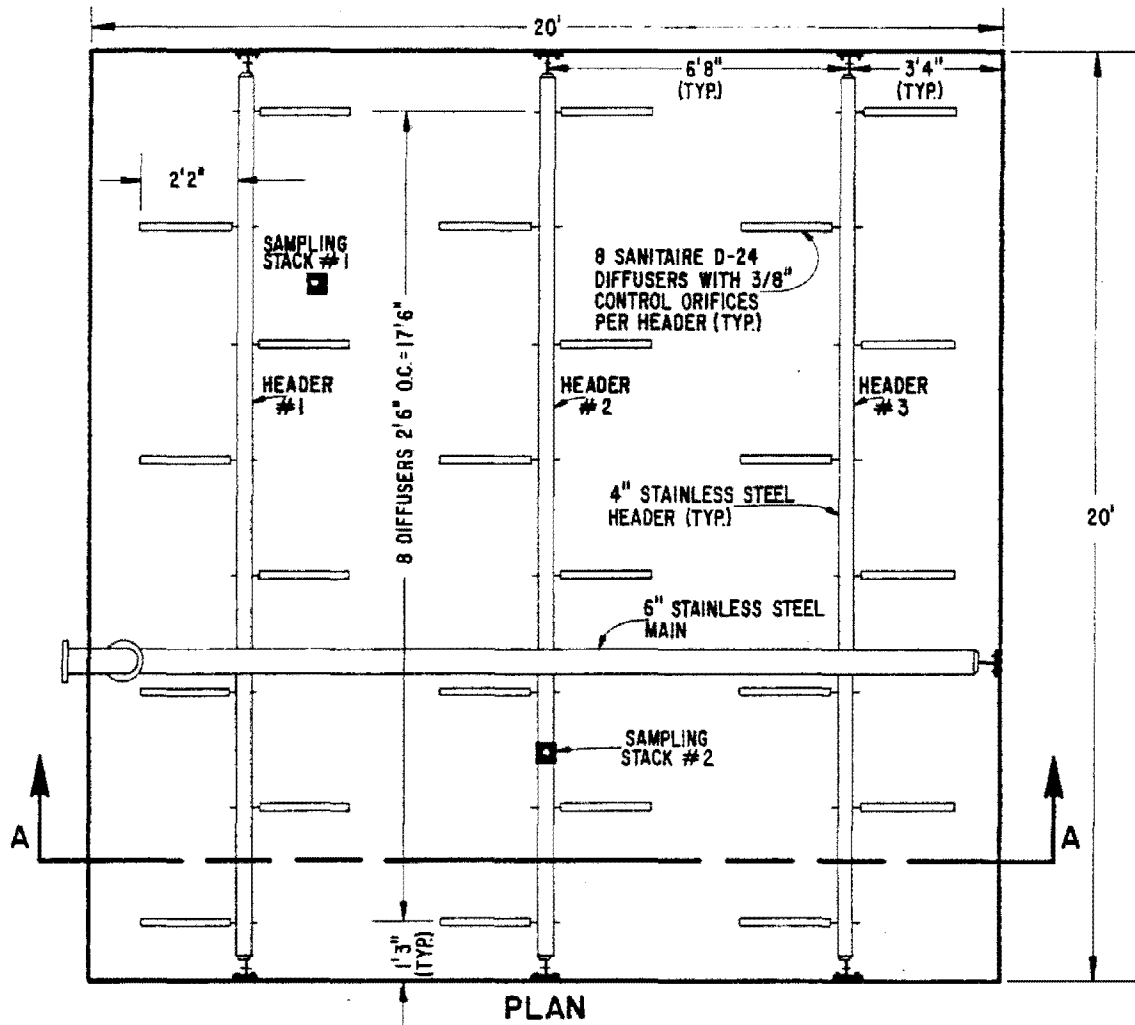


Figure 23. Test tank configuration for the Sanitaire D-24 aeration system at the 10- and 20-ft water depths.

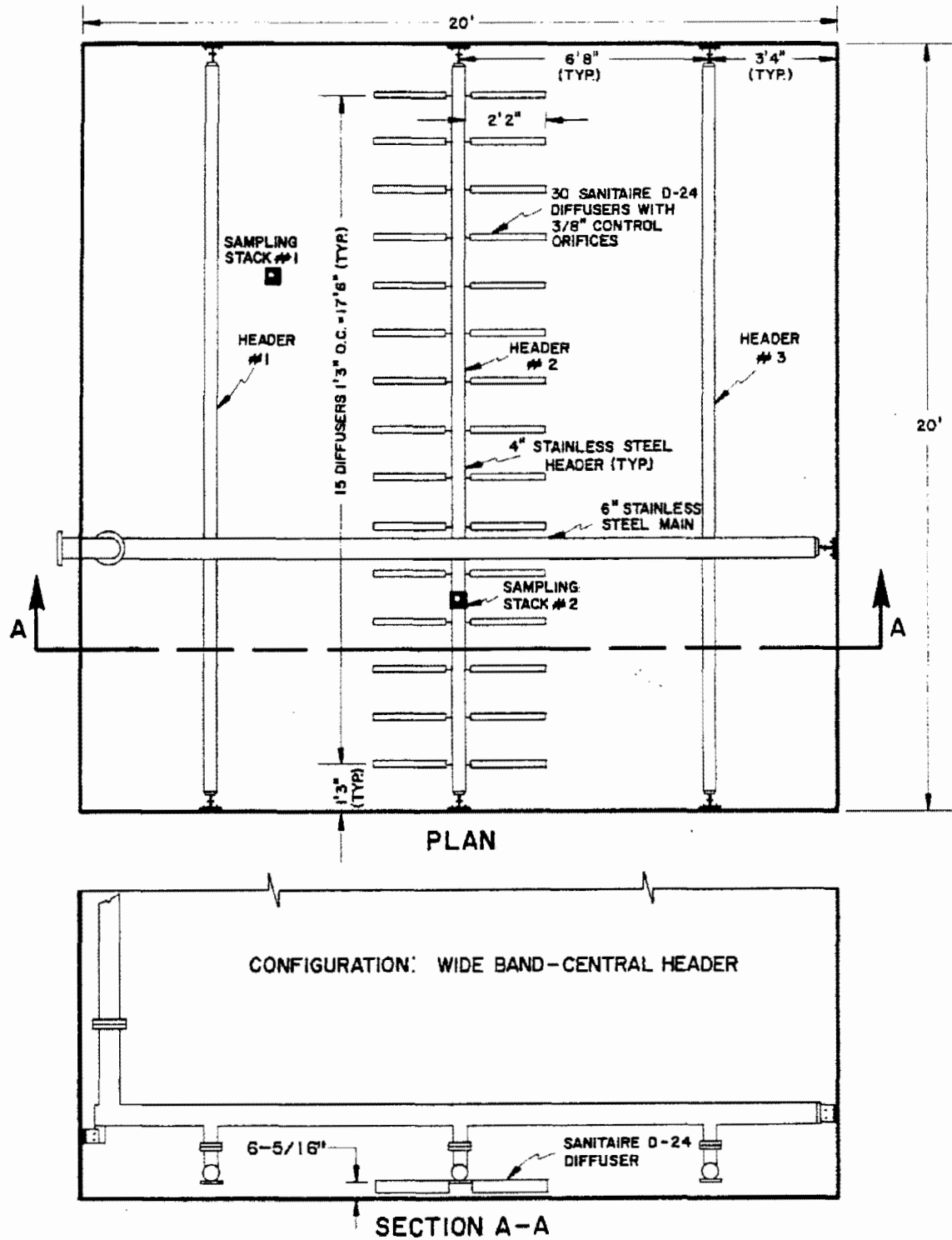


Figure 24. Test tank configuration for the Sanitaire D-24 aeration system at the 15- and 25-ft water depths.

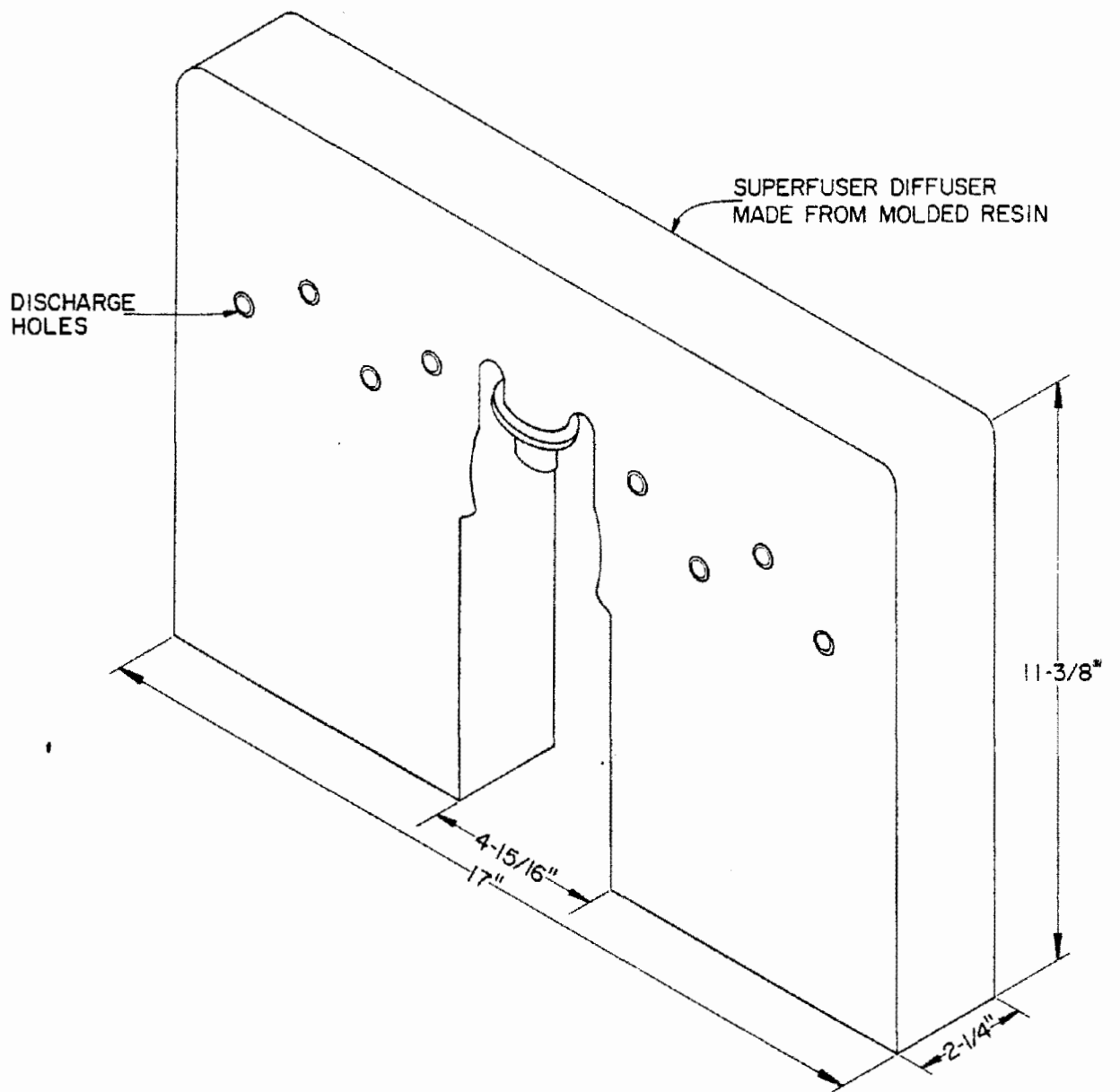


Figure 25. Envirex Superfuser diffuser.

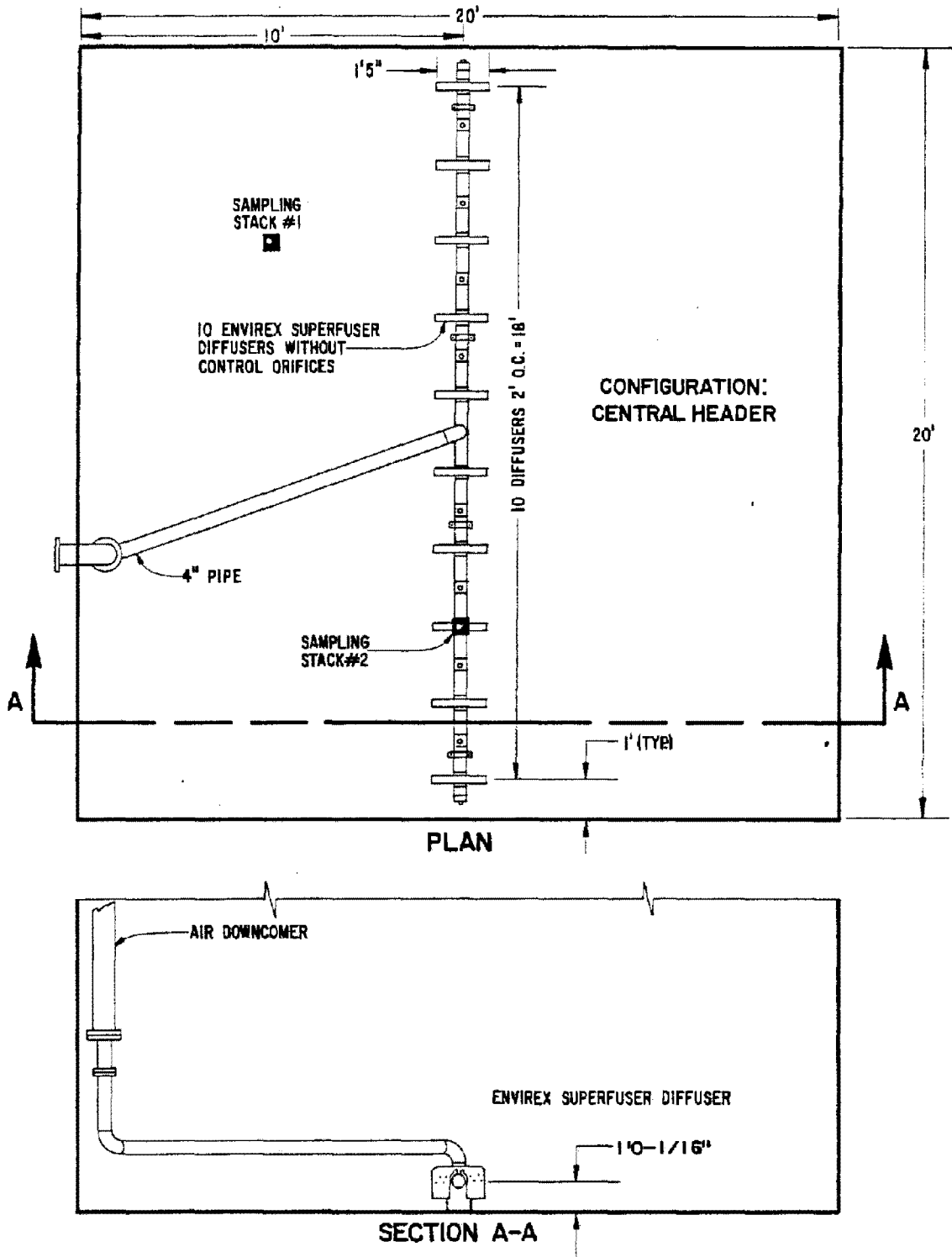


Figure 26. Test tank configuration for the Envirex Superfuser aeration system.

FIXED ORIFICE COARSE BUBBLE DIFFUSERS - DEFLECTOFUSER

Near the conclusion of this study, it was decided that the inclusion of a common coarse bubble diffuser would be worthwhile. The Deflectofuser was chosen because this simple sparger-type diffuser is commonly used throughout the industry and in LACSD facilities.

In a separate LACSD study, the sparger was tested in both dual aeration and single-side aeration configurations. This comparison study also investigated the use of wide-band width configurations using 20 diffusers in one case and 40 diffusers in the other case. The configuration yielding the best results, dual aeration using 40 diffusers, was tested in this study.

The Deflectofuser is a fixed orifice coarse bubble diffuser manufactured by the FMC Corporation (Figure 27). The installation consisted of 40 Deflectofusers, with 20 mounted on each header (Figure 28). It should be noted that this configuration was designed by the LACSD engineering staff and not the equipment manufacturer. The unit was made of acrylonitrile butadiene styrene (ABS) plastic. It measured 7.6 cm (3 in.) in diameter and 5.6 cm (2-3/16 in.) in height. Air was discharged through a discharge ring of four jets 9.5 mm (3/8 in.) in diameter at right angles to the adjacent openings. Each diffuser had an 8.7-cm (11/32-in.) orifice and was directly mounted to a 19.0-mm (3/4-in.) NPT 90° pipe elbow. Diffusers were mounted on both sides of the header using pipe nipples of 25-cm (10-in.) and 51-cm (20-in.) lengths alternately. The air release point of this system was at an elevation of 69 cm (27.1 in.) above the tank floor. This installation was supported by floor stands.

The system was tested at only the 4.6-m (15-ft) SWD at nominal power densities of 13.2, 26.3, and 39.5 W/m³ (0.5, 1.0, and 1.5 hp/1000 ft³). Air rates for this installation ranged from 63 to 188 L/sec (134 to 398 scfm). Corresponding airflow rates per diffuser were 1.6 to 4.7 L/sec (3.4 to 10 scfm). Diffuser headlosses for the system ranged from 8.1 cm (3.2 in.) to 52 cm (20.4 in.) of water.

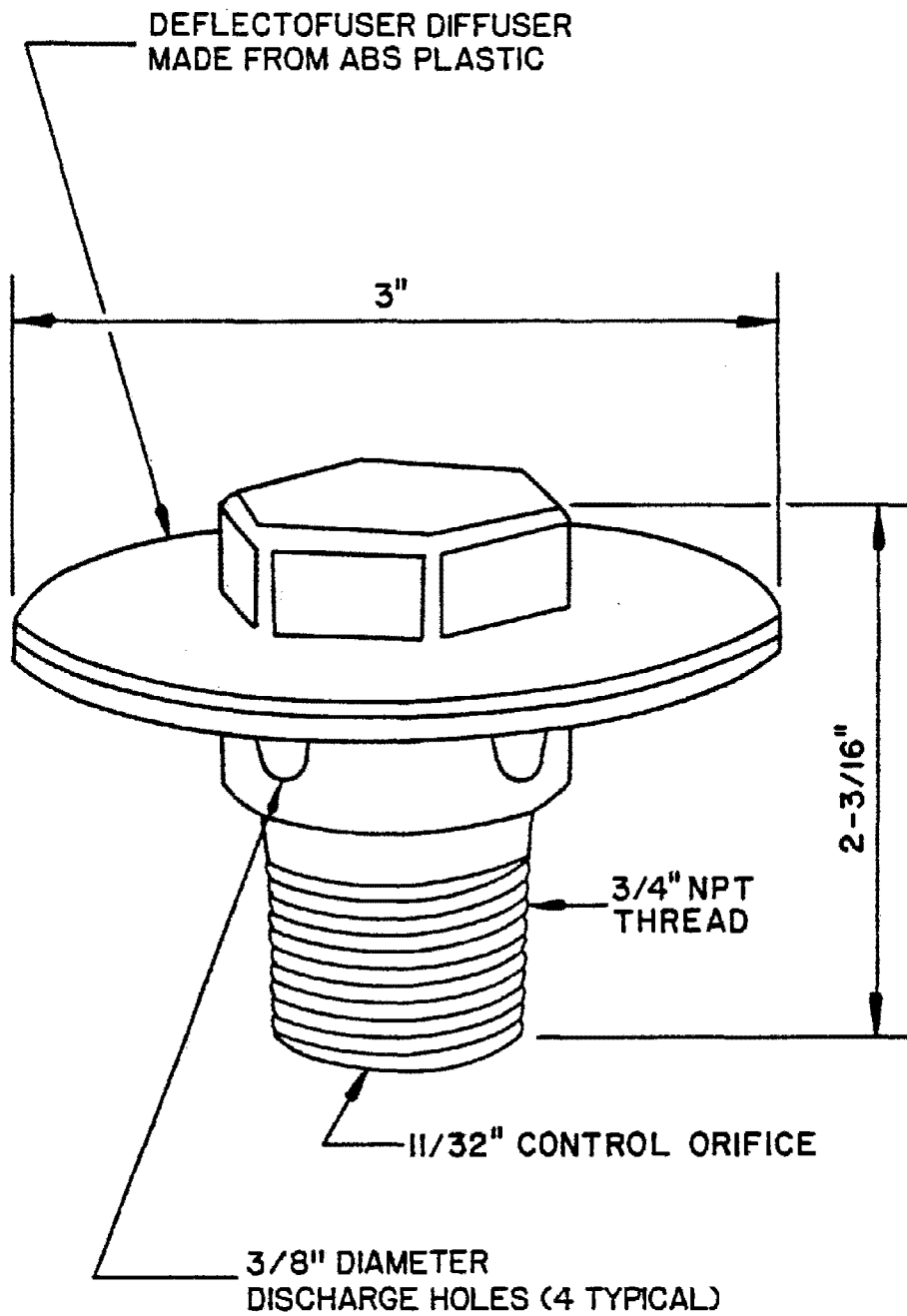


Figure 27. FMC Deflectofuser diffuser.

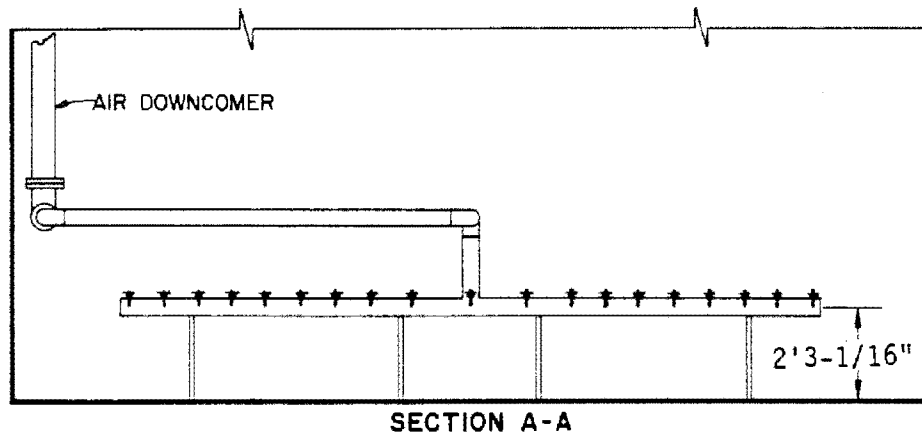
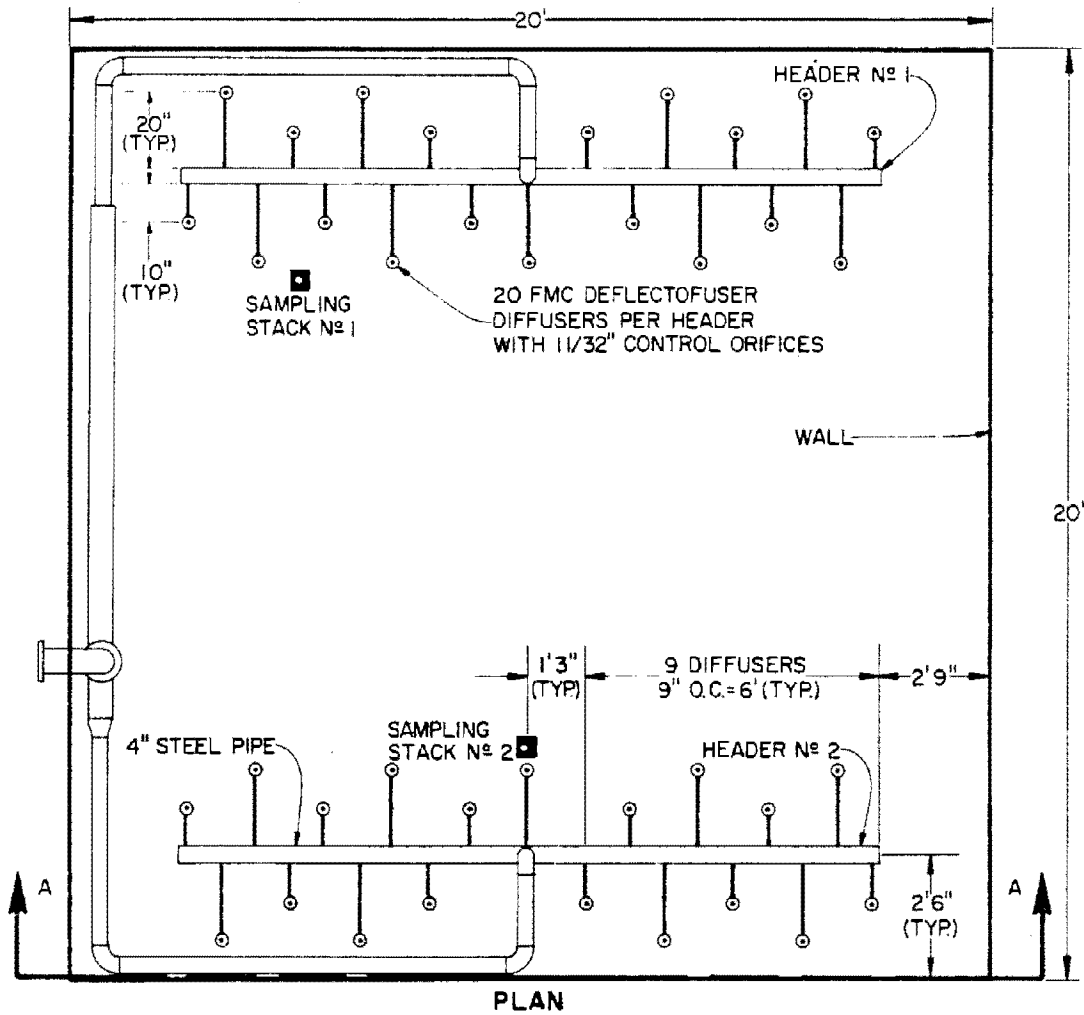


Figure 28. Test tank configuration for the FMC Deflectofuser (Sparger) aeration system at the 15-ft water depth.

SECTION 6

TEST RESULTS

OVERVIEW

Before proceeding with a discussion of test results, it is important to realize the limitations of clean water test data. Clean water data alone cannot be used to predict oxygen transfer performance in mixed liquor. To relate clean water oxygen transfer results to anticipated aerator performance in mixed liquor, two correction factors are required. The first factor, alpha (α), is the oxygen transfer coefficient correction factor. The second factor, beta (β), is the oxygen saturation correction factor. These correction factors are applied to the basic aeration equation as follows:

$$dC/dt = \alpha K_L a (\beta C^* - C) \quad (33)$$

Only with accurate alpha and beta factors, used in conjunction with clean water data, can successful prediction of oxygen transfer performance in activated sludge be achieved. It is important to stress that alpha factors, the ratio of wastewater $K_L a$ to clean water $K_L a$, vary widely as a function of the type of aeration device, wastewater characteristics and degree of prior treatment, aeration system configuration, aeration tank geometry, and other considerations. For the type of equipment tested during this study, alpha factors from 0.35 to 0.95 have been reported. This variation is significant and could cause the relative performance of the oxygen transfer devices in mixed liquor to be completely different than as indicated in clean water.

The results obtained in this clean water study are accurate. It should be stressed, however, that the data were obtained under very specific conditions of test medium, tank geometry, and diffuser configuration, utilizing specific test procedures and data analysis techniques. The results could have been much different under different conditions, not only from an absolute standpoint, but in terms of the comparison between the various generic oxygen transfer devices. Changing conditions, such as the test medium or tank geometry, could affect the performance of one generic device to a greater extent than that of another.

Equipment efficiency may be affected by testing liquid characteristics; consequently, it is common to specify a manufacturer's compliance using clean water tests. Because a clean water test is repeatable, it may be used to demonstrate general trends in aeration

performance with regard to airflow rates, diffuser location, tank geometry, and other parameters. When the aerator's alpha and beta factors are known for a particular wastewater, clean water tests also provide meaningful data for activated sludge aeration system design. Even then, the flow regime used will have a significant effect on alpha. For example, alpha will tend to approach a constant value throughout a completely mixed aeration tank, whereas it will increase from inlet to outlet of a plug flow tank as the influent wastewater becomes progressively more treated.

TABULAR PRESENTATIONS

Presentation of Analysis Results for the Exponential and Equilibrium Methods

Tables 3 through 18 contain the results produced by the eight aeration systems tested in this study. For each system, two tables of results are presented. The tables contain the results of analysis by both the Exponential and the Equilibrium methods of analysis. While the primary analysis method is the Exponential method, results of analysis by the second method are supplied for comparison purposes. Every table is generally composed of the same columns; an extra column is supplied for the jet aeration system results. In the first five or six columns, information is supplied that identifies and characterizes the tests. These columns are Date, Run, Water Depth, Delivered Power Density, and Airflow Rate. For the jet aeration system, the Delivered Pump-Air Power Split is also indicated. The column identified as "Date" refers to the date on which a test was conducted. "Run" differentiates between tests taking place on the same day. Run Nos. 1, 2, 3, and 4 were conducted in that order. "Water Depth" is the measured aeration tank water depth during aerator testing (inflated condition). "Delivered Power Density", "Airflow Rate", and "Delivered Pump-Air Power Split" are as described earlier in this report. The last five columns summarize results of analysis. These columns are $K_L a_{20}$, C^*_O , Standard Oxygen Transfer Efficiency, and Standard Delivered and Standard Wire Aeration Efficiencies. Data presented in the tables are expressed in U.S. customary units. Factors for the conversion of U.S. customary units to SI units are supplied in the front of this report.

Comparison of Analysis Results for the Exponential and Equilibrium Methods

As indicated above, data obtained in this study were evaluated by the Equilibrium and the Exponential methods of analysis, although the primary analysis method chosen was the Exponential method. Review of the results showed that the difference between results obtained by the two analysis methods is small.

To evaluate the agreement of the results obtained using the two analysis methods, the following procedure was used. For each test, the result obtained by the Exponential method was divided by the result obtained by the Equilibrium method. These ratios were then analyzed to obtain the mean ratio and standard deviation. Data that were compared in

TABLE 3. SUMMARY OF EXPONENTIAL METHOD RESULTS: NORTON FINE BUBBLE DOME DIFFUSERS

Date	Run	Water Depth (ft)	Delivered ¹ Power Density (hp/1000 ft ³)	Air- flow Rate (scfm)	K _L a ₂₀ ² (1/hr)	C* _O (mg/L)	Standard Oxygen Transfer Efficiency (%)	Standard ³ Aeration Efficiency (lb O ₂ /hp-hr)	
								Delivered	Wire
03/24/78	1	25	0.28	73.8	5.34	11.42	49.48	13.44	8.22
04/21/78	1	10	0.57	125.8	11.31	9.81	21.30	12.10	7.40
04/24/78	1	10	0.32	73.9	7.17	9.88	23.20	13.95	8.53
04/25/78	1	15	0.31	74.5	6.41	10.24	32.03	13.37	8.18
04/26/78	1	15	0.54	126.0	9.87	10.45	29.71	11.98	7.33
04/27/78	1	15	1.24	253.4	17.66	10.60	26.61	9.33	5.71
05/04/78	1	20	0.51	126.9	9.47	11.12	39.81	12.72	7.78
05/05/78	1	20	1.15	256.1	16.39	11.02	33.80	9.68	5.92
05/08/78	1	25	1.16	272.4	14.61	11.67	37.16	9.11	5.57
05/09/78	1	25	0.50	127.5	8.54	11.65	46.69	12.46	7.62
05/10/78	1	20	0.30	76.3	6.07	11.33	43.55	14.17	8.66
05/15/78	1	10	1.37	248.3	19.30	10.17	19.14	8.94	5.47
05/16/78	1	20	0.30	75.0	5.82	11.44	42.85	13.96	8.54

1. The delivered horsepower numbers are based on the adiabatic compression equation. Standard ambient conditions of 20°C, 14.70 psia, and 36% relative humidity have been used. Blower inlet and discharge pressures were determined in accordance with Equations 4 and 6.
2. Based on the Exponential model analysis using Winkler data.
3. The wire horsepower used in this analysis is related to delivered horsepower by a blower efficiency of 0.70, a coupling efficiency of 0.95, and a motor efficiency of 0.92 (an overall or combined efficiency of 0.612).

TABLE 4. SUMMARY OF EQUILIBRIUM METHOD RESULTS: NORTON FINE BUBBLE DOME DIFFUSERS

Date	Run	Water Depth (ft)	Delivered ¹ Power Density (hp/1000 ft ³)	Air- flow Rate (scfm)	K _L a ₂₀ ² (1/hr)	C* _o (mg/L)	Standard Oxygen Transfer Efficiency (%)	Standard ³ Aeration Efficiency (lb O ₂ /hp-hr)	
								Delivered	Wire
03/24/78	1	25	0.28	73.8	5.36	11.42	49.60	13.47	8.24
04/21/78	1	10	0.57	125.8	11.64	9.72	21.72	12.34	7.55
04/24/78	1	10	0.32	73.9	7.18	9.88	23.21	13.96	8.54
04/25/78	1	15	0.31	74.5	6.22	10.36	31.40	13.10	8.01
04/26/78	1	15	0.54	126.0	9.92	10.40	29.70	11.98	7.33
04/27/78	1	15	1.24	253.4	17.95	10.53	26.87	9.42	5.76
05/04/78	1	20	0.51	126.9	9.57	11.08	40.10	12.81	7.83
05/05/78	1	20	1.15	256.1	16.33	10.97	33.94	9.71	5.94
05/08/78	1	25	1.16	272.4	14.72	11.66	37.42	9.18	5.61
05/09/78	1	25	0.50	127.5	8.42	11.73	46.36	12.37	7.57
05/10/78	1	20	0.30	76.3	6.21	11.25	44.27	14.40	8.81
05/15/78	1	10	1.37	248.3	19.93	10.07	19.58	9.15	5.59
05/16/78	1	20	0.30	75.0	5.85	11.40	42.88	13.97	8.54

1. The delivered horsepower numbers are based on the adiabatic compression equation. Standard ambient conditions of 20°C, 14.70 psia, and 36% relative humidity have been used. Blower inlet and discharge pressures were determined in accordance with Equations 4 and 6.
2. Based on the Equilibrium model analysis using Winkler data.
3. The wire horsepower used in this analysis is related to delivered horsepower by a blower efficiency of 0.70, a coupling efficiency of 0.95, and a motor efficiency of 0.92 (an overall or combined efficiency of 0.612).

TABLE 5. SUMMARY OF EXPONENTIAL METHOD RESULTS: FMC FINE BUBBLE TUBE DIFFUSERS

Date	Run	Water Depth (ft)	Delivered ¹ Power Density (hp/1000 ft ³)	Air- flow Rate (scfm)	K _L a ₂₀ ² (1/hr)	C* _O (mg/L)	Standard Oxygen Transfer Efficiency (%)	Standard ³ Aeration Efficiency (lb O ₂ /hp-hr)	
								Delivered	Wire
08/29/78	1	10	2.02	412.2	17.46	9.87	10.06	5.29	3.23
08/29/78	2	10	1.16	276.6	13.37	9.99	11.68	7.14	4.37
08/29/78	3	10	0.54	142.1	7.63	10.05	12.95	8.86	5.42
08/30/78	1	25	1.66	414.5	14.99	11.23	23.93	6.23	3.81
08/30/78	2	25	1.07	281.1	11.12	11.26	24.40	7.25	4.44
08/30/78	3	25	0.51	139.0	6.39	11.54	31.71	8.99	5.50
09/29/78	1	10	1.19	277.6	13.39	9.98	11.61	6.99	4.27
02/08/79	1	15	1.81	408.6	16.61	10.50	15.34	5.94	3.63
02/08/79	2	15	1.05	264.4	11.90	10.54	17.07	7.36	4.51
02/08/79	3	15	0.51	136.0	6.88	10.63	19.87	9.12	5.58
02/09/79	1	20	1.74	417.4	16.73	10.80	20.69	6.39	3.91
02/09/79	2	20	1.08	277.5	11.62	11.05	22.17	7.37	4.51
02/09/79	3	20	0.49	131.8	6.10	11.19	25.04	8.69	5.31

1. The delivered horsepower numbers are based on the adiabatic compression equation. Standard ambient conditions of 20°C, 14.70 psia, and 36% relative humidity have been used. Blower inlet and discharge pressures were determined in accordance with Equations 4 and 6.
2. Based on the Exponential model analysis using Winkler data.
3. The wire horsepower used in this analysis is related to delivered horsepower by a blower efficiency of 0.70, a coupling efficiency of 0.95, and a a motor efficiency of 0.92 (an overall or combined efficiency of 0.612).

TABLE 6. SUMMARY OF EQUILIBRIUM METHOD RESULTS; FMC FINE BUBBLE TUBE DIFFUSERS

Date	Run	Water Depth (ft)	Delivered ¹ Power Density (hp/1000 ft ³)	Air- flow Rate (scfm)	K _L a ₂₀ ² (1/hr)	C* _O (mg/L)	Standard Oxygen Transfer Efficiency (%)	Standard ³ Aerston Efficiency (lb O ₂ /hp-hr)	
								Delivered	Wire
08/29/78	1	10	2.02	412.2	17.19	9.96	10.00	5.26	3.21
08/29/78	2	10	1.16	276.6	13.02	9.96	11.34	6.93	4.24
08/29/78	3	10	0.54	142.1	8.05	9.86	13.41	9.18	5.61
08/30/78	1	25	1.66	414.5	15.49	11.10	24.44	6.36	3.89
08/30/78	2	25	1.07	281.1	11.26	11.21	26.62	7.30	4.47
08/30/78	3	25	0.51	139.0	6.53	11.47	32.16	9.12	5.58
09/29/78	1	10	1.19	277.6	13.38	9.95	11.57	6.96	4.26
02/08/79	1	15	1.81	408.6	16.78	10.47	15.44	5.98	3.66
02/08/79	2	15	1.05	264.4	12.10	10.49	17.28	7.45	4.56
02/08/79	3	15	0.51	136.0	7.01	10.56	20.09	9.22	5.64
02/09/79	1	20	1.74	417.4	16.86	10.81	20.87	6.45	3.94
02/09/79	2	20	1.08	277.5	11.87	10.90	22.32	7.42	4.54
02/09/79	3	20	0.49	131.8	6.35	11.00	25.64	8.89	5.44

1. The delivered horsepower numbers are based on the adiabatic compression equation. Standard ambient conditions of 20°C, 14.70 psia, and 36% relative humidity have been used. Blower inlet and discharge pressures were determined in accordance with Equations 4 and 6.
2. Based on the Equilibrium model analysis using Winkler data.
3. The wire horsepower used in this analysis is related to delivered horsepower by a blower efficiency of 0.70, a coupling efficiency of 0.95, and a motor efficiency of 0.92 (an overall or combined efficiency of 0.612).

TABLE 7. SUMMARY OF EXPONENTIAL METHOD RESULTS: PENTECH JET AERATORS

Date	Run	Water Depth (ft)	Delivered ¹	Air-flow Rate (scfm)	Delivered	K_{La20} ² (1/hr)	C* _o (mg/L)	Oxygen Transfer Efficiency (%)	Standard ³ Aeration Efficiency (lb O ₂ /hp-hr)	
			Power Density (hp/1000 ft ³)		Pump/Air Power Split (%/%)				Delivered	Wire
07/05/78	1	25	1.56	336.2	82.2/17.8	12.23	11.29	23.85	5.36	3.36
07/07/78	1	20	1.62	322.4	78.7/21.3	12.83	10.99	20.83	5.34	3.36
07/07/78	2	20	0.96	170.8	64.4/35.6	7.95	11.10	24.98	5.72	3.67
07/07/78	3	20	0.51	52.9	33.9/66.1	3.24	11.22	32.85	4.41	2.95
07/08/78	1	25	0.48	64.3	44.2/55.8	3.46	11.97	37.79	5.22	3.44
07/08/78	2	25	1.01	202.1	72.4/27.6	8.82	11.41	29.44	6.19	3.92
07/10/78	2	10	1.89	329.3	77.8/22.2	10.98	9.68	7.84	3.53	2.23
07/10/78	3	10	0.50	32.7	18.6/81.4	2.52	10.35	18.24	3.04	2.09
07/12/78	1	15	1.64	302.9	81.2/18.8	12.26	10.34	15.26	4.78	3.00
07/19/78	1	15	1.03	180.2	69.9/30.1	7.56	10.68	16.12	4.86	3.09
07/20/78	1	15	0.51	54.6	39.1/60.9	3.23	11.11	23.80	4.40	2.93
07/27/78	1	15	1.63	300.4	80.7/19.3	12.05	10.42	15.01	4.74	2.97
07/28/78	1	15	1.02	176.7	69.3/30.7	7.84	10.61	17.12	5.13	3.27
08/01/78	1	10	1.17	203.4	64.4/35.6	7.76	9.76	9.10	4.08	2.62
08/01/78	2	10	0.59	54.5	29.3/70.7	3.16	10.07	14.19	3.41	2.30
08/09/78	1	25	0.49	65.2	44.3/55.7	3.14	11.94	34.35	4.78	3.15
08/14/78	1	25	0.49	65.6	44.5/55.5	3.28	11.96	35.49	4.95	3.26
08/16/78	1	20	0.50	49.3	32.0/68.0	2.89	11.41	31.73	4.08	2.74

1. The delivered horsepower numbers are based on the adiabatic compression equation. Standard ambient conditions of 20°C, 14.70 psia, and 36% relative humidity have been used. Blower inlet and discharge pressures were determined in accordance with Equations 4 and 6.
2. Based on the Exponential model analysis using Winkler data.
3. The wire horsepower used in this analysis is related to delivered horsepower by a blower efficiency of 0.70, a coupling efficiency of 0.95, and a motor efficiency of 0.92 (an overall or combined efficiency of 0.612).

TABLE 8. SUMMARY OF EQUILIBRIUM METHOD RESULTS: PENTECH JET AERATORS

Date	Run	Water Depth (ft)	Delivered ¹	Air-flow Rate (scfm)	Delivered	$K_L a_{20}$ ² (1/hr)	C^*_O (mg/L)	Oxygen Transfer Efficiency (%)	Standard ³ Aeration Efficiency (lb O ₂ /hp-hr)	
			Power Density (hp/1000 ft ³)		Pump/Air Power Split (%/%)				Delivered	Wire
07/05/78	1	25	1.56	336.2	82.2/17.8	12.09	11.16	23.85	5.36	3.36
07/07/78	1	20	1.62	322.4	78.7/21.3	12.62	10.90	20.67	5.30	3.33
07/07/78	2	20	0.96	170.8	64.4/35.6	7.89	11.11	24.80	5.68	3.64
07/07/78	3	20	0.51	52.9	33.9/66.1	3.12	11.07	32.14	4.32	2.89
07/08/78	1	25	0.48	64.3	44.2/55.8	3.29	11.72	36.62	5.05	3.33
07/08/78	2	25	1.01	202.1	72.4/27.6	8.72	11.37	29.22	6.14	3.90
07/10/78	2	10	1.89	329.3	77.8/22.2	11.29	9.73	8.02	3.61	2.28
07/10/78	3	10	0.50	32.7	18.6/81.4	2.21	9.74	16.96	2.83	1.94
07/12/78	1	15	1.64	302.9	81.2/18.8	12.21	10.33	15.22	4.77	2.99
07/19/78	1	15	1.03	180.2	69.9/30.1	7.45	10.61	16.00	4.82	3.07
07/20/78	1	15	0.51	54.6	39.1/60.9	3.20	11.08	23.63	4.37	2.91
07/27/78	1	15	1.63	300.4	80.7/19.3	12.16	10.40	15.18	4.79	3.01
07/28/78	1	15	1.02	176.7	69.3/30.7	7.95	10.67	17.27	5.17	3.30
08/01/78	1	10	1.17	203.4	64.4/35.6	7.91	9.86	9.19	4.12	2.64
08/01/78	2	10	0.59	54.5	29.3/70.7	3.13	10.08	14.08	3.38	2.28
08/09/78	1	25	0.49	65.2	44.3/55.7	3.13	11.93	34.28	4.77	3.14
08/14/78	1	25	0.49	65.6	44.5/55.5	3.23	11.87	35.19	4.91	3.24
08/16/78	1	20	0.50	49.3	32.0/68.0	2.74	11.20	30.67	3.94	2.64

1. The delivered horsepower numbers are based on the adiabatic compression equation. Standard ambient conditions of 20°C, 14.70 psia, and 36% relative humidity have been used. Blower inlet and discharge pressures were determined in accordance with Equations 4 and 6.
2. Based on the Equilibrium model analysis using Winkler data.
3. The wire horsepower used in this analysis is related to delivered horsepower by a blower efficiency of 0.70, a coupling efficiency of 0.95, and a motor efficiency of 0.92 (an overall or combined efficiency of 0.612).

TABLE 9. SUMMARY OF EXPONENTIAL METHOD RESULTS; KENICS STATIC TUBE AERATORS

Date	Run	Water Depth (ft)	Delivered ¹ Power Density (hp/1000 ft ³)	Air-flow Rate (acfm)	K _L a ₂₀ ² (1/hr)	C* _O (mg/L)	Standard Oxygen Transfer Efficiency (%)	Standard ³ Aeration Efficiency (lb O ₂ /hp-hr)	
								Delivered	Wire
05/25/78	1	20	0.49	122.6	3.53	10.88	15.13	4.88	2.99
05/26/78	1	20	1.02	245.0	6.62	10.71	13.95	4.32	2.64
06/02/78	1	25	1.05	262.3	8.09	10.63	19.68	5.13	3.14
06/08/78	1	15	0.48	115.4	3.16	9.98	10.39	4.29	2.62
06/13/78	1	15	1.74	356.7	11.05	9.56	11.13	3.92	2.40
06/13/78	2	15	1.08	243.5	7.74	9.42	11.43	4.40	2.69
06/14/78	2	10	1.11	230.6	6.59	9.50	6.41	3.69	2.26
06/14/78	3	10	0.50	115.5	3.43	9.24	7.04	4.14	2.53
06/22/78	1	25	1.60	381.0	10.99	10.80	18.47	4.59	2.81
06/23/78	1	25	0.48	125.8	3.58	11.23	19.10	5.18	3.17
06/26/78	1	20	1.70	377.5	10.76	10.41	14.28	4.08	2.50
06/28/78	1	10	1.90	345.6	9.32	9.87	6.47	3.01	1.84

81

1. The delivered horsepower numbers are based on the adiabatic compression equation. Standard ambient conditions of 20°C, 14.70 psia, and 36% relative humidity have been used. Blower inlet and discharge pressures were determined in accordance with Equations 4 and 6.
2. Based on the Exponential model analysis using Winkler data.
3. The wire horsepower used in this analysis is related to delivered horsepower by a blower efficiency of 0.70, a coupling efficiency of 0.95, and a motor efficiency of 0.92 (an overall or combined efficiency of 0.612).

TABLE 10. SUMMARY OF EQUILIBRIUM METHOD RESULTS: KENICS STATIC TUBE AERATORS

Date	Run	Water Depth (ft)	Delivered ¹ Power Density (hp/1000 ft ³)	Air- flow Rate (scfm)	K _L a ₂₀ ² (1/hr)	C* _O (mg/L)	Standard Oxygen Transfer Efficiency (%)	Standard ³ Aeration Efficiency (lb O ₂ /hp-hr)	
								Delivered	Wire
05/25/78	1	20	0.49	122.6	3.47	10.91	14.89	4.80	2.94
05/26/78	1	20	1.02	245.0	6.73	10.59	14.02	4.34	2.65
06/02/78	1	25	1.05	262.3	8.09	10.75	19.75	5.15	3.15
06/08/78	1	15	0.48	115.4	3.21	10.34	10.49	4.33	2.65
06/13/78	1	15	1.74	356.7	10.76	9.96	10.86	3.83	2.34
06/13/78	2	15	1.08	243.5	7.33	10.11	11.06	4.26	2.61
06/14/78	2	10	1.11	230.6	6.53	10.00	6.88	3.67	2.25
06/14/78	3	10	0.50	115.5	3.40	9.72	6.97	4.10	2.51
06/22/78	1	25	1.60	381.0	10.99	10.82	18.50	4.60	2.82
06/23/78	1	25	0.48	125.8	3.62	11.21	19.26	5.22	3.19
06/26/78	1	20	1.70	377.5	10.63	10.34	14.01	4.01	2.45
06/28/78	1	10	1.90	345.6	9.55	9.78	6.57	3.06	1.87

1. The delivered horsepower numbers are based on the adiabatic compression equation. Standard ambient conditions of 20°C, 14.70 psia, and 36% relative humidity have been used. Blower inlet and discharge pressures were determined in accordance with Equations 4 and 6.
2. Based on the Equilibrium model analysis using Winkler data.
3. The wire horsepower used in this analysis is related to delivered horsepower by a blower efficiency of 0.70, a coupling efficiency of 0.95, and a motor efficiency of 0.92 (an overall or combined efficiency of 0.612).

TABLE 11. SUMMARY OF EXPONENTIAL METHOD RESULTS: BAUER VARIABLE ORIFICE DIFFUSERS

Date	Run	Water Depth (ft)	Delivered ¹ Power Density (hp/1000 ft ³)	Air-flow Rate (scfm)	K _L a ₂₀ ² (1/hr)	C* _O (mg/L)	Standard Oxygen Transfer Efficiency (%)	Standard ³ Aeration Efficiency (lb O ₂ /hp-hr)	
								Delivered	Wire
12/05/78	1	20	1.75	380.7	12.51	10.32	16.28	4.57	2.80
12/05/78	2	20	1.10	254.9	7.63	10.47	15.14	4.53	2.77
12/05/78	3	20	0.53	130.0	3.54	10.58	13.93	4.37	2.67
12/06/78	1	10	0.53	118.9	3.33	9.69	6.59	3.79	2.32
12/06/78	2	10	1.18	234.8	7.04	9.50	6.91	3.53	2.16
12/06/78	3	10	2.14	369.6	11.76	9.48	7.31	3.26	1.99
12/07/78	1	15	1.82	363.2	11.32	10.04	11.40	3.89	2.38
12/07/78	2	15	1.18	253.2	7.51	10.09	10.83	4.00	2.45
12/07/78	3	15	0.53	121.7	3.27	10.14	9.85	3.91	2.39
12/08/78	1	25	0.52	132.1	3.51	11.07	17.52	4.67	2.86
12/08/78	2	25	1.07	260.4	7.47	11.12	18.93	4.84	2.96
12/08/78	3	25	1.74	403.9	12.51	10.79	19.63	4.78	2.92
12/15/78	1	10	2.05	362.9	10.76	9.53	6.93	3.11	1.90
12/15/78	2	10	0.54	117.6	3.32	9.46	6.54	3.67	2.25

83

1. The delivered horsepower numbers are based on the adiabatic compression equation. Standard ambient conditions of 20°C, 14.70 psia, and 36% relative humidity have been used. Blower inlet and discharge pressures were determined in accordance with Equations 4 and 6.
2. Based on the Exponential model analysis using Winkler data.
3. The wire horsepower used in this analysis is related to delivered horsepower by a blower efficiency of 0.70, a coupling efficiency of 0.95, and a motor efficiency of 0.92 (an overall or combined efficiency of 0.612).

TABLE 12. SUMMARY OF EQUILIBRIUM METHOD RESULTS; BAUER VARIABLE ORIFICE DIFFUSERS

Date	Run	Water Depth (ft)	Delivered ¹ Power Density (hp/1000 ft ³)	Air-flow Rate (scfm)	K _L a ₂₀ ² (1/hr)	C* ₀ (mg/L)	Standard Oxygen Transfer Efficiency (%)	Standard ³ Aeration Efficiency (lb O ₂ /hp-hr)	
								Delivered	Wire
12/05/78	1	20	1.75	380.7	12.46	10.33	16.22	4.56	2.79
12/05/78	2	20	1.10	254.9	7.82	10.40	15.40	4.60	2.82
12/05/78	3	20	0.53	130.0	3.57	10.52	13.98	4.38	2.68
12/06/78	1	10	0.53	118.9	3.49	9.55	6.81	3.92	2.40
12/06/78	2	10	1.18	234.8	7.12	9.46	6.95	3.55	2.17
12/06/78	3	10	2.14	369.6	11.83	9.48	7.35	3.28	2.01
12/07/78	1	15	1.82	363.2	11.57	10.02	11.62	3.96	2.42
12/07/78	2	15	1.18	253.2	7.61	10.04	10.93	4.04	2.47
12/07/78	3	15	0.53	121.7	3.32	10.09	9.98	3.96	2.42
12/08/78	1	25	0.52	132.1	3.67	10.85	17.98	4.79	2.93
12/08/78	2	25	1.07	260.4	8.06	10.84	19.92	5.09	3.11
12/08/78	3	25	1.74	403.9	12.81	10.66	19.87	4.83	2.96
12/15/78	1	10	2.05	362.9	10.71	9.56	6.92	3.11	1.90
12/15/78	2	10	0.54	117.6	3.25	9.50	6.44	3.62	2.21

1. The delivered horsepower numbers are based on the adiabatic compression equation. Standard ambient conditions of 20°C, 14.70 psia, and 36% relative humidity have been used. Blower inlet and discharge pressures were determined in accordance with Equations 4 and 6.
2. Based on the Equilibrium model analysis using Winkler data.
3. The wire horsepower used in this analysis is related to delivered horsepower by a blower efficiency of 0.70, a coupling efficiency of 0.95, and a motor efficiency of 0.92 (an overall or combined efficiency of 0.612).

TABLE 13. SUMMARY OF EXPONENTIAL METHOD RESULTS: SANITAIRE COARSE BUBBLE DIFFUSERS

Date	Run	Water Depth (ft)	Delivered ¹ Power Density (hp/1000 ft ³)	Air-flow Rate (scfm)	K _L a ₂₀ ² (1/hr)	C* _O (mg/L)	Standard Oxygen Transfer Efficiency (%)	Standard ³ Aeration Efficiency (lb O ₂ /hp-hr)	
								Delivered	Wire
11/06/78	1	20	1.74	375.3	15.08	10.76	20.67	5.76	3.52
11/06/78	2	20	1.09	257.7	9.71	10.81	19.59	5.96	3.64
11/06/78	3	20	0.51	127.6	4.15	10.89	17.12	5.54	3.39
11/07/78	1	10	0.50	115.5	3.31	9.85	6.83	4.09	2.50
11/07/78	2	10	1.19	240.9	7.72	9.84	7.64	3.97	2.43
11/07/78	3	10	2.11	354.8	12.52	9.77	8.28	3.60	2.20
11/09/78	1	15	1.90	362.2	11.93	10.34	12.35	4.03	2.47
11/09/78	2	15	1.13	245.8	7.65	10.31	11.60	4.35	2.66
11/09/78	3	15	0.52	125.2	3.50	10.38	10.53	4.38	2.68
11/15/78	1	25	0.49	128.7	3.47	11.00	17.74	4.83	2.95
11/15/78	2	25	1.08	265.8	8.11	10.93	19.83	5.09	3.11
11/15/78	3	25	1.80	402.1	13.65	10.82	21.73	5.07	3.10

1. The delivered horsepower numbers are based on the adiabatic compression equation. Standard ambient conditions of 20°C, 14.70 psia, and 36% relative humidity have been used. Blower inlet and discharge pressures were determined in accordance with Equations 4 and 6.
2. Based on the Exponential model analysis using Winkler data.
3. The wire horsepower used in this analysis is related to delivered horsepower by a blower efficiency of 0.70, a coupling efficiency of 0.95, and a motor efficiency of 0.92 (an overall or combined efficiency of 0.612).

TABLE 14. SUMMARY OF EQUILIBRIUM METHOD RESULTS: SANITAIRE COARSE BUBBLE DIFFUSERS

Date	Run	Water Depth (ft)	Delivered ¹ Power Density (hp/1000 ft ³)	Air- flow Rate (scfm)	K _L a ₂₀ ² (1/hr)	C* _O (mg/L)	Standard Oxygen Transfer Efficiency (%)	Standard ³ Aeration Efficiency (lb O ₂ /hp-hr)	
								Delivered	Wire
11/06/78	1	20	1.74	375.3	14.94	10.76	20.49	5.71	3.49
11/06/78	2	20	1.09	257.7	9.66	10.85	19.55	5.95	3.64
11/06/78	3	20	0.51	127.6	4.26	10.78	17.35	5.62	3.44
11/07/78	1	10	0.50	115.5	3.39	9.75	6.94	4.15	2.54
11/07/78	2	10	1.19	240.9	7.82	9.78	7.70	4.00	2.45
11/07/78	3	10	2.11	354.8	12.40	9.81	8.23	3.58	2.19
11/09/78	1	15	1.90	362.2	12.46	10.18	12.70	4.14	2.53
11/09/78	2	15	1.13	245.8	7.94	10.21	11.91	4.47	2.73
11/09/78	3	15	0.52	125.2	3.58	10.31	10.67	4.44	2.72
11/15/78	1	25	0.49	128.7	3.54	10.96	17.99	4.89	2.99
11/15/78	2	25	1.08	265.8	8.05	10.95	19.73	5.06	3.09
11/15/78	3	25	1.80	402.1	13.46	10.85	21.49	5.02	3.07

85

1. The delivered horsepower numbers are based on the adiabatic compression equation. Standard ambient conditions of 20°C, 14.70 psia, and 36% relative humidity have been used. Blower inlet and discharge pressures were determined in accordance with Equations 4 and 6.
2. Based on the Equilibrium model analysis using Winkler data.
3. The wire horsepower used in this analysis is related to delivered horsepower by a blower efficiency of 0.70, a coupling efficiency of 0.95, and a motor efficiency of 0.92 (an overall or combined efficiency of 0.612).

TABLE 15. SUMMARY OF EXPONENTIAL METHOD RESULTS: ENVIREX COARSE BUBBLE DIFFUSERS

Date	Run	Water Depth (ft)	Delivered ¹ Power Density (hp/1000 ft ³)	Air- flow Rate (scfm)	K _L a ₂₀ ² (1/hr)	C* _o (mg/L)	Standard Oxygen Transfer Efficiency (%)	Standard ³ Aeration Efficiency (lb O ₂ /hp-hr)	
								Delivered	Wire
01/08/79	1	25	0.49	131.0	3.61	11.20	18.39	5.10	3.12
01/08/79	2	25	1.01	259.5	9.05	10.47	21.59	5.77	3.53
01/09/79	1	20	1.69	384.4	12.88	10.44	16.87	4.94	3.02
01/09/79	2	20	0.49	126.5	3.56	10.83	14.98	4.96	3.03
01/10/79	1	20	1.02	252.0	7.68	10.75	15.82	5.01	3.07
01/10/79	2	15	1.79	377.3	11.56	10.19	11.29	4.10	2.51
01/10/79	3	15	1.08	251.6	7.46	10.19	10.97	4.40	2.69
01/10/79	4	15	0.50	125.7	3.51	10.22	10.33	4.42	2.71
01/11/79	1	10	0.49	119.1	3.15	9.76	6.25	3.93	2.41
01/11/79	2	10	1.10	242.5	7.05	9.76	6.88	3.89	2.38
01/11/79	3	10	1.93	363.2	11.36	9.73	7.36	3.57	2.18
01/19/79	1	25	1.64	394.7	12.68	10.85	20.46	5.19	3.17
01/19/79	2	25	0.50	133.2	3.81	10.97	18.70	5.19	3.17
01/25/79	1	25	1.65	400.3	12.89	11.00	20.93	5.30	3.24
01/25/79	2	25	0.51	136.4	3.71	11.31	18.31	5.09	3.11

87

1. The delivered horsepower numbers are based on the adiabatic compression equation. Standard ambient conditions of 20°C, 14.70 psia, and 36% relative humidity have been used. Blower inlet and discharge pressures were determined in accordance with Equations 4 and 6.
2. Based on the Exponential model analysis using Winkler data.
3. The wire horsepower used in this analysis is related to delivered horsepower by a blower efficiency of 0.70, a coupling efficiency of 0.95, and a motor efficiency of 0.92 (an overall or combined efficiency of 0.612).

TABLE 16. SUMMARY OF EQUILIBRIUM METHOD RESULTS: ENVIREX COARSE BUBBLE DIFFUSERS

Date	Run	Water Depth (ft)	Delivered ¹ Power Density (hp/1000 ft ³)	Air- flow Rate (scfm)	K _L a ₂₀ ² (1/hr)	C* _O (mg/L)	Standard Oxygen Transfer Efficiency (%)	Standard ³ Aeration Efficiency (lb O ₂ /hp-hr)	
								Delivered	Wire
01/08/79	1	25	0.49	131.0	3.67	11.02	18.35	5.09	3.12
01/08/79	2	25	1.01	259.5	8.23	10.88	20.39	5.45	3.33
01/09/79	1	20	1.69	384.4	12.86	10.47	16.89	4.95	3.03
01/09/79	2	20	0.49	126.5	3.64	10.70	15.12	5.01	3.06
01/10/79	1	20	1.02	252.0	7.89	10.66	16.11	5.11	3.12
01/10/79	2	15	1.79	377.3	11.76	10.15	11.44	4.16	2.54
01/10/79	3	15	1.08	251.6	7.48	10.16	10.95	4.39	2.69
01/10/79	4	15	0.50	125.7	3.51	10.20	10.32	4.42	2.70
01/11/79	1	10	0.49	119.1	3.32	9.51	6.42	4.04	2.47
01/11/79	2	10	1.10	242.5	7.22	9.66	6.97	3.94	2.41
01/11/79	3	10	1.93	363.2	11.50	9.61	7.36	3.57	2.18
01/19/79	1	25	1.64	394.7	12.75	10.82	20.51	5.20	3.18
01/19/79	2	25	0.50	133.2	3.83	10.97	18.81	5.22	3.19
01/25/79	1	25	1.65	400.3	12.68	11.08	20.73	5.25	3.21
01/25/79	2	25	0.51	136.4	3.88	11.09	18.78	5.22	3.19

88

1. The delivered horsepower numbers are based on the adiabatic compression equation. Standard ambient conditions of 20°C, 14.70 psia, and 36% relative humidity have been used. Blower inlet and discharge pressures were determined in accordance with Equations 4 and 6.
2. Based on the Equilibrium model analysis using Winkler data.
3. The wire horsepower used in this analysis is related to delivered horsepower by a blower efficiency of 0.70, a coupling efficiency of 0.95, and a motor efficiency of 0.92 (an overall or combined efficiency of 0.612).

TABLE 17. SUMMARY OF EXPONENTIAL METHOD RESULTS: FMC COARSE BUBBLE DIFFUSERS

Date	Run	Water Depth (ft)	Delivered ¹ Power Density (hp/1000 ft ³)	Air- flow Rate (scfm)	K _L a ₂₀ ² (1/hr)	C* _o (mg/L)	Standard Oxygen Transfer Efficiency (%)	Standard ³ Aeration Efficiency (lb O ₂ /hp-hr)	
								Delivered	Wire
03/06/79	1	15	1.84	397.8	12.51	10.10	11.52	4.28	2.62
03/06/79	2	15	1.08	266.1	7.44	10.20	10.34	4.37	2.67
03/06/79	3	15	.50	133.6	3.57	10.26	9.91	4.57	2.80

89

1. The delivered horsepower numbers are based on the adiabatic compression equation. Standard ambient conditions of 20°C, 14.70 psia, and 36% relative humidity have been used. Blower inlet and discharge pressures were determined in accordance with Equations 4 and 6.
2. Based on the Exponential model analysis using Winkler data.
3. The wire horsepower used in this analysis is related to delivered horsepower by a blower efficiency of 0.70, a coupling efficiency of 0.95, and a motor efficiency of 0.92 (an overall or combined efficiency of 0.612).

TABLE 18. SUMMARY OF EQUILIBRIUM METHOD RESULTS: FMC COARSE BUBBLE DIFFUSERS

Date	Run	Water Depth (ft)	Delivered ¹ Power Density (hp/1000 ft ³)	Air- flow Rate (scfm)	K _L a ₂₀ ² (1/hr)	C* _o (mg/L)	Standard Oxygen Transfer Efficiency (%)	Standard ³ Aeration Efficiency (lb O ₂ /hp-hr)	
								Delivered	Wire
03/06/79	1	15	1.84	397.8	12.27	10.14	11.35	4.21	2.58
03/06/79	2	15	1.08	266.1	7.25	10.21	10.08	4.26	2.61
03/06/79	3	15	.50	133.6	3.67	10.11	10.07	4.64	2.84

06

1. The delivered horsepower numbers are based on the adiabatic compression equation. Standard ambient conditions of 20°C, 14.70 psia, and 36% relative humidity have been used. Blower inlet and discharge pressures were determined in accordance with Equations 4 and 6.
2. Based on the Equilibrium model analysis using Winkler data.
3. The wire horsepower used in this analysis is related to delivered horsepower by a blower efficiency of 0.70, a coupling efficiency of 0.95, and a motor efficiency of 0.92 (an overall or combined efficiency of 0.612).

this manner included the values of $K_L a_{20}$ and standard wire aeration efficiency (SWAE). Results of this comparison are summarized in Table 19. Also presented in this table are the means and standard deviations of ratios corresponding to the tests of each manufacturer.

TABLE 19. COMPARISON OF ANALYSIS METHODS

Ratios of Results from Exponential and Equilibrium Methods of Analysis

System	$(K_L a_{20})_{ex}/(K_L a_{20})_{eq}$		SWAE _{ex} /SWAE _{eq}		Number of Tests
	Mean	Standard Deviation	Mean	Standard Deviation	
A	0.9927	0.0160	0.9954	0.0109	13
B	0.9855	0.0204	0.9920	0.0150	13
C	0.9837	0.0329	0.9911	0.0199	18
D	1.0053	0.0211	1.0049	0.0147	12
E	0.9817	0.0230	0.9878	0.0156	14
F	0.9885	0.0189	0.9928	0.0121	12
G	0.9928	0.0331	0.9974	0.0192	15
H	1.0062	0.0238	1.0081	0.0160	3
Overall	0.9900	0.0263	0.9946	0.0169	100

The magnitude of the $K_L a_{20}$ AND SWAE values obtained by the Exponential method of analysis were generally less than those obtained using the Equilibrium method of analysis. For the 100 tests conducted, the $K_L a_{20}$ values determined using the Equilibrium method are greater in 69 cases. For the SWAE data, the Equilibrium method produced a higher number in 68 cases. For $K_L a_{20}$, the maximum ratio was 1.10; the minimum ratio was 0.88. For SWAE, the maximum ratio was 1.06; the minimum ratio was 0.93.

GRAPHICAL PRESENTATIONS

In addition to determining clean water test results, this study also illustrated the performance of the various aeration devices with changes in water depth and delivered power. A total of 84 graphs were prepared to facilitate the understanding of the effects of water depth and delivered power level on oxygen transfer performance. These graphs are divided into two categories: graphs that compare performance results of the various manufacturers' equipment and graphs that summarize the individual performance of each manufacturer's equipment. Fifteen of the 84 graphs compare equipment performance and are presented in this subsection. The other 69 graphs summarize individual equipment performance for the eight aeration systems tested and are presented in Appendices C through J. A preamble for Appendices C through J is provided in Appendix B.

The graphs are all based on the data shown in the Exponential method tables. It should be pointed out that straight-line connections are used to connect data points for consistency and fairness to all manufacturers. The reader may elect to use smoother curve fits.

Of the 15 graphs comparing equipment performance, 12 illustrate the effects of changes in power and three show the effects of changes in water depth. Each comparison graph includes data from all manufacturers. (Note: Deflectofuser testing was carried out only at the 4.6-m (15-ft) water depth and, therefore, is not included on graphs illustrating the effect of water depth variation.) On graphs that illustrate the effects of power variation, the data are divided into four groups, each representing a given water depth. On graphs that illustrate the effects of water depth variation, the plotted results correspond to the middle power level. Parameters plotted against water depth and power variation include standard oxygen transfer rate (SOTR), standard oxygen transfer efficiency (SOTE), and standard wire aeration efficiency (SWAE).

Water Depth Relationships

The relationship between SOTR and water depth is shown in Figure 29. The results of the seven manufacturers tested at multiple water depths are presented. For each manufacturer and water depth, only a single result is plotted. This plotted result represents the middle nominal power density at which the manufacturer was evaluated. Note that the middle nominal power density for all manufacturers tested is the same [26.3 W/m^3 (1.0 hp/1000 ft^3)] with the exception of System A, Norton, which was tested over a lower power density range with a middle nominal power density of 13.2 W/m^3 (0.5 hp/1000 ft^3).

Data plotted in this graph are connected by straight lines. Also, where the data appear to be influenced by a manufacturer's configuration change at different depths, only points from the same configuration are connected (see data for System D, Kenics, and System F, Sanitaire).

It is apparent that increases in water depth resulted in increases in SOTR. This is true for each manufacturer's configuration tested. In this collection of data, the two highest curves represent fine bubble aeration equipment. Coarse bubble aeration equipment is represented by generally lower curves. The jet aeration equipment curve is in the middle above most but not all of the coarse bubble aeration devices.

Comparative results of the SOTE vs. water depth for the seven manufacturers tested at multiple water depths are presented in Figure 30. Stipulations made for Figure 29 regarding plotting only the middle nominal power density evaluated and connection of data points also apply to this figure.

It is apparent that increases in water depth produced increases in SOTE for each manufacturer configuration tested. The three highest curves represent the fine bubble diffusers and jet aerators. Coarse bubble

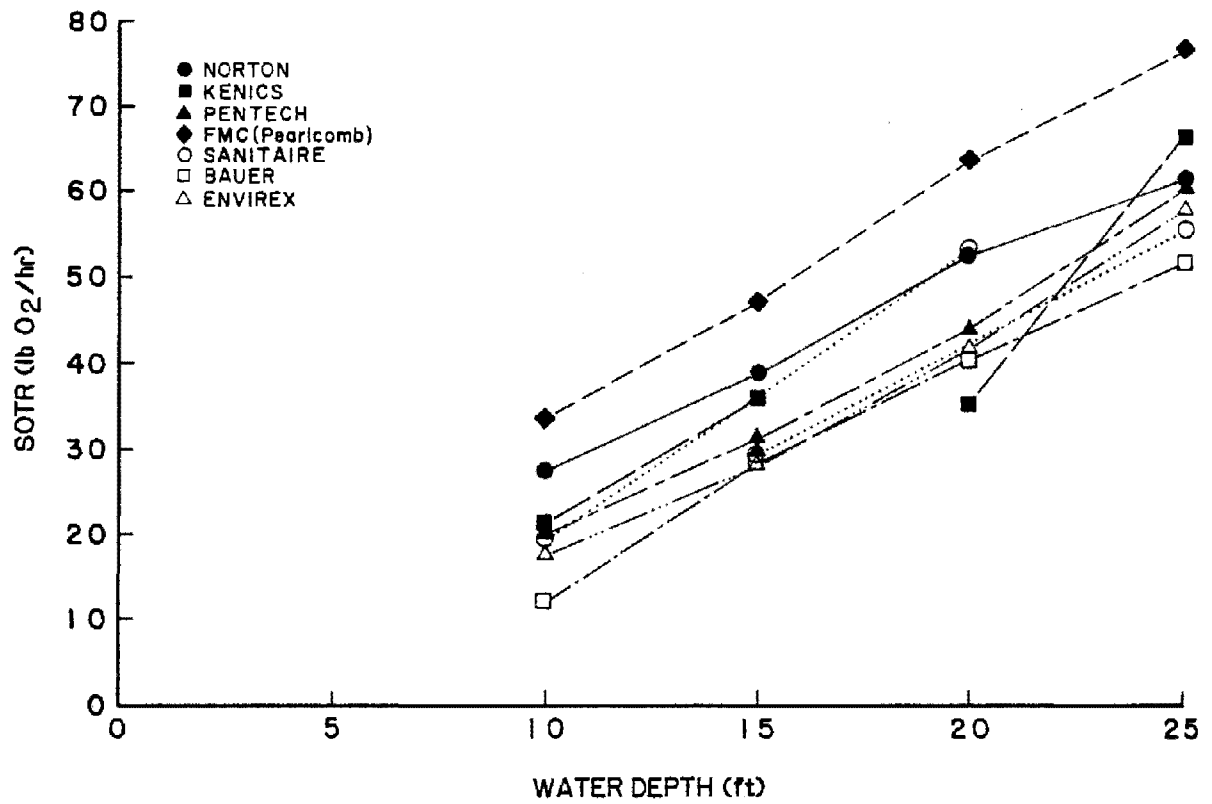


Figure 29. Comparative plot of SOTR vs. water depth at middle power density tested.

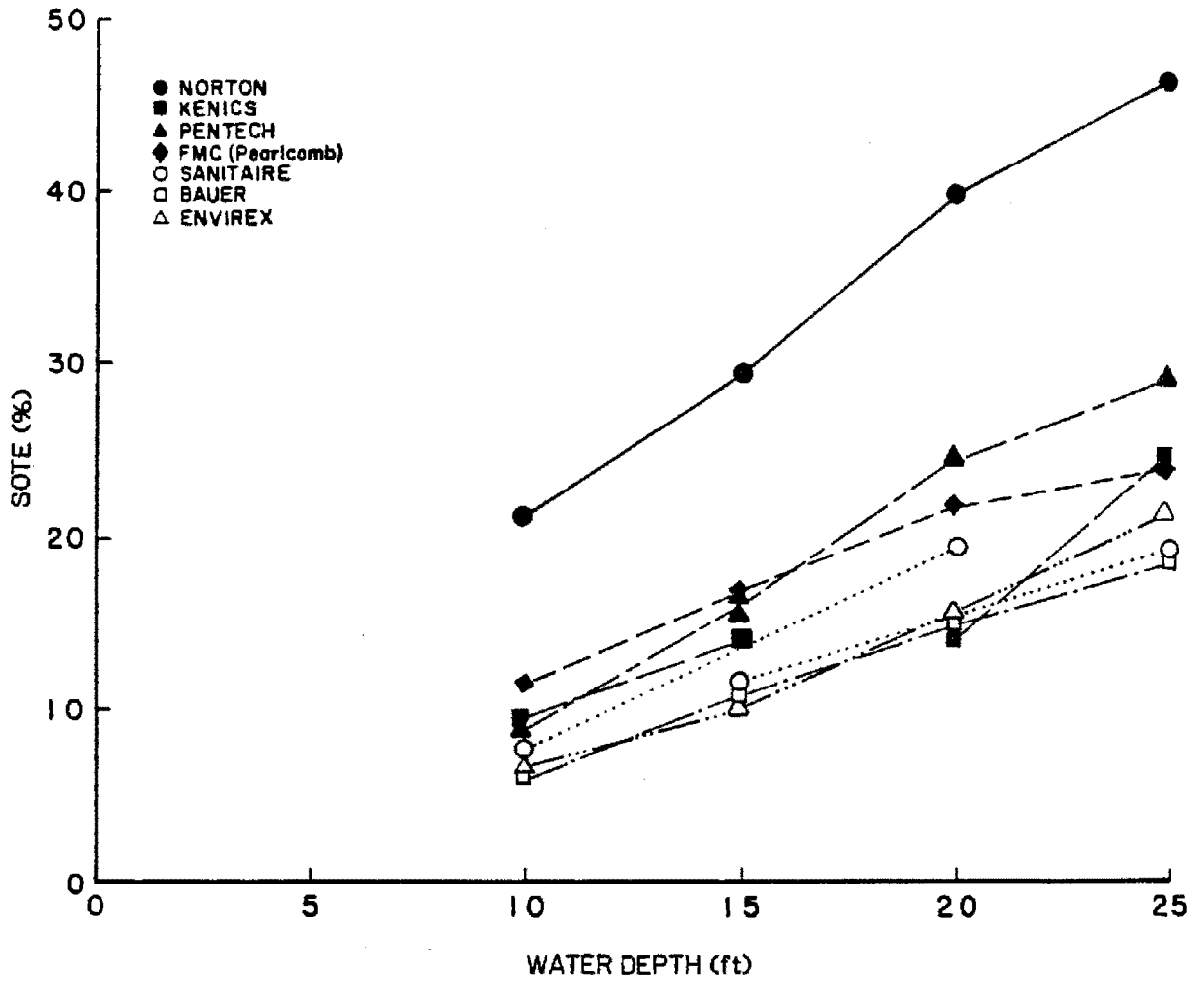


Figure 30. Comparative plot of SOTE vs. water depth at middle power density tested.

aeration equipment is generally represented by lower curves. The variable orifice diffusers showed no improvement over the other coarse bubble diffusers.

In Figure 31, SWAE is plotted against water depth for the seven manufacturers tested at multiple water depths. Stipulations made for Figures 29 and 30 regarding plotting only the middle power density evaluated and connection of data points also apply to this figure.

The data in Figure 31 indicate that the effects of increasing water depth depend on the generic type of aeration equipment tested. While the fine bubble diffusers appear to have been relatively unaffected by changes in water depth, SWAE improved with increasing water depth for the coarse bubble diffusers and jet aerators. In this collection of data, the two highest curves represent the fine bubble diffusers while the jet aeration equipment and coarse bubble diffusers generally grouped together in the lower band of curves. The variable orifice diffuser results again were the lowest. This graph indicates that coarse bubble devices appear to be sensitive to changes in configuration (see data for System D, Kenics, and System F, Sanitaire).

Delivered Power Density Relationships

Figure 32 is a plot of SOTR vs. delivered power density for the 3.0-m (10-ft) water depth. This graph presents the results of the seven manufacturers' equipment tested at this depth. The FMC Deflectofuser, a coarse bubble diffuser, was tested only at the 4.6-m (15-ft) water depth. Results plotted in this graph and the 11 other delivered power density relationship graphs (Figures 33 through 43) to follow are connected by straight lines.

Increases in delivered power density resulted in increasing SOTR. The two highest SOTR curves represent the fine bubble diffusion equipment. Other generic types of aeration equipment produced similar but lower SOTR results at this water depth.

SOTE is plotted against delivered power density for the 3.0-m (10-ft) water depth in Figure 33. Results of the seven aeration systems tested at this depth are presented in this graph. The FMC Deflectofuser was not tested at this depth.

The coarse bubble and variable orifice systems (Kenics, Sanitaire, Bauer, and Envirex) exhibited similar performance. The SOTE of these systems remained the same or improved only slightly with increasing delivered power density. The two fine bubble diffusers produced the highest SOTE values, but in a pattern opposite to that of the coarse bubble and variable orifice diffusers. Peak values for the fine bubble diffusers occurred at the lowest delivered power density and declined for higher power density levels. The jet system, like the fine bubble diffusion systems, produced its peak SOTE value at the lowest delivered power density.

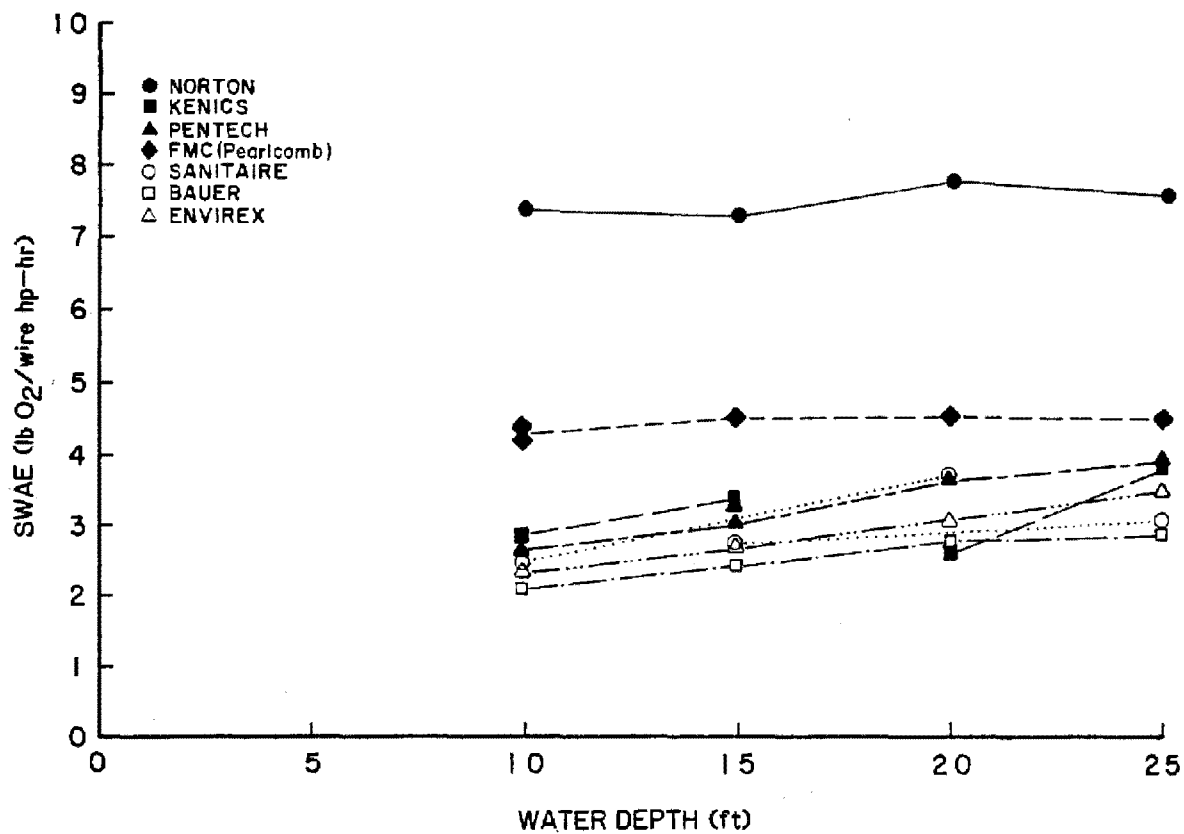


Figure 31. Comparative plot of SWAE vs. water depth at middle power density tested.

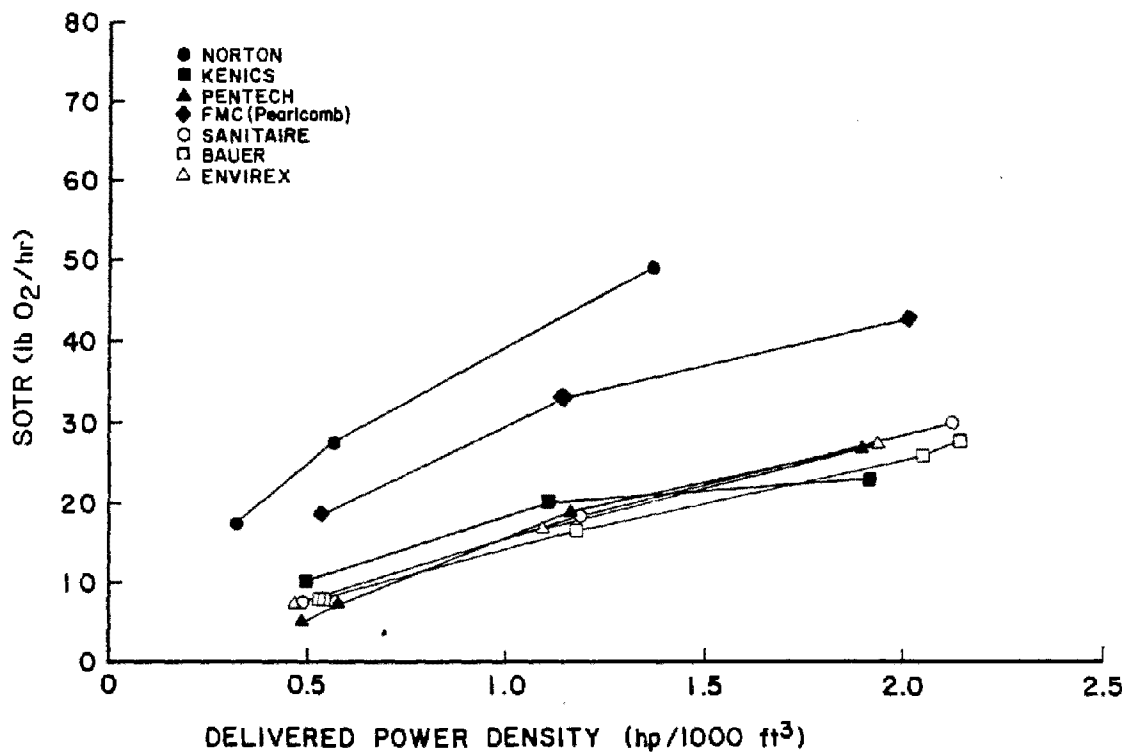


Figure 32. Comparative plot of SOTR vs. delivered power density at 10-ft water depth.

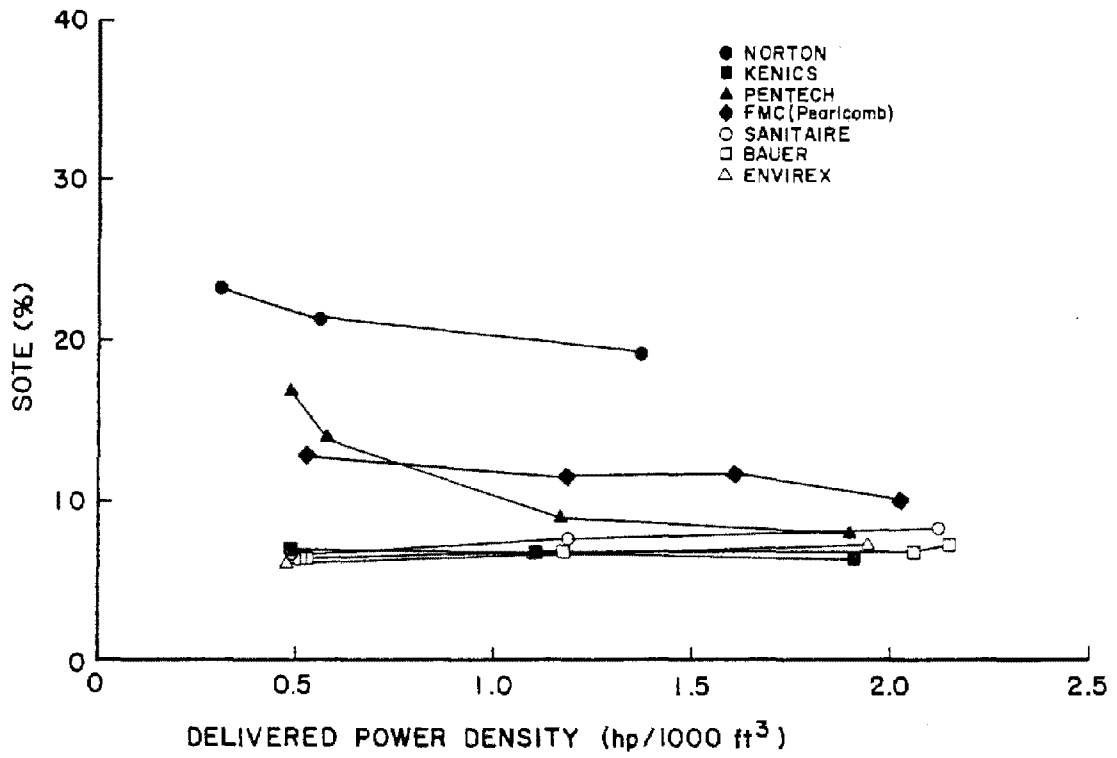


Figure 33. Comparative plot of SOTE vs. delivered power density at 10-ft water depth.

The relationship between SWAE and delivered power density for the 3.0-m (10-ft) water depth is shown in Figure 34. In this graph, data for the seven manufacturers' equipment tested at this depth are presented. The FMC Deflectofuser was not tested at this water depth.

All systems, with the exception of the jet aerators, demonstrated their highest SWAE value at the lowest delivered power density level. For the jet aeration system, peak SWAE performance occurred at the middle delivered power density. The highest SWAE values were produced by the two fine bubble aeration systems. All other systems exhibited nearly the same SWAE results at this depth.

SOTR vs. delivered power density for the 4.6-m (15-ft) water depth is plotted in Figure 35 for the eight aeration devices (including the FMC Deflectofuser) tested at this depth.

It is apparent that increases in delivered power density resulted in SOTR increases. The highest SOTR curves again represent the fine bubble diffusion equipment. The order in SOTR values for the eight systems tested, from highest to lowest, is as follows: Norton; FMC Pearlcomb; Kenics; Pentech; Envirex, Sanitaire, and FMC Deflectofuser grouped together; and Bauer.

SOTE vs. delivered power density for the 4.6-m (15-ft) water depth is illustrated in Figure 36. All eight manufacturers' systems were tested at this depth.

The order in SOTE values, from highest to lowest, is as follows: Norton, Pentech, FMC Pearlcomb, and Kenics, followed by the other coarse bubble systems clustered closely together. The equipment producing fine bubbles, Norton, FMC Pearlcomb, and Pentech, exhibited peak performance at the lowest delivered power density. Equipment that produces coarse bubbles generally showed the opposite trend, with peak values occurring at the greatest delivered power density. The curves for most of the equipment are relatively straight with the exception of the jet aeration system.

SWAE is plotted against delivered power density for the 4.6-m (15-ft) water depth in Figure 37. All eight aeration systems were tested at this depth.

The order in SWAE values, from highest to lowest, is Norton; FMC Pearlcomb; Kenics; Pentech; FMC Deflectofuser, Envirex, and Sanitaire grouped together; and Bauer. Five of the systems demonstrated little variation in SWAE over the range of delivered power densities evaluated. The systems that did exhibit significant variation over this range were Norton, FMC Pearlcomb, and Pentech. These three systems all produce small bubbles. Both Norton and FMC produced their peak SWAE values at the lowest delivered power density, while for Pentech, the peak SWAE occurred at the middle delivered power density.

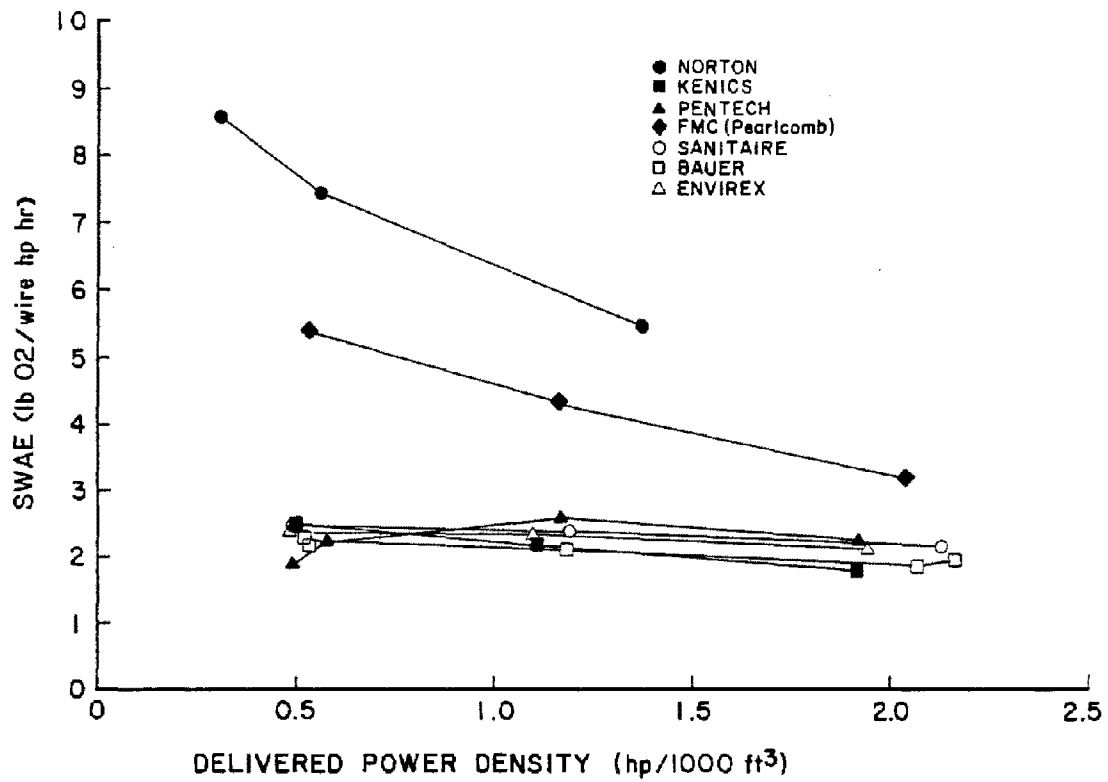


Figure 34. Comparative plot of SWAE vs. delivered power density at 10-ft water depth.

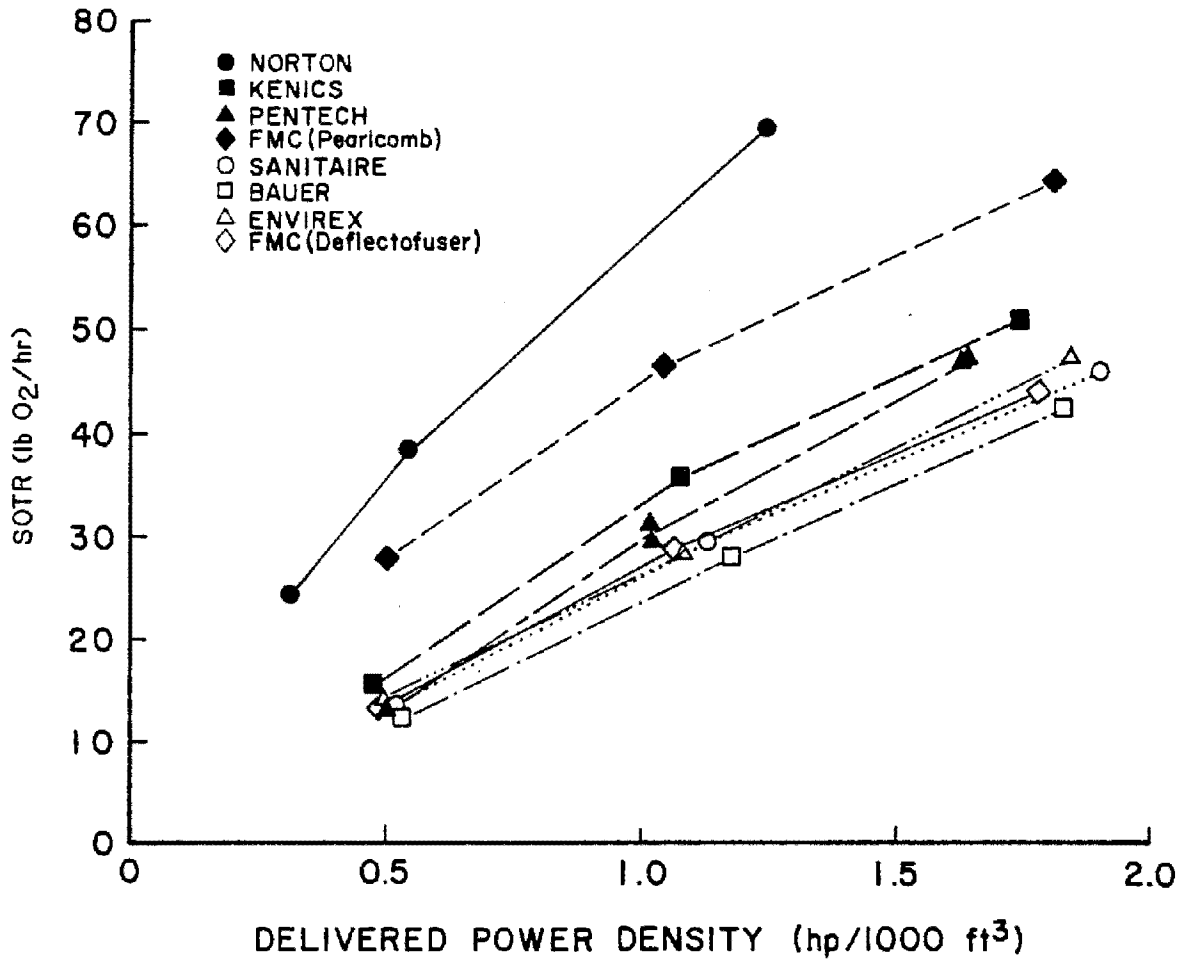


Figure 35. Comparative plot of SOTR vs. delivered power density at 15-ft water depth.

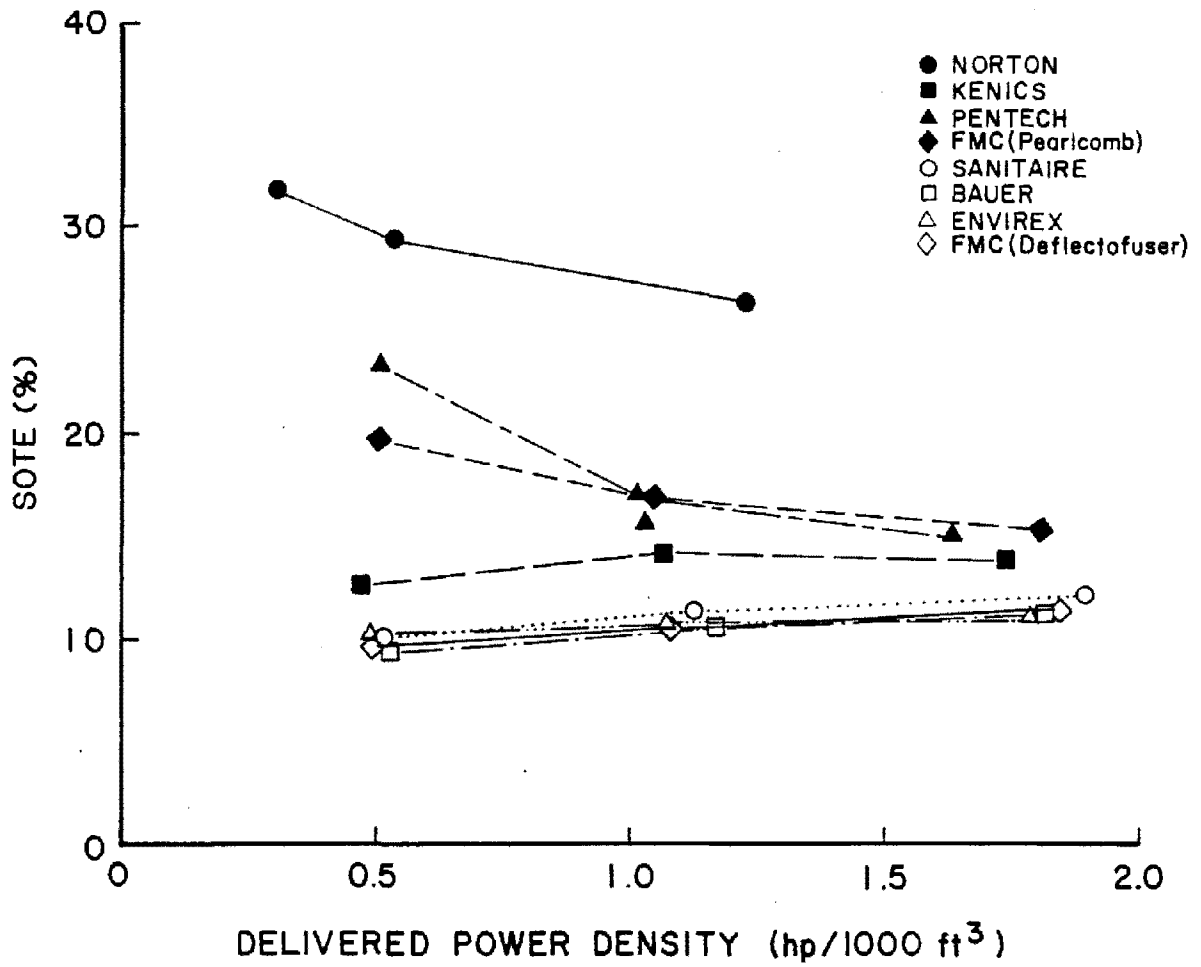


Figure 36. Comparative plot of SOTE vs. delivered power density at 15-ft water depth.

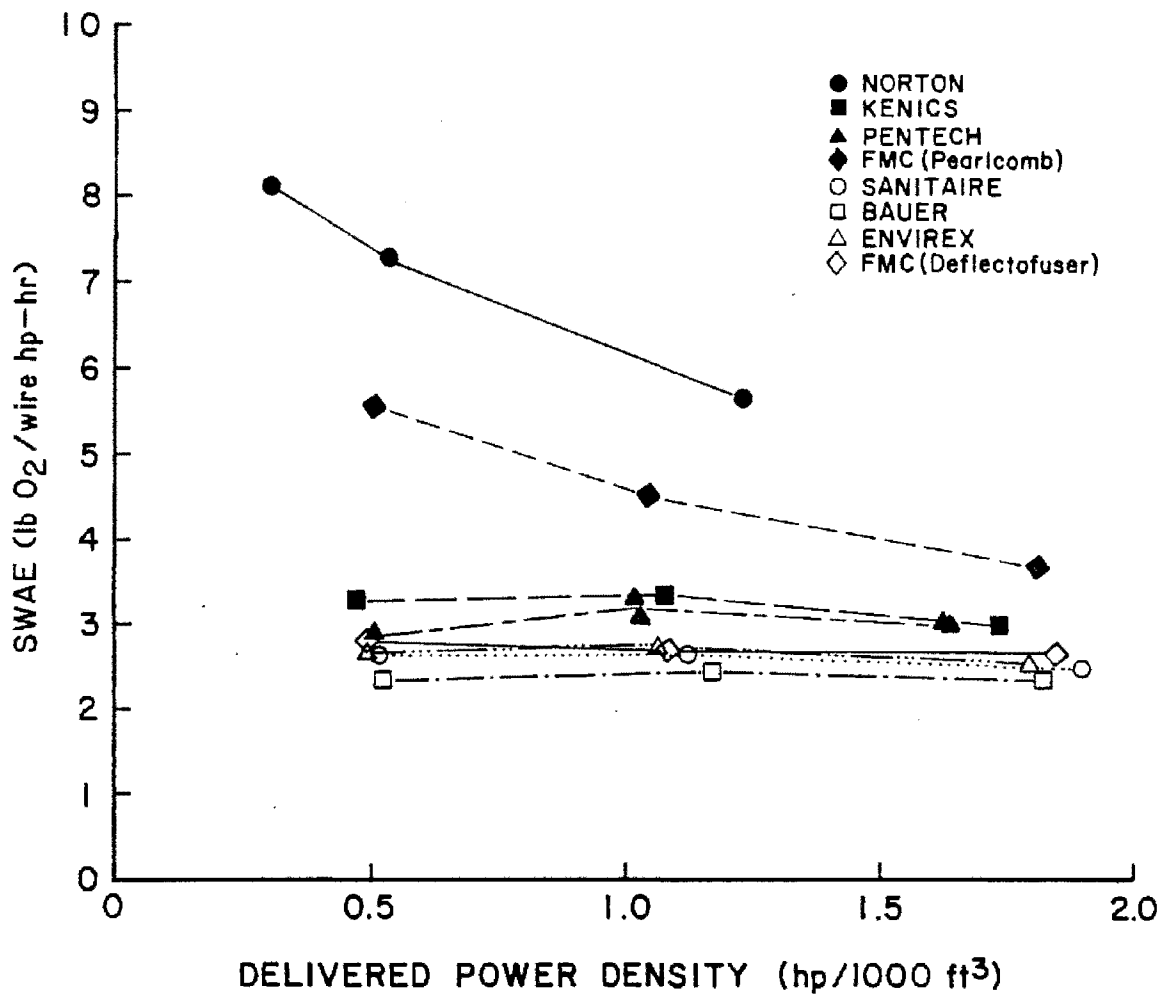


Figure 37. Comparative plot of SWAE vs. delivered power density at 15-ft water depth.

Figure 38 is a plot of SOTR vs. delivered power density for the 6.1-m (20-ft) water depth. Data for the seven aeration systems tested at this depth are presented in this graph. The FMC Deflectofuser was not tested at this depth.

It is clear from this figure that increasing delivered power density resulted in increasing SOTR. The order of the system SWAE curves, from highest to lowest, is Norton, FMC Pearlcomb, Sanitaire, Pentech, Envirex, Bauer, and Kenics.

SOTE is plotted against delivered power density for the 6.1-m (20-ft) water depth in Figure 39 for the seven manufacturers' devices tested at this depth. The FMC Deflectofuser was not tested at this water depth.

Two opposite trends are apparent in this graph. Four aeration systems (Norton, FMC Pearlcomb, Pentech, and Kenics) produced peak SOTE values at the lowest delivered power density. Two coarse bubble systems and the variable orifice system (Sanitaire, Envirex, and Bauer) showed peak SOTE at the highest delivered power density. The order of the system SOTE curves, from highest to lowest, is as follows: Norton, Pentech, FMC Pearlcomb, Sanitaire, Envirex, Bauer, and Kenics.

The relationship of SWAE and delivered power density for the 6.1-m (20-ft) water depth is shown in Figure 40. This graph presents data for the seven aeration devices tested at this depth. The FMC Deflectofuser was not tested at this water depth.

The Norton, FMC Pearlcomb, and Kenics systems achieved peak SWAE values at the lowest delivered power density. The Sanitaire, Envirex, and Bauer systems exhibited little variation of SWAE over the range of delivered power densities tested. The Pentech system produced its peak SWAE at the middle delivered power density. The order of the system SWAE curves, from highest to lowest, is Norton, FMC Pearlcomb, Sanitaire, Pentech, Envirex, Bauer, and Kenics.

Figure 41 shows the relationship of SOTR vs. delivered power density for the 7.6-m (25-ft) water depth. Results of the seven manufacturers' equipment tested at this depth are given in this graph. The FMC Deflectofuser was not tested at this water depth.

It is clear that increasing delivered power density produced increases in SOTR. The order of the system SOTR curves, from highest to lowest, is as follows: Norton, FMC Pearlcomb, Kenics, Pentech, Envirex, Sanitaire, and Bauer, although the Kenics curve crosses the latter four in the higher portion of the range.

SOTE vs. delivered power density for the 7.6-m (25-ft) water depth is shown in Figure 42. This graph presents data for the systems tested at this depth. The FMC Deflectofuser was not tested at this water depth.

In this graph, many system SOTE trends are apparent. The Norton and Pentech data exhibit a steeply sloped linear relationship between SOTE and

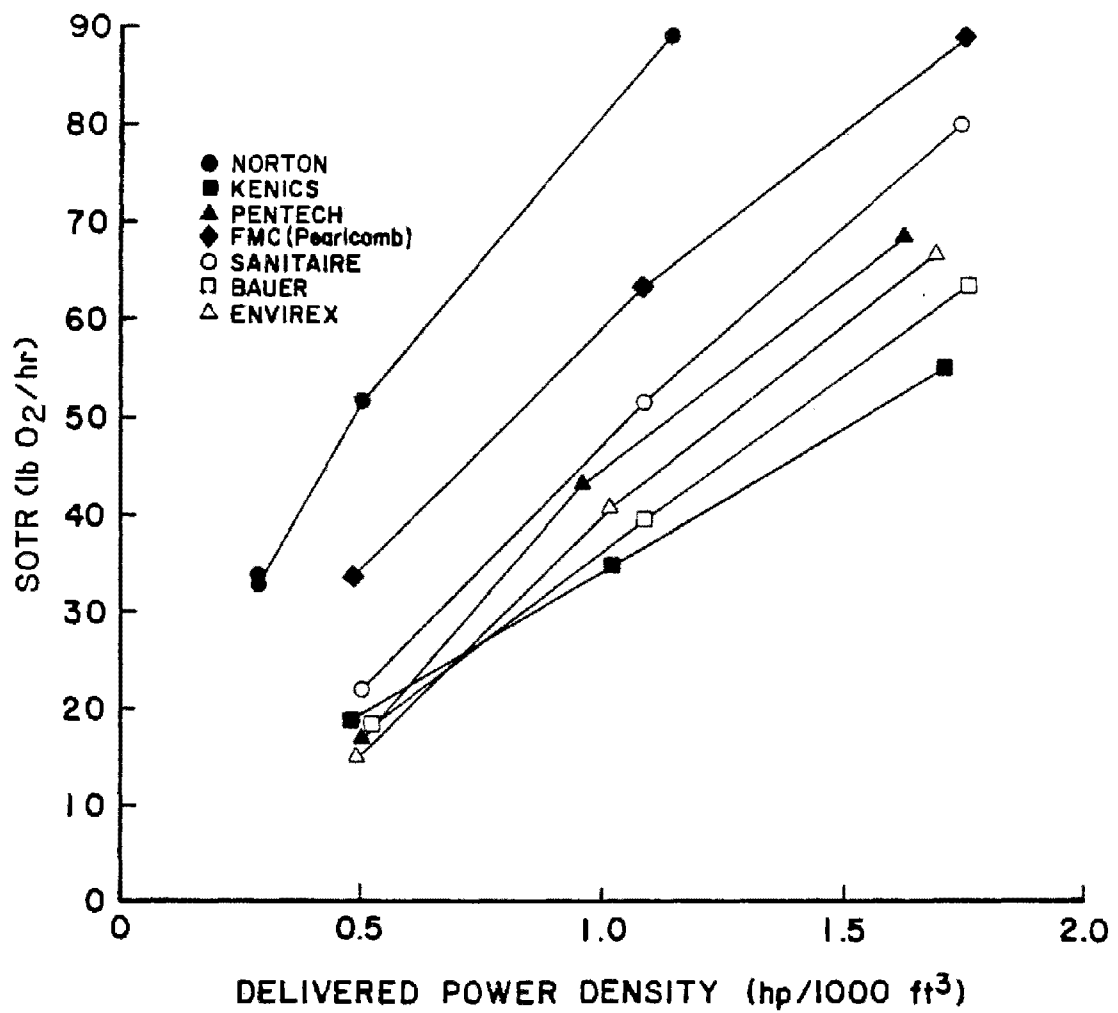


Figure 38. Comparative plot of SOTR vs. delivered power density at 20-ft water depth.

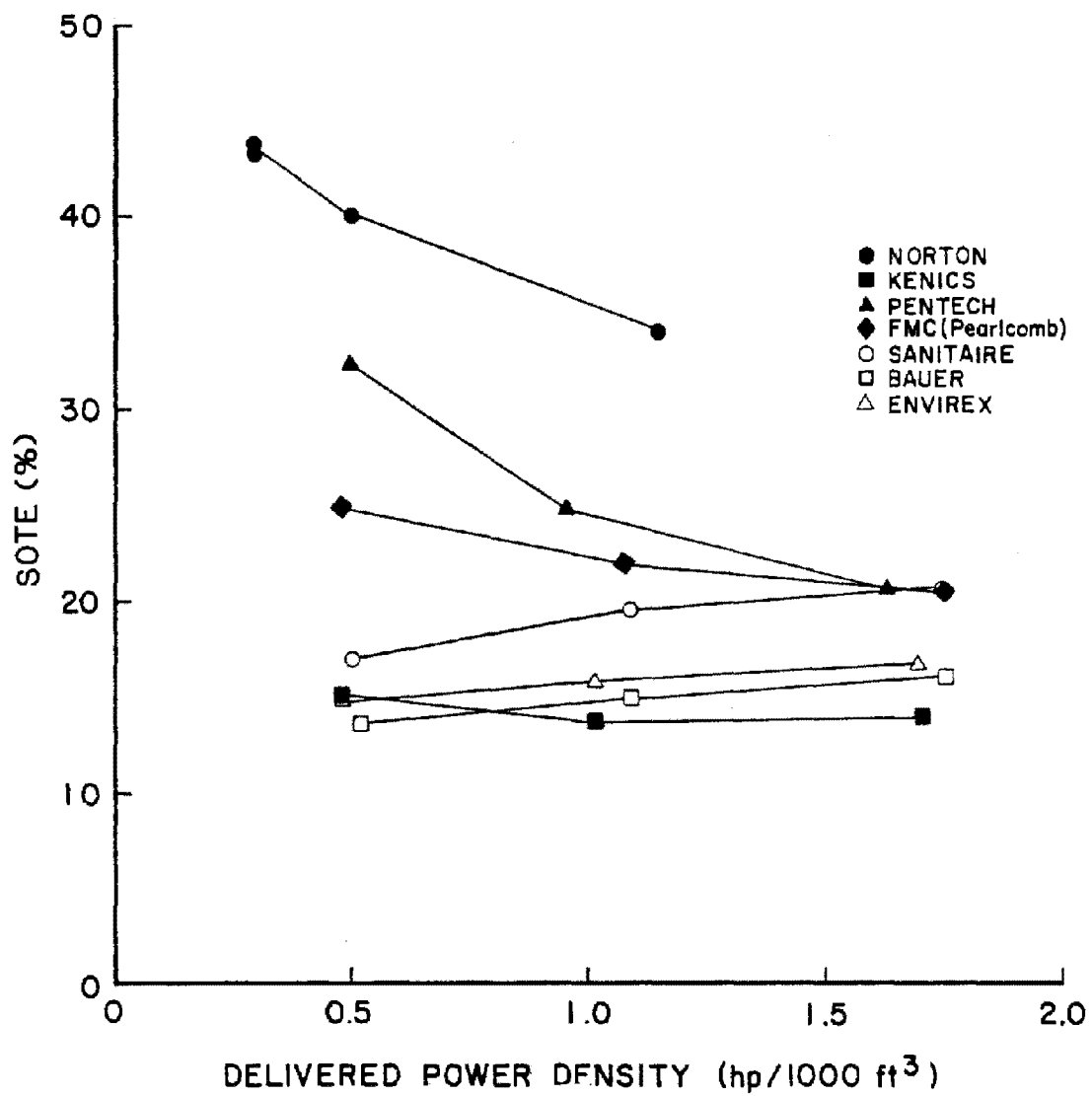


Figure 39. Comparative plot of SOTE vs. delivered power density at 20-ft water depth.

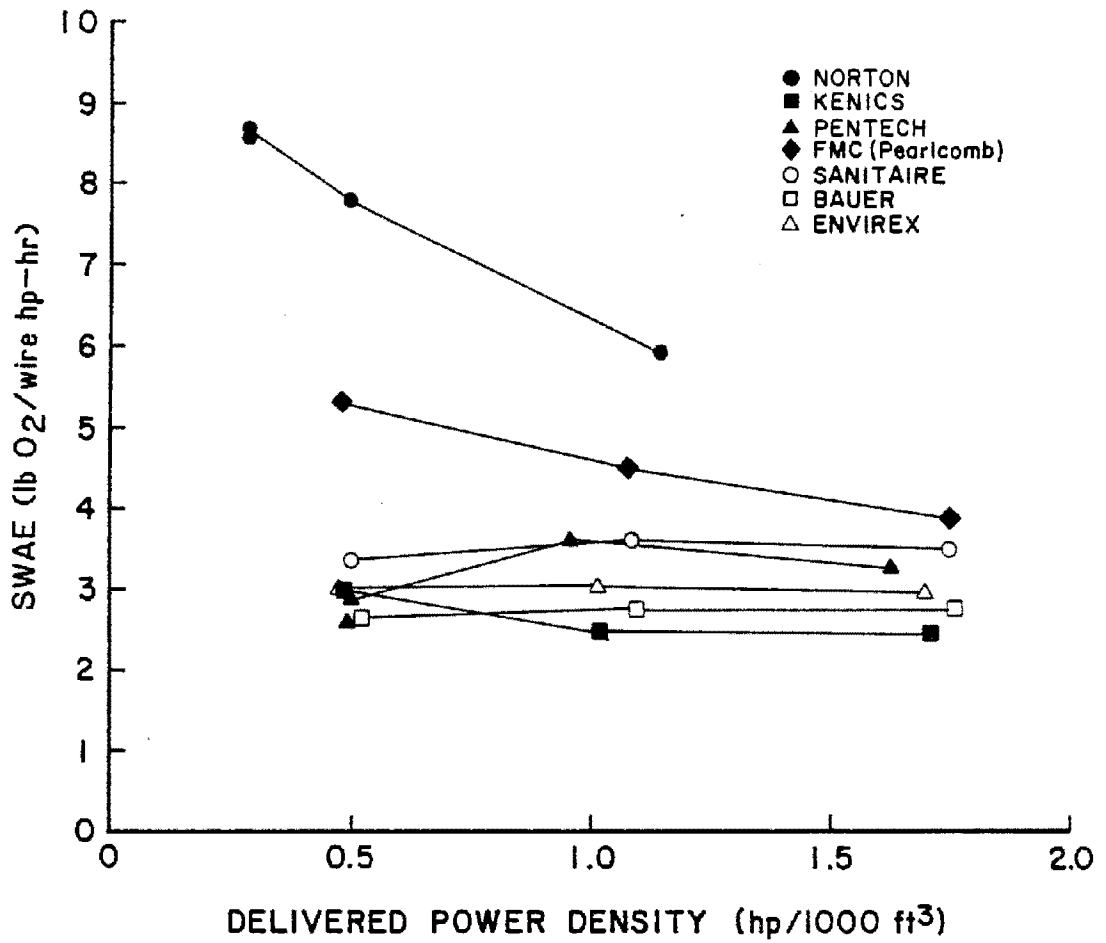


Figure 40. Comparative plot of SWAE vs. delivered power density at 20-ft water depth.

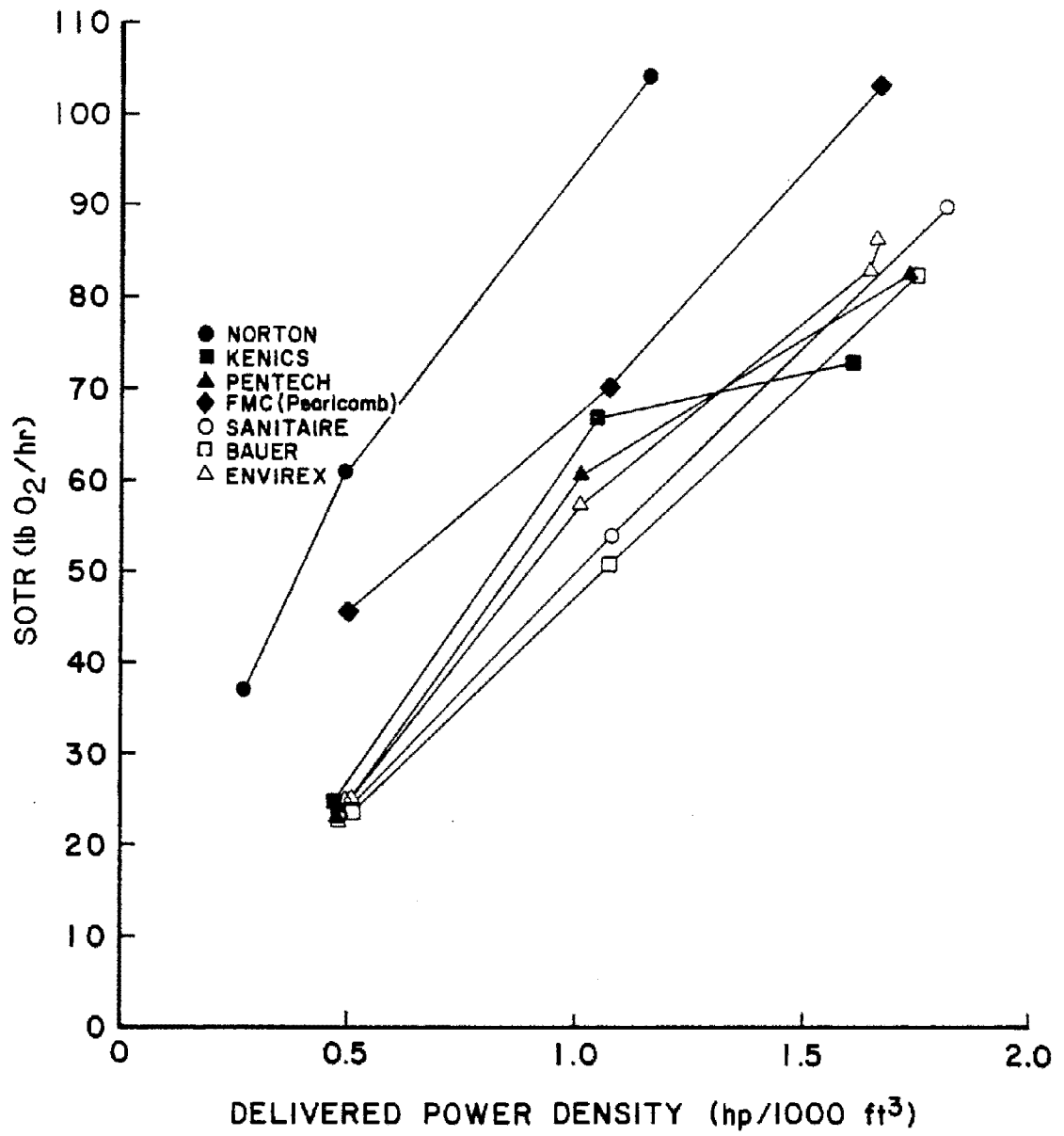


Figure 41. Comparative plot of SOTR vs. delivered power density at 25-ft water depth.

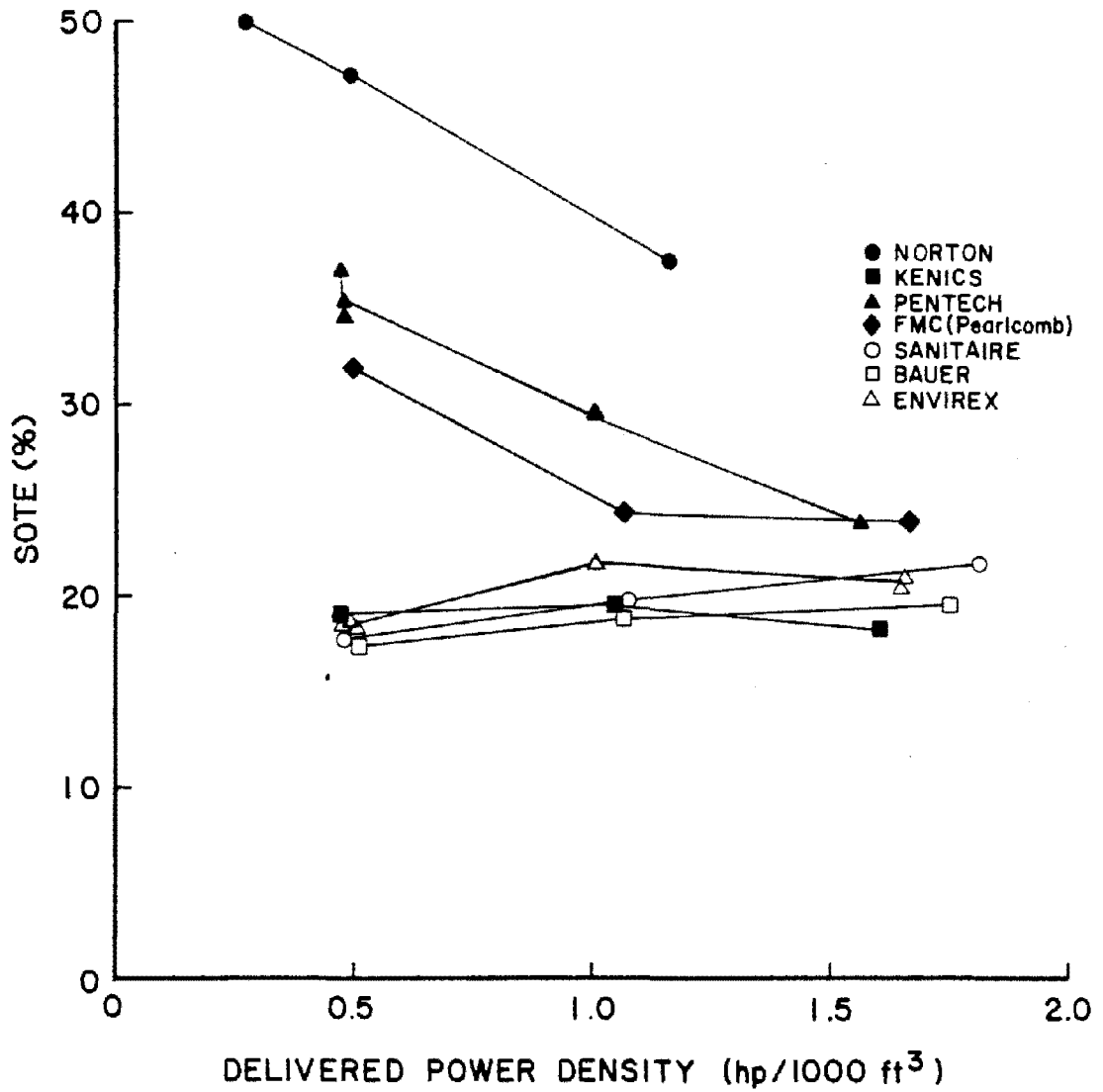


Figure 42. Comparative plot of SOTE vs. delivered power density at 25-ft water depth.

delivered power density. The peak value of SOTE for both systems occurred at the lowest delivered power density. The peak SOTE value also occurred at the lowest delivered power density for the FMC Pearlcomb system. Unlike the first two systems, the SOTE vs. delivered power density relationship of this system is not linear, but is steeply sloped in the lower portion of the delivered power density range and horizontal in the higher portion of the range. Other systems generally showed minor variations in SOTE. The order of the system SOTE curves, from highest to lowest is Norton, FMC Pearlcomb, Pentech, Envirex, Sanitaire, Kenics, and Bauer, although the Kenics plot does cross the Envirex, Sanitaire, and Bauer curves between the lower and middle portions of the range.

SWAE is plotted against delivered power density for the 7.6 (25-ft) water depth in Figure 43 for the seven aeration devices tested at this depth. The FMC Deflectofuser was not tested at this water depth.

The Norton and FMC Pearlcomb systems produced linear, downward sloping curves with peak SWAE values at the lowest delivered power density. The Pentech and Envirex systems also demonstrated similar relationships with peak SWAE values occurring at the middle delivered power density. These two systems, in addition to the remaining aeration systems, exhibited minor variation in SWAE over the range of delivered power densities evaluated. The order of the system SWAE curves, from highest to lowest, is as follows: Norton, FMC Pearlcomb, Pentech, Envirex, Sanitaire, Kenics, and Bauer, although the Kenics curve crosses the Sanitaire and Bauer curves between the middle and upper portions of the range.

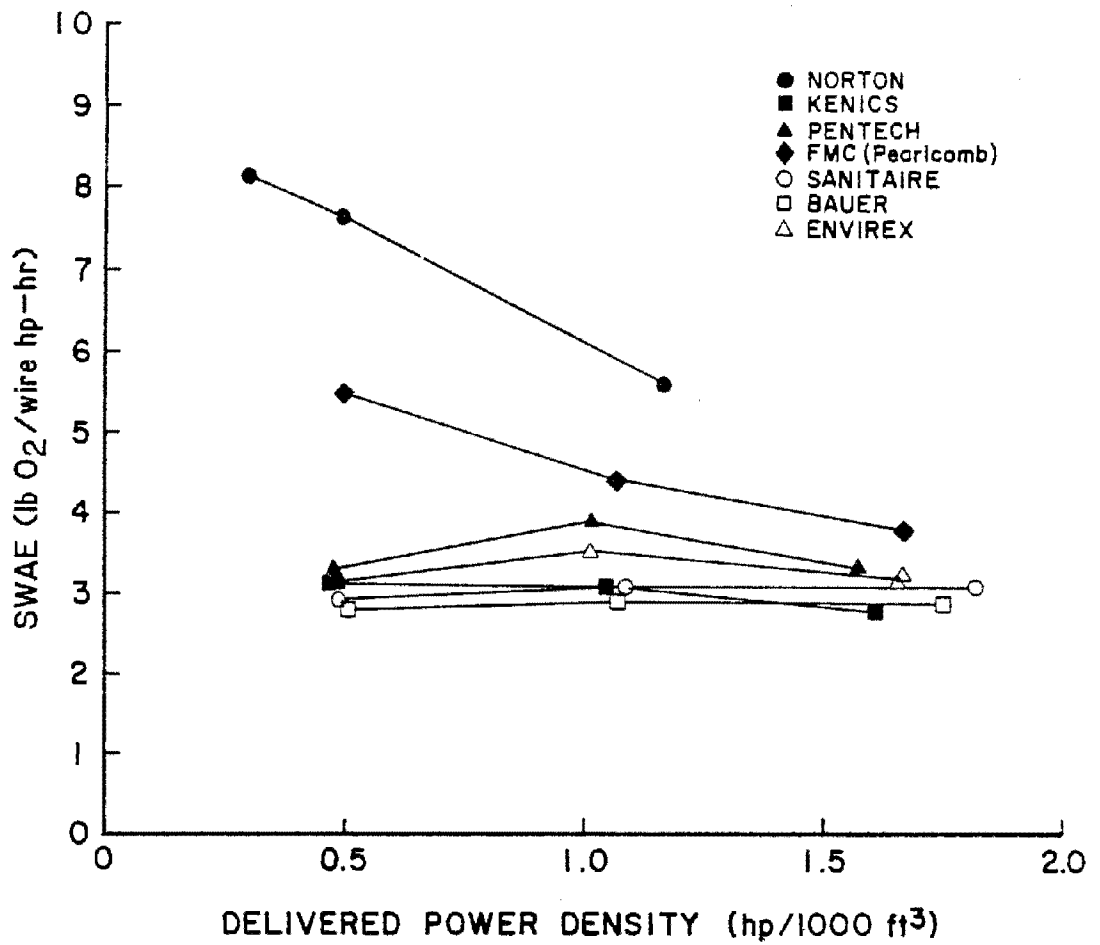


Figure 43. Comparative plot of SWAE vs. delivered power density at 25-ft water depth.

SECTION 7

PROBLEMS ASSOCIATED WITH CLEAN WATER TESTING

OVERVIEW

Prior to the initiation of clean water testing, a literature review was conducted and equipment manufacturers and other experts in the field were consulted. However, problems were still encountered, which often were not immediately obvious. It was, in many cases, not until after several tests were run that a problem became evident. During this evaluation, a total of 144 tests were completed. Of these tests, only 100 were acceptable for reporting. Reasons for the exclusion of test data from this report included excessive variation of $K_L a$ values, unacceptable testing conditions, and problems with primary data measurements. These problems are discussed below in the order in which they were encountered.

DEGASSING OF HIGH LEVEL DISSOLVED OXYGEN SAMPLES

The original testing procedure was to measure the D.O. concentration in all samples collected in the BOD bottles by using a D.O. meter and probe. Following probe analysis, one of the four sample locations would be analyzed using the Winkler method. A problem became apparent when the probe measurements began to disagree with the Winkler method measurement of the same sample. The disagreement was most evident in the equilibrium (saturated) samples, where the oxygen concentration levels were the highest. A number of potential explanations for this discrepancy were explored. Among the possibilities investigated were chemical interference with the Winkler method, improper concentration of the titrant used in the Winkler method, probe membrane condition, probe stirring rate, probe calibration procedure, and degassing of saturated samples. After examining all of the above, it became evident that degassing of the high D.O. samples was occurring. Degassing resulted from sample agitation by the D.O. probe stirrer. This agitation caused the formation of small bubbles that collected on the probe membrane and interfered with the probe's performance.

A number of possible corrections for this problem were considered. An attempt was made to modify the BOD bottle stirrer to produce less agitation. However, modification of the stirrer shape or speed was not successful. Because the equilibrium concentration of D.O. in water increased as the water temperature decreased, the possibility of chilling the samples was also considered. Although it appeared that this solution would work, implementation was viewed as impractical. A decision was instead made to analyze all samples by the Winkler method, which was

expected to be unaffected by high level D.O. concentrations. Although the Winkler method is a more time-consuming method for analysis, it is believed that the improved quality of the data generated made the added effort worthwhile.

BLOWER PULSATION

After a few months of testing, a blower pulsation problem was discovered. The effect of blower pulsation on airflow measurements was not obvious. No pulsating manometer fluid levels were detected, as one might at first expect. When the oxygen transfer test results were reviewed with the manufacturer and did not meet expectations, a decision was made to examine the airflow measurement system in detail.

The air delivery system consisted of two separate air lines, each made for a different range of airflow rates. In each line, there were two different types of airflow meters. One was an orifice plate; the other was an Annubar. Considerable care was exercised in the original design of the air piping system. All pipes were placed in a single plane. In locating the airflow measurement devices, proper upstream and downstream distances were maintained from bends or other airflow disturbances.

Before any oxygen transfer testing began, a typical range of airflow rates was run through each line at a typical range of line pressures. The line pressures were simulated by throttling a valve downstream of the flow meter section (no water was in the aeration tank at the time). Under these conditions, nearly perfect agreement was obtained between the orifice plate and Annubar at all flows tested. At that time, there was no reason to expect problems of any kind.

Measurements taken after the tank was filled with water made it clear that the agreement was no longer satisfactory. Furthermore, certain phenomena were observed that were difficult to explain. At low airflow rates, the Annubar manometer read negative instead of positive. Extensive leak checks were performed to no avail, and a conclusion was reached that a pressure disturbance of some type in the line was occurring. Even more baffling, however, was the fact that by changing the lengths of the manometer tubing, particularly on the Annubar, varying differential pressure readings could be produced. Short tubing lengths of approximately 1 m (3 ft) tended to produce differential pressure readings that differed by as much as 5 cm (2 in.) of water from those produced by longer tubing lengths [approximately 3.8 m (12 to 13 ft)]. Again, extensive leak checks were performed to no avail. After consulting a number of experts in the field, it was decided to use larger diameter tubing [6.4 mm (1/4 in.) I.D., instead of 4 mm (5/32 in.) I.D.] as well as to make the tubing leads exactly the same length on both sides of the manometer. After making these corrections, the problem was still experienced with the Annubar but apparently not with the orifice plate. A decision was made at that time to disregard readings from the Annubar, as it was obviously being affected by some type of pressure disturbance in the

line. Because the disturbance was located upstream from a check valve and other fittings, it was felt that in some way they might be interfering with the readings. It was not known at that time that the cause of the problem was pulsation.

After several more tests were conducted, the pulsation problem was discovered. During a second complete recheck of the air measurement system, a valve was closed downstream of the Annubar such that all the blower air was wasted through the waste valve. Under these conditions, the Annubar manometer should have read zero since there was no net flow past it. Instead, it registered approximately 1.3 cm (0.5 in.) of water in a negative direction with short tubing leads and approximately 6.4 cm (2.5 in.) of water in a negative direction with long tubing leads. It was at this time that pulsation was suspected. The Annubar manometer reading went to zero when a valve upstream of the flow meter was shut off. This confirmed the existence of a pulsation phenomenon.

In an attempt to dampen the pulsation, a decision was made soon afterwards to install a large in-line air reservoir downstream of the blower. This was one of the recommended procedures to help eliminate pulsation. The tank used was cylindrical, 0.8 m (2.5 ft) in diameter and 2.2 m (7.25 ft) high, with a capacity of approximately 1 m³ (35 ft³). The tank air inlet was mounted near the top perpendicular to the outlet mounted on the bottom. After the tank was installed, essentially perfect agreement was obtained between the Annubar and the orifice plate over the full range of flows and pressures. Furthermore, the manometer zeroed perfectly when the downstream valve was closed and the manometer readings were not affected by short and long tubing leads. The Annubar manometer no longer read negative at low airflows as it did prior to the installation of the reservoir.

Although the exact amount of error is not known, it does appear that the effect of pulsation on airflow measurements was greater at the combination of low airflow rates and high water depths. This was determined by a comparison of all the orifice plate and Annubar data from the tests performed when the problem existed. A relationship between the differences in the Annubar and orifice plate measurements with air flow rate and water depth was evident. It appears that the data collected at high airflow rates and low water depths were very nearly correct; however, as the airflow rate decreased and the water level increased, the error became much worse. It is interesting to note that based on these findings it would appear that the pulsation problem was worse at low line velocities.

It should be mentioned that after the problem was corrected, a clean water test was run at the 6.0-m (20 ft) depth. The oxygen transfer results obtained then met the manufacturers' expectations.

EXCESSIVE $K_L a$ VARIATION

The original limitations set for defining acceptable tests included a minimum number of data points per analyzed location and a maximum variation level of the $K_L a$ values resulting from analysis of data from four locations. These $K_L a$ values were calculated using the Equilibrium method analysis of data between 20 and 80% of measured D.O. saturation. Each location was required to be within 6% of the average of the four locations. This criterion for maximum allowable $K_L a$ variation was set up prior to the conducting of any tests. The intent was to invalidate a test if the tank did not appear to be completely mixed. It was based on the recommendations of people experienced in clean water evaluation of aeration equipment. Of the 100 accepted tests, four runs did not meet this criterion. Of these four, one test was on the variable orifice diffuser and the remaining three were on the static tube aerator.

It was during testing of the static tube aerator that problems were initially encountered with regard to excessive $K_L a$ variation. In addition to the excessive percent variation, the tests showed a significant degree of scatter on plots of the log-deficit saturation vs. time. The log-deficit saturation is the logarithm of the difference between measured D.O. concentration and measured D.O. saturation level. In general, this graph clearly defined a linear relationship between the log-deficit saturation and time. Low correlation values calculated for static tube aerator test regression lines indicated that a significant degree of scatter was present at each sample location.

Difficulties result from the bottom sample location. In an attempt to better understand the problem and to verify that the original sample location was representative, an additional bottom sample point was installed. The original bottom location was relatively close to an aerator. The new location, on the other hand, was centered between four static tube aerators. The additional sample location was sampled on 10 of the 19 runs. After further testing, a considerable but random difference between the two bottom locations was frequently found. A decision was made to use results only from the original sample location since the problem did not appear to be directly attributable to the position of the bottom sample pump.

Altogether, a total of 19 tests were run on the static tube aerator. Of these tests, only nine satisfied the projects' original limitation of allowable $K_L a$ variation. Three of the tests had variations between 6 and 7%, and a decision was made to include these tests in the final results. This was decided after additional tests conducted under the same conditions produced no better results.

It is possible that problems experienced with the static tube aerator configuration tested may have been the result of non-uniform mixing. However, such an evaluation was not a primary aim of the study and more specific testing would have been needed to support this conclusively.

JET AERATOR PUMP POWER MEASUREMENT

With the exception of the jet aerator system, all systems tested required power only to supply compressed air. As mentioned previously, air power for all systems was calculated using the adiabatic compression equation and typical full-scale values for blower and motor efficiencies were assumed. In the testing of the jet system, pump power was measured two ways. A wattmeter/recorder was used to monitor the actual power being supplied to the pump. A pressure tap at the discharge side of the pump allowed the measurement of total dynamic head (TDH) on the pump. The initial analysis employed measured power values to determine the total nominal horsepower values. The manufacturer indicated that because of the relatively small volume of the clean water test tank, the pump being used was of unusually low efficiency and the results would be neither fair to the manufacturer nor representative of full-scale operational efficiencies. It was also pointed out that in computing air power, the blower and motor efficiencies being used were typical of full-scale operations. Following discussions with the EPA Project Officer and the Project Consultant, it was decided that full-scale efficiencies would be permitted. The TDH measurements were used with pump curves to determine the pumping rate. Using these flow rates, TDH measurements, and pump and motor efficiencies typical of full-scale designs, the power values were calculated. The following equation was used for this determination:

$$P_{pd} = \frac{Q_p (\gamma \text{ water}) (\text{TDH})}{550} \quad (34)$$

in which:

P_{pd} = jet aerator pump delivered power
 Q_p = liquid flow rate produced by jet aerator pump
 $\gamma \text{ water}$ = specific weight of water at 20°C (62.4 lb/ft³)

Unfortunately, this calculation could not be easily generalized. It was complicated by the fact that typical pump and motor efficiencies differed, depending on whether submersible or dry pit pumps were employed. For a submersible pump, the manufacturer recommended an overall efficiency of 65.6% (assumed a pump efficiency of 75% and a motor efficiency of 87.5%). For a dry pit pump, the manufacturer recommended a typical overall efficiency of 75.2% (assumed a pump efficiency of 86%, a motor efficiency of 92%, and a coupling efficiency of 95%). The manufacturer also mentioned that both types of pumps were used with nearly the same frequency. Since it was desired to have only one set of horsepower numbers for the jet aeration analysis, a decision was made to use the average of the typical overall efficiencies for each type of pump. Thus, the jet aerator data were reevaluated using an overall pump-motor-coupling efficiency of 70.4%. If a design engineer is considering using power numbers from this report, the pump power percentage of the total power should be adjusted up or down, depending on the type of pump proposed.

To calculate the SWAE of a jet aerator using a different pump efficiency, the following factor may be applied:

$$\text{Factor} = \frac{100\%}{100\% - \% P_{pw}[(e' - 0.704)/e']} \quad (35)$$

in which:

$\% P_{pw}$ = percent of total delivered aerator power supplied by pump
 e' = new assumed overall (pump, coupling, and motor) efficiency

This correction to the standard wire aeration efficiency, N_{wo} , may be applied as follows:

$$N'_{wo} = \text{Factor} \times N_{wo} \quad (36)$$

in which:

N'_{wo} = corrected value of standard wire aeration efficiency

TAP WATER FOAMING

During the testing of the fine bubble tube diffuser, significant foaming problems developed after 12 tests on the system were completed. Foaming was first experienced with a new batch of water. The onset of the foaming seemed to correlate with the beginning of rain in the general area, although not with any direct rainfall on the test tank.

The test tank foam was white, billowy, and at times as thick as 0.8 m (2.5 ft). It did not cover the entire water surface, but usually occupied two circular regions on the east and west walls of the test tank. These circular regions were observed to be as large as 1.5 m (5 ft) in diameter. The foam was very stable and tended to cling to the test tank walls. It did not break down even after relatively long periods of aeration. It was also not uncommon to see bubbles as large as 20 to 30 cm (8 to 12 in.) in diameter breaking on the surface of the tank during aeration.

The problem did not appear to be entirely confined to the surface of the tank as water being pumped from the mid-depth location past an in-line probe showed a tendency to form some bubbles. Other observations were that foam formed fairly rapidly when the air was turned on and broke up immediately when the air was shut off. Finally, the level of foaming seemed to increase with either an increase in depth or an increase in airflow rates.

When the foaming problem first developed, the local water supplier and the wholesale distribution agency were contacted; however, they could shed no direct light on the situation. A decision was made at that time to suspend testing until the cause of the foaming could be determined and corrected. It has been well substantiated that surface active agents can have a tremendous effect on oxygen transfer tests.^{12/} Laboratory personnel

attempted to determine the chemical characteristics of the tap water and foam; the engineering staff conducted various field tests and procedures to determine the source of the contaminants. A number of possible contamination sources were considered, including the tap water supply, the test tank and/or diffuser system, and the air supply. At that time, the preponderance of the laboratory and field evidence seemed to indicate that the water supply was the source of the problem.

The laboratory staff determined that linear alkylate sulfonate (LAS), the common surfactant present in detergents, was not measurable in the test tank water. It was also determined that, upon coalescence, the bubbles in the foam formed a deep brown liquid with well flocculated suspended solids readily apparent. The staff also began an involved chemical extraction procedure in an attempt to isolate the foaming agent. Other tests conducted included surface tension, amine concentration, and pH.

Surface tension tests were performed on water samples from the following locations: 1) the test tank, 2) the test tank water faucet, 3) the plant's non-potable water supply tank, and 4) the bottled drinking water supply (Sparkletts). The results of the tests showed that there was essentially no difference in surface tension between the four samples and that the surface tension obtained agreed with handbook values. This was somewhat baffling, but additional testing revealed that the surface tension of the condensed foam liquid was a little lower than that corresponding to tap water. This information led to the belief that perhaps the foaming problem was primarily a surface phenomenon, with aeration serving to concentrate the surfactant on top of the tank.

Further proof of the concentrating phenomenon was obtained from laboratory amine tests performed on both bulk liquid and foam samples. Very high concentrations were found in the foam, while insignificant concentrations were obtained in the bulk liquid. It was felt that the high level of amines in the foam might be related to the cause of the foaming. Among other things, the high amine concentration could have been due to the presence of polymers in the water supply or to proteins from living cells.

It may be of interest to review some of the field tests that were performed to determine the cause of the foaming problem. First, small-scale aeration tests (500-ml beakers) were conducted on separate water samples from the test tank, the test tank water faucet, the plant's water supply tank, and the bottled drinking water supply. Surprisingly enough, none of the samples, including the test tank sample, could be made to foam at this small a scale. It was concluded that the scale of the test was very important and that further testing would have to be conducted on a sufficiently large scale.

To determine whether a cross-connection into the plant's non-potable water supply system existed, it was decided to fill the aeration tank with water from a separate distribution system; the plant's fire water system was used. The aeration tank foaming was not reduced by this method, however, and it was concluded that plant cross-connections were not the problem.

In an attempt to determine whether the problem was related to the incoming water, air diffusers were installed in the plant's water supply tank. This tank was much smaller than the aeration test tank used for the clean water evaluation. Aeration produced essentially no foam. It was then concluded that either the scale of the test was too small or that the problem was not related to the incoming water, but to some other source such as aeration test tank contamination.

Aeration test tank contamination was eventually eliminated as a possibility. Six or seven batches of water were used in the tank, and between fillings, the tank was always hosed out thoroughly. Each successive batch of water indicated no decrease in the severity of the foam. This indicated that the source was either not present in the test tank or that it was an extremely large source, which was unlikely. Furthermore, it was determined that the foam could be vacuumed from the top of the tank (a somewhat slow and incomplete process) and that the foam did not return to its original level. With the next water batch, however, the foam returned completely. This indicated that the source of the foaming was not the aeration test tank, the air supply, or atmospheric contamination.

Since the causative agent was felt to be in the incoming water, a decision was made to try and remove the contaminant by some means. It was believed that surfactant was probably an organic compound at a fairly low concentration; consequently, removal by carbon adsorption seemed a likely possibility.

Concern was expressed by EPA that pretreatment of the water should be avoided, if possible, since this was not done for the earlier manufacturers in the study. It was conceded that to avoid further delays, an activated carbon column should be installed in an attempt to remove the surfactant before it entered the aeration test tank.

The column was initially operated in a downflow mode, but large carbon particles escaped around the retaining plate at the bottom of the column. Fortunately, this was discovered before any attempt was made to fill the aeration tank. To correct this problem, a decision was made to operate the column in an upflow mode. The carbon column piping was revised to accommodate this change in operation. The carbon column was backwashed extensively to get rid of carbon fines. Unfortunately, the first batch of aeration tank water showed that this operation had not been successful. A noticeable quantity of fine colloidal carbon was present in the treated water, so much, in fact, that the water took on a deep black appearance. The fine colloidal carbon particles had an almost neutral buoyancy and were carried out of the column at even the lowest of surface loading rates. It was interesting to note that under aeration the treated tank water produced no trace of foam or other surfactant phenomena of any kind. The fine colloidal carbon in the water was not acceptable, however, so a means of correcting the problem was sought.

It was felt that the escape of fine colloidal carbon could not be controlled in the upflow mode of operation, and a decision was made to

revert back to the downflow mode. This time, however, a 20-cm (8-in.) bed of #20 silica sand was backwashed down to the bottom of the column in an attempt to filter the #12 to #40 activated carbon. This attempt was only partially successful and an additional 13 cm (5 in.) of #12 silica sand was added in the same manner. After approximately 8 hr of downflow operation with a 10-min contact time [3.2 L/sec (50 gpm)], essentially no carbon or sand was observed in the carbon column effluent. The aeration test tank was filled to the 3-m (10-ft) depth with this treated water, but although the water was noticeably clearer than regular tap water, it soon became apparent that a portion of the surfactant still remained. Under aeration no buildup of foam occurred as before, but surface bubbles were noticeably larger than in regular tap water [bubbles as large as 10 to 13 cm (4 to 5 in.) in diameter were observed]. While the carbon column removed the major portion of the surfactant, it was obvious that a greater contact time was required to achieve complete removal. To increase the contact time to 20 min, the flow rate through the carbon column was reduced to 1.6 L/sec (25 gpm). Unfortunately, even this contact time was insufficient to achieve complete surfactant removal. It was not considered feasible to go to even lower flow rates through the carbon column, or on the other hand, to use a larger carbon column. With this in mind, it was decided to try and show that the available water was equivalent to previously used "clean" water as far as the oxygen transfer testing was concerned.

To show the effect of both the surfactant and the activated carbon process on the oxygen transfer results, the results of five tests were analyzed for the 3.0-m (10-ft) water depth and the 26.3-W/m³ (1.0-hp/1000 ft³) power level. The only difference between these tests was the quality of the water used in each case. The first data set evaluated was from a background test (8/29/78) conducted at a time before the foaming problem was observed. The second data set was from a test (9/29/78) conducted when the foaming problem was very much in evidence. The third test (10/13/78) was conducted with water that was obtained from the upflow carbon column operation and, as a result, contained a great deal of the fine colloidal carbon, but no evidence of a surfactant. For the fourth test (10/19/78), the test tank water was obtained from the high-rate [3.2-L/sec (50-gpm)] carbon column operation in a downflow mode; some evidence of a surfactant was present. For the fifth test (10/26/78), the test tank water was obtained from the low-rate [1.6-L/sec (25-gpm)] carbon column operation in a downflow mode. Again, some evidence of a surfactant was present. The results of these five tests are compared in Table 20 below.

TABLE 20. FOAMING PROBLEM COMPARISON TESTS

Date	Run	Average Water Depth (ft)	Delivered Power Level (hp/1000 ft ³)	Airflow Rate (scfm)	K _L a ₂₀ (1/hr)	Standard Oxygen Transfer Efficiency (%)
8/29/78	2	10.06	1.16	276.6	13.02	11.31
9/29/78	1	10.04	1.18	277.6	13.37	11.54
10/13/78	1	9.98	1.17	274.5	14.02	12.06
10/19/78	1	10.12	1.22	284.0	13.98	11.76
10/26/78	1	10.06	1.19	278.8	14.65	12.41

The first two tests indicate that the surfactant had no effect on SOTE transfer. The SOTE obtained with foam in the tank was 11.5% as compared to 11.3% without it. Even though this comparison was noted early in the foaming problem investigation, it was still considered necessary to eliminate the cause of the problem. The credibility of the tests might be questioned by the presence of foam in the water no matter how many comparative tests gave evidence to the contrary.

Additional proof that the surfactant did not affect the oxygen transfer results was obtained after the carbon column was installed. In the test with no surfactant present (10/13/78 - Run 1), the SOTE obtained was 12.1%. The following two tests both had some surfactant remaining in the water and yielded an average SOTE identical to that from the 10/13/78 run.

After the carbon adsorption unit was installed, the data indicated that the SOTE values increased slightly. The average of the three "carbon adsorption" tests produced an SOTE of 12.1% as compared to 11.4% for the two tests before the carbon adsorption unit was installed. This was an increase of 5.7% and would appear to be significant. This phenomenon was best explained by the possibility that the carbon column removed an oxygen transfer inhibiting compound(s) that occurs naturally in local tap water. It was also possible, however, that the change in SOTE was not related to the carbon column at all, but was due to other factors such as water temperature variation [water temperature decreased steadily from 24.5°C (76.1°F) during the first test to 21.9°C (71.4°F) during the last test].

After considering the results of the first four comparison tests (the fifth test was not run until later), a decision was made to go ahead and

run the remaining fine bubble tube diffuser tests on water from the carbon column. Unfortunately, the results of these latter tests strongly supported the hypothesis that the activated carbon process (or possibly some other factor) was having a significant influence on the oxygen transfer results. The transfer efficiencies obtained exhibited an increase of 13 to 15% over what would be projected from tests at the 3.0- and 7.6-m (10- and 25-ft) depths. Pounds of oxygen transferred per wire horsepower-hour vs. delivered power was plotted for the various depths. It was evident that the curves for the 4.6- and 6.1-m (15- and 20-ft) depths were on considerably higher curves than those for the 3.0- and 7.6-m (10- and 25-ft) depths. This would not be expected if the tests were conducted on water of identical quality. The tests for the 4.6- and 6.1-m (15- and 20-ft) depths were conducted with carbon treated water, while the others were conducted on non-foaming tap water. It was clear from the plot that the effect was very significant for all power levels. Furthermore, the magnitude of the difference was much more significant than what would have been predicted from the comparison tests at the 3.0-m (10-ft) water depth.

A decision was made to run the rest of the tests for the study without the carbon treated water. As mentioned previously, the surfactant causing the foaming problem did not appear to be affecting the oxygen transfer results, whereas the use of the activated carbon process did. It should be mentioned that it is likely that the oxygen transfer results obtained from the carbon treated water are closer to actual "clean" water transfer results. It appears, however, that there may have been some natural surfactant present in the tap water from the start of the study. Since our main objective was to compare the different manufacturers' equipment under the same conditions, it did not seem appropriate to use the carbon treated water only for the manufacturers that remained to be tested. The fine bubble tube diffuser tests for the 4.6- and 6.1-m (15- and 20-ft) water depths that were conducted with carbon treated water initially were repeated using untreated tap water.

SECTION 8

FOLLOW-ON RESEARCH ACTIVITIES

To determine the wastewater correction factors associated with some of the generic oxygen transfer devices evaluated in the clear water study, LACSD, in conjunction with EPA, conducted full-scale oxygen transfer tests in mixed liquor (Aeration Equipment Evaluation - Phase II). Not all of the equipment evaluated during Phase I could be tested in Phase II due to space and manpower limitations. A decision was made, therefore, to test the three most promising devices from a potential energy conservation standpoint. The tests were carried out in parallel trains at the Districts' Whittier Narrows Water Reclamation Plant. The aeration systems selected included

- o fine bubble (dome/disc) diffusers applied in a total floor coverage configuration,
- o fine bubble tube diffusers applied in a dual aeration configuration, and
- o jet aerators.

Operation of the three aeration systems in mixed liquor began in December 1980. For 6 mo, information on oxygen transfer and mechanical reliability was collected on the three systems. After this initial screening, the most promising system was tested on an expanded scale for 8 mo at nominal aeration detention times of 4 to 6 hr. This system was the fine bubble ceramic (dome/disc) diffusers. Mixed liquor testing was completed in December 1982. A final report of the results of the Phase II study is in preparation.

REFERENCES

1. Personal communication with Dominguez Water Corporation, Long Beach, CA, September 20, 1978.
2. Cusick, C.F. Flow Meter Engineering Handbook. Fourth Edition, Honeywell, Fort Washington, PA, 1968. pp. 1-14, 57-79, 85-165.
3. Fluid Meters, Their Theory and Application. Fifth Edition, ASME, 1959.
4. American Public Health Association. Standard Methods for the Examination of Water and Wastewater. 14th Edition, Washington, D.C., 1975.
5. Spink, L.K. Principles and Practice of Flow Meter Engineering. Ninth Edition, Foxboro Company, Foxboro, MA, 1967. pp. 3-127, 415-530, 545-564.
6. Metcalf and Eddy, Inc., Wastewater Engineering. McGraw-Hill, New York, NY., 1972.
7. Lewis, W.K. and W.C. Whitman. Principles of Gas Adsorption. Ind. Eng. Chem., 16:1215, 1924.
8. Proceedings: Workshop Toward an Oxygen Transfer Standard. Edited by W. C. Boyle. EPA 600/9-78-021, NTIS No. PB-296557/2, U.S. EPA, Cincinnati, OH, April 1979.
9. Stukenberg, J.R., V.N. Wahbeh, and R.E. McKinney. Experiences in Evaluating and Specifying Aeration Equipment. Journal WPCF, 49(1):66-82, January 1977.
10. Beveridge, G.F.G. and R.F. Schechter. Optimization - Theory and Practice. McGraw Hill, New York, NY, 1970. pp. 453-456.
11. Stenstrom, M.K., L.C. Brown, and H.J. Hwang. Oxygen Transfer Parameter Estimation. Journal of the Environmental Engineering Division, ASCE, 107(E2):379-397, April 1981.
12. Houck, D.K. and A.G. Boon. Survey and Evaluation of Fine Bubble Dome Diffuser Aeration Equipment. EPA 600/2-81-222, NTIS No. PB82-105578, U.S. EPA, Cincinnati, OH, September 1981.

APPENDIX A

AIRFLOW METER EQUATIONS

The equations that follow can be used to determine airflow rate at standard conditions based on measured data. The orifice plate and Annubar equations are shown separately. Standard conditions for airflow measurement are 20°C (68°F), 101.3 kPa (14.7 psia), and 36% relative humidity.

ORIFICE PLATE AIRFLOW EQUATIONS

For a definition of the variables used in this appendix subsection, refer to the Nomenclature section of this report. The following orifice plate airflow equation was used for this project:

$$Q_o = (K)(S_o)(F_a)(F_m)(F_{pe})(F_{wv})Y \sqrt{\frac{(h_o) (0.01934p_a + 0.491p_{fo})}{(T_f + 460)}} \quad (A1)$$

The equations common to both orifice plates are shown below:

$$F_a = 2 \times 10^{-5} (T_f + 460) + 0.9891 \quad (A2)$$

For ZK red fluid-filled manometer:

$$F_m = \sqrt{1 - 0.05448 \frac{(0.01934p_a + 0.491p_f)}{(T_{am} + 460)}} \quad (A3)$$

For water-filled manometer:

$$F_m = \sqrt{1 - 0.04331 \frac{(0.01934p_a + 0.491p_f)}{(T_{am} + 460)}} \quad (A4)$$

$$F_{pe} = 1.333 \times 10^{-5} (T_f + 460) + 0.9930 \quad (A5)$$

$$F_{WV} = \frac{1 - (p_{W1}/(0.01934p_a + 0.491p_f))}{\sqrt{1 - 0.3775 [p_{W1}/(0.01934p_a + 0.491p_f)]}} \quad (A6)$$

in which:

$$p_{W1} = \frac{(0.01934p_a + 0.491p_f)(RH)(p_{VP}T)}{1.934p_a} \quad (A7)$$

and

$$p_{VP}T = \log^{-1} \left[8.13254 - \left(\frac{1764.42}{236.139 + T_w} \right) \right] (0.01934) \quad (A8)$$

3-in. Orifice Plate

$$K = 1256.93$$

$$S_o = -0.001 \sqrt{15.392 - \left(\frac{Re-96,800}{20,000} \right)^2} + 0.19658 \quad (A9)$$

(for R_e from 19,000 to 120,000)

$$Y = 1 - 0.01141 h_o/(0.01934p_a + 0.491p_{fo}) \quad (A10)$$

4-in. Orifice Plate

$$K = 2201.56$$

$$S_o = -0.002 \sqrt{12.527 - \left(\frac{Re-383,000}{100,000} \right)^2} + 0.32871 \quad (A11)$$

(for R_e from 30,000 to 500,000)

$$Y = 1 - 0.01257 h_o/(0.01934p_a + 0.491p_{fo}) \quad (A12)$$

Note:

$$R_e = 28.943 Q/d \mu \quad (A13)$$

in which:

$$\mu = 2.218 \times 10^{-5} (T_f + 460) + 0.00641 \quad (A14)$$

ANNUBAR AIRFLOW EQUATIONS

For a description of the variables used in this appendix subsection, refer to the Nomenclature section of this report. The following Annubar airflow equation was used.

$$Q_a = K' \sqrt{\frac{h_a}{0.491(p_t - p_{fa})(T_f + 460)}} \left[\left(\frac{(0.01934p_a + 0.491p_t)^{0.2857}}{(0.01934p_a + 0.491p_{fa})} \right)^{-1} \right] \quad (A15)$$

in which:

$$K' = (K)(F_m)(F_{pe})(F_{wv})(P_{fa}) \quad (A16)$$

$$F_m = (\text{See Eqs. A3 and A4})$$

$$F_{wv} = (\text{See Eq. A6})$$

3/4-in. Annubar

$$K = 100.55$$

$$F_{pe} = 1.6989 \times 10^{-5} (T_f + 460) + 0.99097 \quad (A17)$$

2-in. Annubar

$$K = 742.58$$

$$F_{pe} = (\text{See Eq. A5})$$

3-in. Annubar

$$K = 1690.74$$

$$F_{pe} = (\text{See Eq. A5})$$

APPENDIX B

PREAMBLE TO APPENDICES C THROUGH J

The results of clean water testing for the eight aeration systems evaluated in this study were summarized previously in Section 6 in Tables 3 through 18. Two tables were prepared for each system, one based on the Exponential method of analysis and the other on the Equilibrium method of analysis. Also in Section 6, the oxygen transfer performance of these systems was compared graphically in Figures 29 through 43.

In addition to the above graphs that compared the performance of all the manufacturers' equipment, a total of 69 graphs were prepared to summarize individual equipment performance for the eight aeration systems tested. These graphs are presented for each system in Appendices C through J. Nine graphs each were generated for Norton, FMC (fine bubble tubes), Pentech, Kenics, Bauer, Sanitaire, and Envirex (Appendices C through I, respectively), while just six graphs were produced for the FMC Deflectofuser (Appendix J) because it was tested at one water depth only.

Data from all water depths and power levels tested are included in the individual performance graphs. The nine graphs for each of the first seven systems listed above (Appendices C through I) illustrate in order the following relationships: Airflow Rate vs. Delivered Power Density, $K_L a_{20}$ vs. Delivered Power Density, SOTR vs. Delivered Power Density, SOTE vs. Delivered Power Density, SWAE vs. Delivered Power Density, SOTR vs. Water depth, SOTE vs. Water Depth, and SWAE vs. Water Depth. Only the first six of these graphs are included for the FMC Deflectofuser (Appendix J).

In the plots illustrating the effects of power variation, points representing the same water depth are connected. For the graphs depicting the effects of water depth variation, points of equal nominal power are connected. All connections between points were made using straight lines; the reader may elect to use smoother curve fits.

APPENDIX C

INDIVIDUAL PERFORMANCE RESULTS FOR NORTON FINE BUBBLE DOME DIFFUSERS

A total of 13 acceptable tests were conducted on the Norton fine bubble dome diffuser system in this study. The results of these tests were summarized tabularly in Tables 3 and 4 in Section 6 and are presented graphically here in Figures C-1 through C-9.

The effect of variations in airflow rate on delivered power density is shown in Figure C-1 for the various water depths. As expected, an increase in airflow rate resulted in an increase in delivered power density.

Figure C-2 shows the relationship between nominal power density and delivered power density. The effect that is generally demonstrated is that as power density increased, the differences between nominal and delivered power densities increased. The differences became larger with decreasing water depth.

Figure C-3 illustrates the relationship between delivered power density and K_{La20} . In this plot, the K_{La20} rate of increase is initially high, then appears to decrease slightly with increasing delivered power density. Also apparent is that increasing water depth resulted in decreasing K_{La20} values.

SOTR is plotted against delivered power density in Figure C-4. SOTR is expressed in both U.S. customary units (left vertical axis) and SI units (right vertical axis). For the Norton system, an increase in delivered power density produced an increase in SOTR. The rate of SOTR increase of this system was essentially linear at the 3.0-m (10-ft) water depth. Both nonlinearity and the rate of increase in SOTR increased with increasing water depth. The nonlinearity effect was characterized by an initial rapid increase in SOTR at low delivered power densities followed by a lower rate of increase at higher delivered power densities. The effect of increasing water depth on SOTR was greater than on K_{La20} . For every system tested, the same trend was noted; SOTR increased with increasing water depth.

Figure C-5 is a plot of the relationship between SOTE and delivered power density. SOTE values are clearly the greatest at the lowest delivered power density level tested. For three of the four water depths, the rate of SOTE decrease was greater at the lower delivered power densities than the higher ones. Also evident in this graph is the existence of a relationship between SOTE and water depth; an increase in

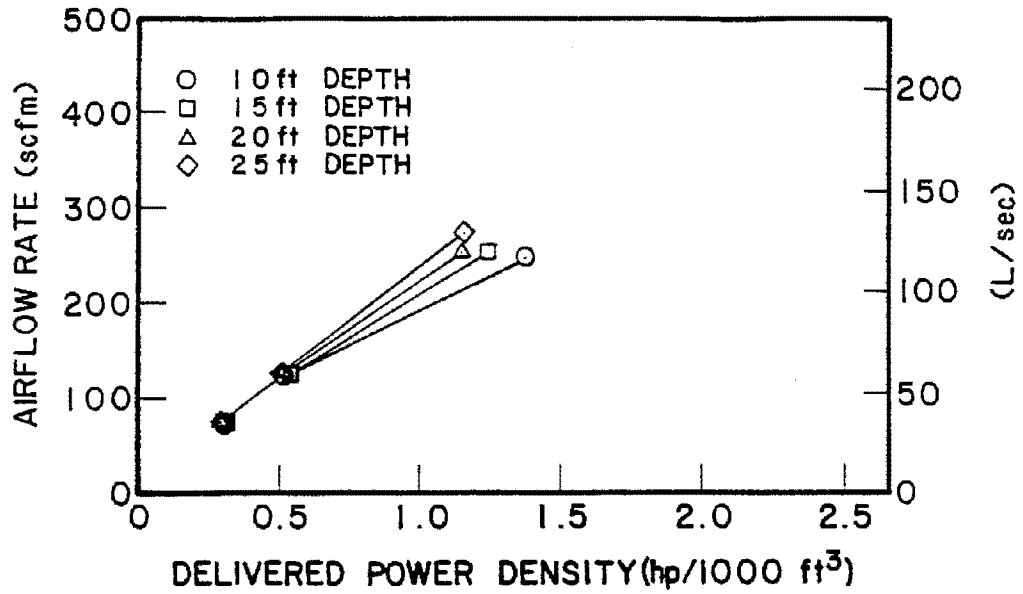


Figure C-1 Airflow rate vs. delivered power density for Norton fine bubble dome diffusers.

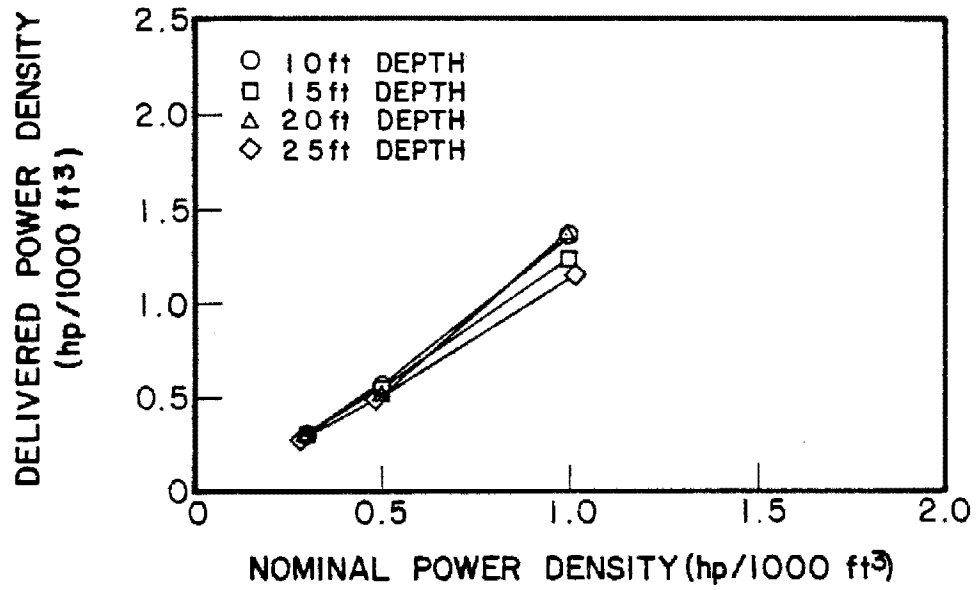


Figure C-2. Delivered power density vs. nominal power density for Norton fine bubble dome diffusers.

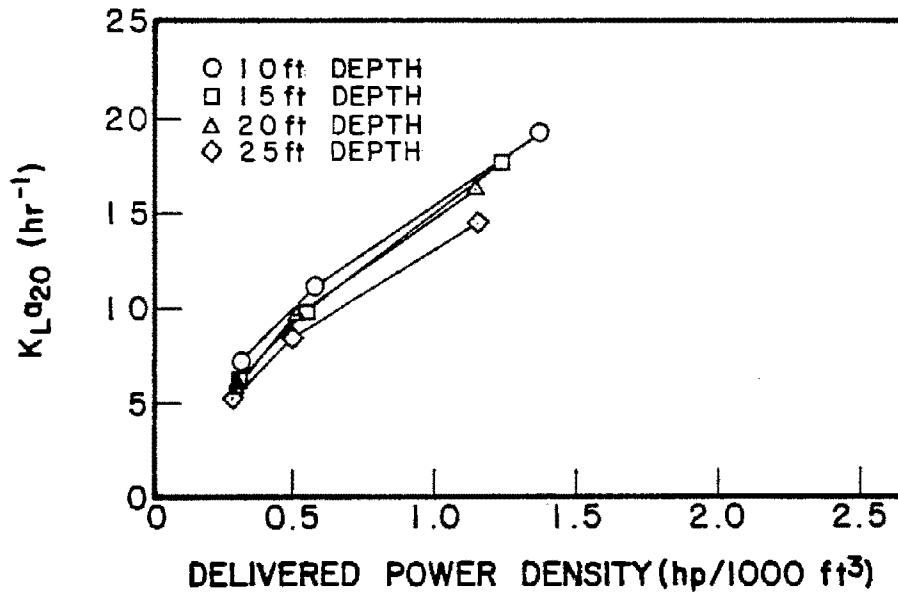


Figure C-3. $K_{La_{20}}$ vs. delivered power density for Norton fine bubble dome diffusers.

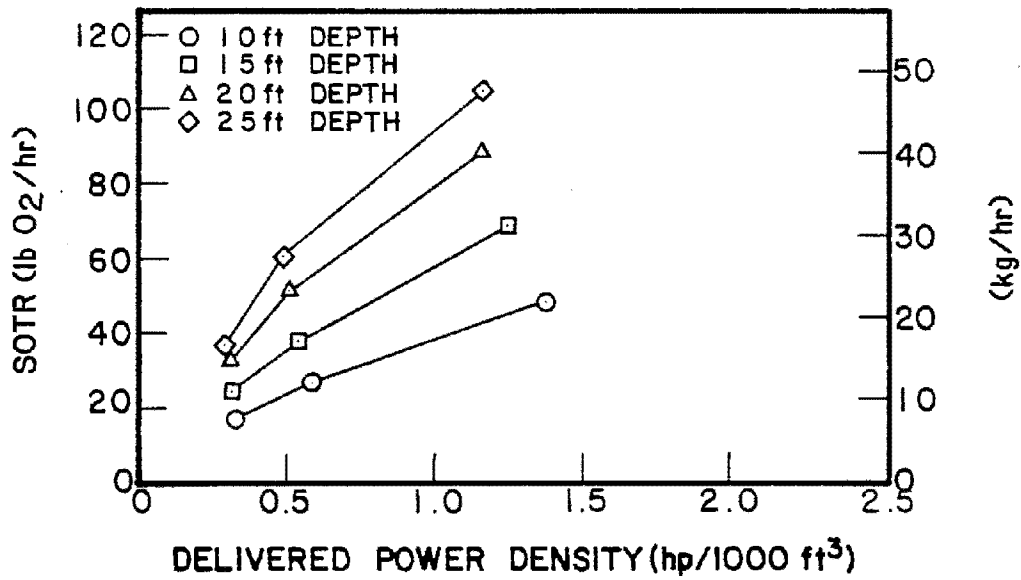


Figure C-4. SOTR vs. delivered power density for Norton fine bubble dome diffusers.

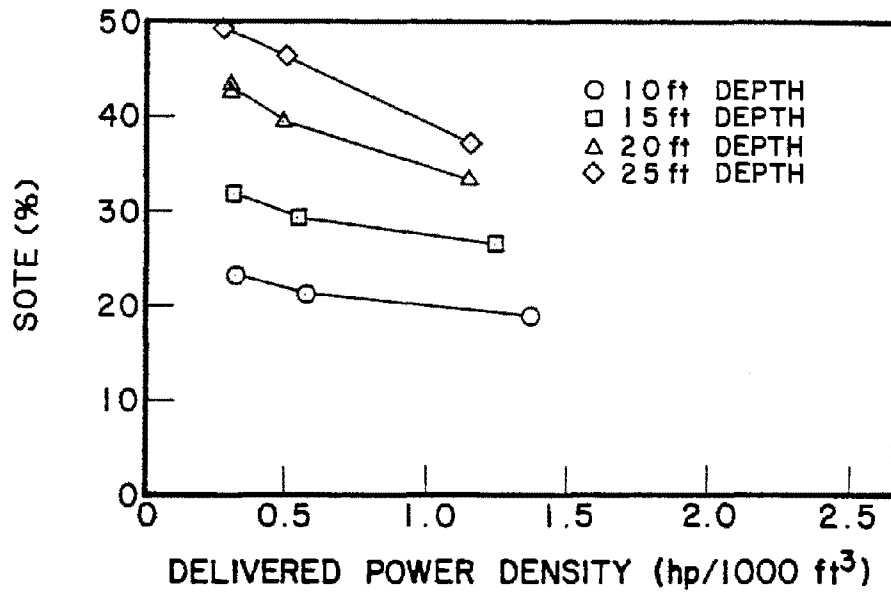


Figure C-5. SOTE vs. delivered power density for Norton fine bubble dome diffusers.

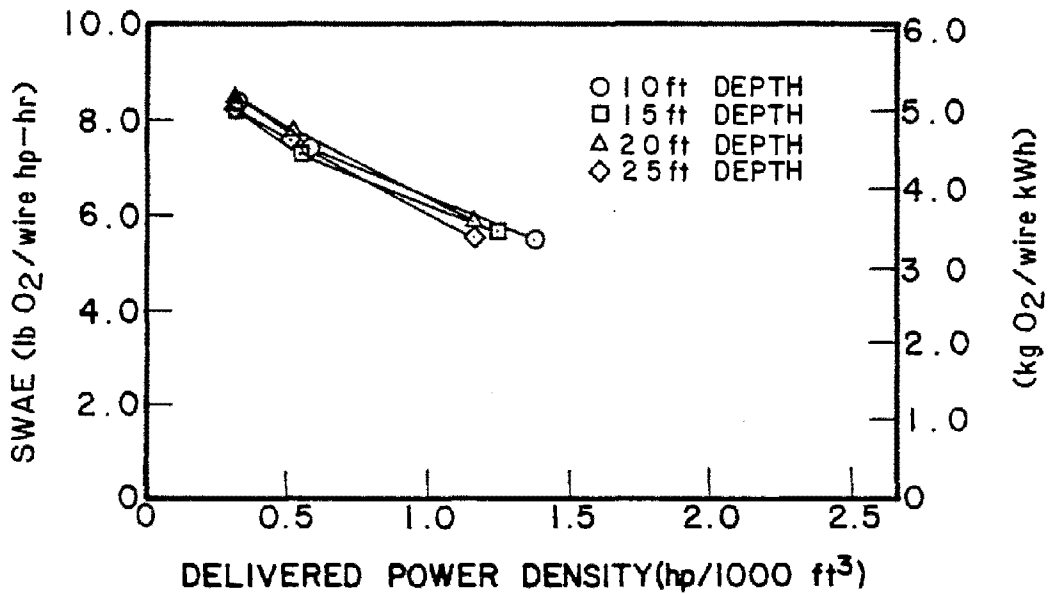


Figure C-6. SWAE vs. delivered power density for Norton fine bubble dome diffusers.

water depth resulted in an improvement in SOTE. In fact, this relationship is exhibited by the equipment of every manufacturer tested in this study.

SWAE vs. delivered power density is shown for Norton in Figure C-6. SWAE is given in both U.S. customary units and SI units. This graph is possibly the most important of those presented; the sensitivity or insensitivity of a system's efficiency to variations in delivered power density is demonstrated. For this system, the highest SWAE values occurred at the lowest delivered power density. The trend of the data is such that SWAE decreased almost linearly with increasing values of delivered power density. Unlike the preceding two figures, an increase in water depth generally did not result in increased values of the dependent variable (vertical axis). The effect of increasing water depth on this system appears minimal. Results representing various depths are clustered very closely for this system, indicating an insensitivity of the system to changes in water depth.

Figure C-7 illustrates the relationship between SOTR and water depth, with SOTR expressed in both U.S. customary units and SI units. An increase in water depth implies that for a given nominal power density to be maintained [i.e., $26.3 \text{ W/m}^3 = (1.0 \text{ hp}/1000 \text{ ft}^3)$], the delivered power must be increased by a comparable amount. It might, therefore, be expected that an increase in water depth would result in increased SOTR. This trend is indicated by results from each of the seven aeration systems tested at multiple water depths. The Norton system exhibited an almost linear increase in SOTR with increasing water depth. The highest SOTR values were observed at the highest nominal power density.

SOTE vs. water depth is plotted in Figure C-8. An increase in water depth produces an increase in pressure on discharged air in addition to increasing the detention time of air bubbles in the tank liquid. The theoretical impact of such changes is an increase in SOTE at greater depths.

Increasing SOTE with increasing water depth was observed for each of the seven aeration systems tested at multiple water depths. With the Norton fine bubble, an almost linear increase in SOTE was observed with increasing water depth. The highest values of SOTE were associated with the lowest nominal power density.

Figure C-9 depicts the Norton system's relationship between SWAE and water depth, with SWAE expressed in both U.S. customary units and SI units. In this illustration, SWAE appears to have been unaffected by changes in water depth. This system's peak SWAE performance was at the 6.1-m (20-ft) water depth. It is apparent that variations in nominal power density significantly affected SWAE. Optimum SWAE occurred at the lowest nominal power density evaluated.

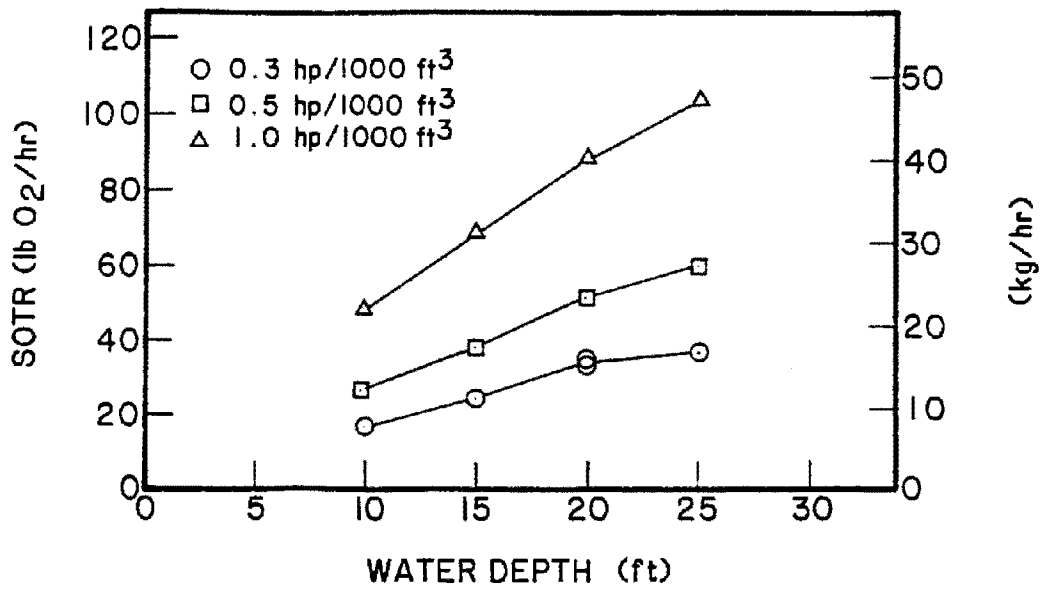


Figure C-7. SOTR vs. water depth for Norton fine bubble dome diffusers.

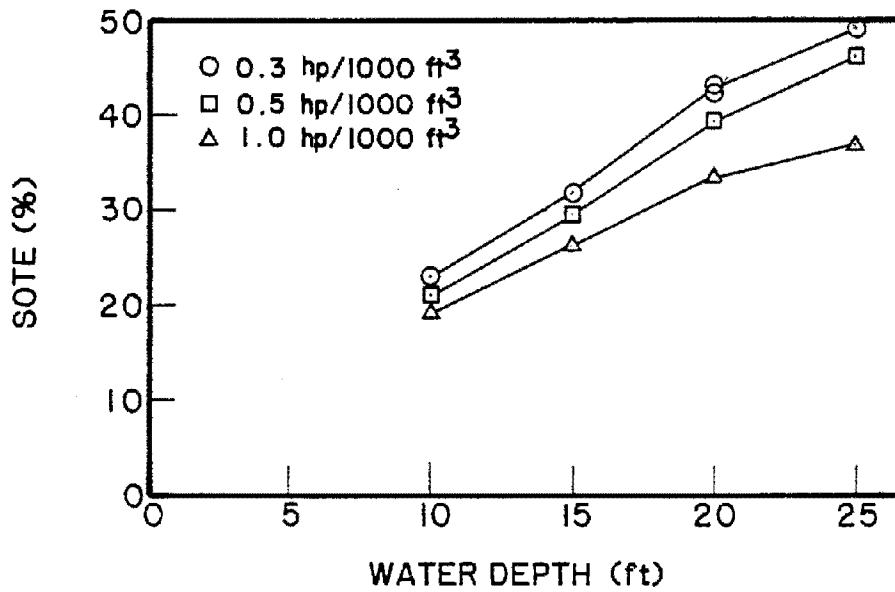


Figure C-8. SOTE vs. water depth for Norton fine bubble dome diffusers.

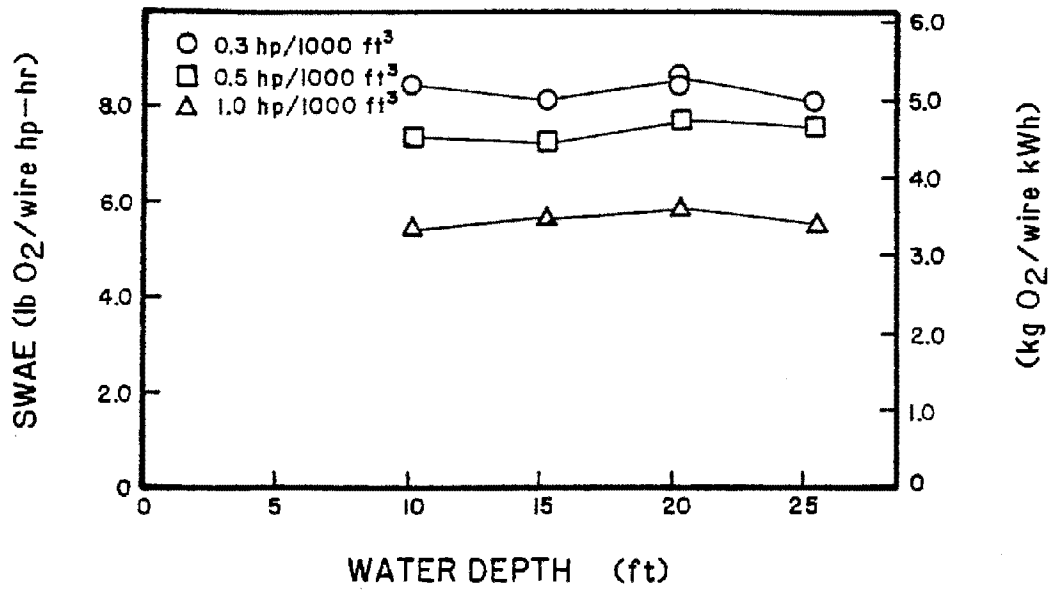


Figure C-9. SWAE vs. water depth for Norton fine bubble dome diffusers.

APPENDIX D

INDIVIDUAL PERFORMANCE RESULTS FOR FMC FINE BUBBLE TUBE DIFFUSERS

A total of 13 acceptable tests were conducted on the FMC Pearlcomb fine bubble tube diffusers in this study. Test results for this system were summarized tabularly in Tables 5 and 6 (Section 6) and are shown graphically here in Figures D-1 through D-9.

Figure D-1 illustrates the effect that variations in airflow rate have on delivered power density at the various water depths. As expected, an increase in airflow rate produced an increase in delivered power density.

The relationship between nominal power density and delivered power density is shown in Figure D-2. As with the Norton system, as power density increased, discrepancies between nominal and delivered power densities increased. The discrepancies became larger as water depth decreased.

The relationship of delivered power density to $K_L a_{20}$ is plotted in Figure D-3. For this system, $K_L a_{20}$ increased linearly with increasing power density. It is not apparent that increased water depth had any effect on $K_L a_{20}$ values for the FMC fine bubble tube diffuser.

Figure D-4 is a plot of SOTR vs. delivered power density. This plot gives SOTR values in both U.S. customary units (left vertical axis) and SI units (right vertical axis). An increase in delivered power density results in an increase in this system's SOTR. The rate of increasing SOTR appears to have been almost constant at the 6.1-m (20-ft) and 7.6-m (25-ft) water depths. At lower water depths, a small degree of nonlinearity was characterized by a higher rate of increase in SOTR values at low delivered power densities. Also apparent is the significant effect of increasing water depth on SOTR, an effect much greater than that observed on $K_L a_{20}$.

The relationship between SOTE and delivered power density is graphed in Figure D-5. SOTE decreased moderately with increasing delivered power density except at the 7.6-m (25-ft) water depth where the decrease was more evident. An increase in water depth resulted in higher SOTE values.

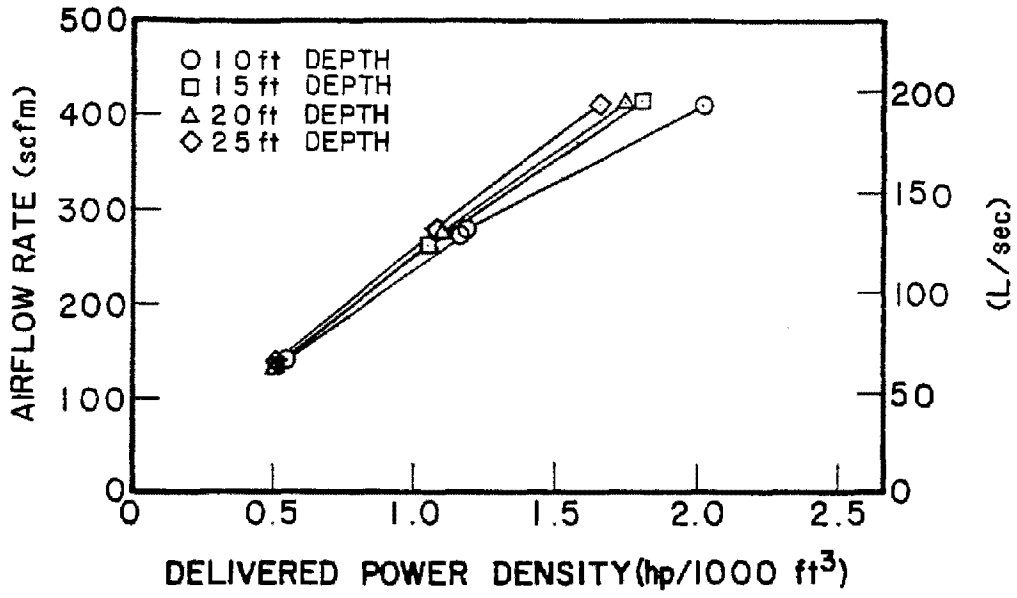


Figure D-1. Airflow rate vs. delivered power density for FMC fine bubble tube diffusers.

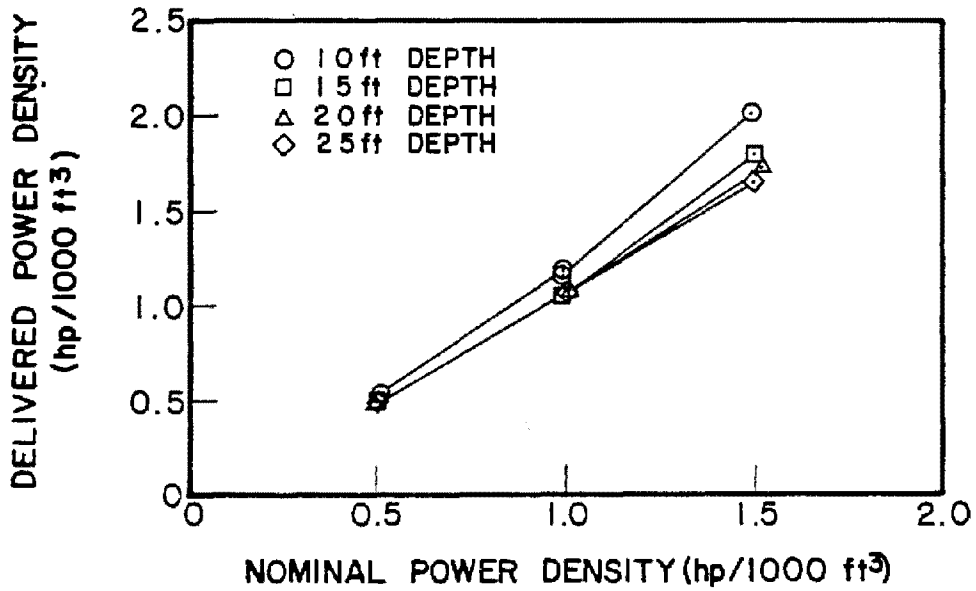


Figure D-2. Delivered power density vs. nominal power density for FMC fine bubble tube diffusers.

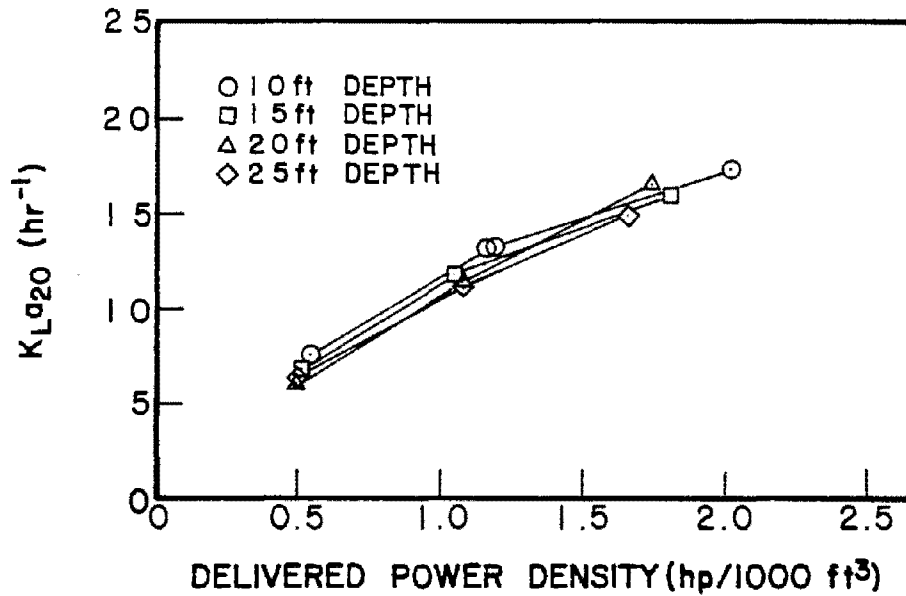


Figure D-3. $K_{La_{20}}$ vs. delivered power density for FMC fine bubble tube diffusers.

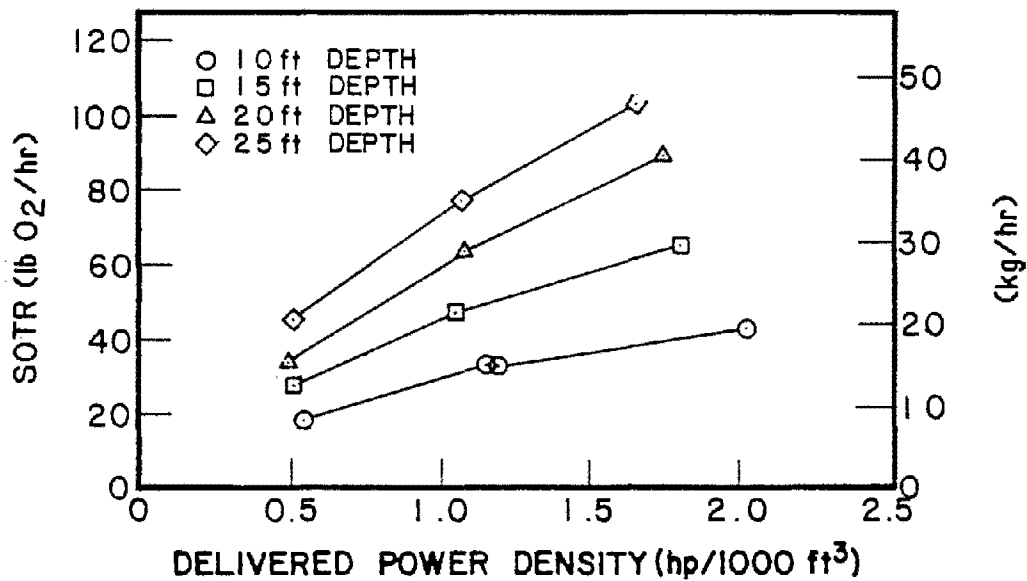


Figure D-4. SOTR vs. delivered power density for FMC fine bubble tube diffusers.

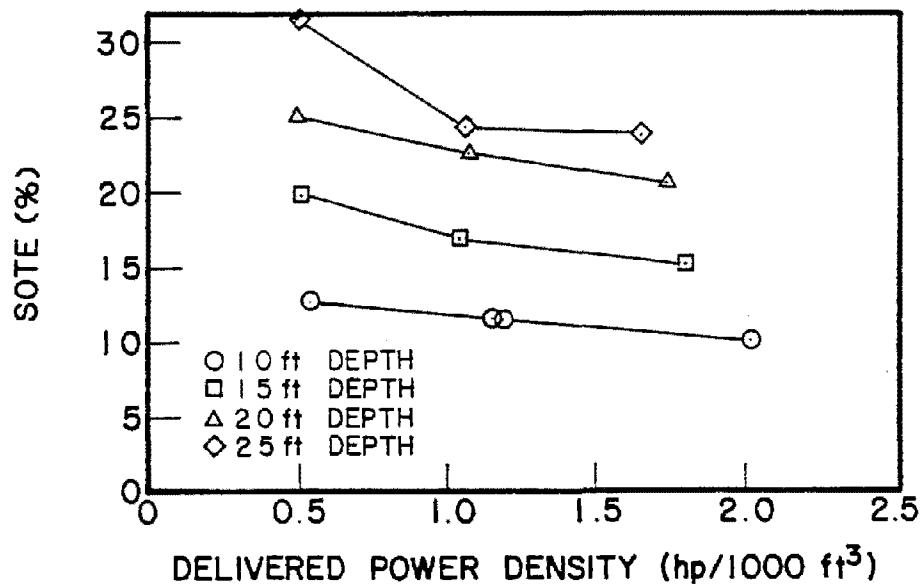


Figure D-5. SOTE vs. delivered power density for FMC fine bubble tube diffusers.

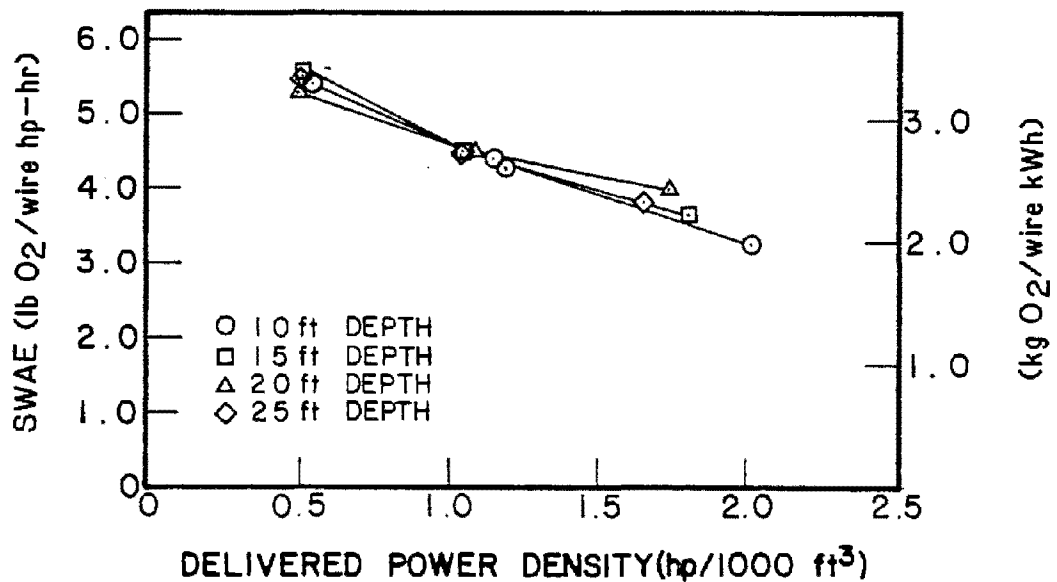


Figure D-6. SWAE vs. delivered power density for FMC fine bubble tube diffusers.

SWAE is plotted against delivered power density in Figure D-6, with SWAE provided in both U.S. customary units and SI units. For this fine bubble system, the highest SWAE values occurred at the lowest delivered power density. SWAE decreased almost linearly with increasing values of delivered power density. Increasing water depth did not always result in increased SWAE values, however. The effect of increasing water depth on this system's SWAE appears to have been small. Results representing various water depths at a given power level are clustered closely for this system, indicating an insensitivity of the system's SWAE to changes in depth.

The relationship of SOTR to test tank water depth is illustrated in Figure D-7, with SOTR given in both U.S. customary units and SI units. This system exhibited an almost linear increase in SOTR with increasing water depth, with the highest SOTR observed at the highest nominal power density.

Figure D-8 is a plot of SOTE vs. test tank water depth. Increasing SOTE with increasing water depth was noted for this system, as with each of the other six aeration systems tested at multiple water depths. Two of the three nominal power density curves indicate that the SOTE rate of increase dropped off slightly at the 7.6-m (25-ft) water depth with this system. The remaining curve indicates a somewhat linear relationship. In this graph, the highest SOTE values are associated with the lowest nominal power density.

This system's relationship of SWAE to water depth is shown in Figure D-9. SWAE is expressed in both U.S. customary units and SI units. As with the Norton system, SWAE appears unaffected by changes in water depth. For this system, it is unclear what water depth produced the best performance. It is apparent, however, that variations in nominal power density significantly affected SWAE results. Optimum SWAE occurred at the lowest nominal power density.

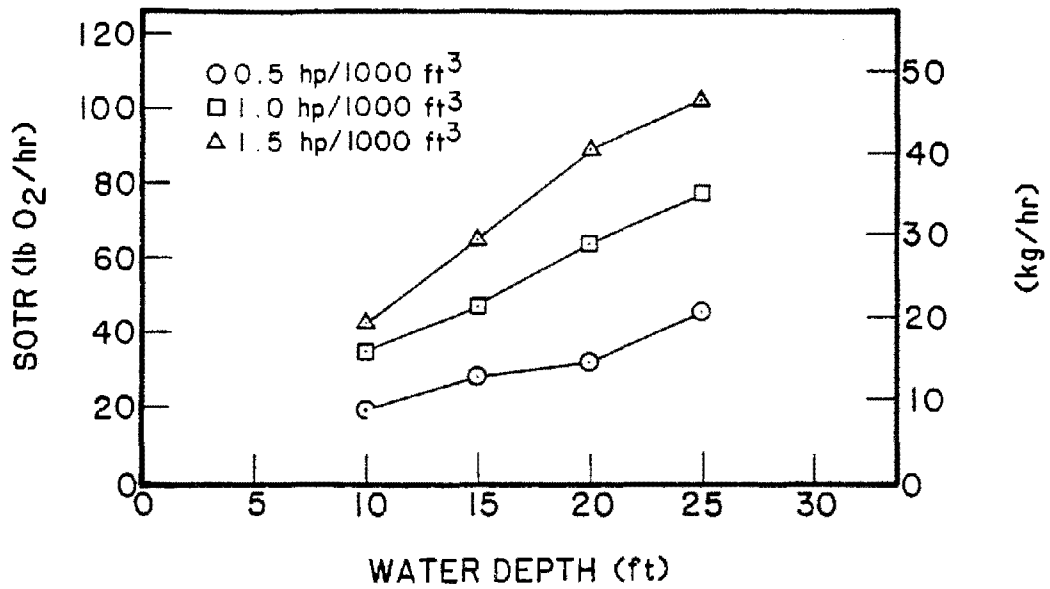


Figure D-7. SOTR vs. water depth for FMC fine bubble tube diffusers.

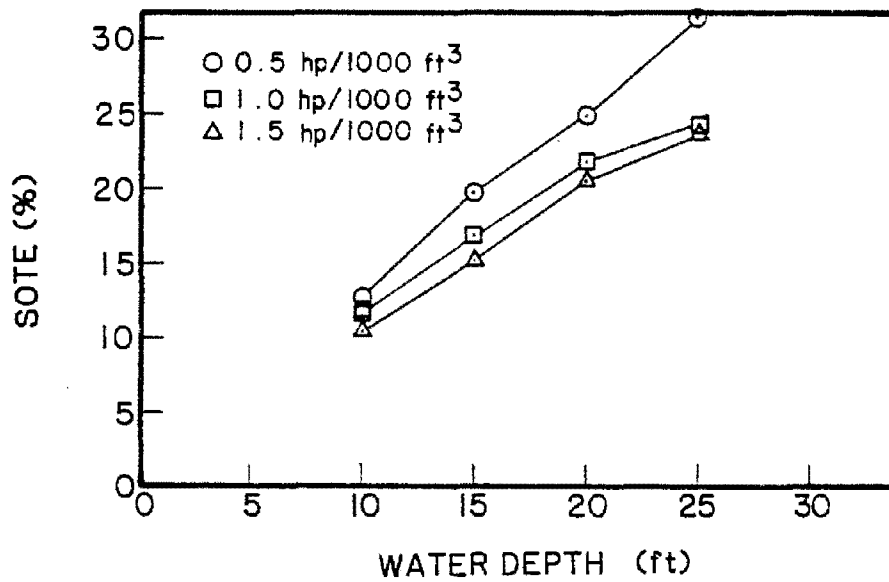


Figure D-8. SOTE vs. water depth for FMC fine bubble tube diffusers.

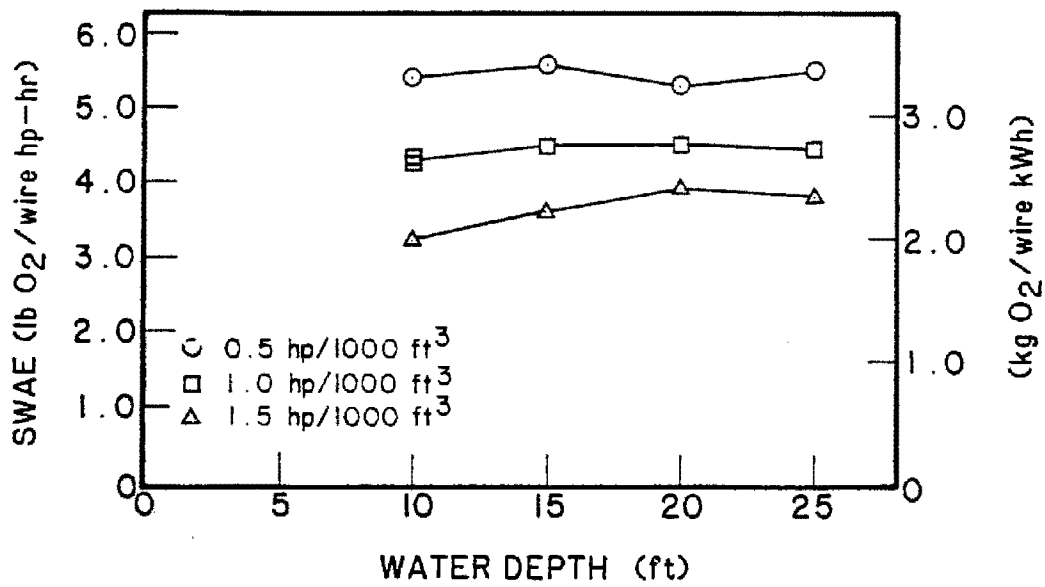


Figure D-9. SWAE vs. water depth for FMC fine bubble tube diffusers.

APPENDIX E

INDIVIDUAL PERFORMANCE RESULTS FOR PENTECH JET AERATORS

A total of 18 acceptable tests were conducted on the Pentech jet aeration system in this study. The results of these tests were summarized tabularly in Tables 7 and 8 in Section 6 and are presented graphically here in Figures E-1 through E-9.

The effect of variations in airflow rate on delivered power density is shown in Figure E-1 for the various water depths. As expected, an increase in airflow rate resulted in an increase in delivered power density.

Figure E-2 shows the relationship between nominal power density and delivered power density. The effect that is generally demonstrated is that as power density increased, the differences between nominal and delivered power densities increased. The differences became larger with decreasing water depth.

Figure E-3 illustrates the relationship between delivered power density and $K_L a_{20}$. In this plot, the $K_L a_{20}$ rate of increase is initially high, then appears to decrease slightly with increasing delivered power density. Also apparent is that increasing water depth resulted in increasing $K_L a_{20}$ values.

SOTR is plotted against delivered power density in Figure E-4. SOTR is expressed in both U.S. customary units (left vertical axis) and SI units (right vertical axis). For the Pentech system, an increase in delivered power density produced an increase in SOTR. The rate of SOTR increase of this system was nonlinear at all water depths. The nonlinearity was essentially the same for all depths and was characterized by a higher rate of increase in SOTR values at low delivered power densities. Also apparent in this graph is the substantial effect of increasing water depth on SOTR. Increasing water depth had a much smaller effect on $K_L a_{20}$ (Figure E-3).

Figure E-5 is a plot of the relationship between SOTE and delivered power density. The values of SOTE for each water depth are clearly the highest at the lowest delivered power density level tested. The trend of SOTE values for this system was a moderate decrease with increasing delivered power density. Also evident in

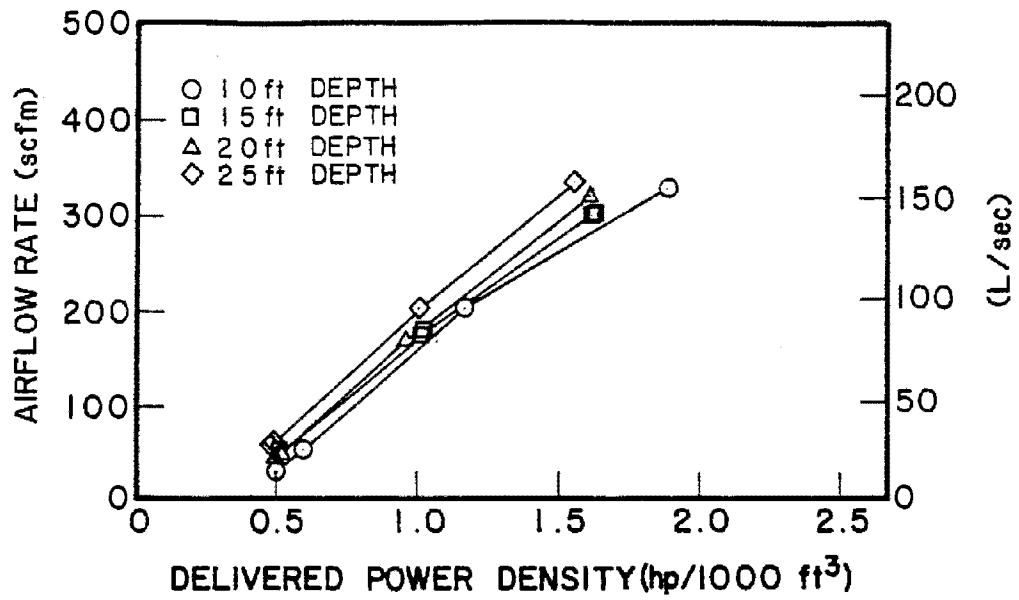


Figure E-1. Airflow rate vs. delivered power density for Pentech jet aerators.

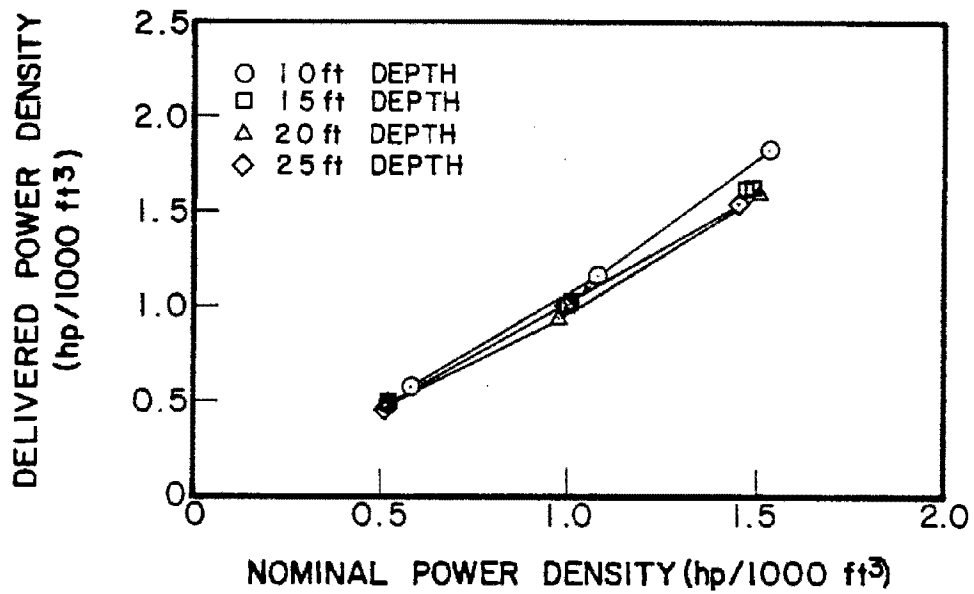


Figure E-2. Delivered power density vs. nominal power density for Pentech jet aerators.

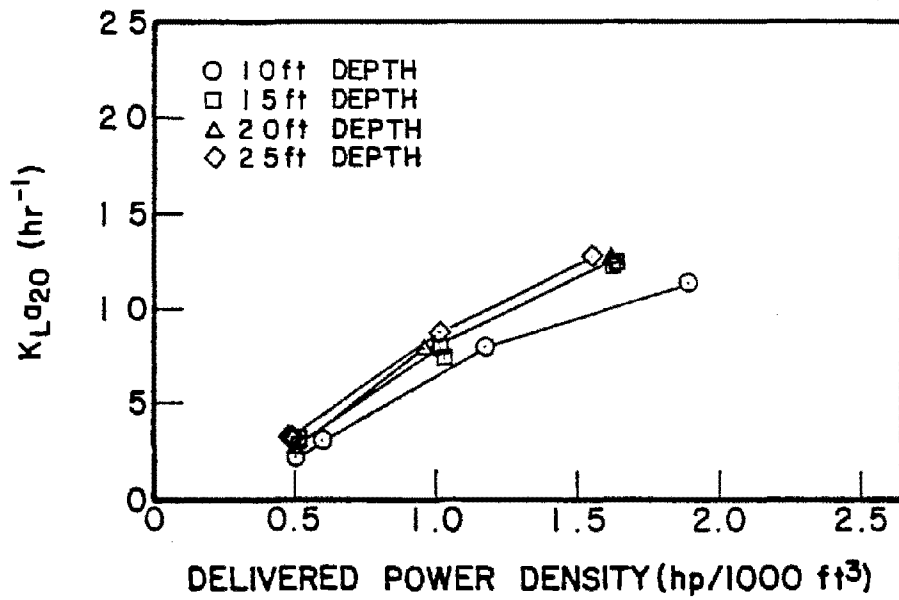


Figure E-3. K_La₂₀ vs. delivered power density for Pentech jet aerators.

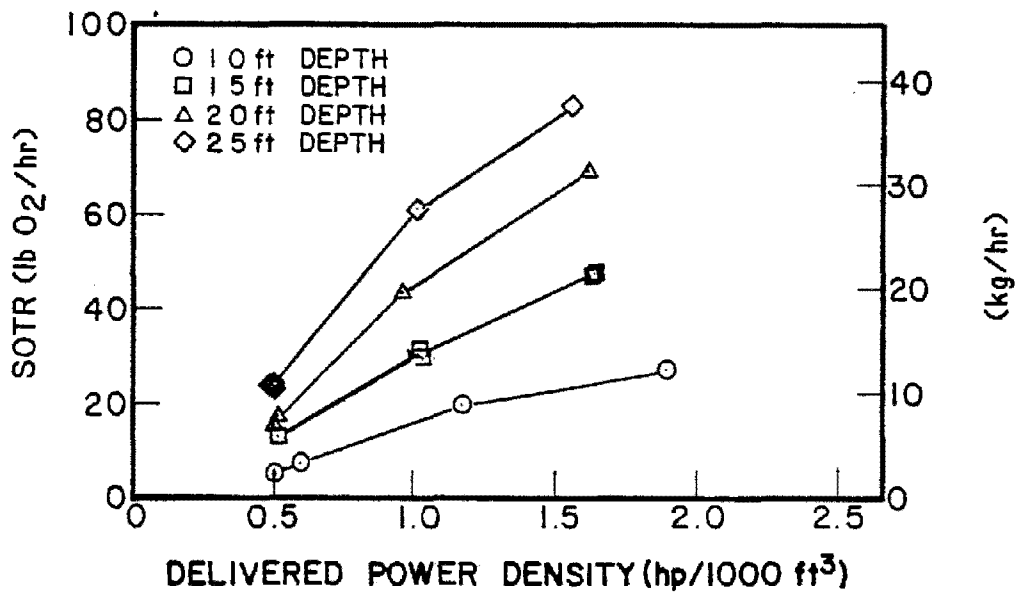


Figure E-4. SOTR vs. delivered power density for Pentech jet aerators.

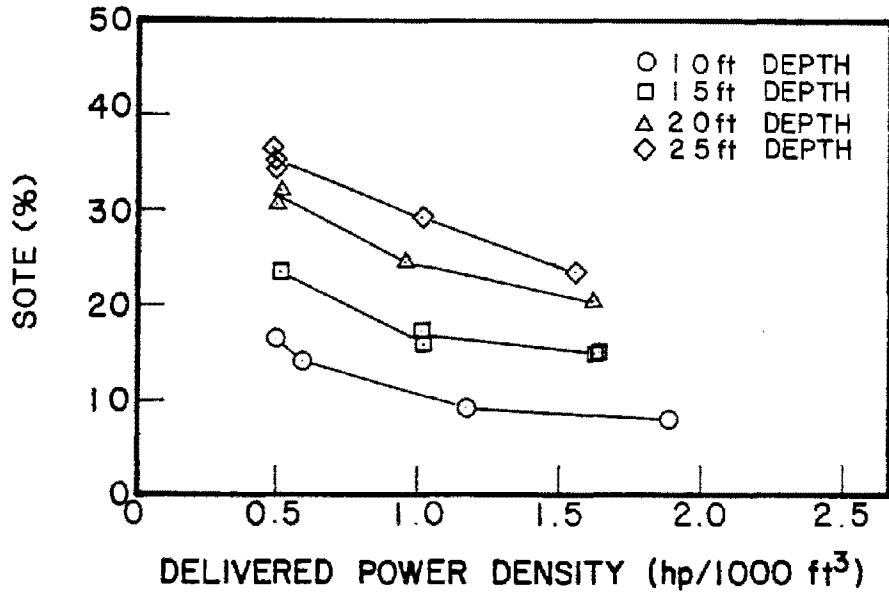


Figure E-5. SOTE vs. delivered power density for Pentech jet aerators.

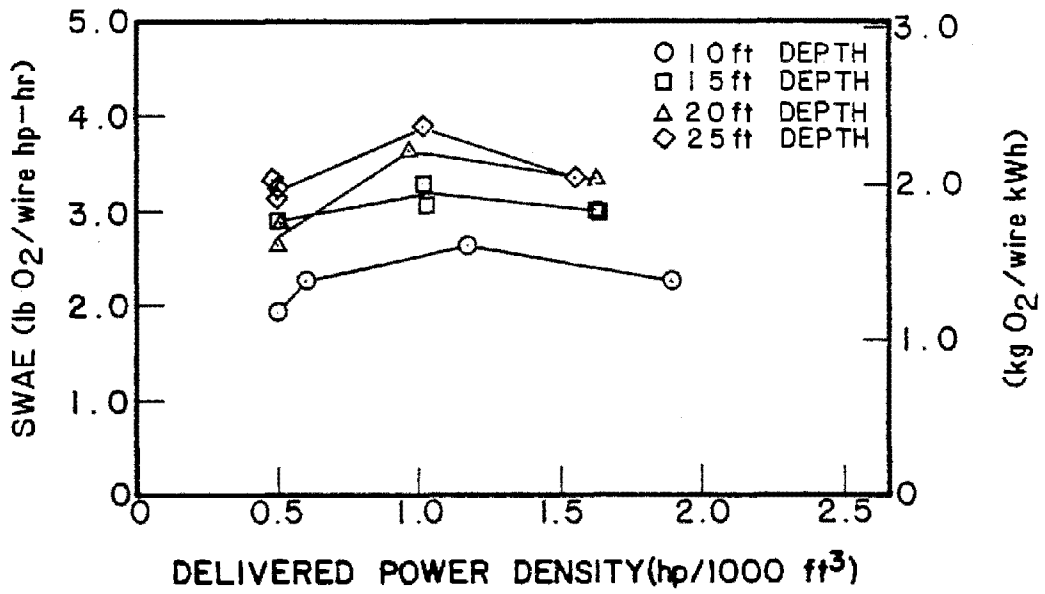


Figure E-6. SWAE vs. delivered power density for Pentech jet aerators.

this graph is the existence of a relationship between SOTE and water depth; an increase in water depth resulted in an improvement in SOTE.

SWAE vs. delivered power density is shown for Pentech in Figure E-6. SWAE is given in both U.S. customary units and SI units. For this system, the highest SWAE values occurred at the middle delivered power density. The trend of the data is such that any variation of the delivered power density either above or below the middle value caused a decrease in SWAE. Unlike the preceding two graphs, increasing water depth did not necessarily result in increased values of the dependent variable (vertical axis). Increasing water depth clearly produced changes in SWAE for this system, however. The highest values of SWAE occurred at the 7.6-m (25-ft) water depth.

Figure E-7 illustrates the relationship between SOTR and test tank water depth, with SOTR expressed in both U.S. customary units and SI units. The Pentech system exhibited an almost linear increase in SOTR with increasing water depth. The highest SOTR values were observed at the highest nominal power density.

SOTE vs. water depth is plotted in Figure E-8. Increasing SOTE was observed with increasing water depth for this aeration system as with each of the other six systems tested at multiple water depths. For this system, all three power density curves indicate that the rate of increase in SOTE dropped off slightly at the 7.6-m (25-ft) water depth. In this graph, the highest values of SOTE were associated with the lowest nominal power density.

This system's relationship of SWAE to water depth is shown in Figure E-9. SWAE is expressed in both U.S. customary units and SI units. SWAE generally increased with increasing water depth. Peak SWAE performance for this system was noted at the 7.6-m (25-ft) water depth. Variations in nominal power density appear to have significantly affected the results, with the optimum SWAE occurring at the middle nominal power density evaluated.

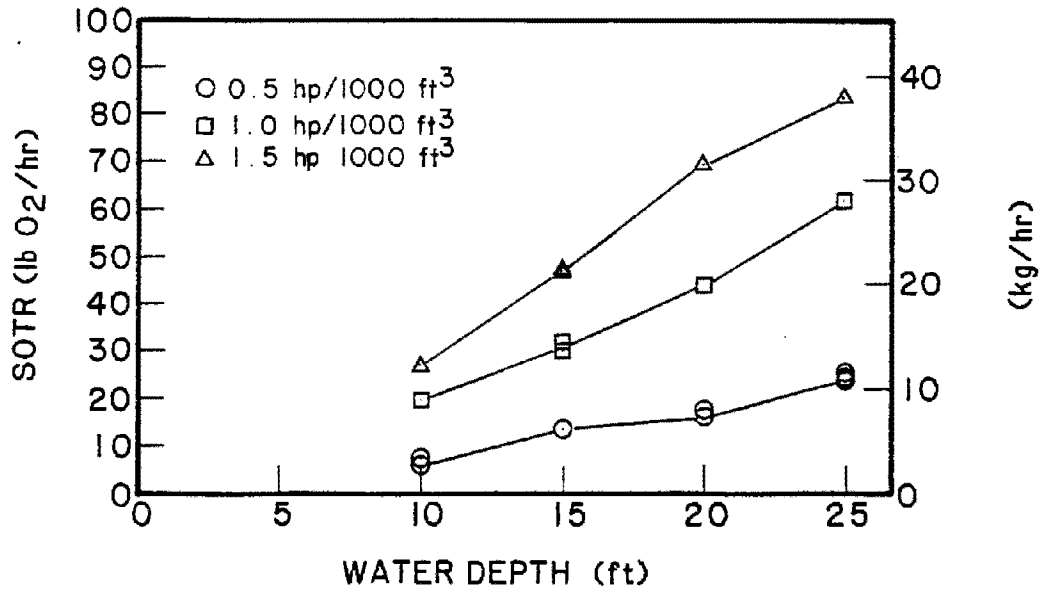


Figure E-7. SOTR vs. water depth for Pentech jet aerators.

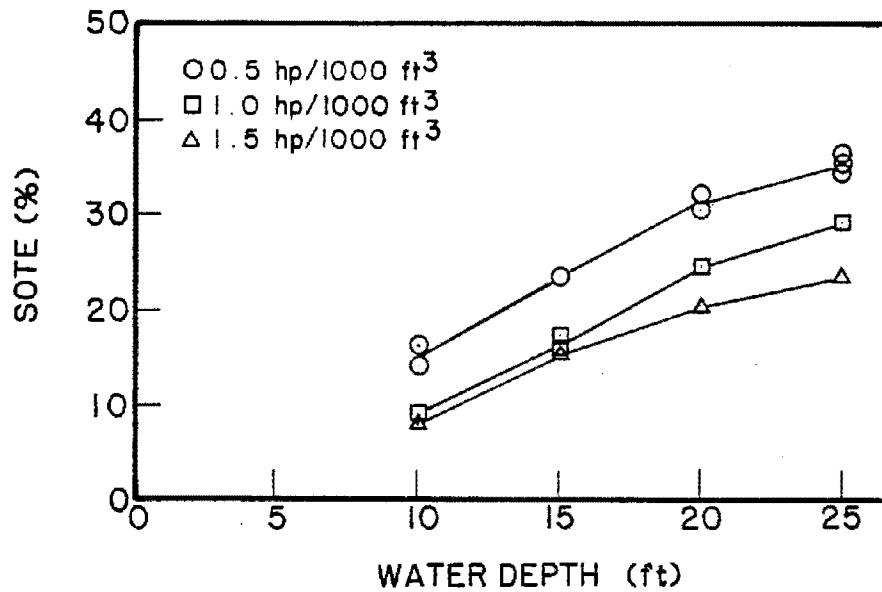


Figure E-8. SOTE vs. water depth for Pentech jet aerators.

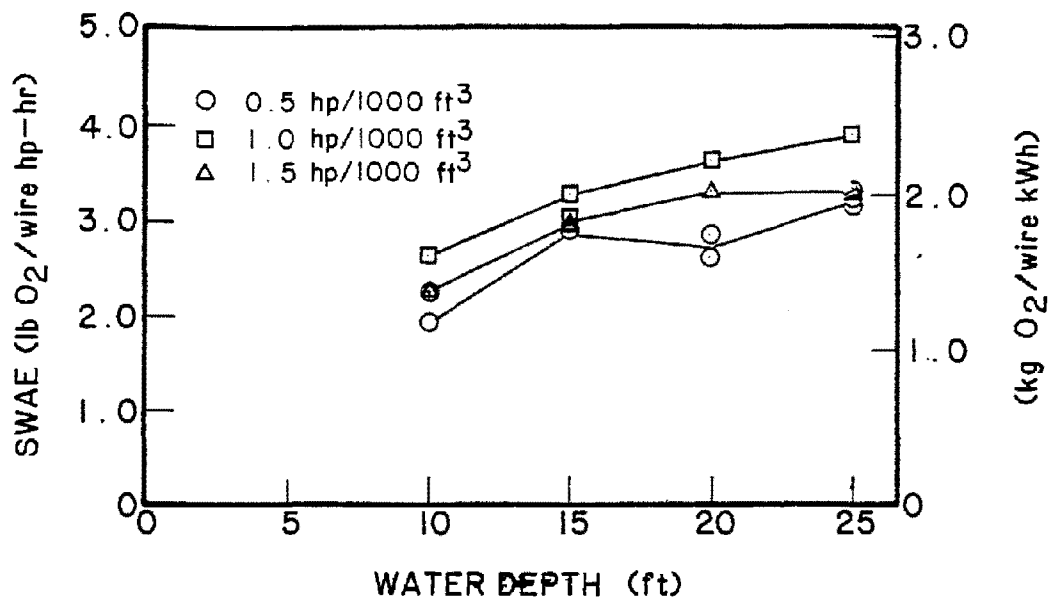


Figure E-9. SWAE vs. water depth for Pentech jet aerators.

APPENDIX F

INDIVIDUAL PERFORMANCE RESULTS FOR KENICS STATIC TUBE AERATORS

A total of 12 acceptable tests were conducted on the Kenics static tube aeration system in this study. Test results for this system were summarized tabularly in Tables 9 and 10 (Section 6) and are shown graphically here in Figures F-1 through F-9.

Figure F-1 illustrates the effect that variations in airflow rate have on delivered power density at the various water depths. As expected, an increase in airflow rate produced an increase in delivered power density.

The relationship between nominal power density and delivered power density is shown in Figure F-2. As with the other systems, as power density increased, discrepancies between nominal and delivered power densities increased. The discrepancies became larger as water depth decreased.

The relationship of delivered power density to $K_L a_{20}$ is plotted in Figure F-3. $K_L a_{20}$ increased in a similar manner for curves representing three of the four water depths. In these three cases, the $K_L a_{20}$ rate of increase was high, then decreased slightly with increasing delivered power density. Also apparent is that increasing water depth generally resulted in increasing $K_L a_{20}$ values for the Kenics static tube aerator.

Figure F-4 is a plot of SOTR vs. delivered power density. This plot gives SOTR values in both U.S. customary units (left vertical axis) and SI units (right vertical axis). An increase in the delivered power density resulted in an increase in this system's SOTR. The rate of increase in SOTR appears to have been almost linear at all water depths. For curves representing three of the four water depths, a slight nonlinearity was observed. This minor nonlinearity was characterized by a higher rate of increase in SOTR values at low delivered power densities. Also apparent is the significant effect of increasing water depth on SOTR, an effect much greater than that noted in $K_L a_{20}$.

The relationship between SOTE and delivered power density is shown graphically in Figure F-5. SOTE was unaffected by changes in

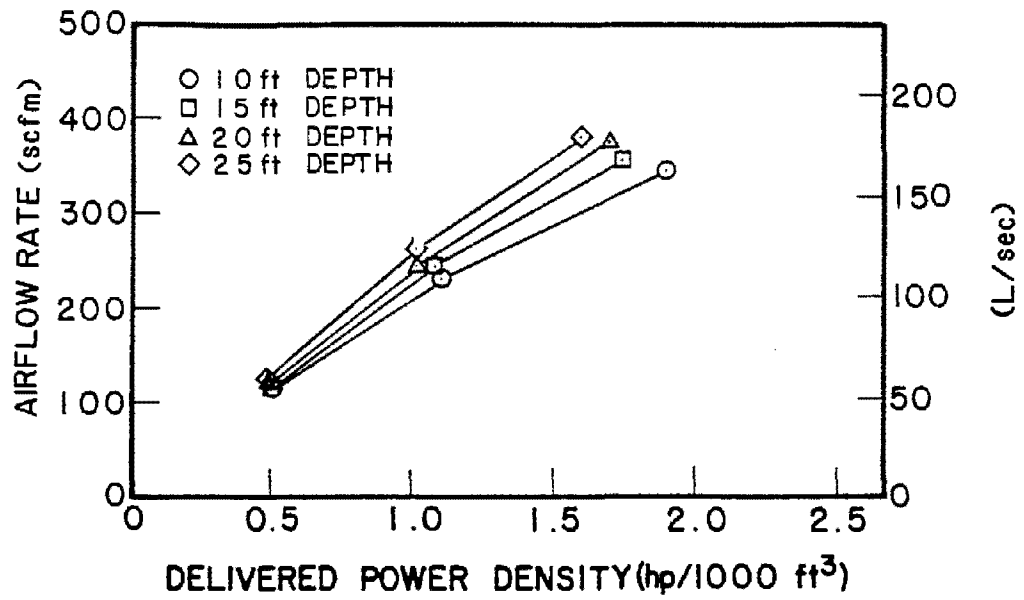


Figure F-1. Airflow rate vs. delivered power density for Kenics static tube aerators.

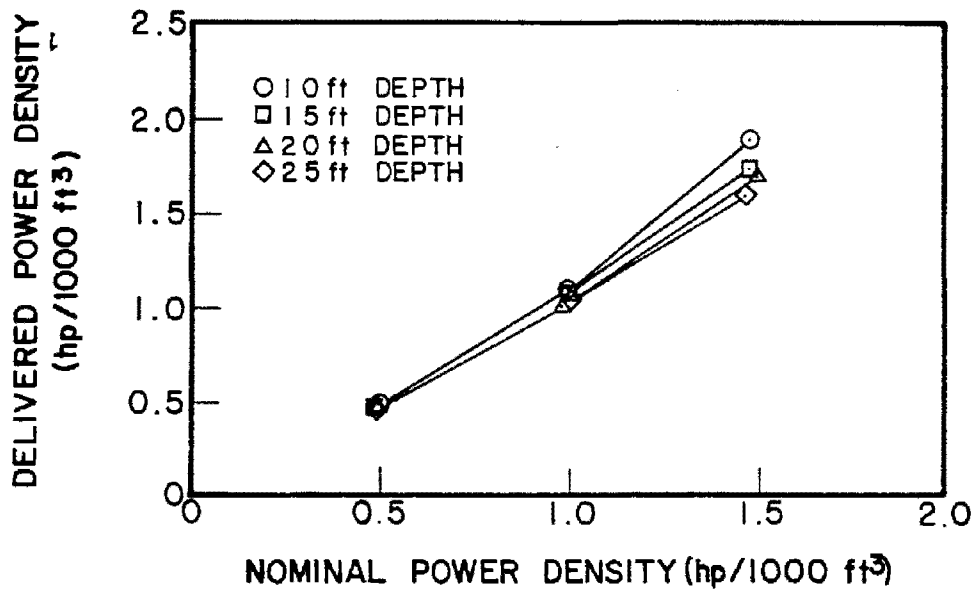


Figure F-2. Delivered power density vs. nominal power density for Kenics static tube aerators.

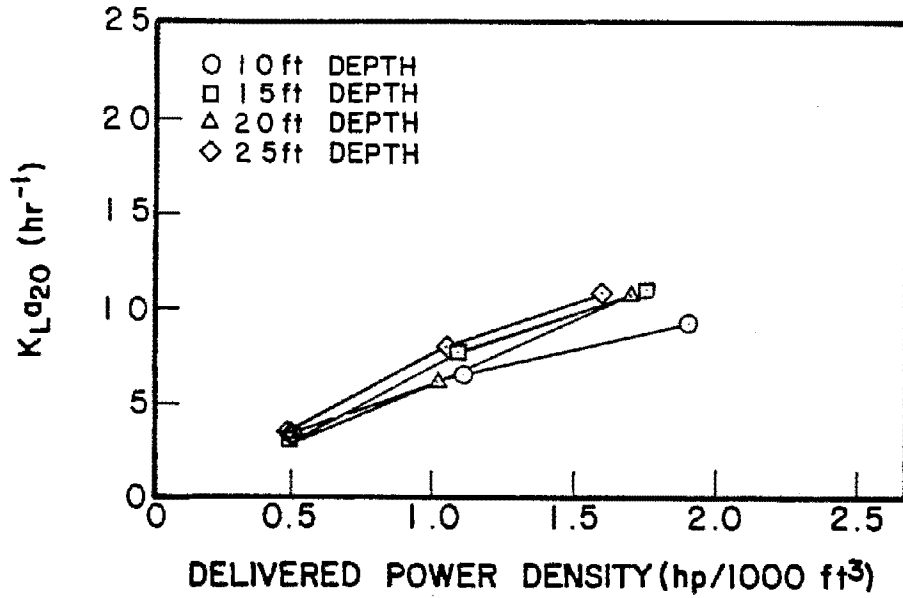


Figure F-3. K_{La20} vs. delivered power density for Kenics static tube aerators.

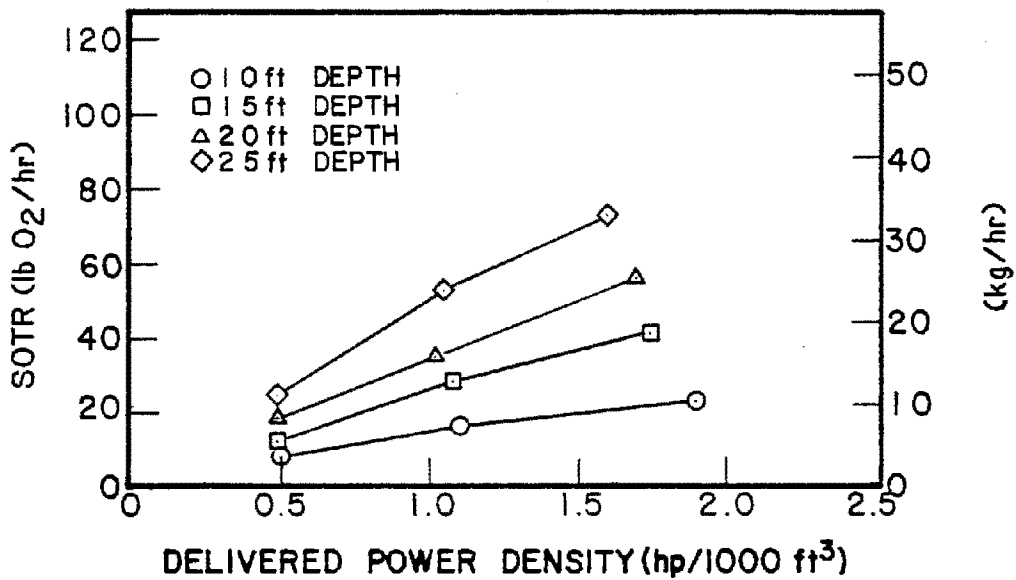


Figure F-4. SOTR vs. delivered power density for Kenics static tube aerators.

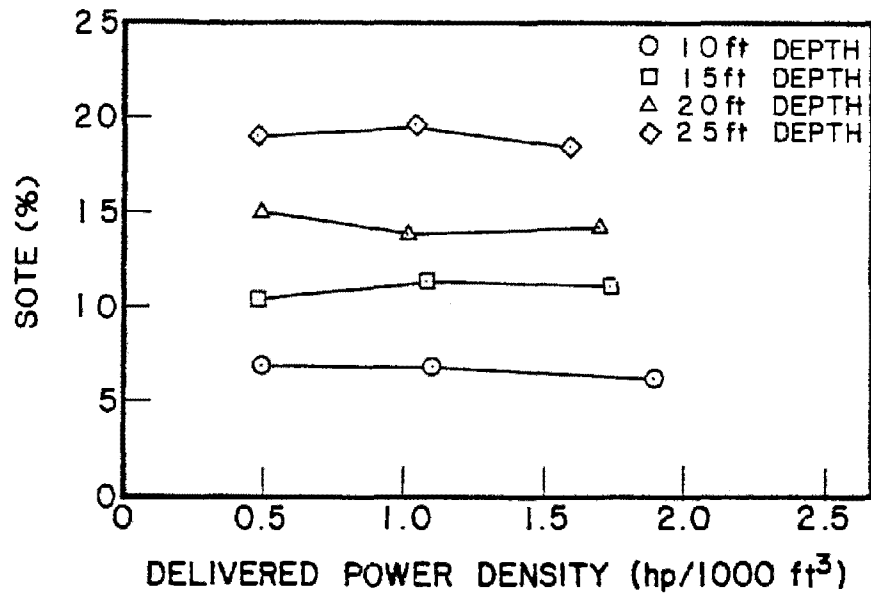


Figure F-5. SOTE vs. delivered power density for Kenics static tube aerators.

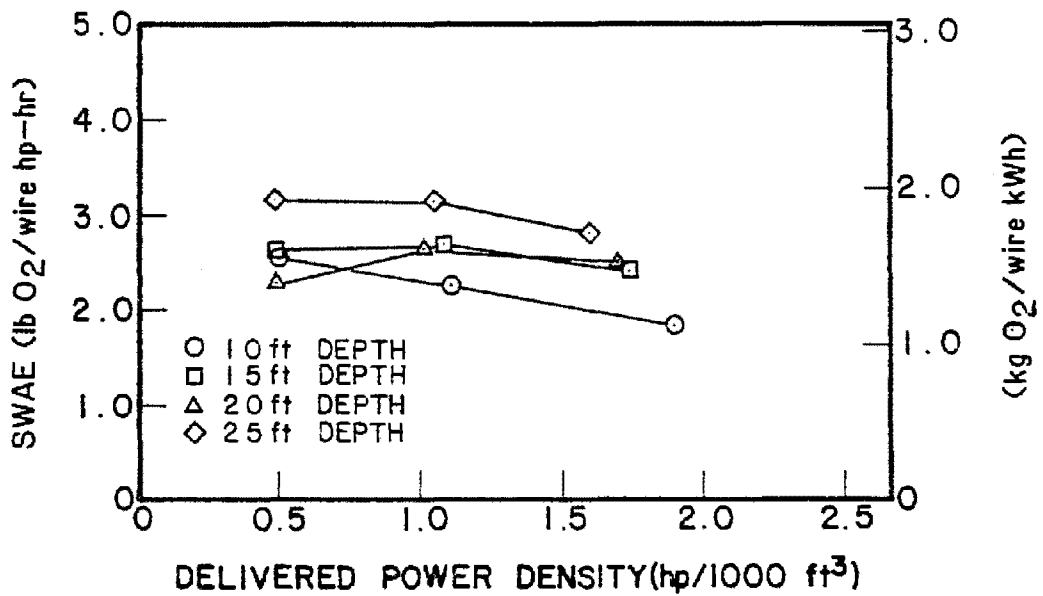


Figure F-6. SWAE vs. delivered power density for Kenics static tube aerators.

delivered power density. An increase in water depth resulted in higher SOTE VALUES.

SWAE is plotted against delivered power density in Figure F-6, with SWAE provided in both U.S. customary units and SI units. For this coarse bubble system, the highest SWAE values occurred at the lowest delivered power density except at the 6.1-m (20-ft) water depth. SWAE generally decreased with increasing values of delivered power density. Increasing water depth did not always result in increased SWAE values, however. The effect of increasing water depth on this system's SWAE does appear to have been significant, however, with the highest values of SWAE observed at the 7.6-m (25-ft) water depth.

The relationship of SOTR to test tank water depth is illustrated in Figure F-7, with SOTR given in both U.S. customary units and SI units. This system exhibited a somewhat linear increase in SOTR with increasing water depth, with the highest SOTR observed at the highest nominal power density.

Figure F-8 is a plot of SOTE vs. test tank water depth. Increasing SOTE with increasing water depth was noted for this system as with each of the other six aeration systems tested at multiple water depths. For this system, the data indicate a somewhat linear relationship between SOTE and depth. The various SOTE values representing different nominal power densities are tightly clustered. In this graph, the highest SOTE values do not appear to be associated with any particular nominal power density.

This system's relationship of SWAE to water depth is shown in Figure F-9. SWAE is expressed in both U.S. customary units and SI units. The data indicate that SWAE tended to improve with increasing water depth. Peak values of SWAE occurred at the 7.6-m (25-ft) water depth. Significant variations in SWAE occurred with changes in nominal power density; however, the cause of these changes was not evident. Although the highest nominal power density generally produced the lowest SWAE values, it is not clear which of the other two power densities represents better performance.

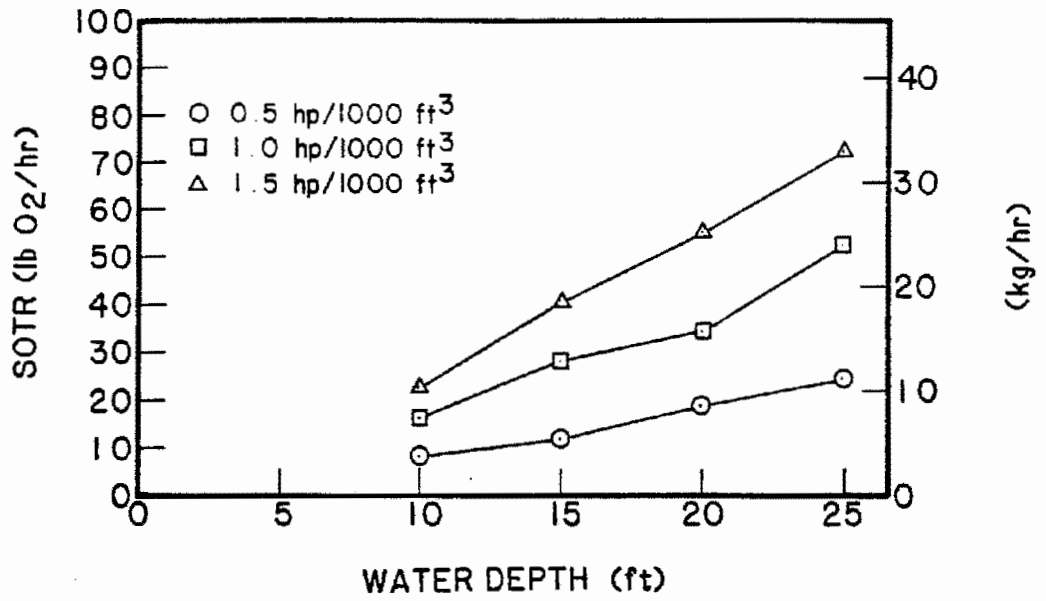


Figure F-7. SOTR vs. water depth for Kenics static tube aerators.

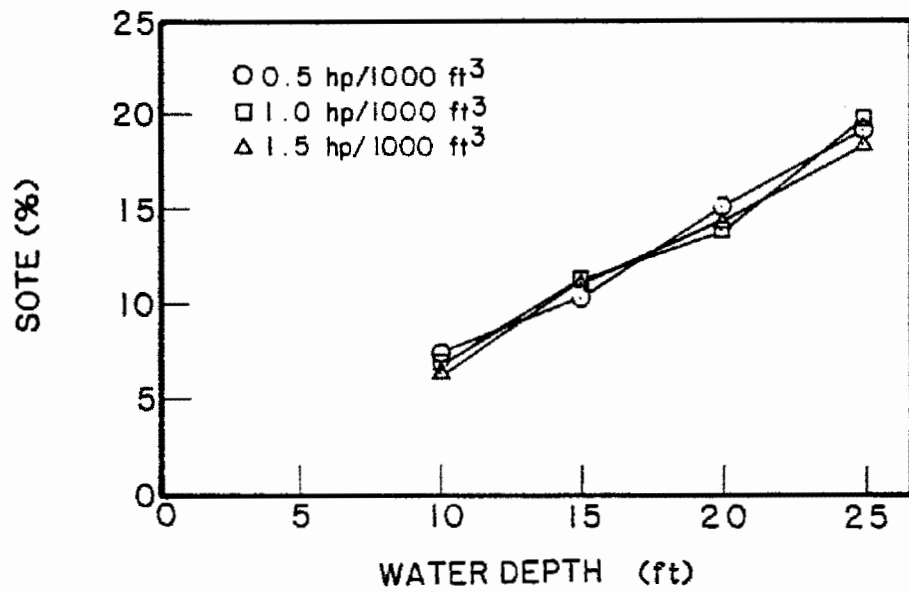


Figure F-8. SOTE vs. water depth for Kenics static tube aerators.

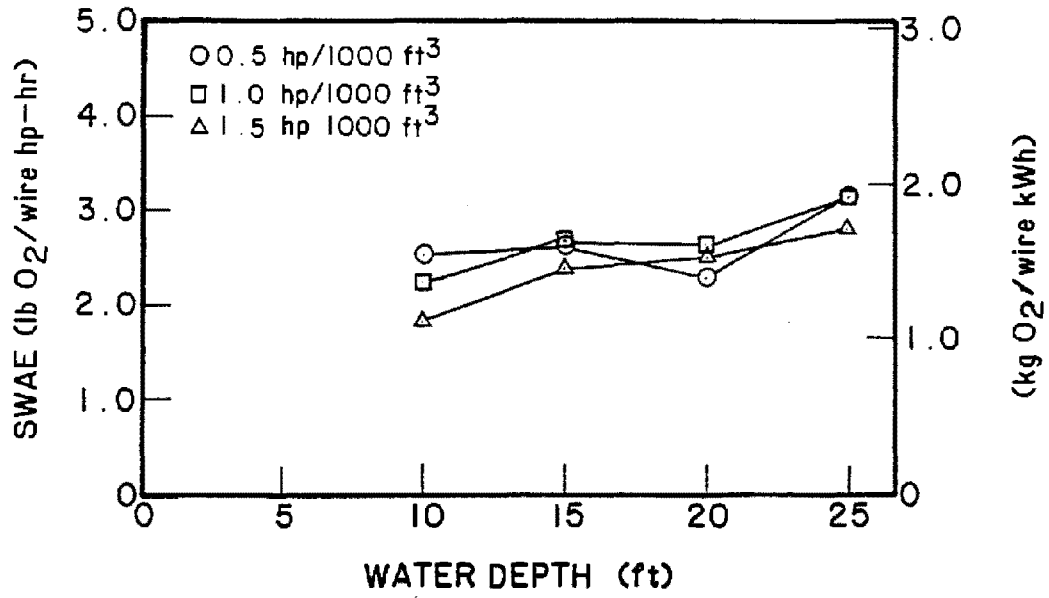


Figure F-9. SWAE vs. water depth for Kenics static tube aerators.

APPENDIX G

INDIVIDUAL PERFORMANCE RESULTS FOR BAUER VARIABLE ORIFICE DIFFUSERS

A total of 14 acceptable tests were conducted on the Bauer variable orifice diffusion system in this study. The results of these tests were summarized tabularly in Tables 11 and 12 in Section 6 and are presented graphically here in Figures G-1 through G-9.

The effect of variations in airflow rate on delivered power density is shown in Figure G-1 for the various water depths. As expected, an increase in airflow rate resulted in an increase in delivered power density.

Figure G-2 shows the relationship between nominal power density and delivered power density. The effect that is generally demonstrated is that as power density increased, the differences between nominal and delivered power densities increased. The differences became larger with decreasing water depth.

Figure G-3 illustrates the relationship between delivered power density and K_{La20} . As shown in this plot, K_{La20} increased almost linearly for the various water depths. Also apparent is that increasing water depth resulted in increasing K_{La20} values.

SOTR is plotted against delivered power density in Figure G-4. SOTR is expressed in both U.S. customary units (left vertical axis) and SI units (right vertical axis). For the Bauer system, an increase in delivered power density produced an increase in SOTR. The rate of increase in SOTR for this system appears to have been almost linear for all water depths. Also apparent is the considerable effect of increasing water depth on SOTR. Increasing water depth had a much smaller effect on K_{La20} (Figure G-3).

Figure G-5 is a plot of the relationship between SOTE and delivered power density. SOTE increased slightly with increasing delivered power density at each water depth. Also evident is that an increase in water depth was accompanied by an improvement in SOTE.

SWAE vs. delivered power density is shown for Bauer in Figure G-6. SWAE is given in both U.S. customary units and SI units. For this system, SWAE was clearly affected by water depth, increasing with

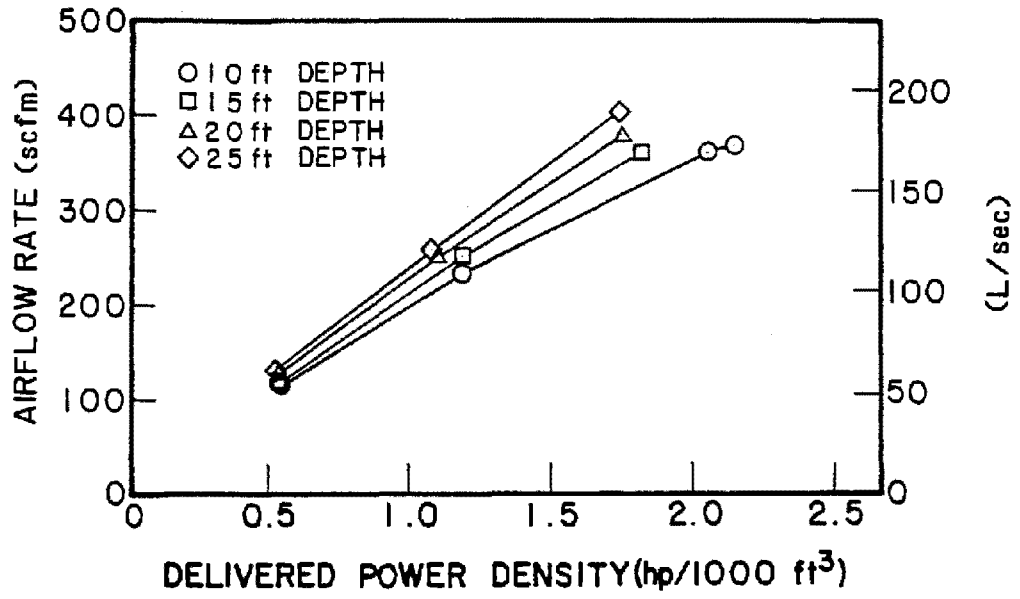


Figure G-1. Airflow rate vs. delivered power density for Bauer variable orifice diffusers.

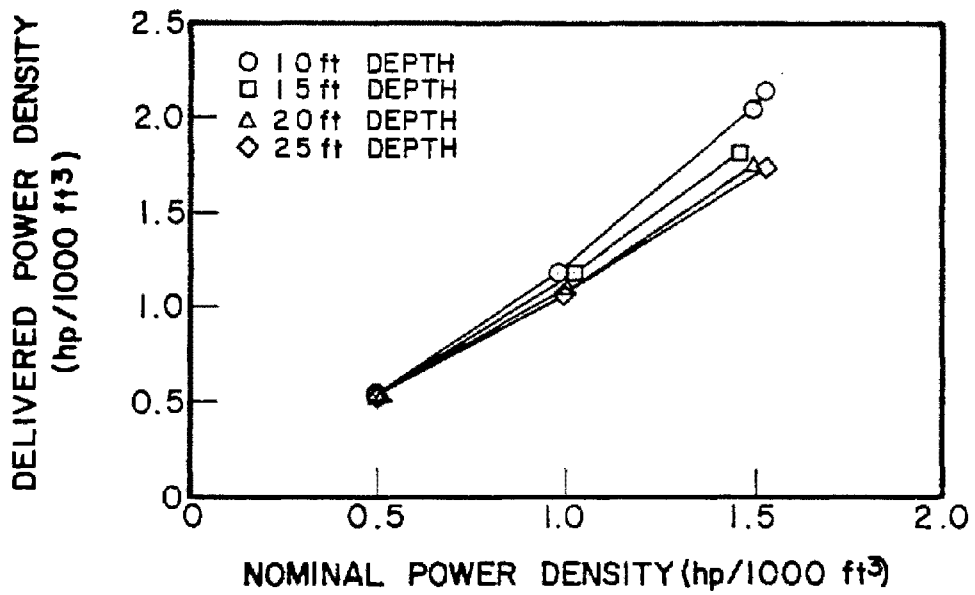


Figure G-2. Delivered power density vs. nominal power density for Bauer variable orifice diffusers.

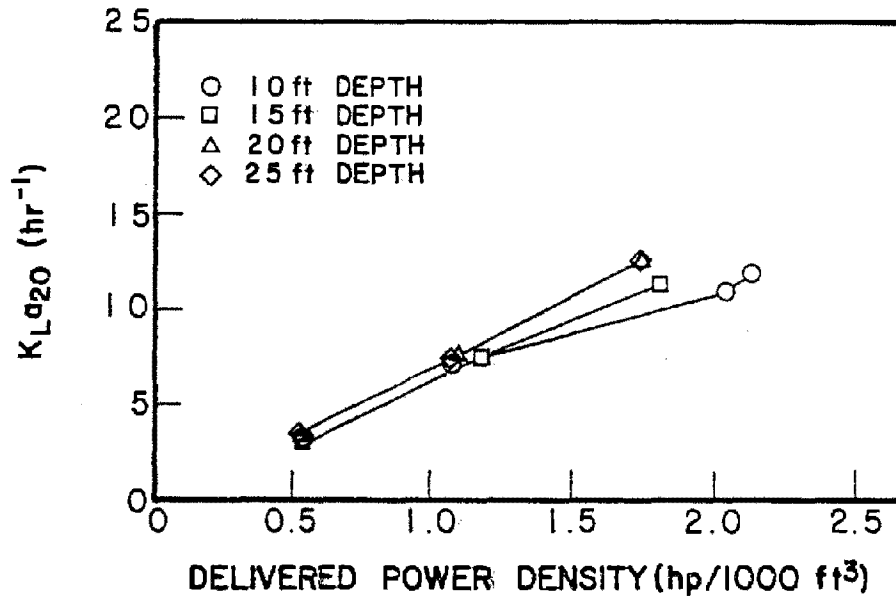


Figure G-3. $K_L a_{20}$ vs. delivered power density for Bauer variable orifice diffusers.

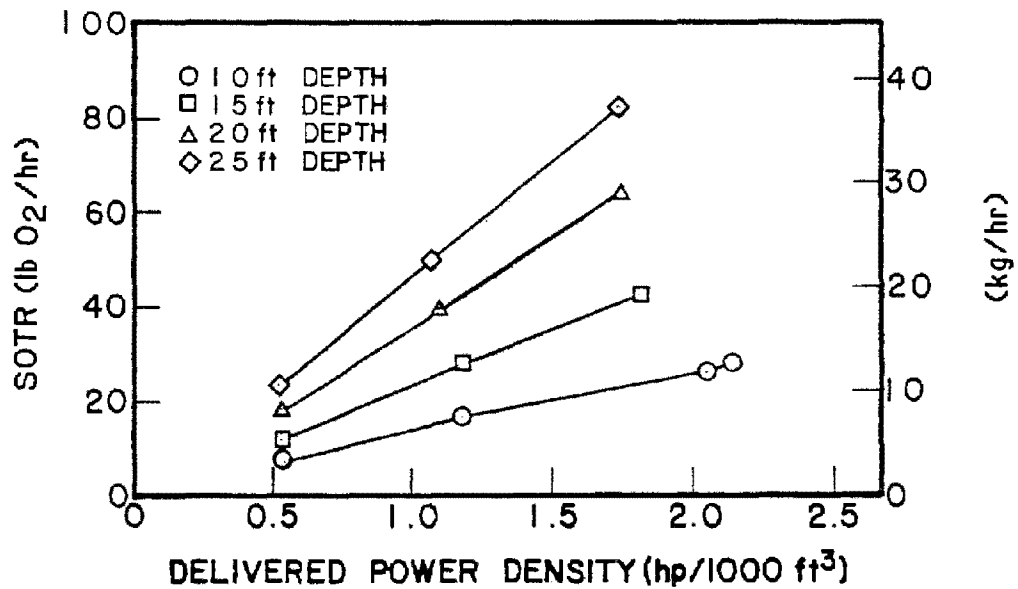


Figure G-4. SOTR vs. delivered power density for Bauer variable orifice diffusers.

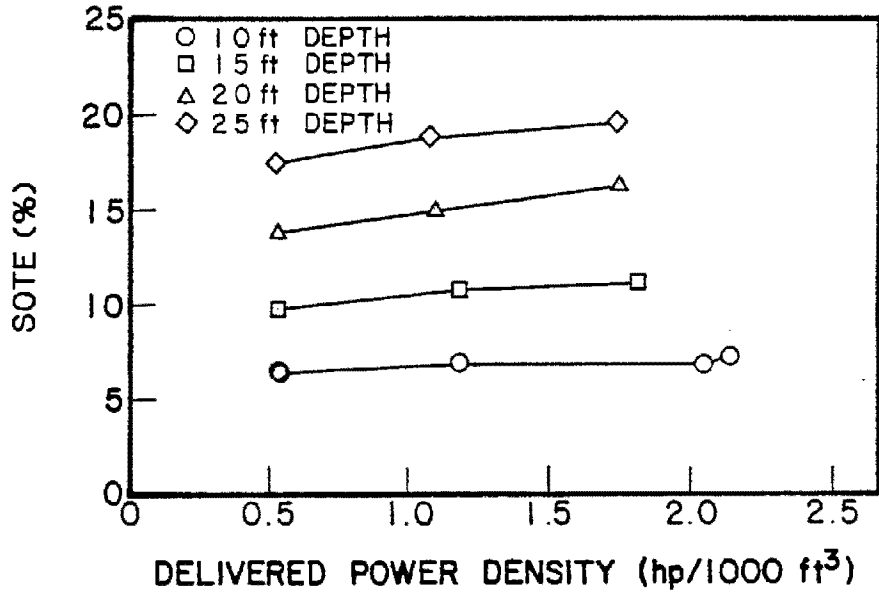


Figure G-5. SOTE vs. delivered power density for Bauer variable orifice diffusers.

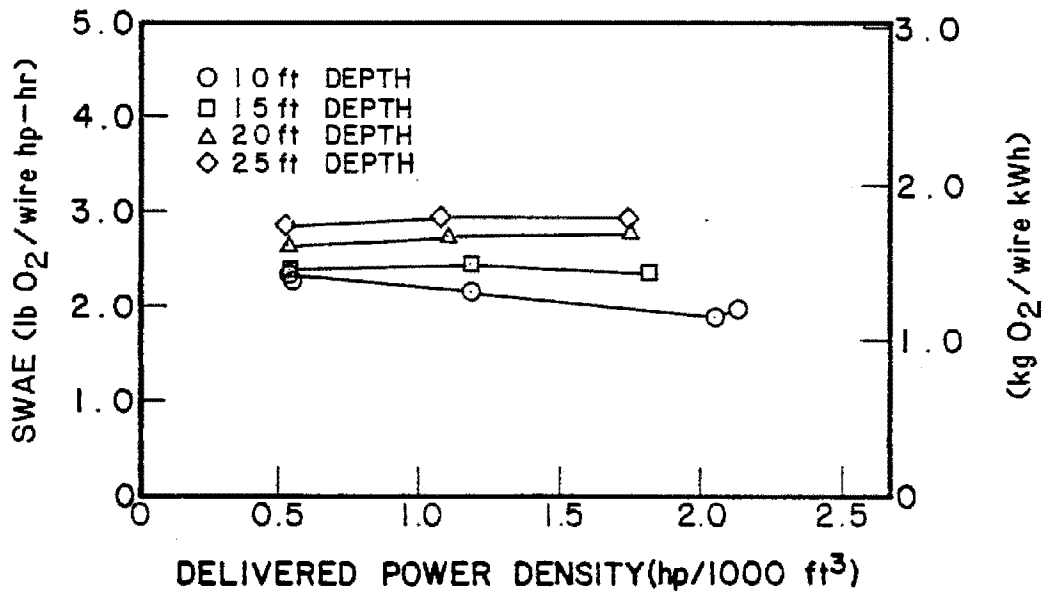


Figure G-6. SWAE vs. delivered power density for Bauer variable orifice diffusers.

each increase in depth. For the 4.6-, 6.1-, and 7.6-m (15-, 20-, and 25-ft) water depths, SWAE was virtually unaffected by changes in delivered power density. At the 3.0-m (10-ft) water depth, SWAE decreased with increasing delivered power density.

Figure G-7 illustrates the relationship between SOTR and test tank water depth, with SOTR expressed in both U.S. customary units and SI units. The Bauer system exhibited an almost linear increase in SOTR with increasing water depth. The highest SOTR values were observed at the highest nominal power density.

SOTE vs. water depth is plotted in Figure G-8. Increasing SOTE was observed with increasing water depth for this aeration system as with each of the other six systems tested at multiple water depths. For this system, the data indicate a linear relationship between SOTE and water depth at all three nominal power densities. The highest values of SOTE were associated with the highest nominal power density.

This system's relationship of SWAE to water depth is shown in Figure G-9. SWAE is expressed in both U.S. customary units and SI units. SWAE generally increased with increasing water depth, although not at a rapid rate. Peak values of SWAE occurred at the 7.6-m (25-ft) water depth. At three of the four water depths, SWAE appears to have been unaffected by changes in nominal power density.

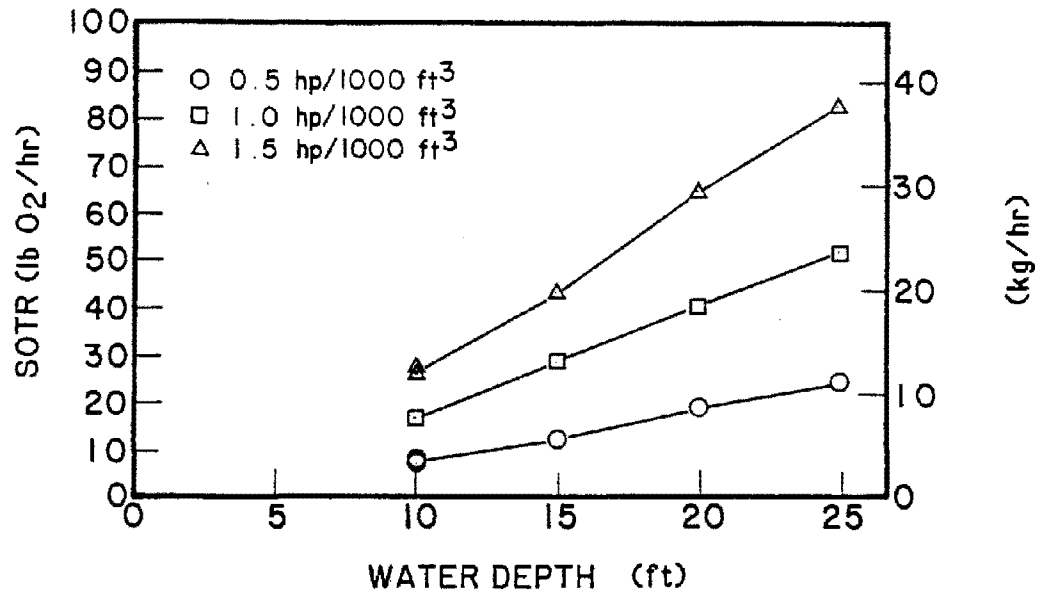


Figure G-7. SOTR vs. water depth for Bauer variable orifice diffusers.

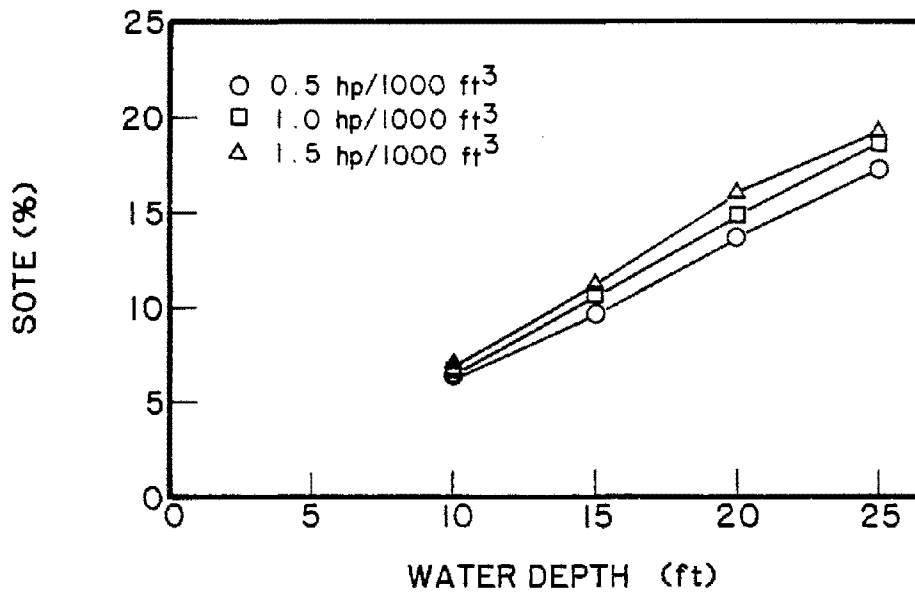


Figure G-8. SOTE vs. water depth for Bauer variable orifice diffusers.

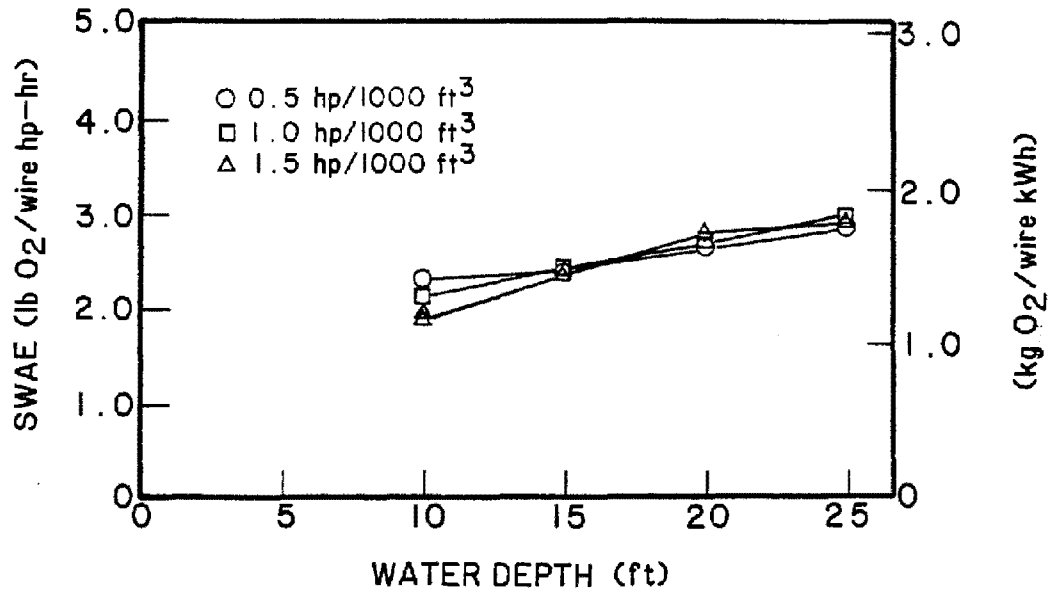


Figure G-9. SWAE vs. water depth for Bauer variable orifice diffusers.

APPENDIX H

INDIVIDUAL PERFORMANCE RESULTS FOR SANITAIRE COARSE BUBBLE DIFFUSERS

A total of 12 acceptable tests were conducted on the Sanitaire coarse bubble diffusion system in this study. Test results for this system were summarized tabularly in Tables 13 and 14 (Section 6) and are shown graphically here in Figures H-1 through H-9.

Figure H-1 illustrates the effect that variations in airflow rate have on delivered power density at the various water depths. As expected, an increase in airflow rate produced an increase in delivered power density.

The relationships between nominal power density and delivered power density is shown in Figure H-2. As with the other systems, as power density increased, discrepancies between nominal and delivered power densities increased. The discrepancies became larger as water depth decreased.

The relationship of delivered power density to $K_L a_{20}$ is plotted in Figure H-3. $K_L a_{20}$ increased almost linearly for all four water depths with increasing delivered power density. Also apparent is that increasing water depth was not a controlling influence on the relative positions of the $K_L a_{20}$ curves.

Figure F-4 is a plot of SOTR vs. delivered power density. This plot gives the SOTR in both U.S. customary units (left vertical axis) and SI (right vertical axis). An increase in the delivered power density resulted in an increase in this system's SOTR. The rate of increase for the SOTR of this system appears to have been essentially linear for all water depths. Also apparent in this graph is the significant effect of increasing water depth on SOTR, particularly separating the two higher from the two lower water depths. This effect was much greater than that observed with $K_L a_{20}$.

The relationship between SOTE and delivered power density is shown graphically in Figure H-5. SOTE values were the lowest at the lowest levels of delivered power density, and increased steadily with increasing delivered power density. An increase in water depth also resulted in higher SOTE values.

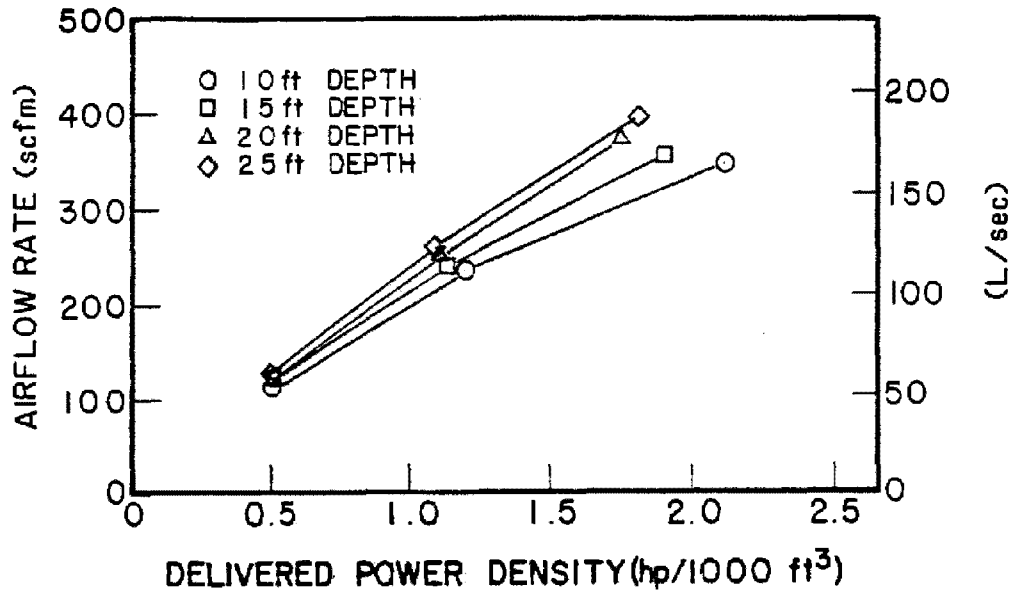


Figure H-1. Airflow rate vs. delivered power density for Sanitaire coarse bubble diffusers.

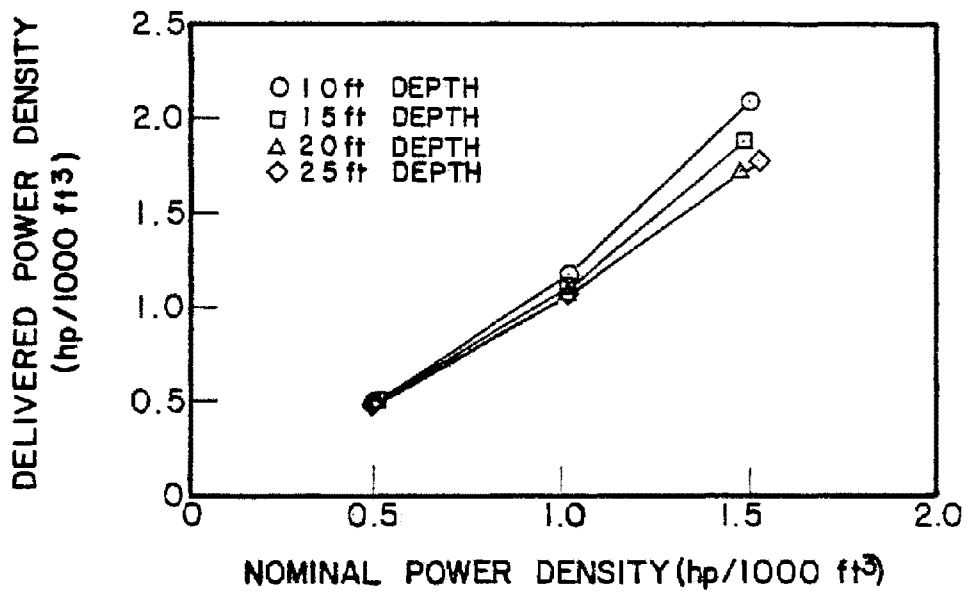


Figure H-2. Delivered power density vs. nominal power density for Sanitaire coarse bubble diffusers.

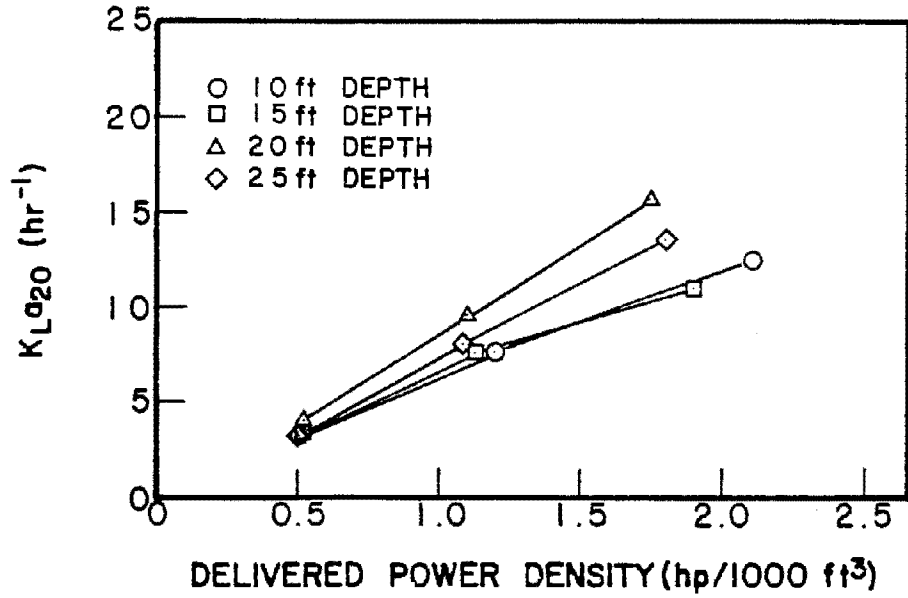


Figure H-3. K_{La20} vs. delivered power density for Sanitaire coarse bubble diffusers.

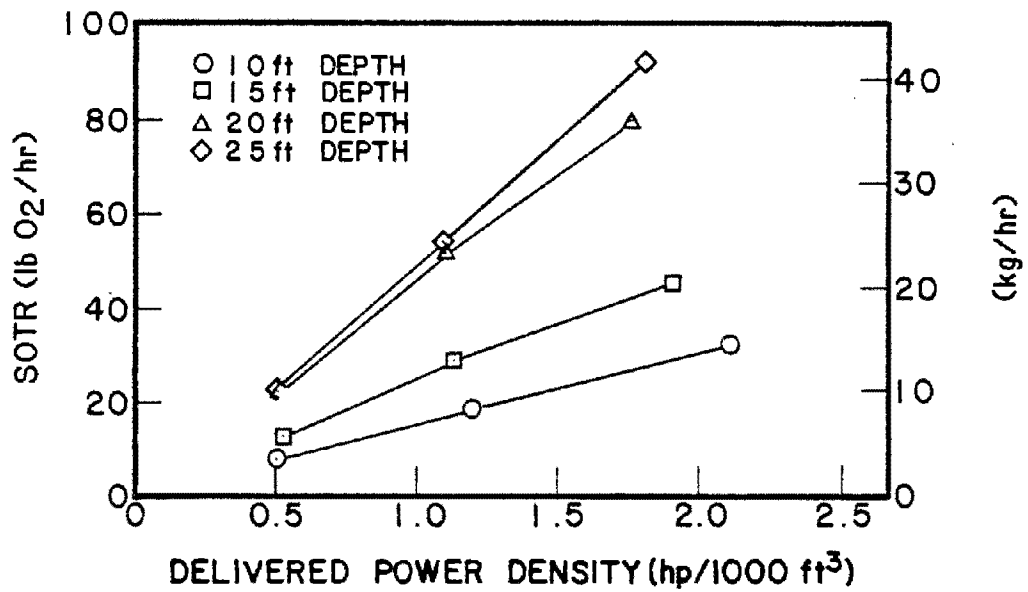


Figure H-4. SOTR vs. delivered power density for Sanitaire coarse bubble diffusers.

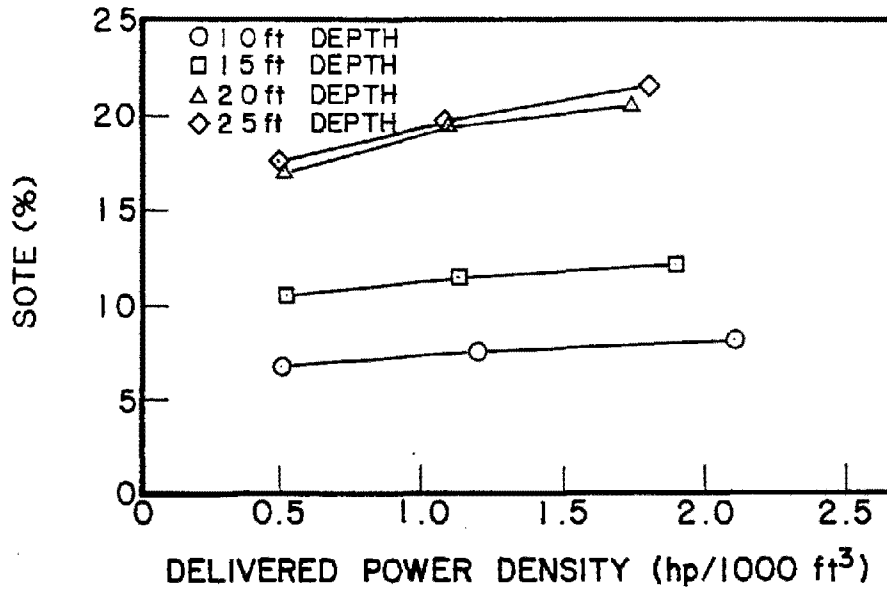


Figure H-5. SOTE vs. delivered power density for Sanitaire coarse bubble diffusers.

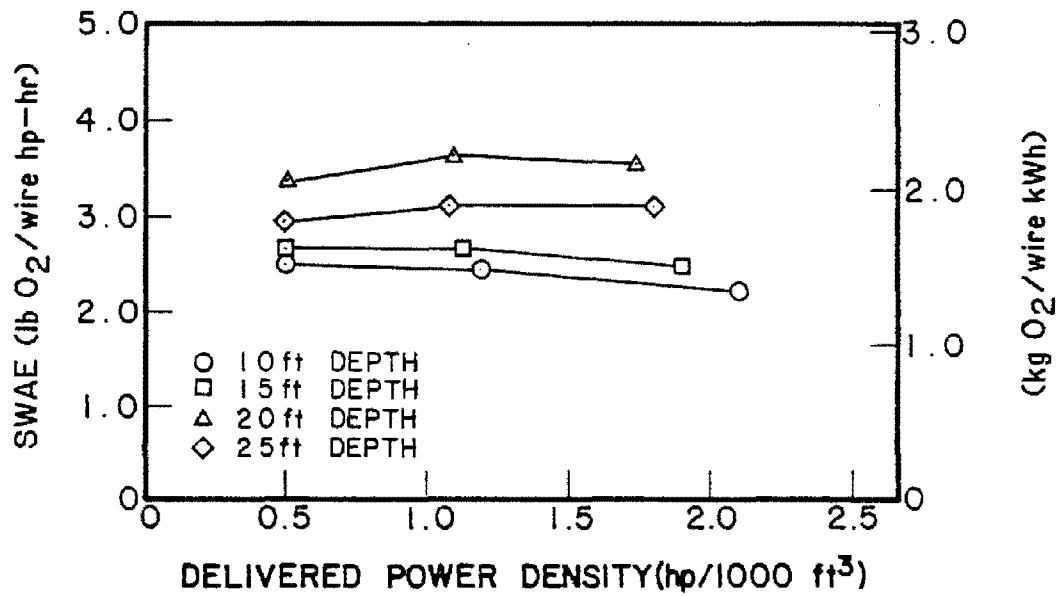


Figure H-6. SWAE vs. delivered power density for Sanitaire coarse bubble diffusers.

SWAE is plotted against delivered power density in Figure H-6, with SWAE provided in both U.S. customary units and SI units. For this coarse bubble system, SWAE values increased slightly with increasing power density for the two higher water depths and decreased slightly with increasing power density at the two lower water depths. The effect of increased water depth on this system appears to have had an influence on SWAE; however, it should be noted that the highest values of SWAE occurred at the 6.1 (20), not 7.6-m (25-ft), water depth.

The relationship of SOTR test tank water depth is illustrated in Figure H-7, with SOTR given in both U.S. customary units and SI units. Although increasing water depth definitely influenced the magnitude of the SOTR values, diffuser configuration also appears to have played a role in determining SOTR for this system. A different configuration was used for the 3.0- and 6.1-m (10- and 20-ft) water depths than for the 4.6- and 7.6-m (15- and 25-ft) water depths. Rather than connecting all points in succession at a given nominal power density, points of like configuration have been connected because of the apparent relationship that existed between SOTR and configuration for the Sanitaire diffuser. The highest SOTR values were observed at the highest nominal power density at each water depth.

Figure H-8 is a plot of SOTE vs. test tank water depth. Increasing SOTE with increasing water depth was noted for this system as with each of the other six aeration systems tested at multiple water depths. As in preceding figure, however, diffuser configuration appears to have strongly influenced the data observed at a given nominal power density. For this system, the highest values of SOTE were associated with the highest nominal power density.

This system's relationship of SWAE to water depth is shown in Figure H-9. SWAE is expressed in both U.S. customary units and SI units. Again, the apparent influence of diffuser configuration is evident. Increasing water depth generally produced increasing SWAE. However, peak SWAE values did not occur at 7.6-m (25-ft) water depth, but at 6.1-m (20-ft) water depth. The variation in nominal power density at each depth does not appear to have significantly affected SWAE and it is not clear at which nominal power density peak SWAE performance occurred.

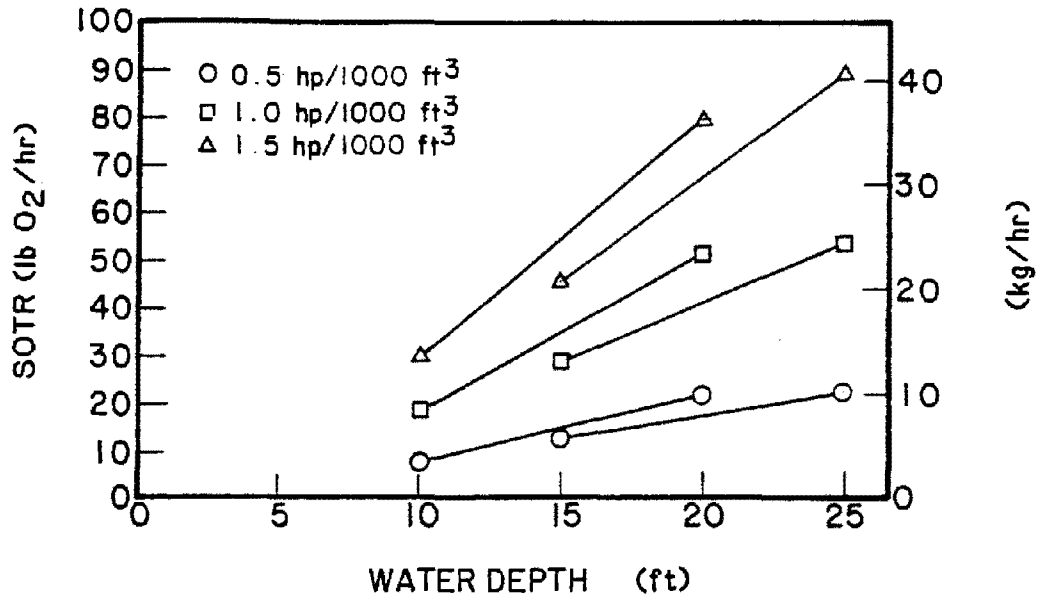


Figure H-7. SOTR vs. water depth for Sanitaire coarse bubble diffusers.

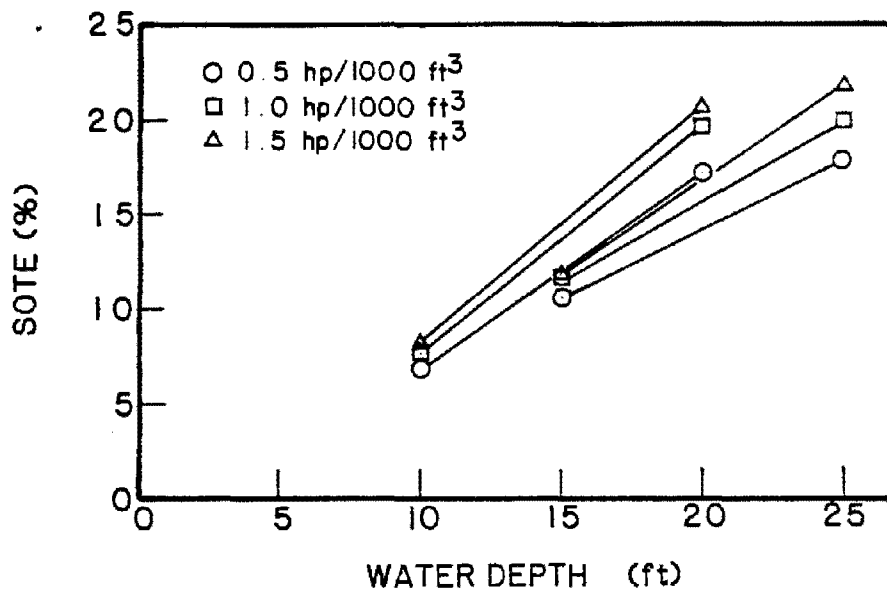


Figure H-8. SOTE vs. water depth for Sanitaire coarse bubble diffusers.

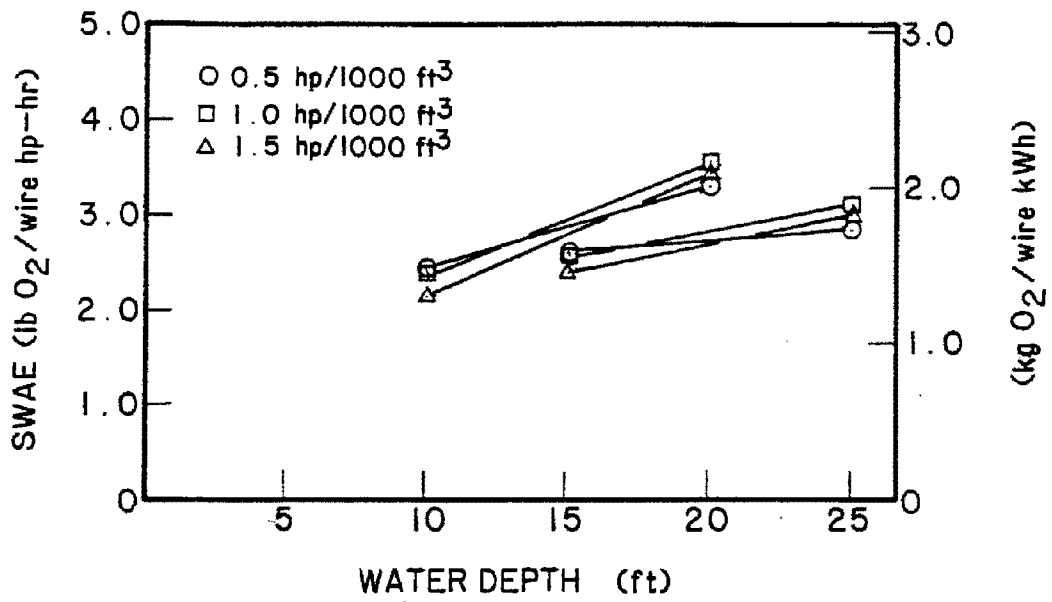


Figure H-9. SWAE vs. water depth for Sanitaire coarse bubble diffusers.

APPENDIX I

INDIVIDUAL PERFORMANCE RESULTS FOR ENVIREX COARSE BUBBLE DIFFUSERS

A total of 15 acceptable tests were conducted on the Envirex coarse bubble diffusion system in this study. The results of these tests were summarized tabularly in Tables 15 and 16 in Section 6 and are presented graphically here in Figures I-1 through I-9.

The effect of variations in airflow rate on delivered power density is shown in Figure I-1 for the various water depths. As expected, an increase in airflow rate resulted in an increase in delivered power density.

Figure I-2 shows the relationship between nominal power density and delivered power density. The effect that is generally demonstrated is that as power density increased, the differences between nominal and delivered power densities increased. The differences became larger as water depth decreased.

Figure I-3 illustrates the relationship between delivered power density and K_{La20} . As shown in this plot, K_{La20} increased linearly for the 6.1-m (20-ft) water depth. For the other three depths, the K_{La20} rate of increase was high initially, then decreased slightly with increasing power density. Also apparent is that increasing water depth resulted in increasing K_{La20} values.

SOTR is plotted against delivered power density in Figure I-4. SOTR is expressed in both U.S. customary units (left vertical axis) and SI units (right vertical axis). For the Envirex system, an increase in delivered power density produced an increase in SOTR. The rate of increase in SOTR for this system appears to have been almost linear for all water depths. Also apparent is the substantial effect of increasing water depth on SOTR. Increasing water depth had a much smaller effect on K_{La20} (Figure I-3).

Figure I-5 is a plot of the relationship between SOTE and delivered power density. The lowest SOTE values corresponded with the lowest delivered power density level at each water depth. For three of the four water depths, SOTE increased almost linearly with increasing levels of delivered power density. At the 7.6-m (25-ft) water depth, however, the highest SOTE value occurred at the middle delivered power density tested. Also evident is that an increase in water depth was accompanied by a consistent improvement in SOTE.

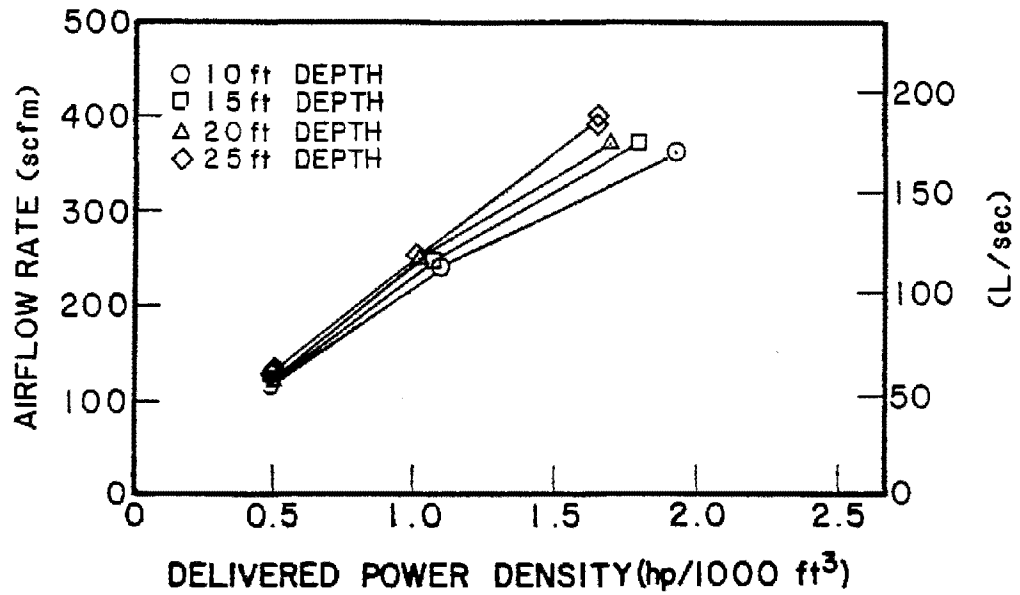


Figure I-1. Airflow rate vs. delivered power density for Envirex coarse bubble diffusers.

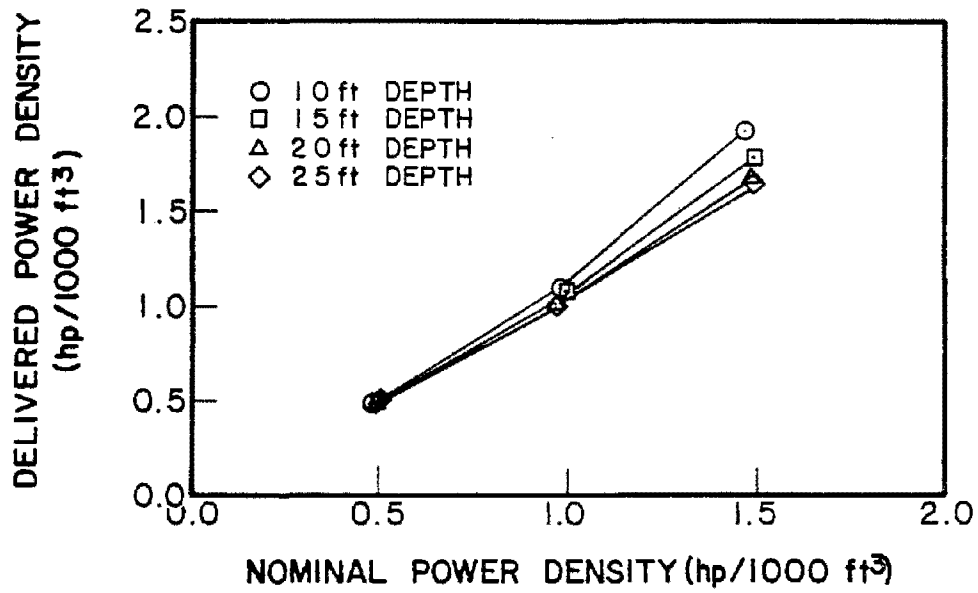


Figure I-2. Delivered power density vs. nominal power density for Envirex coarse bubble diffusers.

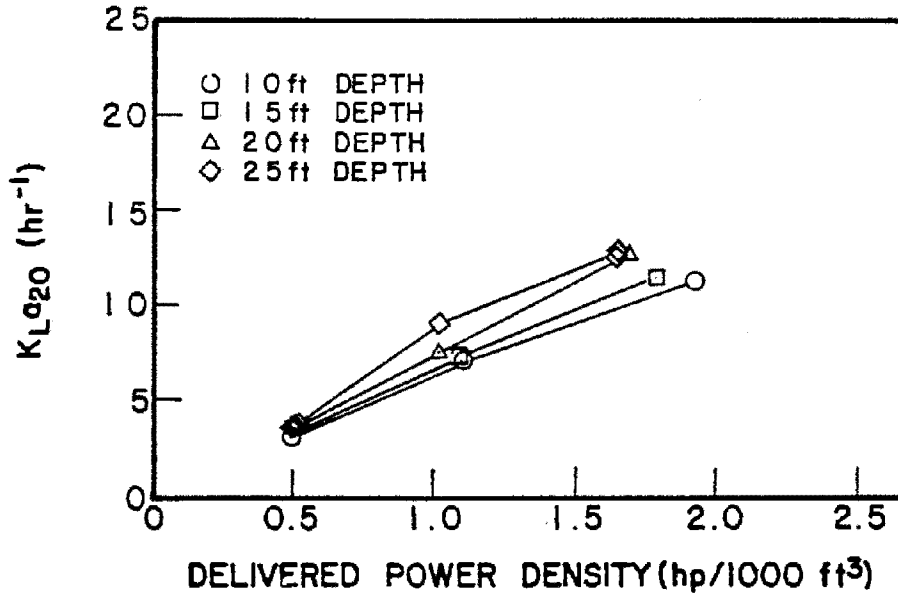


Figure I-3. K_{La20} vs. delivered power density for Envirex coarse bubble diffusers.

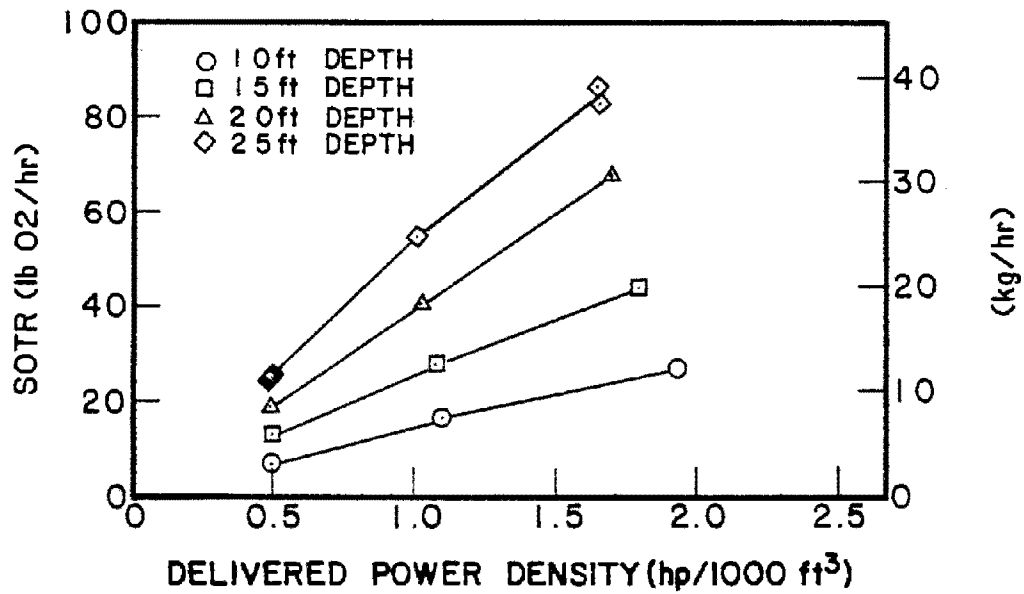


Figure I-4. SOTR vs. delivered power density for Envirex coarse bubble diffusers.

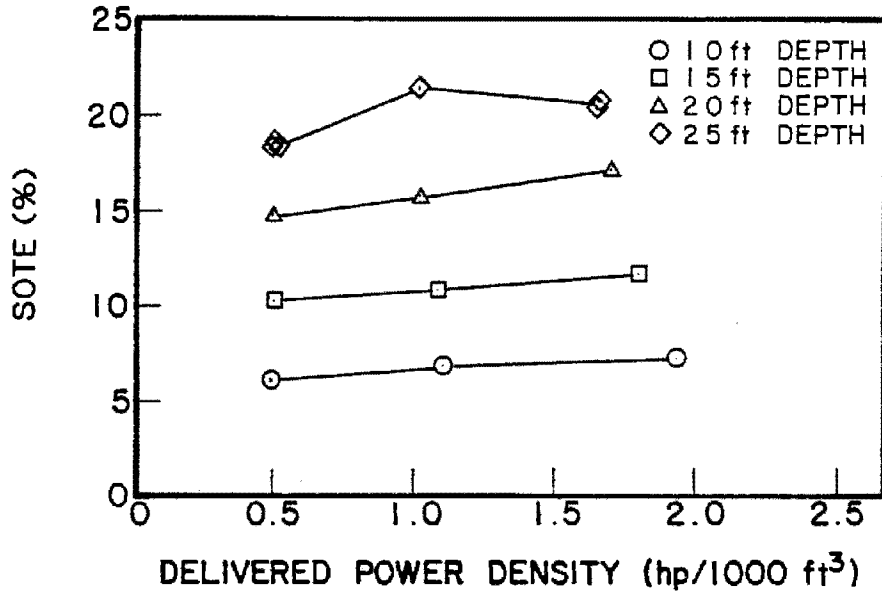


Figure I-5. SOTE vs. delivered power density for Envirex coarse bubble diffusers.

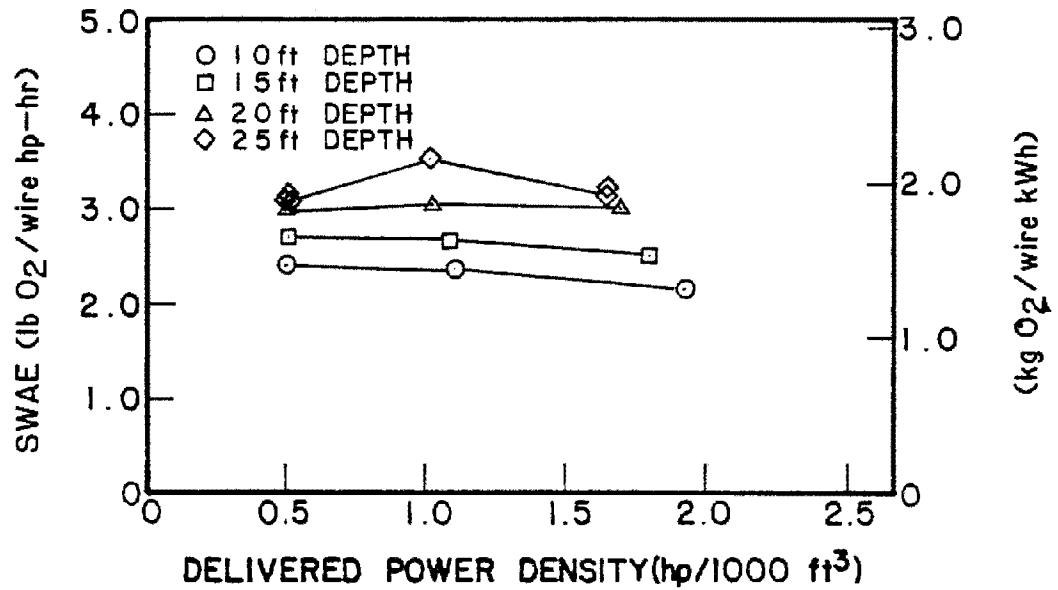


Figure I-6. SWAE vs. delivered power density for Envirex coarse bubble diffusers.

SWAE vs. delivered power density is shown for Envirex in Figure I-6. SWAE is given in both U.S. customary units and SI units. For this system, SWAE was virtually unaffected by changes in delivered power density except at the 7.6-m (25-ft) water depth. SWAE values increased with each increase in water depth.

Figure I-7 illustrates the relationship between SOTR and test tank water depth, with SOTR expressed in both U.S. customary units and SI units. For the Envirex system, two of the three nominal power density curves exhibited an increasing rate of increase in SOTR with increasing water depth, while the third curve indicated a constant rate of increase. The highest SOTR values were observed at the highest nominal power density.

SOTE vs. water depth is plotted in Figure I-8. Increasing SOTE was observed with increasing water depth for this aeration system as with each of the other six systems tested at multiple water depths. For this system, the data indicate a mostly linear relationship between SOTE and water depth. The highest values of SOTE generally corresponded with the highest nominal power density.

This system's relationship of SWAE to water depth is shown in Figure I-9. SWAE is expressed in both U.S. customary units and SI units. A trend of increasing SWAE is evident with increasing water depth. Peak values of SWAE occurred at the 7.6-m (25-ft) water depth. The nominal power density values are clustered closely together at three of the four water depths, indicating this system's insensitivity to variations in power density.

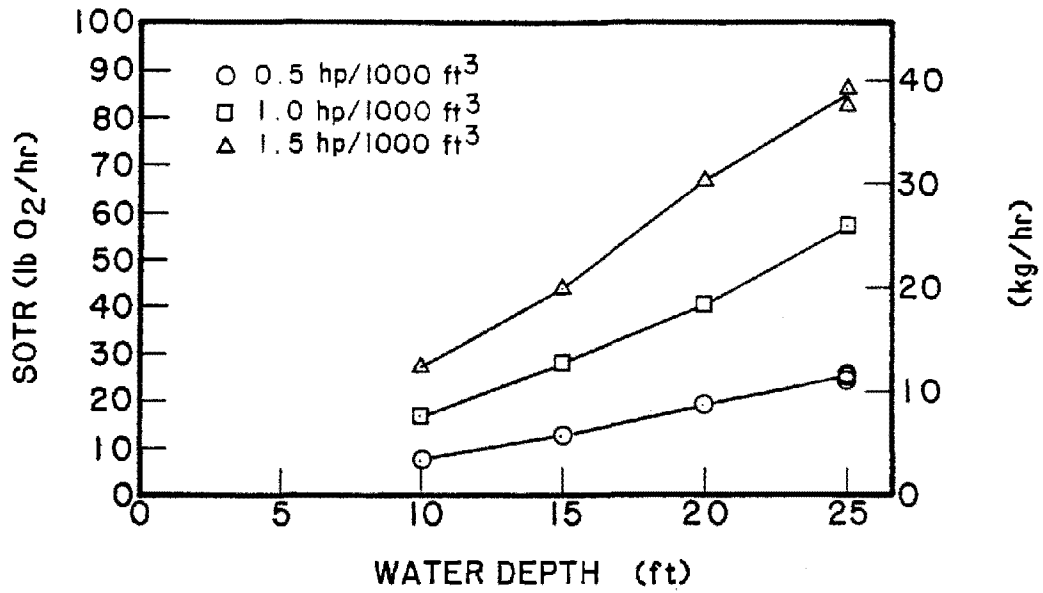


Figure I-7. SOTR vs. water depth for Envirex coarse bubble diffusers.

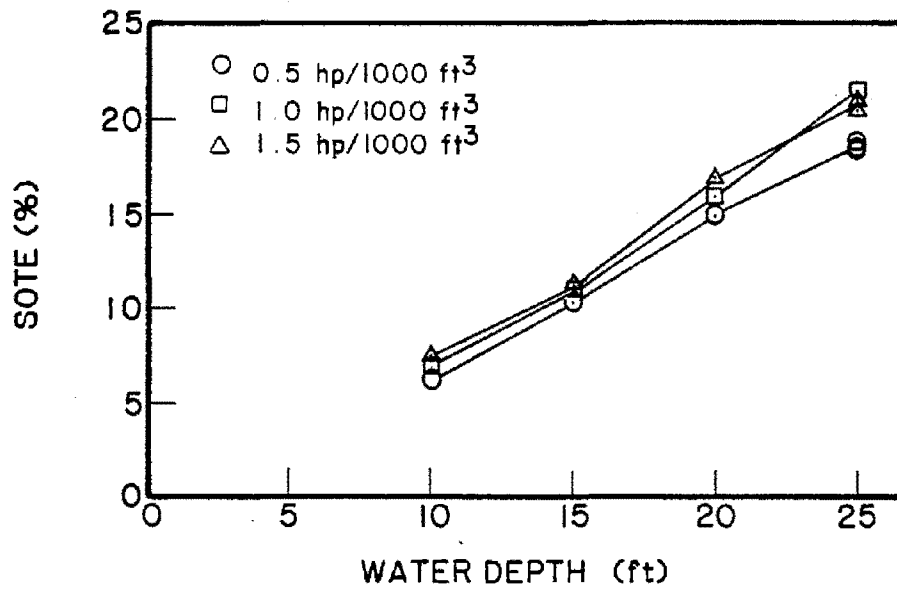


Figure I-8. SOTE vs. water depth for Envirex coarse bubble diffusers.

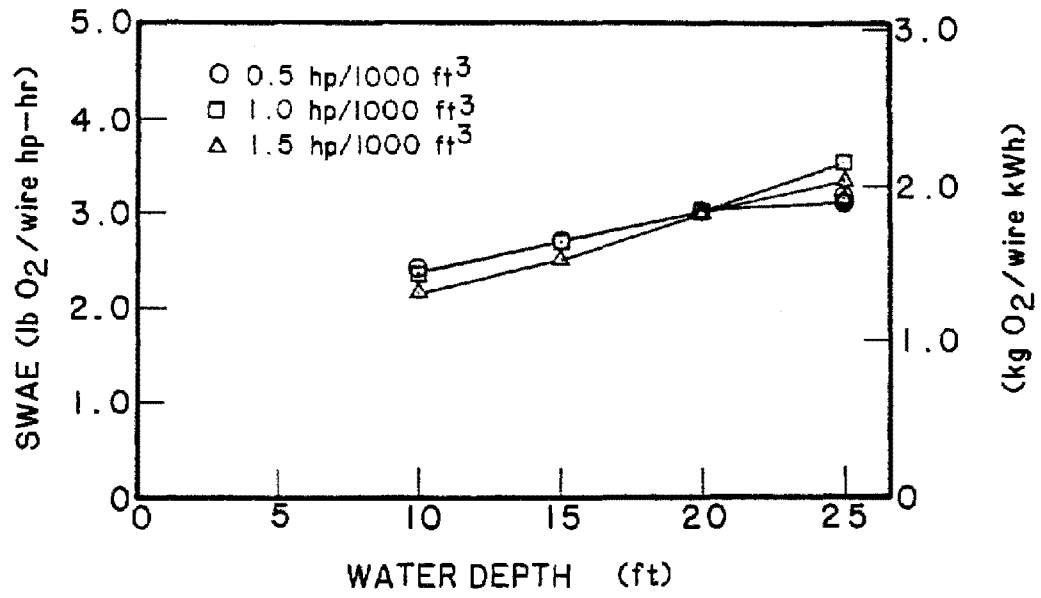


Figure I-9. SWAE vs. water depth for Envirex coarse bubble diffusers.

APPENDIX J

INDIVIDUAL PERFORMANCE RESULTS FOR FMC COARSE BUBBLE DIFFUSERS

A total of three acceptable tests were run on the FMC coarse bubble diffusion system (Deflectofuser) in this study. Test results for this system were summarized tabularly in Tables 17 and 18 (Section 6) and are shown graphically here in Figures J-1 through J-6.

Figure J-1 illustrates the effect that variations in airflow rate have on delivered power density. As expected, an increase in airflow rate produced an increase in delivered power density.

The relationship between nominal power density and delivered power density is shown in Figure J-2. The effect that is generally demonstrated is that as power density increased, the discrepancy between nominal and delivered power densities also increased.

The relationship of delivered power density to $K_L a_{20}$ is plotted in Figure J-3. $K_L a_{20}$ increased linearly with increasing delivered power density.

Figure J-4 is a plot of SOTR vs. delivered power density. This plot gives SOTR values in both U.S. customary units (left vertical axis) and SI units (right vertical axis). An increase in the delivered power density resulted in an increase in this system's SOTR. The rate of increase was approximately constant for the water depth tested.

The relationship between SOTE and delivered power density is graphed in Figure J-5. SOTE increased with each increase in delivered power density, but only at a very moderate rate.

SWAE is plotted against delivered power density in Figure J-6, with SWAE provided in both U.S. customary units and SI units. For this coarse bubble system, although the highest SWAE value occurred at the lowest delivered power density, the curve indicates that changes in delivered power density had little impact on SWAE.

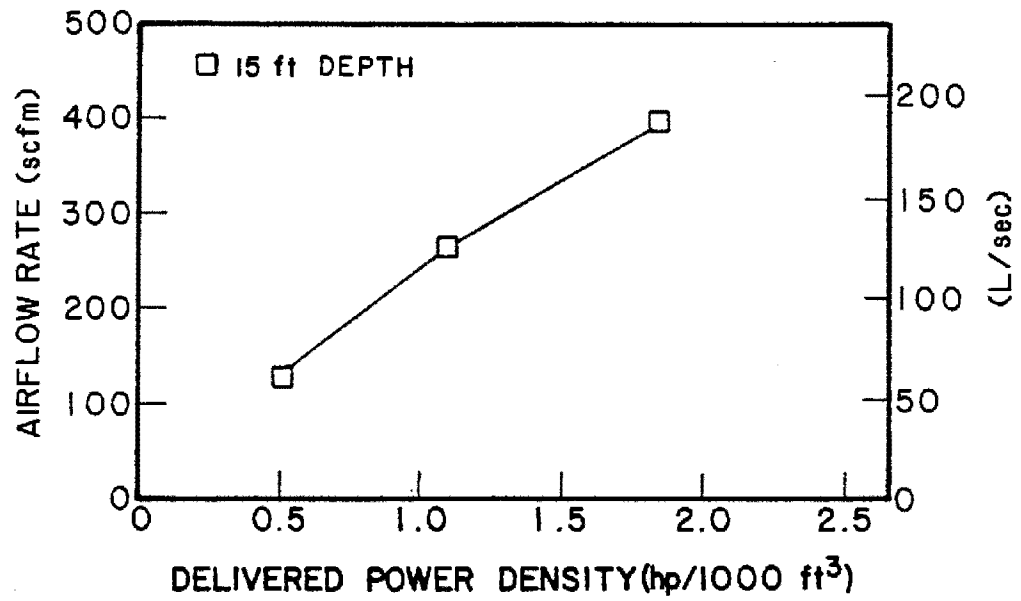


Figure J-1. Airflow rate vs. delivered power density for FMC coarse bubble diffusers.

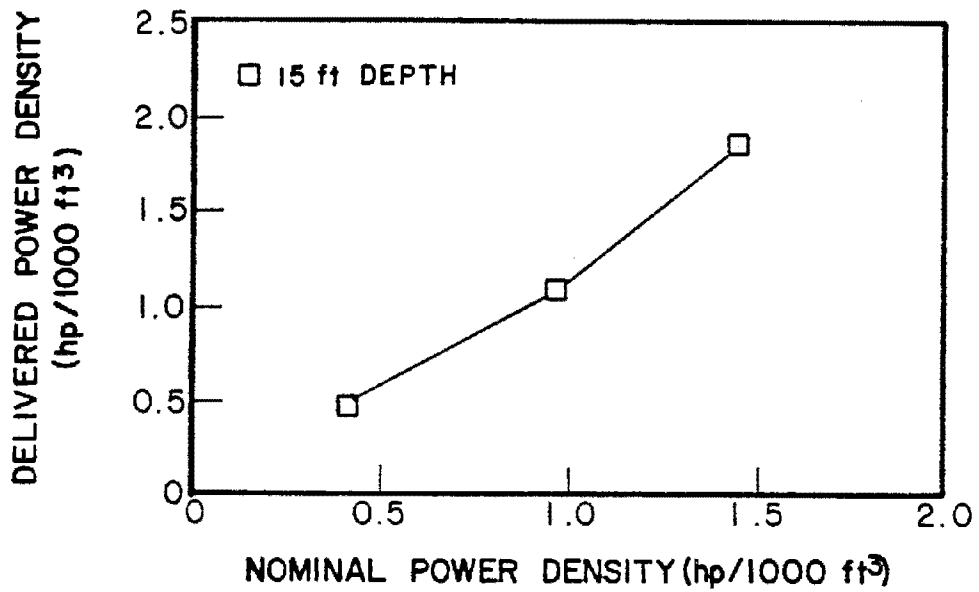


Figure J-2. Delivered power density vs. nominal power density for FMC coarse bubble diffusers.

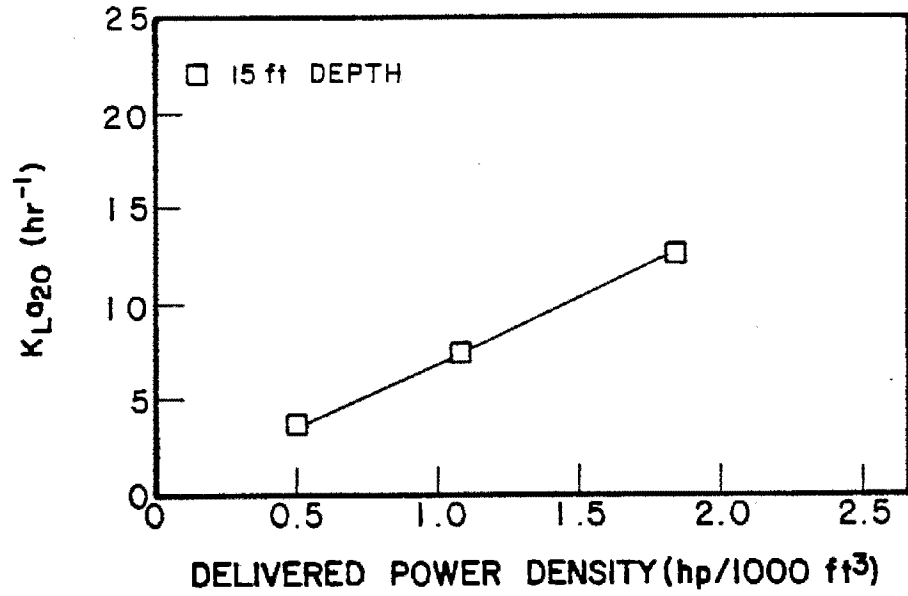


Figure J-3. K_La₂₀ vs. delivered power density for FMC coarse bubble diffusers.

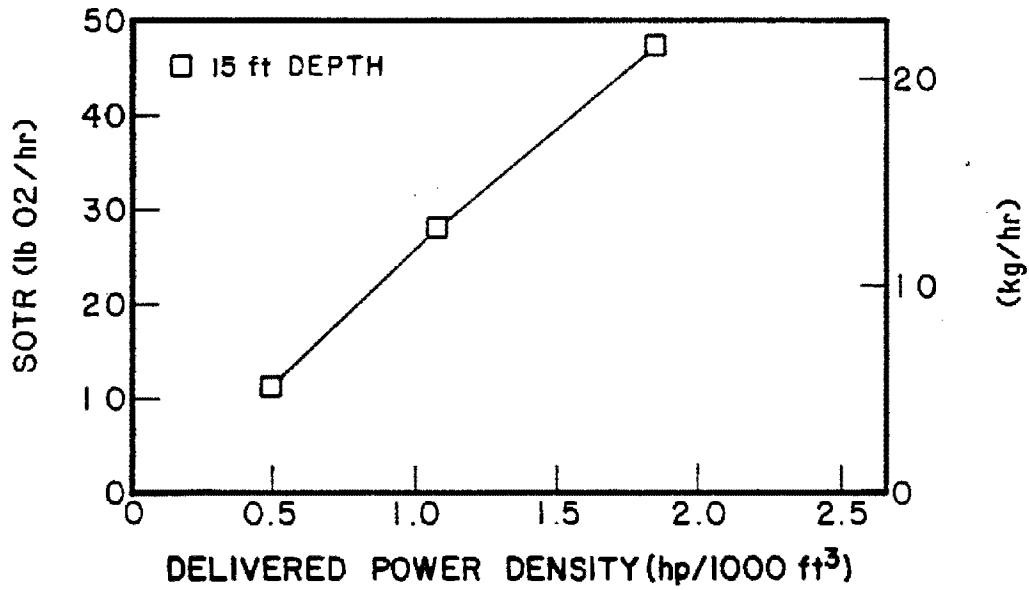


Figure J-4. SOTR vs. delivered power density for FMC coarse bubble diffusers.

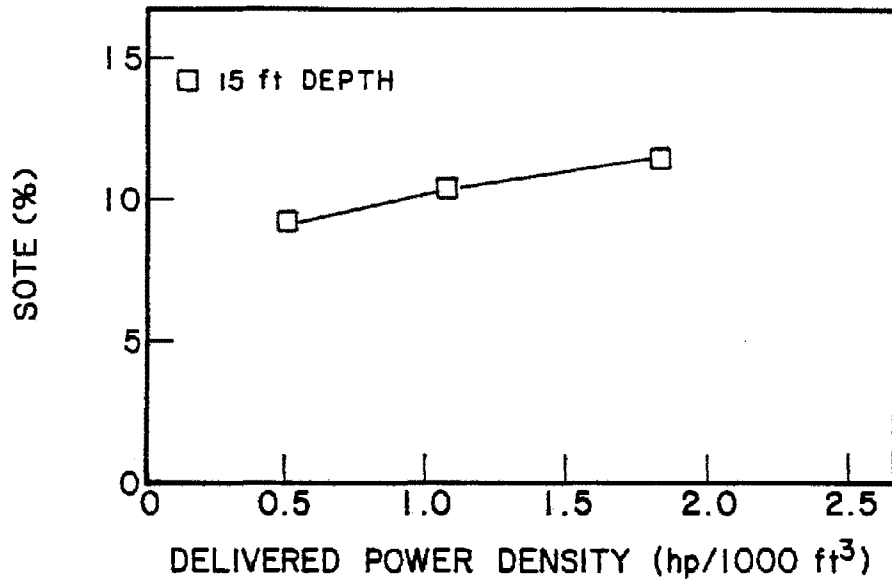


Figure J-5. SOTE vs. delivered power density for FMC coarse bubble diffusers.

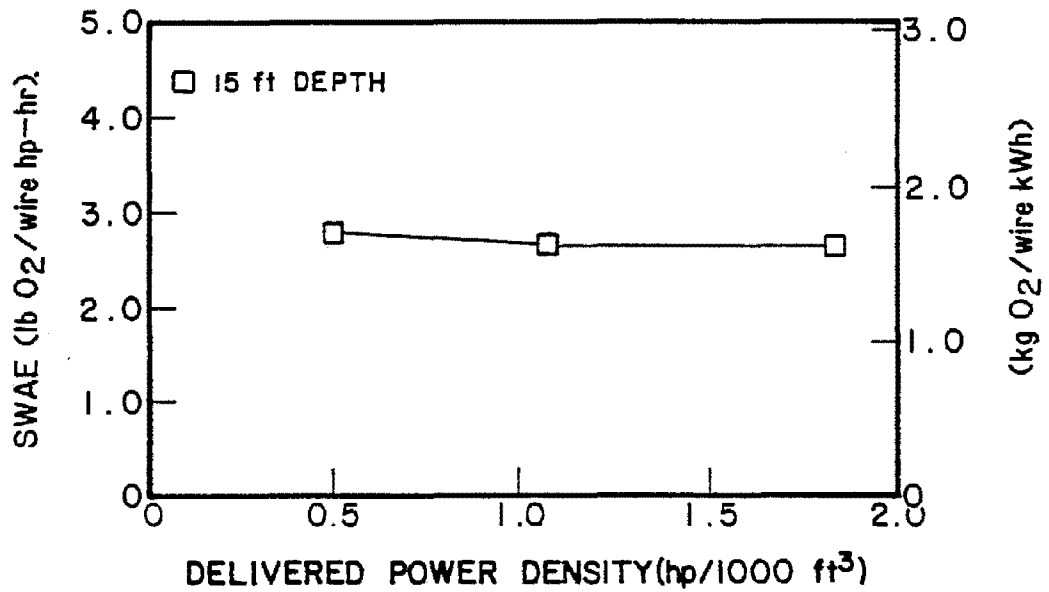


Figure J-6. SWAE vs. delivered power density for FMC coarse bubble diffusers.